

The structural design of earthen structures with robotic shotearth fabrication

Master Thesis

Yi Yu Shirley Feng

Delft University of Technology

The structural design of earthen structures with robotic shotearth fabrication

by

Yi Yu Shirley Feng

Institution: Delft University of Technology
Place: Faculty of Civil Engineering and Geosciences
Project Duration: January, 2021 - March, 2022
Committee: Branko Šavija
Michela Turrin
Pierre Hoogenboom
Jelle Feringa
Diederik Veenendaal

Cover Image: Tecla house by Mario Cucinella and WASP

Acknowledgements

This thesis marks the end of my MSc Building Engineering degree at TU Delft. I would like to thank my thesis committee for the guidance and support over this long period of time and during these challenging circumstances. Thank you to my committee chair Branko Šavija for showing up week after week and guiding me through this challenging work. Thank you to Diederik Veenendaal and Jelle Feringa for introducing me and giving me the opportunity to work on this fascinating topic that has radically changed my way of thinking about our built environment. Thank you to Michela Turrin and Pierre Hoogenboom for your support and valuable feedback whenever needed. Thank you to Yask Kulshreshtha for helping me understand earth materials and behaviour, without your valuable insights my work would probably not be the same. Thank you to the Summum Engineering office (Diederik and Rik) for being available to help during technical difficulties and for being so flexible. Thank you to all the external academics who have provided me experimental data and shared experiences working with earthen materials and structures. It was so nice to get validated on common struggles.

I would also like to thank everyone who have been part of my journey during my time here. Thank you to Roel Schipper for your patience and support in us students whenever we need it. Thank you to my fellow programme buddies for helping me get through challenging group projects, intense discussions and passing exams. Thank you to everyone at U-BASE for organising interesting talks and events, and for just wanting to have a chat and a good time. Thank you to all the lunch and study buddies that have shown up every day in the last many many months, I will miss our breaks and banter. Last but not least I would like to give special thanks to my family (爸爸, 妈妈, 弟弟, 姐姐, 姑丈, 奶奶) and Patrick for supporting me through all these years of higher education and my decision to do it all abroad.

This thesis not only marks the end of my time in Delft but is also the culmination of many years of living in a different country, meeting new people from different backgrounds, exploring new places and trying new things. All these experiences have changed the way I think and view the world. My journey has both challenged and enriched my life in ways that I could never imagine. I would like to thank all the people who have been part of this longer journey and I am looking forward to many more years of challenges, growth and laughter.

*Yi Yu Shirley Feng
Delft, March 2022*

“Socialism collapsed because it did not allow prices to tell the economic truth.
Capitalism may collapse because it does not allow prices to tell the ecological truth.”

LESTER R. BROWN

Abstract

In the near future, pressure on sustainability requirements in building structures will increase further as governments around the world are forced to tackle climate change issues. The construction industry is one of the most resource intensive and wasteful sectors in the world and is estimated to keep growing at a fast pace due to growing populations. Earth building materials and construction systems are perhaps one of the most attractive options available. The advantages of raw earth are that it is considered to be widely available, recyclable, can be sourced at low costs, can exhibit high strength and can provide an excellent indoor climate for occupants. The interest in building with earth is experiencing a renaissance but advancements in Earth Building Technology is currently at its infancy. Most improvement in earth buildings has been related to fabrication methods, where current developments and opportunities in additive manufacturing has potential to create a new form of earth architecture. From a mechanical perspective, earth materials are strong in compression and weak tension, making compression-only structures like arches, vaults and domes especially interesting.

The purpose of this thesis is to determine how feasible it is to combine earth material with a robotic sprayed earth fabrication method to build wall and arch structures. Emphasis has been put in understanding the material for robotic fabrication. Therefore, an in-depth literature study of earth materials and their properties was conducted to understand how they gain strength. In AM, modelling the structural-up of a printed structure requires time-dependent material properties where early-age behaviour is especially critical. As a result, time-dependent compressive strength and Young's modulus of potential shotearth with and without cement stabilisation was predicted. Equations from the material predictions were input into the design tool developed by Witteveen+Bos to explore geometrical shapes, assess printing time and dimensions that can be achieved.

The results of this work show that earth building materials is essentially impossible to predict without testing as soil composition has a big influence on mechanical strength. Prediction of raw earth properties was based on understanding of soil consistencies and water content. Prediction of cement stabilised earth properties was based on existing data from 3D extruded and sprayed concrete experiments. 3D printed structures, extruded and sprayed, can be compared to ancient masonry structures in their structural design and inspiration from these structures sees different layering techniques adopted to minimise formwork and maximise structural efficiency and strength. Through a geometrical non-linear FE analysis with the time-dependent properties defined and varying robotic printing speeds between 1000 -6000 mm/min, a free standing wall structure of one meter width can reach heights between 0.1 and 0.62 m. For the overhanging structures, a barrel vault and a half dome, considering no formwork, an 8.5 -10.5 degrees arch or tilt can be achieved, compared to the vertical free wall. It is found that for lower printing speeds, more structure can be printed before failure. For the half dome almost the full geometry can be achieved. The unstabilised and cement stabilised upper bound material models resulted in comparable geometric dimensions for all structures analysed. Results of this study also compared the barrel vault and half dome using the roman (radial) and nubian (inclined) layering techniques.

Contents

Acknowledgements	i
Abstract	iii
List of Figures	vii
List of Tables	xii
1 Earth construction for future sustainability of our built environment	1
1.1 Climate crisis, housing shortage and public health	1
1.2 Earth building and construction	2
1.3 Why we are not building with earth?	3
1.4 Earth architecture from antiquity to the 21st century	5
1.4.1 Earthen arches, vaults and domes	7
1.5 Research in earth building materials and fabrication	7
1.6 Future trends	9
2 Research scope	11
3 Historic overview	14
4 Overview of Advances in current Earth Building Technology	20
4.1 Earth building materials	20
4.1.1 Definitions	20
4.1.2 Classification of soils for earth building	21
4.1.3 Materials for modern earth building	25
4.1.4 Stabilisation	26
4.2 Earth construction techniques	29
4.2.1 Construction systems	29
4.2.2 Technical standards	31
4.3 Physical properties	31
4.3.1 Determining physical properties	31
4.3.2 Water content in soils.	32
4.3.3 Compaction of soil	35
4.4 Mechanical properties.	38
4.4.1 Determining mechanical properties	38
4.4.2 Mechanical properties of cement stabilised rammed earth	39
4.4.3 Mechanical properties of unstabilised earth.	41
4.5 Hygrothermal properties	44
4.5.1 Determining hygrothermal properties	45
4.5.2 Moisture buffering capacity	45
4.5.3 Thermal performance	46
4.6 Durability	47
4.7 Challenges in current earth building technology	50

5 Additive Manufacturing for Earth Construction	51
5.1 Additive manufacturing and 3D printing	51
5.2 AM in the context of earthen construction and architecture	53
5.2.1 Robotic rammed earth	54
5.2.2 3D printing earth and clay materials	54
5.2.3 Sprayed earth	55
5.3 Material and processing requirements for digital earth.	55
5.3.1 Material requirements	55
5.3.2 Processing requirements	57
5.4 Design and computational modelling	60
5.5 Challenges of AM technologies with earth building materials.	60
6 Design and Model Part 1: Defining material models	62
6.1 Material and processing requirements for SE3DP	62
6.2 Defining material models for Shotearth 3D printing.	64
6.2.1 Stress and stiffness over time development	64
6.2.2 Unstabilised robotic shotearth.	64
6.2.3 Cement stabilised robotic shotearth	70
6.2.4 Discussion on results.	78
6.2.5 Discussion on procedure	83
7 Design and Model Part 2: Assessment of shotearth structures	84
7.1 Structural design of earthen wall structures	84
7.2 Structural design of earthen arch structures.	85
7.2.1 Roman, Nubian and Corbelling techniques	86
7.3 Design of shotearth structures with shotearth 3D printing	87
7.3.1 Model setup	87
7.3.2 Processing parameters considered	88
7.3.3 Material models	89
7.3.4 Analysis	90
7.4 Monolithic shotearth wall structure	91
7.4.1 Wall geometry and element definition	91
7.4.2 Analysis check	92
7.4.3 Results	93
7.4.4 Discussion	95
7.5 Barrel vault and half dome structures.	98
7.5.1 Geometry, element definition and loads	98
7.5.2 Analysis check	99
7.5.3 Results	100
7.5.4 Discussion	108
8 Conclusion	114
8.1 Main question: Fabrication feasibility of shotearth structures	114
8.2 Future outlook on earth and shotearth construction	118
8.2.1 Standardisation	118
8.2.2 Sustainability	119
8.2.3 Cost benefits.	119
8.3 Recommendations and further work	120

A	Additives, biopolymers and fibres found in earth material research	122
B	Overview of earth building standards, codes and normative documents	124
C	Unstabilised shotearth calculations	127
C.1	Data entries for predictions	127
D	Cement stabilised shotearth calculations	130
D.1	Concrete and shotcrete models	130
D.1.1	Eurcode 2 and ACI	130
D.1.2	Shotcrete models	131
D.2	Data on early age strength and stiffness development for 3DCP and SC3DP . .	133
D.2.1	Suiker's data	133
D.2.2	Dressler's data	133
D.2.3	Perrot's data	134
D.3	Curvefitting calculation	134
E	Assessment of shotearth structures	139
E.1	Recommendations for the design of earthen walls	139
E.2	Linear regression of data for material models	140
E.3	Monolithic wall	146
E.4	Overhang roman layering	147
E.4.1	Barrel vault	147
E.4.2	Half dome	148
E.5	Overhang nubian layering	149
E.5.1	Barrel vault	149
E.5.2	Half dome	150

List of Figures

1.1	Life cycle of raw earth materials (adapted from Ref [7])	2
1.2	Hospital of Feldkirch, Austria [9]	6
1.3	Ricola Kräuterzentrum, Switzerland [10]	6
1.4	Arch of Ctesiphon, Iraq [11]	6
1.5	Rwanda Cricket Stadium in Kigali [12]	6
1.6	Sharanam conference hall, India [13]	6
1.7	Rammed earth arch in Lyon, France [14]	6
1.8	Prefabricated rammed earth pavilion ETH, Zürich [15]	6
1.9	Tecla house by Mario Cucinelli and WASP [16]	6
1.10	Cumulative number of research and review articles discussing earthen construction techniques recorded per year as indicated by Science Direct keyword searches (adapted from Ref [18])	8
1.11	Sciences involved in Earth Building Engineering (adapted from Ref [19])	8
2.1	Methodology of work	12
3.1	Presence of earth architecture with black dots indicating UNESCO world heritage sites [23]	15
3.2	Bagdir or windcatcher, a traditional persian architectural element to create natural ventilation [26]	16
3.3	The oldest known earthen settlement in Catal Höyük, Anatolia (Turkey and Palestine) (reconstruction) [27]	16
3.4	Present day White Temple of Uruk, one of the earliest examples of raw earth brick construction [28]	16
3.5	Dur-Sharrukin, capital of King Sargon II, 713-707 BCE (present day Iraq). The city was built using raw earth bricks (reconstruction) [29]	16
3.6	Shibam, Yemen, one of earliest examples of vertical master planning [30]	16
3.7	Alhambra fortress in Spain built with rammed earth in 889 CE [31]	16
3.8	Section of the Great Wall of China built using rammed earth [32]	17
3.9	Tulou houses in Fujian, China built with rammed earth [33]	17
3.10	Pueblo style houses in Santa Fe, New Mexico, using adobe bricks [34]	17
3.11	Icelandic turf houses. Turf is a great insulation material for cold climates [35]	17
3.12	Ennis Brown House by Frank Lloyd Wright 1924 [36]	19
3.13	New Baris village in Egypt by Hasan Fathy [37]	19
4.1	Soil layers. Subsoil is usually used for earth building purposes.	21
4.2	Soil classification systems by different standards (adapted from Ref [38])	22
4.3	PSD envelope found by Houben & Guillaud and PSD envelopes used by other authors in research (adapted from Ref [41])	23
4.4	Recommended upper and lower proportions of clay, silt, sand/gravel in earth building materials according to a) Houben & Guillaud, b) Norton, c) SAZS 724, d) Schrader, e) McHenry, f) Radanovic (adapted from Ref [2])	23

4.5	Composition of subsoil and clay minerals	25
4.6	Selection criteria for common stabilizers with different soil characteristics, described in Australian Earth Building Handbook HB195 (adapted from Ref [40], [51])	28
4.7	Twelve ways of using earth for construction by CRAterre	30
4.8	The concept of soil suction (adapted from Ref [7], [55])	33
4.9	Earth construction systems classified as wet and dry methods (partially adapted from Ref [21])	34
4.10	Atterberg limits (adapted from Ref [38])	35
4.11	Optimum moisture content and maximum dry density of a soil (adapted from Ref [58])	36
4.12	Compaction curves from different soils (adapted from Ref [58])	36
4.13	Compaction curve of a soil with higher compactive effort, from B to C (adapted from Ref [58])	37
4.14	Compaction curves at 25, 50, 100 MPa and standard Proctor (adapted from Ref [62])	38
4.15	Relative increase in compressive strength over % cement content for different soil groups (adapted from Ref [40])	40
4.16	MBV of stabilised and unstabilised earth samples (adapted from Ref [95])	47
4.17	Measured moisture adsorption in g/m ² at 8 hours for different earth products (adapted from Ref [92])	47
4.18	Effect of humidity on strength (adapted from Ref [97])	48
4.19	Linear and non-linear erosion over time (adapted from Ref [103])	49
5.1	Process of 3D concrete printing	51
5.2	First 3D printed office in Dubai [122]	52
5.3	First 3D printed bridge, Netherlands [123]	52
5.4	"The Bridge Project", Netherlands [124]	52
5.5	Project Milestone, Netherlands [125]	52
5.6	Opportunities for application of SC3DP (adapted from Ref [131])	53
5.7	Reinforced curved wall using SC3DP [131]	53
5.8	Cylinder with overhang using SC3DP [132]	53
5.9	Gantry system [152]	58
5.10	Delta system [153]	58
5.11	Industrial robot arm system [154]	58
5.12	Cooperative robot [155]	58
5.13	Mesh mould system at ETH Zürich [156]	58
5.14	Comparison of processing parameters in 3DCP and SC3DP and their target values	59
6.1	Water content of different earth building applications and where printed earth is assumed to be	63
6.2	Assumed range of SE3DP relative to plasticity index based on data gathered	66
6.3	Assumed maximum dry density (MDD) and moisture content (W _{opt}) of unstabilised robotic shotearth relative to rammed earth and 3DP earth, assumed same soil composition.	66
6.4	Yield stress data from Perrot (adapted from Ref [137])	67
6.5	Stiffness data from Perrot (adapted from Ref [137])	67
6.6	Strength: upper and lower limits of unstabilised shotearth	68
6.7	Stiffness: upper and lower limits of unstabilised shotearth	68

6.8	Stress: Proposed shotearth relative to the bounds	69
6.9	Stiffness: Proposed shotearth relative to the bounds	69
6.10	Assumed strength of cement stabilised robotic shotearth	71
6.11	Assumed stiffness of cement stabilised robotic shotearth	71
6.12	Strength predictions from concrete and shotcrete models	72
6.13	Stiffness predictions from concrete and shotcrete models	72
6.16	Shotcrete in tunnelling compressive strength development	73
6.14	Stress data from SC3DP and 3DCP	74
6.15	Stiffness data from SC3DP and 3DCP	74
6.17	Comparison of strength development	75
6.18	Comparison of stiffness development	75
6.19	Stress data from SC3DP and 3DCP compared to alginate stabilised earth	76
6.20	Stiffness data from SC3DP and 3DCP compared to alginate stabilised earth	76
6.21	Shape of the first order differential function	77
6.22	Curvefitting for upper bound strength	79
6.23	Curvefitting for lower bound strength	79
6.24	Curvefitting for upper bound stiffness	80
6.25	Curvefitting for lower bound stiffness	80
6.26	Results of the strength development over 28 days	81
6.27	Results of the stiffness development over 28 days	81
6.28	Comparison of Curto's results to Houben & Guillaud.	83
7.1	Roman, Nubian and Corbelling layering techniques used in masonry structures (adapted from Ref [145])	86
7.2	Model setup for wall structure	87
7.3	Functions and types of analysis of Karamba	88
7.4	Left: Processing parameters assumed and applied for SE3DP, only rows marked in yellow is considered in the design tool. Right: Printing parameters considered in the tool where only layer count and printing speed is varied	88
7.5	Linear regression in Excel to GHPython conditionals	89
7.6	Left: Wall geometry and dimensions. Right: triangular shell elements	91
7.7	Karamba model verification of Suiker's results where red is compression stress and blue is tension stress. The table shows resulting maximum compression and tension stresses of the model compared to those allowed and the buckling load factor. The highlighted yellow cell is the governing failure mode.	93
7.8	Visualisation of maximum wall height that can be printed before failure either through material crushing or buckling for the unstabilised material models at speed 6000 mm/min. Red =compression stress. Blue =tension stress.	94
7.9	Visualisation of maximum wall height that can be printed before failure either through material crushing or buckling for the cement stabilised material models at speed 6000 mm/min. Red =compression stress. Blue =tension stress.	94
7.10	The first four buckling modes for the wall upper bound models unstabilised and cement stabilised	94
7.11	Maximum number layers for the unstabilised material models	95
7.12	Maximum number layers for the stabilised material models	95
7.13	Mesh resolution influence on results, U count =1, V count =1 -110 where max. stress = maximum tension stress and min. stress = maximum compression stress	96
7.14	Comparison of maximum wall height for upper bound material models	97
7.15	Comparison of maximum wall height for lower bound material models	97

7.16 Top: geometric setup of the barrel vault. Bottom: geometric setup of the half dome. Middle: Roman layering for both geometries. Right: Nubian layering for both geometries.	98
7.17 Grasshopper definition for both the barrel vault, labelled arch surface, and the half dome, labelled dome surface, geometries.	99
7.18 Setup of the slicing direction for the geometries	99
7.19 Half of the barrel vault with roman layering technique using unstabilised lower bound material model at printing speed 1000 and 6000 mm/min. The horizontal lines show the expected printing path. Red =compression stress. Blue =tension stress.	101
7.20 Half of the barrel vault with roman layering technique using unstabilised upper bound material model at printing speed 1000 and 6000 mm/min. The horizontal lines show the expected printing path. Red =compression stress. Blue =tension stress.	101
7.21 Half of the barrel vault with roman layering technique using cement stabilised lower bound material model at printing speed 1000 and 6000 mm/min. The horizontal lines show the expected printing path. Red =compression stress. Blue =tension stress.	102
7.22 Half of the barrel vault with roman layering technique using cement stabilised upper bound material model at printing speed 1000 and 6000 mm/min. The horizontal lines show the expected printing path. Red =compression stress. Blue =tension stress.	102
7.23 Half of the barrel vault with nubian layering technique using unstabilised material models at printing speed 1000 mm/min. The inclined lines show the expected printing path. Red =compression stress. Blue =tension stress.	103
7.24 Half of the barrel vault with nubian layering technique using cement stabilised material models at printing speed 1000 mm/min. The inclined lines show the expected printing path. Red =compression stress. Blue =tension stress.	103
7.25 Half dome with roman layering technique using unstabilised lower bound material model at printing speed 1000 and 6000 mm/min. Red =compression stress. Blue =tension stress	104
7.26 Half dome with roman layering technique using unstabilised upper bound material model at printing speed 1000 and 6000 mm/min. Red =compression stress. Blue =tension stress	104
7.27 Half dome with roman layering technique using cement stabilised lower bound material model at printing speed 1000 and 6000 mm/min. Red =compression stress. Blue =tension stress	105
7.28 Half dome with roman layering technique using cement stabilised upper bound material model at printing speed 1000 and 6000 mm/min. Red =compression stress. Blue =tension stress.	105
7.29 Half dome with nubian layering technique using unstabilised material models at printing speed 1000 mm/min. The inclined lines show the expected printing path. Red =compression stress. Blue =tension stress.	106
7.30 Half dome with nubian layering technique using cement stabilised material models at printing speed 1000 mm/min. The inclined lines show the expected printing path. Red =compression stress. Blue =tension stress.	106
7.31 Barrel vault with nubian layering buckling modes 1 and 2	109
7.32 Barrel vault and half dome mesh and support definitions	109
7.33 a / t ratio (adapted from Ref [169])	111

7.34	Finite element analysis of shells (adapted from Ref [170])	112
7.35	Comparison of barrel vault with (b) and without imperfections (a)	113
7.36	Comparison of half dome with (b) and without imperfections (a)	113
8.1	Design considerations taken into account in this work	114
E.1	Recommended values for wall thickness and slenderness of earth walls (adapted from Ref [7])	139
E.2	Python code: conditions for unstabilised material models	140
E.3	Linear regression of Perrots stress development	141
E.4	Linear regression of Perrots stiffness development	141
E.5	Linear regression of assumed URE stress development	142
E.6	Linear regression of assumed URE stiffness development	142
E.7	Python code: conditions for stabilised material models	143
E.8	Linear regression of stress data, upper	143
E.9	Linear regression of stress data, lower	144
E.10	Linear regression of stiffness data, upper	144
E.11	Linear regression of stiffness data, lower	145

List of Tables

1.1	Main advantages of building with earth (adapted from Ref [2])	3
1.2	The main problems with cement and earth as a solution (adapted from Ref [3])	3
1.3	Main limitations of building with earth (adapted from Ref [2], [8])	4
4.1	Definitions on soil, earth, and earth building materials (adapted from Ref [7]) .	20
4.2	Common soil stabilisation methods (adapted from Ref [7], [52])	29
4.3	Earth construction systems and applications (adapted from Ref [19])	30
4.4	Compressive strength of masonry materials vs. hypercompaction (adapted from Ref [2])	38
4.5	Overview of the diversity of testing procedures adopted to measure rammed earth properties	39
4.6	Overview of cement content and compressive strength measured in cement stabilised rammed earth	41
4.7	Measured unconfined compressive strength and Young's modulus from different studies (adapted from Ref [41])	42
4.8	Measured tensile strength of earth bricks and earth mortar (adapted from Ref [82])	43
4.9	Measured shear strength from different studies (adapted from Ref [41])	44
4.10	Thermal conductivity and thermal resistance of earth compared to other materials	45
5.1	Advantages of SC3DP over 3DCP (partially adapted from (Ref [25], [117], [131]))	53
5.2	Key terminology used in 3D concrete printing	56
6.1	Mechanical properties of unstabilised (Perrot and Gomaa) and cement stabilised printed earth (Curto)	63
7.1	Printing parameters (left) and results for a free standing 3DCP wall (right) (adapted from Ref [161])	92
7.2	Overview of results from the both barrel vault and half dome roman and nubian layering techniques	107
A.1	Natural additives and fibers of animal origin for earthen material stabilisation classified by their additive source (adapted from Ref [177])	122
A.2	Natural additives and fibers of plant origin for earthen material stabilisation classified by their additive source (adapted from Ref [177])	123
B.1	Overview of numerical ranges of recommended soil gradation and plasticity for rammed earth and earth blocks from different counties (adapted from Ref [7]) .	124
B.2	Overview of earth building guidelines from different countries (adapted from Ref [7])	125
B.3	Permissible levels of salt content in earth building standards (adapted from Ref [7])	126

B.4	Recommended design values of UCS and specimen details (adapted from Ref [7])	126
C.1	Measured data for stress and stiffness development, original data received from Perrot	127
C.2	Data for stress and stiffness development assumed for URE	128
C.3	Data for stress and stiffness development proposed for unstabilised shotearth .	129
D.1	Original data from Dressler with 0 % accelerator	133
D.2	Assumed stiffness calculation for Dressler based on Suiker's data	133
D.3	Measured data for stress and stiffness development, original data received from Perrot	134
D.4	Curvefitting fcm upper	135
D.5	Curvefitting fcm lower	136
D.6	Curvefitting E upper	137
D.7	Curvefitting E lower	138
E.1	Stress and buckling checks for wall model at different print speeds	146
E.2	Results from the barrel vault roman layering where the highlighted cell is the governing failure mode	147
E.3	Results from the half dome roman layering where the highlighted cell is the governing failure mode	148
E.4	Results from the barrel vault nubian layering where the highlighted cell is the governing failure mode	149
E.5	Results from the half dome nubian layering where the highlighted cell is the governing failure mode	150

Earth construction for future sustainability of our built environment

1.1. Climate crisis, housing shortage and public health

In the last decades, the changing climate, deteriorating wildlife and growing populations have put forth the need to rethink the way we consume materials. In many industries, research and innovation is focused on creating a more sustainable and healthier life for everyone. The construction industry is one of the largest, most resource and energy demanding in the world. In Europe, the construction sector accounts for 10-11% of gross domestic product (GDP) and 28% employment, representing 25% of all European industrial production. The industry accounts for 30% of global carbon emissions and 5% from the production of cement alone. The use of cement is expected to grow from 2.5 billion tons in 2006 to 4.4 billion tons in 2050. In Europe, cement produces about 33% of all waste. Construction and demolition waste account for 13-30% of all landfills worldwide, with demolition waste being twice that of construction waste. The needs for buildings and other infrastructure will further increase the consumption on non-renewable materials, and waste production [1], [2].

On a world scale, the construction industry will keep growing at a fast pace. The world bank estimates that 21 million homes are required per year by 2030, as populations are projected to increase, most notably in Africa. China will need 40 billion square meters of combined residential and commercial floor space over the next 20 years, equivalent to adding on a New York every 2 years [3]. Furthermore, the lack of more affordable housing and rising inequality is threatening economic, social, and political systems. UN Habitat [4] has reported that approximately 860 million families in the world are living in slums and "the net growth of slums continue to outpace the improvements."

Humans spend about 90% of their time indoors, either at work or at home. Indoor air quality plays a significant role in the general state of health and well-being of occupants. Nowadays, residential buildings contain a high amount of chemicals and heavy metals that contaminate indoor air, causing many health-related issues from birth defects to cancer, irritation on skin, throat or eyes to nausea and headaches. Much energy is also spent on mechanically regulating indoor temperature and humidity leading to high building energy consumption during service life [1].

1.2. Earth building and construction

The climate crisis, pressing housing shortage and demand for better indoor environments have triggered a growing interest in alternative and more sustainable building materials and construction methods. Raw earth is one of the most attractive options available as it is one of the oldest and the most widely used building material in the world (not including stone, cement or metals derived from ore). Building with earth is a traditional practice that has taken place all over the world for thousands of years. Several different construction techniques exist, of which earth masonry, rammed earth, cob and adobe are the most popular ways of building. The most suitable technique depends on the location and type of application. It is estimated that around 20-30% of the human population live in an earth-based dwelling today, the majority in less developed countries. In the two most populous states, India and China, it is estimated that around 80 million and 100 million people respectively live in an earthen dwelling. In France, 15% of rural buildings are made of rammed earth and the US is the leading consumer of adobe (mud bricks) in the developed world [5].

The material is considered recyclable, inexhaustible (Fig. 1.1), harmless to humans, and when properly used exhibits high strength, excellent hygrothermal properties, long service life and low embodied energy at little cost. Earth building materials have the potential of cutting the use of natural resources during construction, operation, and end-of-life by reducing unrecyclable demolition waste [2]. When designed properly, earth walls can function as a passive thermal regulator, decreasing or eliminating the need for mechanical ventilators. This gives an additional potential for further decreasing energy consumption in buildings. Furthermore, earth buildings have a positive impact on the outdoors, contributing to the resilience of cities against heat stress [6]. Table 1.1 lists the main advantages of building with earth.

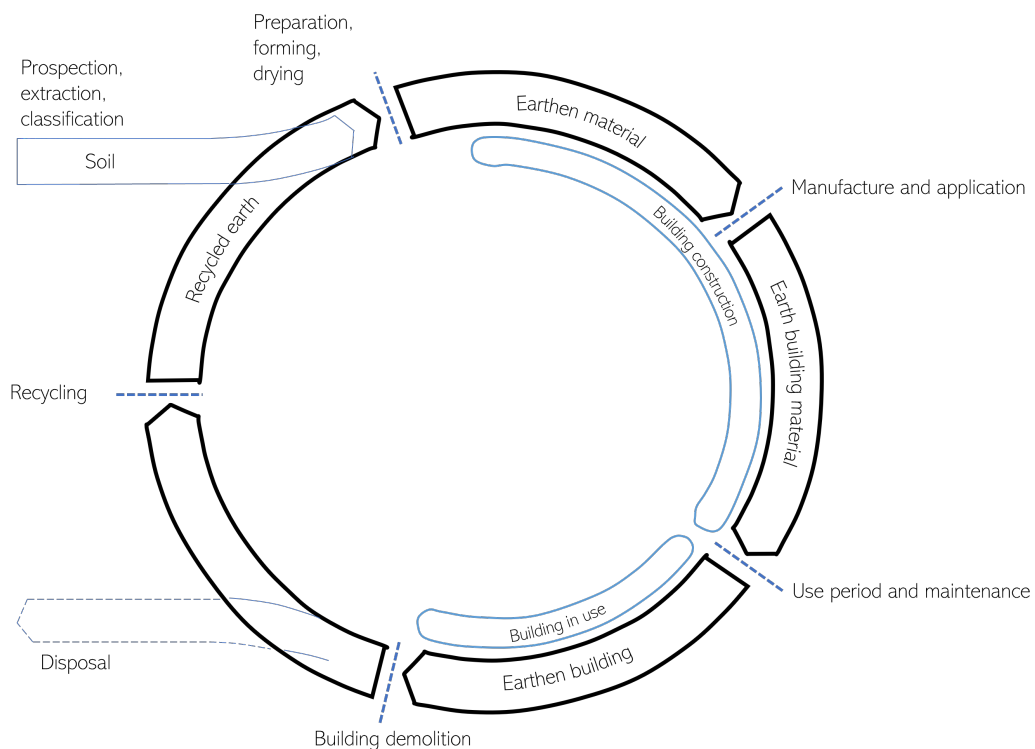


Figure 1.1: Life cycle of raw earth materials (adapted from Ref [7])

Advantages of building with earth as a sustainable material for modern construction	
Reduction of embodied energy	Processing earth materials require 1 % of the energy required to manufacture the same volume of cement.
Reduction of operational energy (hygrothermal regulator)	The porous nature of earth materials result in good hygroscopic properties, the ability to absorb and release humidity. This results in stable indoor temperatures all year round.
Acoustic insulation	Earth walls assumed to have great reverberation properties and therefore good acoustic performance.
Recycling or disposal of demolition waste	Demolition of raw earth structures produces clean waste, natural soils, which can be reused again and again.
Economic impact	Building with earth has the potential of significantly reducing construction costs given its local availability. This is especially advantageous in lower income countries where costs can be reduced 30-60 % compared to concrete based construction. This especially applies to small scale structures.

Table 1.1: Main advantages of building with earth (adapted from Ref [2])

Problems with cement	Earth as a solution
1. Production is capital intensive	1. Building elements (bricks, blocks, rammed earth) require very low capital investment
2. Energy intensive product to make and use	2. Energy embedded in the earth-made building elements is very low
3. The necessary raw materials are not always available	3. Necessary raw materials are almost always available (on-site or close by)
4. Production is at present almost always a large-scale technology	4. Production of earth made building elements is a small-scale technology

Table 1.2: The main problems with cement and earth as a solution (adapted from Ref [3])

In countries, where the cost of cement is high, earth construction is a great opportunity to create low-cost housing, jobs and strengthen local communities. Table 1.2 lists four main reasons why cement is unable to satisfy the worlds housing needs and how earth may be better suited in its place.

1.3. Why we are not building with earth?

Though it has many advantages, building with earth is rare and finding an earth building is not easy, especially in the developed world, and increasingly so in the less developed world. Despite the abundance and low cost, it is also the most ignored solution by governments, developments banks and aid agencies. The reasons for this are mainly due to prejudice, industrialisation and politics but also due to limited knowledge and research in this field. A list of current technical limitations can be found in Table 1.3.

Current limitations in earth building and construction	
Uncertainties of local soil & reliance on chemical stabilisers	The exact influence of soil grading on the material strength is unclear but proper grading indicate better mechanical performance. Some guidelines give recommendation on the amount of clay, silt, sand and gravel. If the recommended proportions are not available they must be sourced elsewhere or the material must be stabilised by binders to compensate for the original substandard properties. Chemical stabilisation is common practice but increases the environmental footprint, cost, and compromises the hygrothermal properties of the material.
Structural integrity & durability	Mechanical performance is much lower compared to conventional materials. Earth building elements are also sensitive to moisture ingress and erosion which can cause structural damage if not properly maintained. Stabilisation helps improve strength and durability.
Tensile strength & reinforcement	Earth materials can be assumed to have zero tensile strength, thus elements in bending and tension cannot be made of earth. Traditional reinforcing material are fibres. Solutions are still being investigated to increase tensile strength.
Uncertainty about energy performance	Few studies have quantified the energy efficiency of the material and its hygrothermal properties. Investigations are still being undertaken.
Quality control and absence of acknowledged standards	There are no standardised tests or recognised procedures that controls the quality from raw material to assessing the thermo-hygro-mechanical properties to maintenance of structures. This makes it hard to compare studies. The lack is due to variability of soils and different construction techniques which vary depending on soil types and tools.
Empiricism of design methods & absence of international standards	Several countries have their own national standards for earth buildings which are based on empiricism rather than engineering science. These standards vary in function of climate, location, skills and experience. On the other hand, recognised codes and regulations do not consider earth materials to live up to "standard".
Lack of skilled craftsmanship	There is a general lack of skilled labour in construction. Earth buildings require specialised skills due to the regional differences of the material, knowledge and experience.
Long construction time	Earth construction is a manual job and not many processing machines have been developed due to its limited consideration in construction. Earth has a lot of potential to be combined with industrial production methods but is still being developed.
Current trends in architecture & maintenance	Exposed texture of structural materials is the current trend in architecture. This undermines the traditional protective measures of earthen walls which utilises big roof overhangs. Exposed earthen walls can be seen as a result of misguided design and ignorance of the limitations and values of earth construction.

Table 1.3: Main limitations of building with earth (adapted from Ref [2], [8])

Prejudice

Earth building materials are currently classified as "alternative" or "primitive". It is often regarded as an inferior material compared to industrially produced materials (concrete, steel, glass) due to the perception that industrial materials are better. The prejudice against earth materials risks a region losing their earth building traditions and further depleting natural resources to produce industrialised materials. Moreover the structural integrity of earth buildings is often questioned due to the lack of knowledge in the building technology. This has been furthered by the 2003 earthquake, which destroyed large parts of the historic city of Bam, Iran, a UNESCO World Heritage site made entirely of earth. The city was home to the largest mud brick structures in the world and the collapses caused widespread fear of earth buildings, garnering a reputation for being dangerous [5].

Industrialisation

Earth building is a largely specialised traditional practice, often studied through conservation and therefore unchanged for thousands of years. Earth has not been subject to large-scale industrialisation and standardisation, making it difficult to choose earth as building material. The reason for this is also its local variability due to different geological and soil formations making it hard to predict the behaviour of the material. Today, more practices and machines are used to "advance" the state of the material but building with earth remains unique and expensive due to the need for specialists and manual labour [5].

Politics

The availability and abundance of earth building materials make the unit price of building with it very low. Past experiences have shown that existing material production facilities for processed materials feel threatened to go out of business as a "free" material does not work in a capitalist society. Furthermore, earth buildings often do not comply to building codes and regulations as these often do not fully take advantage of its mechanical properties. In places where earth is accepted and part of building codes such as the US and Australia, overbuilding of foundations and dimensioning as a result of lack of knowledge of the material results in higher building costs. Here, specially skilled labour and equipment keeps earth construction out of reach for most common people except, perhaps, the wealthy [5].

1.4. Earth architecture from antiquity to the 21st century

"Earthen architecture is one of the most original and powerful expressions of our ability to create a built environment with readily available resources." Our history of building with earth dates back thousands of years and examples can be found everywhere in the world in all climates and cultures. The diversity show a wide spectrum of philosophies, social strata and different traditions represented by this universal material. Today, earth buildings are found in use by every economic and social class. Building typologies include a variety of structures for living, working, worshiping and other forms of architecture not inhabited by humans e.g. agricultural buildings, city walls, monuments, cultural landscapes and archaeological sites.

In the last decades, building with earth has experienced a renaissance and the number of projects has increased substantially in developed countries due to the sustainable construction agenda, where earth buildings can play a big role. The availability and economic quality of the material mean it bears great potential to contribute to poverty alleviation and sustainable development [5]. Examples of modern earth construction incl. the hospital of Feldkirch, Austria, which has a 180m gallery with long sections of rammed earth walls (some places up to 6m), Fig. 1.2. The main aim of using rammed earth was achieving stabilisation of the relative humidity without using conventional mechanical devices for a better indoor climate. The Ricola Kräuterzentrum in Switzerland, completed in 2014, designed by Herzog & de Meuron, was built using prefabricated earth elements, which were manufactured using locally sourced soils. The herb storage facility, with a solid rammed earth facade over 100 meters long and around 11 meters high, is a prime example of a way of expressing the natural attributes of a site through a sustainable construction method that utilises local materials with modern technology, Fig. 1.3.



Figure 1.2: Hospital of Feldkirch, Austria [9]



Figure 1.3: Ricola Kräutercentrum, Switzerland [10]



Figure 1.4: Arch of Ctesiphon, Iraq [11]



Figure 1.5: Rwanda Cricket Stadium in Kigali [12]



Figure 1.6: Sharanam conference hall, India [13]



Figure 1.7: Rammed earth arch in Lyon, France [14]



Figure 1.8: Prefabricated rammed earth pavilion
ETH, Zürich [15]



Figure 1.9: Tecla house by Mario Cucinelli and
WASP [16]

1.4.1. Earthen arches, vaults and domes

The most important mechanical property in earth construction is compressive strength. Compression-only structures are interesting in this regard as they can utilise the material in the most efficient ways to reach an optimal shape. Despite limitations in the material, sustainable and dramatic structures and spaces can be produced. The first arch, vault and dome structures were constructed using earth masonry. The most impressive example from antiquity is the earth masonry arch of Ctesiphon, located in modern-day Iraq. The arch was originally part of a barrel vault that enclosed the Iwan-i-Khosran (throne room) built around 540 AD. The vault was constructed using the methods of corbelling and nubian vaulting to avoid any support structure during construction. The surviving arch is approximately 35 m high at its crown, 25 m wide and 50 m long with a sectional thickness of 7 m at the base, progressively tapering to 1 m at the crown, Fig. 1.4.

Modern examples of earth masonry arches, vaults and domes incl. the Mapungwe Interpretation center, South Africa, the Rwanda Cricket Stadium, Fig. 1.5 and the Sharanam conference hall, India, Fig. 1.6. Other ways of building earthen arches, vaults and domes is with rammed earth. An example can be found in Lyon, France, Fig. 1.7, where a 1000 m² office building, comprising of 14 earthen arches, was built using local materials. The building, designed by Clément Vergély, is a low carbon footprint building, in a forest of concrete buildings, built in accordance with local traditions. Another example is the rammed earth vault, a research project at ETH Zürich, Fig. 1.8. The pavilion demonstrates the utilisation of earth material in a load-bearing vault structure using prefabricated elements. The Tecla house by Mario Cucinella and WASP is the latest example of constructing a dome structure using earthen material and robotic fabrication. The pioneering research and technology behind this project shows the possibilities of a new architectural aesthetic using this ancient material with the technology available today to create low-carbon housing, healthy living, with the most consideration to the local environment.

1.5. Research in earth building materials and fabrication

Since the 90's there has been an exponential increase in earth building research and technology, Fig. 1.10. The field of science for "Earth Building Technology" is currently at its infancy as systematic earth building research has not been conducted for decades due to the fact that earth has not been widely used. To learn and better understand these earth building processes and techniques, scientific methods are being developed to rediscover the movement in building with earth. Fig. 1.11 shows the different areas of sciences that are involved in earth building construction. As of now, individual countries have started to systematically examine the material on a larger scale and incorporate these results into their own national standards. The most notable standards that exist today are found in New Zealand, Australia, USA, Germany, France.

Most advancement in earth building has been in construction methods. The past few decades have seen a rise in digital products and services. Additive manufacturing and 3D printing is now one of the most researched construction methods, as the technology is set to revolutionise the construction sector. New digital tools and processes promises better, faster and even more optimal solutions. Significant sustainability benefits can be realised through the integration of digital fabrication techniques with earth-based materials [17].

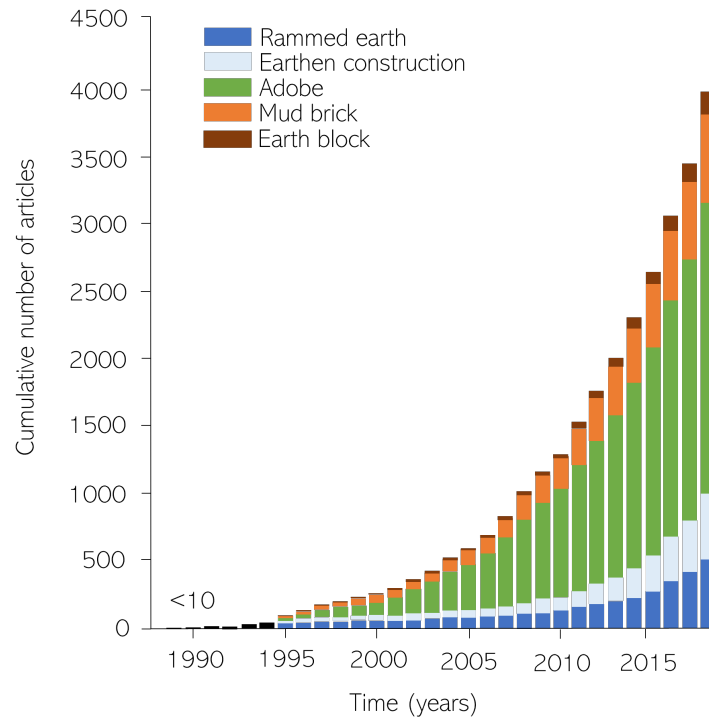


Figure 1.10: Cumulative number of research and review articles discussing earthen construction techniques recorded per year as indicated by Science Direct keyword searches (adapted from Ref [18])

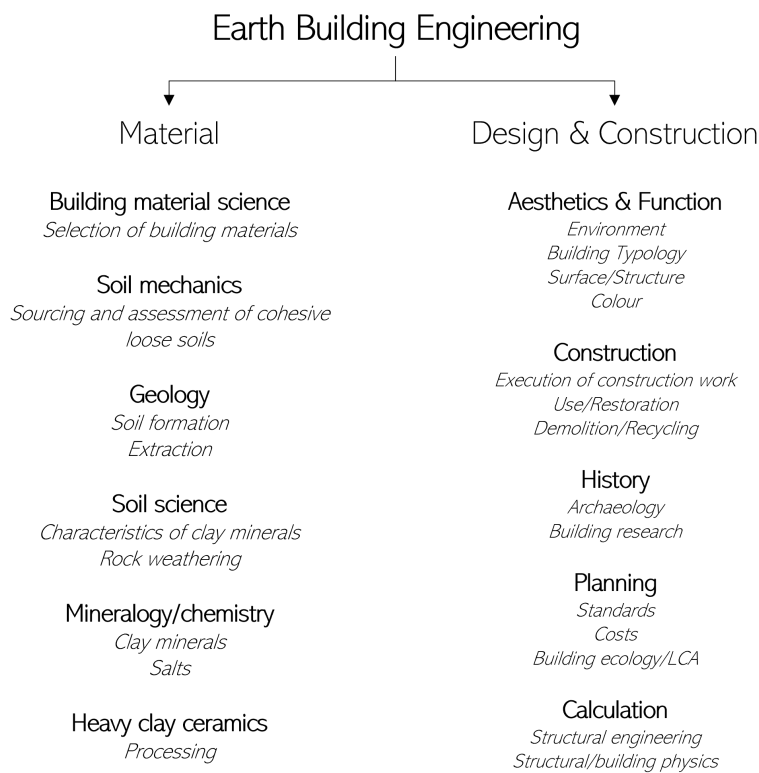


Figure 1.11: Sciences involved in Earth Building Engineering (adapted from Ref [19])

Earth is currently being researched everywhere around the world. Contemporary trends [20] in research focus on:

Granular materials research Improved mechanical resistance and understanding of microstructure. Better quality control. Understanding rheology (flow of matter) which has developed earth concrete. Research into natural dispersants, biopolymers and natural binders which may make it possible to make green concrete or eco concrete. Research into waste products and recycled aggregates for use in earth construction.

Fibre reinforcements Natural and synthetic fibres have been researched to improve tensile properties. Natural fibres such as hemp hurds, shives has led to high performance. Other research focus on elements that will increase absorption of water vapour that help regulate environmental humidity.

Conservation Little written material exists on existing earth structures as much expertise on the construction and the materials was transmitted orally. Much effort is also focused on analysing existing earth buildings built using various techniques to better inform design standards [21].

Prefabricated elements Greatly advanced mainly thanks to Austrian entrepreneur Martin Rauch, who has integrated it into building practice. This development has opened new horizons for contemporary earth architecture. Prefabricated earth elements have been already been demonstrated in different projects as mentioned earlier.

Digital fabrication and additive manufacturing 3D printing and use of robots that apply layers of earth mortar to quickly and precisely build walls has already been experimented with and demonstrated. In 3D concrete printing, research is focused on building analysis tools to assess the structural build-up of straight elements as well as overhangs. The advancement of digital tools has also led to research in functionally graded materials that can further optimise buildings for specific functions and applications. These can be easier realised with digital construction methods.

As the demand for alternative or sustainable solutions and standardised products/ components/ elements increases, the field of earth building technology will become more specialised and developed to be considered in line with other conventional materials. On the other hand, earth building may also remain a non-engineering technology as earth material has traditionally been selected based on visual inspection, smell, feel and taste. The types of buildings constructed were shaped by local cultures, where knowledge was passed down orally through generations [5]. Earth as a building material is, unlike concrete and steel, not synthetically produced, but a natural and non-standardised material. The complexity of the material and the unpredictable influence a local climate can have on its properties make it hard to fully standardise, quantify and predict all aspects of a building construction [19].

1.6. Future trends

In the near future, pressure on sustainability in buildings will increase further. Construction systems with lower environmental impact over their life cycle and materials with low primary energy consumption will become increasingly significant. Embodied energy of construction

will be taken into account rigorously in regulations as countries increasingly set goals for reducing CO₂ emissions. In this context, earth construction systems and building materials are especially favourable. This increasing awareness is also reflected by the increasing number of earth building standards and research. The directions of development, with regards to sustainability of earthen construction, will likely follow the following [7]

1. Development of architectural design able to build with natural construction soil (dug on-site) with no admixtures. This will allow the use and reuse of earthen materials without causing pollution.
2. Use of coatings to protect walls and other elements. Most coatings can provide acoustic and thermal qualities, protection against moisture, while minimising the amount of high embodied energy material used. Use of coatings will be increased by establishing design guides to implement mortars with local or other suitable materials.
3. Use of low embodied energy stabilisers in elements or in coatings e.g. of vegetable origins (fibres or biopolymers). These are interesting because they may increase the durability or mechanical properties of earthen materials.
4. Faster and more customised construction of elements. The implementation of digital fabrication technologies will offer many more potentials for sustainability, increased productivity and faster construction, which will result in cost savings. More design freedom and customisation will result in new architectural styles. Additive manufacturing methods have already played a part in the renewed interest of earth buildings and will play a bigger role in the design and construction for future earth buildings [17].

2

Research scope

Given the advancements made thus far in automation and digital fabrication, plus the increasing awareness and benefits of using earth building materials, a growing number of studies is investigating the properties and feasibility of additive manufacturing earth and clay structures. In the world of 3D printed concrete, much research has been performed on understanding the fresh and hardened properties of the material in an extrusion process. The advancement of material property understanding has led to the development of numerical methods to model the fabrication process and layer-on-layer behaviour of 3D printed structures. Furthermore, the material knowledge and numerical methods have been utilised in the design of overhangs and 3D printing of funicular shapes, drawing inspiration from ancient structures, and returning to the principles of unreinforced masonry to analyse them.

The purpose of this thesis is to look into the possibility of designing and fabricating a wall and an earthen arch /vault or some form of overhang structure combined with a new robotic shotearth technology. The main focus will be on the material influence in the fabrication of such a structure and the aim is to showcase some possible geometries and their structural performances that this material can bring. In order to achieve this, considerations will be given to early-age earth material requirements and influences from processing aspects, such as printing time and layering techniques, as these will impact the fabrication feasibility and resulting structural performance. As there is currently no academic research combining the use of earth materials, spraying it through a robot to fabricate a funicular load bearing structure, and a limited opportunity for testing due to the novelty of the method, much of the work in this thesis will borrow concepts from related disciplines and extended to the case of shotearth. As a result, the work presented will be based on assumptions from existing literature and evaluated using existing tools and theories.

Main question

What is the fabrication feasibility of robotically fabricated shotearth structures?

Sub questions

1. What are the properties of earth building materials and 3D printed cementitious materials and how can this be used to predict shotearth material behaviour?
2. What are the design techniques of existing earthen wall and arch structures and how can these be applied to the design of shotearth wall and arch structures?
3. What are the possible fabrication times and dimensions of shotearth structures?
4. What are the design considerations required for real construction?

Methodology

The methodology follows the general scientific approach in engineering. This is to first identify the gaps in the knowledge through a literature review on earth building materials, additive manufacturing in extruded concrete, shotcrete and lastly additive manufacturing using earth and clay materials. From this the main material properties required and the tool defined by Witteveen +Bos for the modelling of printed structures were identified. The second step looks into methods on how to predict material strength development. This followed mainly two methods, one using the general principles gathered for earth building materials and soil mechanics, the other using principles from concrete technology, where especially normal concrete standards such as Eurocode, American Concrete Institute (ACI), CEB-FIP as well as various time-dependent mathematical equations related to shotcrete for tunnel construction were identified. These models were plotted against existing research data from literature for comparison and to assess their adequacy. The third step uses the defined material model results in the simulation tool to determine the fabrication feasibility of different structural geometries. A wall structure with varying printing speed was first assessed, then two types of arch structures with different layering techniques were assessed.

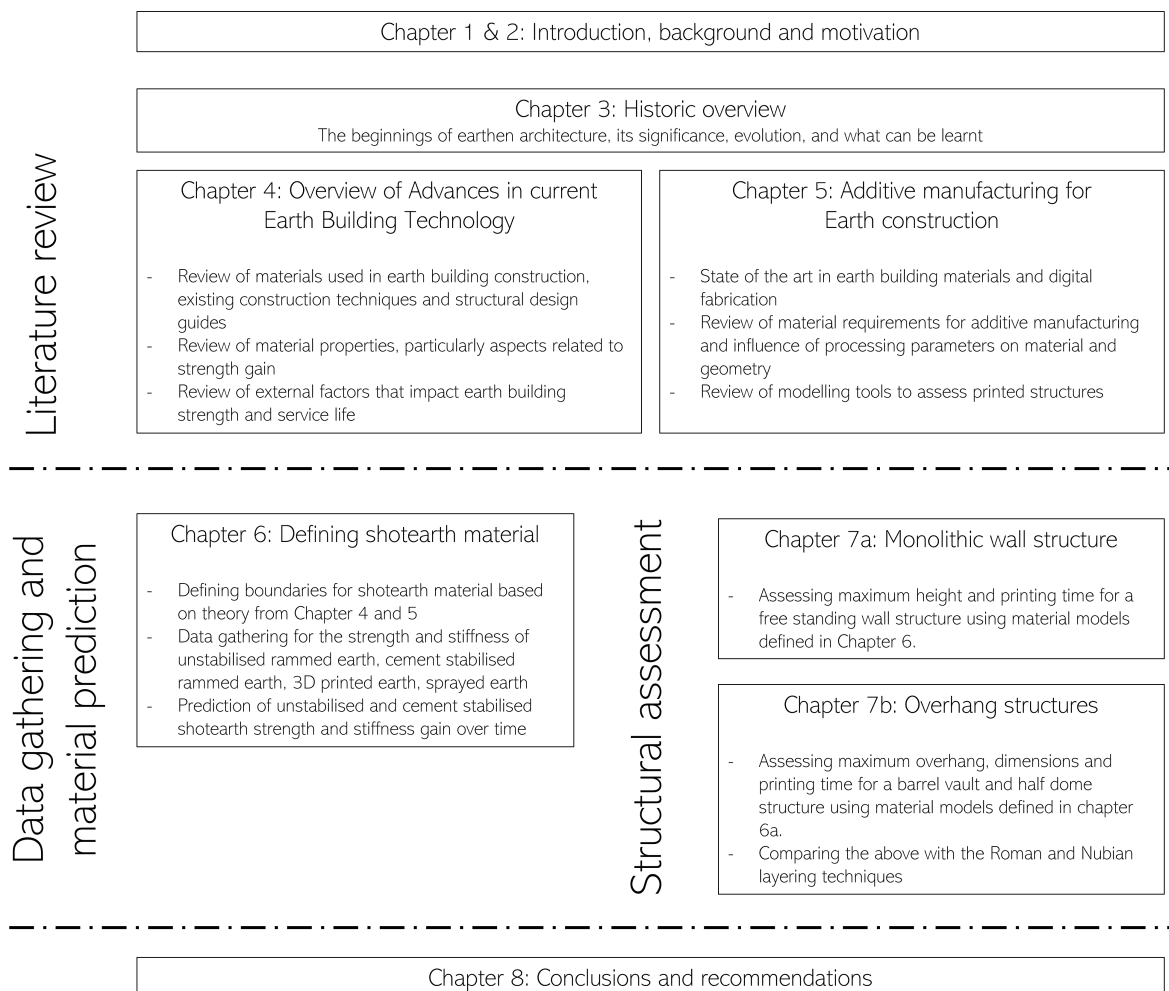


Figure 2.1: Methodology of work

To answer the subquestions, the work has been divided into five objectives, each with their own set of goals.

1. State of the art of earth building material research.
 - (a) Understand soil, earth materials and compositions.
 - (b) Understand the construction techniques and technological advances in fabrication.
 - (c) Understand the mechanical and other properties that have influence on structural design.
2. Overview of 3D printing of cementitious materials, 3D printing of earth materials and shotcrete 3D printing.
 - (a) Understand the material requirements and processing influences that affect strength and stability of 3D printed/sprayed structures.
 - (b) Assessing how to extend these parameters to shotearth fabricated structures.
3. Obtain material models for shotearth based on objectives (1) and (2)
 - (a) How to assume/obtain relations of early strength and stiffness gain of earth materials (concrete models, shotcrete models, unsaturated soil mechanics models, data from existing research).
 - (b) Set requirements for upper and lower bound limits of shotearth based on understanding of earth materials and 3D printing.
4. Design a shotearth wall structure and arched/vaulted structures and assess the stability during printing using the material models obtained in objective (3).
 - (a) Existing design principles for earth and printed structures
 - (b) Evaluate the height and fabrication time of the wall structure obtained with the material models.
 - (c) Evaluate the height and fabrication time of an arch structure obtained with the material models.
5. Discussion and conclusions of work, potentials for the future and recommendations for further work.
 - (a) Final outcomes and results of work
 - (b) Limitations of methodology

3

Historic overview

This chapter aims to understand the history and development of earthen architecture and its importance today. It also aims to look into lessons learnt and challenges from predecessors and what to keep in mind for the context of modern earth construction. This chapter is an additional chapter which does not serve the main story line of this thesis and can thus be skipped but will provide an extra insight to earthen architecture for those interested.

Beginnings

Traditionally, buildings were built using locally available materials only. There is no consensus about when humans began constructing with earth. However, it is believed that earthen architecture developed independently around the globe when humans transitioned from nomadic lifestyles to sedentary settlements around 11 000 BCE. In Mesopotamia, on the plains of Tigris and Euphrates (modern day Iraq and Syria). In Egypt, along the Nile, from Nubia to the Delta. In Pakistan, by the banks of the Indus and the Hakra. In China, on the plateaus overlooking the Yellow River. In Peru, on the desert coastline of the Pacific Ocean fed by watercourses flowing down from the Andes. In Central and North America along the banks of Mississippi. Throughout Africa both north and south of Sahara [20]. Depending on the prevailing climate, vegetation and geological conditions of a region, different building styles and construction methods were developed [22]. In hot and dry climates without major sources of wood, ancient civilisations in the Middle East, Central Asia, Central and South America and Africa built massive constructions using load-bearing earthen walls, often also incorporating building physics considerations, Fig. 3.2. In temperate, transitional climates or mountainous regions with abundant sources of wood, framed construction with wood as a load bearing skeleton and earth combined with stone infill is more commonly found [19]. Over time and with exchanging knowledge, these structures were developed to take greater loads. Countless archaeological sites around the world, Fig. 3.1, many of which have been declared UNESCO World Heritage sites, are testament to the use of earth in walls, floors, furnishings and roofs. The quality of construction on these sites, display a remarkable degree of expertise in the choice of earth materials, technique and workmanship [20].

One of the oldest permanent earthen settlements known is found in present-day's Turkey and Palestine. The 8000 year old structures of Catal Höyük, Anatolia, consists of load-bearing exterior walls of earth blocks with interior wooden supports carrying the roof (Fig. 3.3). The roofs were flat, made of poles and grasses or reed and a layer of earth for protection against rainwater. The houses were entered via the roof and the structures are grouped together like

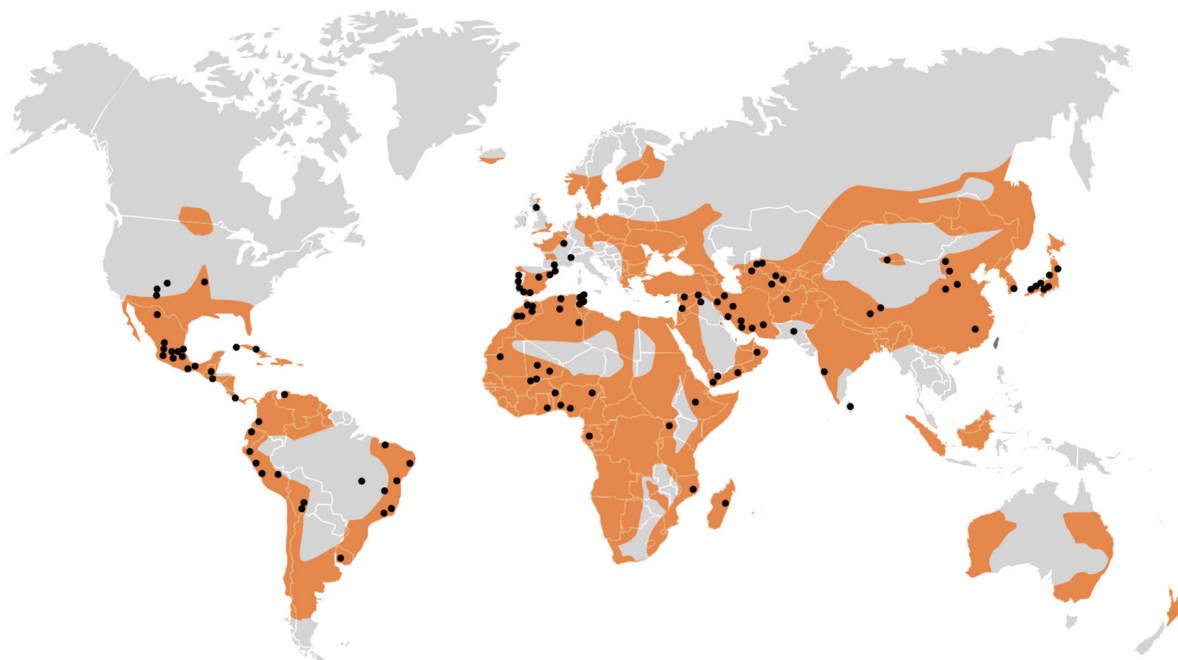


Figure 3.1: Presence of earth architecture with black dots indicating UNESCO world heritage sites [23]

honeycombs touching each other [19], [20]. Furthermore, the region is also home to the oldest known written rules for building, which dates back to the Babylonian ruler of Hammurabi (around 1800 BCE) [24].

The invention of raw earth bricks in Mesopotamia marked a major advance in the evolution of building practices. Originally, modelled by hand, then shaped in wooden moulds, raw earth bricks were used in domestic architecture from the 4th millennium BCE. They were used to construct large structures such as temples and palaces such as the White Temple of Uruk, Fig. 3.4, and Temple of Oval of Khafajah in the Tigris valley. It is hypothesized that the origins of arches, vaults and domes started in this area (Mesopotamia, Syria, Egypt, Afghanistan). Assyrian kings built palaces of staggering dimensions in Mesopotamia using raw earth bricks. An example of this is the capital of King Sargon II, Dur-Sharrukin (Khorsabad), which took 6 years to build (713-707 BCE). Standing 12 m high on a platform of earth and contained within 7 gated walls. It contains a citadel, an arsenal, a throne room, royal apartments, princely residences, a ziggurat, and a temple dedicated to Nabu (god of wisdom and writing), Fig. 3.5.

In Egypt, earthen architecture also dates back thousands of years. The annual floods of the Nile river brought fertile mud which dried in the sun and became solid. When the mud got wet, it became malleable again. This fundamental knowledge formed the basis of the production of sun-dried mud blocks which could be made stronger by adding sand or plant fibres and improved even further through firing. The use of fibers to enhance mechanical properties of materials can be traced back to the ancient Egyptian civilisation. Straw and hair were often incorporated for the fabrication of mud bricks. Later, this technique was used for load bearing walls in houses [25]. The town of Shibam, Yemen, also known as Manhattan of the desert, is dense cluster of tower like structures in the middle of the desert. The town is one of the best examples of urban planning with a vertical masterplan. The mud brick towers create shade for its inhabitants and the rectangular grid plan of the city can operate as wind tunnels, resulting in a liveable desert town, Fig 3.6.



Figure 3.2: Bagdir or windcatcher, a traditional persian architectural element to create natural ventilation [26]



Figure 3.3: The oldest known earthen settlement in Catal Höyük, Anatolia (Turkey and Palestine) (reconstruction) [27]



Figure 3.4: Present day White Temple of Uruk, one of the earliest examples of raw earth brick construction [28]



Figure 3.5: Dur-Sharrukin, capital of King Sargon II, 713-707 BCE (present day Iraq). The city was built using raw earth bricks (reconstruction) [29]



Figure 3.6: Shibam, Yemen, one of earliest examples of vertical master planning [30]



Figure 3.7: Alhambra fortress in Spain built with rammed earth in 889 CE [31]

It is believed that rammed earth was first invented in Tunisia around 814 BCE. The most notable examples with rammed earth is the Alhambra fortress in Spain built around 889 CE, Fig. 3.7. The Great Wall of China, whose construction began about 3000 years ago, has extensive sections built using rammed earth dating back to the Qin dynasty (around 2200 years ago). The 21 000 km long structure, which took 2000 years to build, used materials including wood, stone, earth and vegetal material for reinforcement, Fig. 3.8. The tulou houses in Fujian, China are large enclosed fortified buildings consisting of thick load bearing rammed earth walls between three to five stories high. Located in the mountains, the buildings, constructed between the 15th and 20th century, are an outstanding of example a particular type of communal living and defense organization, Fig. 3.9.



Figure 3.8: Section of the Great Wall of China built using rammed earth [32]



Figure 3.9: Tulou houses in Fujian, China built with rammed earth [33]



Figure 3.10: Pueblo style houses in Santa Fe, New Mexico, using adobe bricks [34]



Figure 3.11: Icelandic turf houses. Turf is a great insulation material for cold climates [35]

Going to the Americas, in Pre-Columbian Peru, people were also familiar with different earth building techniques. The earliest sacred buildings were erected in the 2nd millennium BCE, in the form of stepped pyramids. It is estimated that 130 million sun-dried adobe blocks were used to build the Huaca del Sol pyramid of Moche (200-500 CE). In Mexico, the Aztecs founded the city of Tenochtitlan on an island in Lake Texcoco in 1325 or 1369. In 1529, the Spanish conquistadors triggered its downfall but recorded the discovery of a splendid, gleaming white earthen city with a population of almost half a million spread over 1000 hectares. In North America, examples of earthen architecture are found especially in Santa Fe, New Mexico with Pueblo Indian settlements made of adobe bricks, Fig 3.10 [20].

In Europe, oldest Neolithic settlements are found in Bulgaria and Romania. Earth building in Europe have historically come about due to shortage of other building materials and often in times of crisis. A shortage of wood in central Europe in the 1500s became the driving force behind developing more earth buildings. The 'Saxon Forestry Regulations' of 1560, in Germany, stipulated that a building's ground floor be constructed out of stone or earth, to reduce the use of construction timber. A six story residential building from 1830 in Weilburg an der Lahn, still in use today, is considered Germany's tallest rammed earth building. After WWI, chief architect Adolf Loos, from the Vienna settlement office, designed low-cost rammed earth housing due to the scarcity of materials. As did Edwin Lutyens, British architect, who made designs in earth as a response to the housing shortage. During WWII, German architect Albert Speer, was interested in building with earth, but more as a means to drive the war by conserving "steel and concrete for the construction of weapons and bunkers." [5], [19]. In Norway and Iceland, turf (sod) is a traditional architectural feature. Here grass roofed or turf

houses are found which consist of flat stone foundations with a timber frame filled with one of two layers of turf acting as walls and roof. The turf consist of top soil, unlike other earth construction which consist of subsoil, and is a great insulation for harsh climates, Fig. 3.11.

Pioneers: Francois Cointeraux and Hasan Fathy

Many architects throughout time have had an interest in earth building. The Roman architect Vitruvius' idea that all buildings should reflect the three attributes: firmitas, utilitas, and venustas -durability, usefulness and beauty, is inherently reflected in earth architecture. Chapter two of his book *De Architectura* describes the use of mud bricks. Perhaps the biggest pioneer and promoter of earth architecture is French architect, Francois Cointeraux (1740-1830), who is considered the father of modern earthen architecture. At a time when most houses in the European countryside were constructed using flammable timber frame and wattle and daub, Cointeraux used rammed earth as an inexpensive fireproof construction method. He devoted his life to study and promote rammed earth hoping that it could contribute to improving life in France which had suffered several wars and believed that rammed earth could be a means to the common man to improve the quality of their own life. Cointeraux developed a typology of earth architecture that encompasses a range of housing for the poor and the wealthy in both urban and rural settings. His projects incl. four-storey town houses, country mansions, public buildings, churches and factories. During a rammed earth project in Amiens, Cointeraux was chased out of the city, due to the threat of livelihood that timber and stone merchants and various craftsmen perceived his buildings were. Despite these kinds of setbacks, Cointeraux founded the school of rural architecture in Paris in 1788. He published 50 works on his knowledge of pisé which was translated into 8 languages, which spread across Europe to the USA. He developed a number of stabilisation methods that enabled rammed earth to meet greater creative demands of other architects [5].

Other well known architects who experimented with earth in the 19th and 20th centuries include Antoni Gaudi, who drew from rammed earth traditions in Spain and constructed several projects. Luis Barragán, Mexican architect, also utilised adobe (mud bricks) in his designs. Rudolph Schindler working under Frank Lloyd Wright, was inspired by earth building practices in the American Southwest. He supervised the Ennis-Brown House, which utilised soil excavated from site mixed with cement, Fig. 3.12. This is also in line with Wright's belief that "no house should ever be on a hill or on anything. It should be of the hill. Belonging to it." Wright himself also designed a number of earth buildings using rammed earth and mud brick across the US. Le Corbusier, the most influential architect of the modern movement, began developing architectural solutions using earth for refugee immigration after WWII. His book *Les Constructions Murondins (1942)* outlines methods and techniques for making and constructing with rammed earth and compressed earth block for a wide range of residential, agricultural and civic applications [5].

Around the same time, Hasan Fathy, Egyptian architect, worked on reviving and enhancing the vernacular architecture of Egypt. He adopted the Nubian art of mud brick dome, wall and vault construction, which made it possible for an entire building to be made of earth. He utilised principles of thermodynamics inherent to earth construction to create passive cooling systems at residential and urban scales. However, Fathy experienced several setbacks in his support of earth architecture. A construction project in New Mexico ran over budget due to the local authorities demanding he use formwork in constructing his vaults despite thousands of years of tradition and establishment of formless techniques. Although mud brick had been used in New Mexico, his designs had to comply with strict building codes in the US, which required elaborate foundations and cement plaster skin. Despite these setbacks, Fathy inspired many



Figure 3.12: Ennis Brown House by Frank Lloyd Wright 1924 [36]



Figure 3.13: New Baris village in Egypt by Hasan Fathy [37]

people through his works. He is perhaps, "the earliest, clearest example of a sustainability-oriented architect that we can find. Every sustainable principle, Fathy wrote about, thought about, built and gave us living examples of." [5]. Fig. 3.13 shows one of his most iconic projects in New Baris, Egypt.

Predecessor for modern construction materials

It has been suggested that the use modern materials: glass, steel, concrete was directly influenced by earthen construction techniques. The origins of modern concrete can be directly linked to advancements made in pisé (rammed earth) in France. These included developing efficient formwork, experimenting with aggregate sizes and adding cement stabiliser, which were some of the first steps toward the development of modern béton (concrete) [5]. Technical innovations in firing systems and mechanical engineering in the 19th century led to fundamental changes in the construction industry: large-scale mining of hard and soft coal for modern furnaces and kilns made the transition to gas and oil firing, which led to the industrialisation of brick production. The transition from wood to coal firing also helped develop the cement industry and with it the rise of concrete and reinforced concrete. The goal was to increase strength in building materials and decrease the dimensions of them. This is well accomplished through the combination of steel and concrete. Earth building could not adapt to this development due to their limited strength and their low water resistance. Thus earth buildings became increasingly marginalised and lost its significance [19].

What can be learnt?

The archaeological heritage of earth architecture demonstrates that earth as a building material has historically enabled societies to expand and prosper, simply by taking advantage of this local zero-carbon material. They demonstrate that already in ancient times, the criteria of using local and recycled materials, integration of built space into environment, ecological design, passive heating, and so on, were met. However, the promotion of earth construction in modern times have thus far shown to be tough to implement. Both Cointeraux and especially Fathy experienced setbacks in their promotion of earth buildings. The setbacks they faced, among which are mainly the questions of manufactured material vs. free abundant material and building regulations vs. tradition, are still relevant today. Being aware of this, lessons learnt from the supporters of earth construction along with our archaeological heritage can help us develop new forms of earth architecture and building technology that is in harmony within its surroundings and attuned to today's challenges [20].

4

Overview of Advances in current Earth Building Technology

This chapter aims to give an overview of current earth building technology, knowledge and research. It aims to understand earth materials and the influence of physical, mechanical, hygrothermal properties and durability on the behaviour of earth constructions and their construction techniques. Lastly, the chapter aims to highlight the lack of knowledge and ongoing research in determining different earth properties.

4.1. Earth building materials

4.1.1. Definitions

Earth, as a construction material, by definition is a mixture of clay, silt, sand and sometimes gravel with or without other additives. The terms ‘earth’, ‘raw earth’ or ‘unstabilised earth’ refer to natural subsoil, which does not contain organic matter, unlike topsoil, although it can sometimes be found, see Figure. 4.1. Depending on the methods of soil formation, a soil has distinct properties, different particle sizes and/or mineral structures, which lead to different uses and suitability for certain applications. Soils with high organic content or high shrinking and swelling properties are generally undesirable in earth construction applications. The term ‘stabilised earth’ is a soil with modifications, natural or chemical, usually to increase strength or durability. Table 4.1 defines general terminology when describing the material.

Terminology	Description
Soil	Granular material derived from weathered parent rock
Earth	A soil suitable for building purposes
Earth building materials	Soils sourced in natural deposits or manufactured industrially
Unstabilised earth	Natural soil suitable for building purposes without additives
Stabilised earth	Soil with modifications, to increase certain properties, usually strength and durability
Unshaped	Dry or moist mixtures ready for use in e.g. rammed earth, cob, light clay
Shaped	Mixtures manufactured through moulding with different types of compaction e.g. earth blocks, clay panels

Table 4.1: Definitions on soil, earth, and earth building materials (adapted from Ref [7])

Petrographic maps can be used on site to make general statements about a soil's suitability for its intended use and, if necessary, about possible modifications. Parameters for selecting soils suitable for earth building purposes are [7]:

- Granular composition
- Plasticity and cohesion caused by the amount of clay
- Shrinkage which can be derived by the parameters above

4.1.2. Classification of soils for earth building

Soil is classified by particle sizes ranging from gravel to clay size. It is constantly changing due to any number of chemical, biological, and physical processes, including climatic weathering. The complexity in the composition of soils and local variation of these around the world means no single classification scheme exists. Classification of earth materials in construction on a worldwide basis does not exist and is a challenge.

Classification systems

Numerous different geological rock -and soil classification schemes are available. Many of which have evolved over decades to meet specific local needs. Also depending on which field of science; soil science, geology, sedimentology, soil mechanics, geotechnical engineering or other, the classification of soils by particle size differs [7], [22]. Fig. 4.2 shows the classification of soils following a few different classification systems.

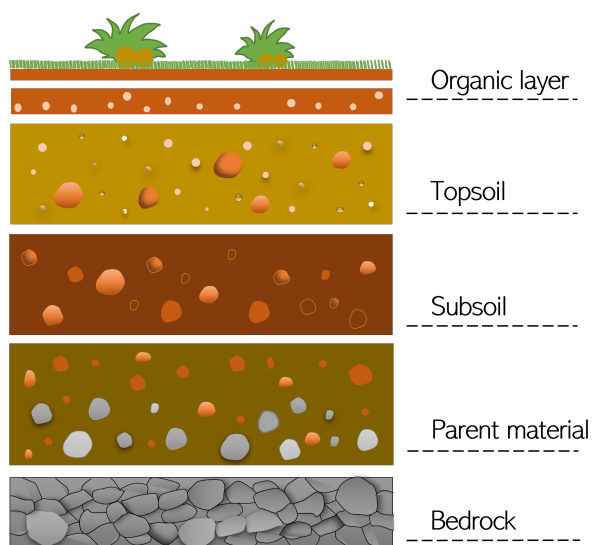


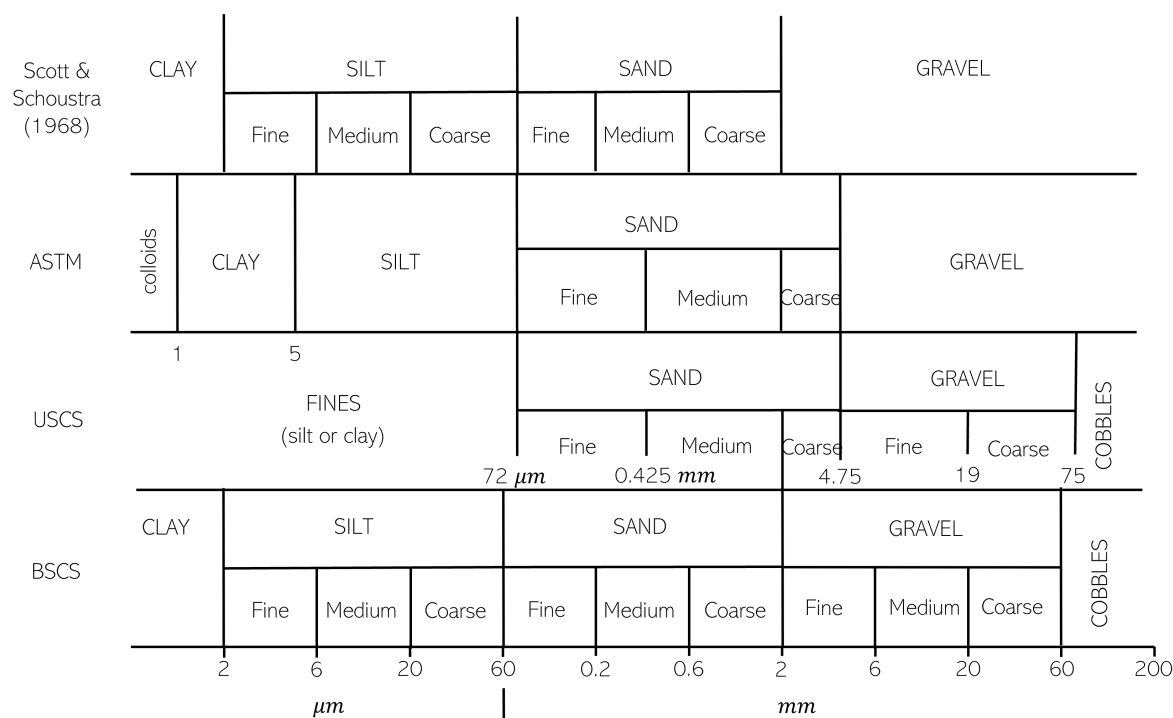
Figure 4.1: Soil layers. Subsoil is usually used for earth building purposes.

The naming of soils also differ according to science. In traditional soil mechanics, if the clay content is less than 15% by weight, the soil is termed a lean clayey soil. If it is more than 30% by weight, it is termed a rich clayey soil. Components that form less than 5% of the total by weight are not mentioned when naming the soils. In earth building engineering, the method of naming soils is less accurate, e.g., a loam with 14% clay which would be called lean clayey in soil mechanics, would be considered a rich clayey soil [7].

A proposed universal classification scheme for earth construction will need to consider the source of the stone or rock (igneous, metamorphic, sedimentary), weathering products (soils or regolith. The latter comprise of clays, muds, silts, sands, gravels or unconsolidated mixtures of several of these components), and will need to be flexible to evolve over time as new studies and interpretations are made. Use of organic materials as binders would need to be evaluated separately [22].

Particle size distribution

Particle size distribution (PSD) curves determine the relative proportions of different grain sizes in a soil. The size of soil particles is most commonly determined by sieve analysis but laser diffraction analysis is commonly used for particle sizes ranging from 0.02 to 2000 μm . For earth construction, it is generally recommended to obtain a uniform PSD curve of a soil which



ASTM –American Society for Testing and Materials
 USCS –Unified Soil Classification System (US Bureau of Reclamation, Corps of Engineers)
 BSCS –British Soil Classification System (BS 5930:1981)

Figure 4.2: Soil classification systems by different standards (adapted from Ref [38])

includes both fine and coarse particles for better mechanical behaviour. Wu et al. [39] demonstrated the significance of soil grading. Four earth materials, with a coarse sandy-gravelly fraction between 60 and 45 % and a fine clayey-silty fraction between 40 and 55%, were lightly compacted at the same water content and then subjected to unconfined compression. Strength and stiffness grew as the fine fraction increased from 40-50% but reduced as the fraction increased further from 50-55%.

Two recommended guides for the classification of granular composition and plasticity of earth building materials are that of Houben & Guillaud [40] and the German Lehmbau Regeln (2009). Fig. 4.3 shows the recommended approximate limits for the particle size distribution and plasticity by Houben & Guillaud. According to this guide, percentage of soil fractions suitable for unstabilised rammed earth (URE) walls is between 20-35% fine-grained particles (clay and silt combined) and 45-75% sand. Permitted tolerances may vary considerably.

The German Lehmbau Regeln recommends limits for plasticity and binding (suction) force between soil particles. However, there is currently no correlation between these, therefore, further research is required. For industrially produced earth building materials, no limits for granular composition and plasticity are specified. The German Technical Recommendation (DVL TM05) defines controls for soil quality for industrially produced earth building materials which include composition, plasticity and soluble salt content.

Other guides include the BS1377 standard and the US National Bureau of Standards, which also define an admissible range of particle grading for earth applications. However, some re-

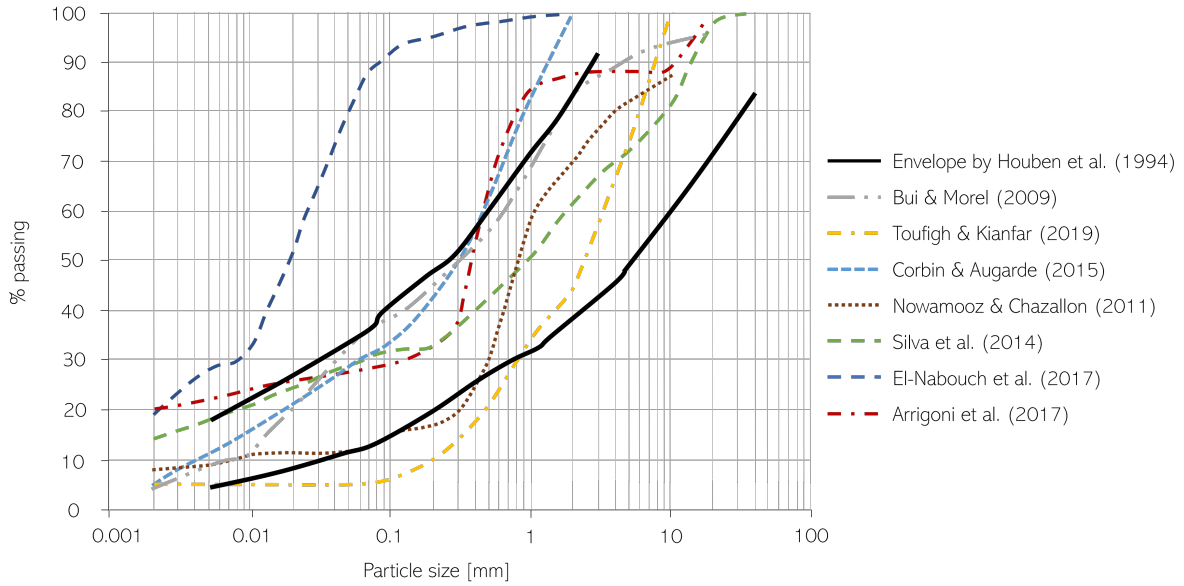


Figure 4.3: PSD envelope found by Houben & Guillaud and PSD envelopes used by other authors in research (adapted from Ref [41])

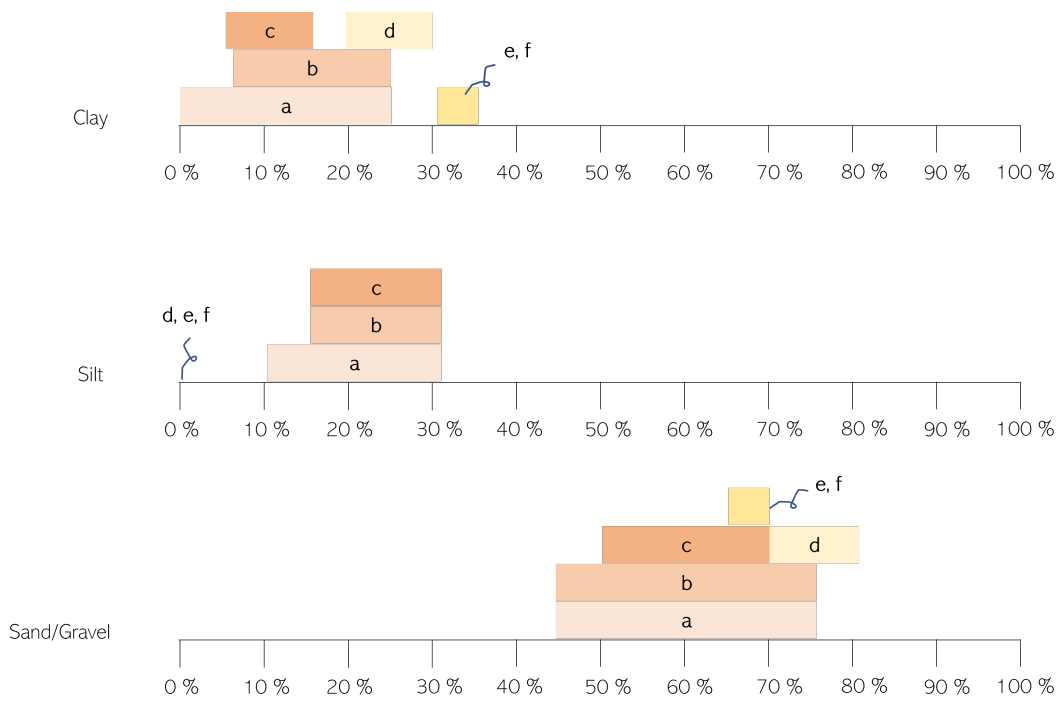


Figure 4.4: Recommended upper and lower proportions of clay, silt, sand/gravel in earth building materials according to a) Houben & Guillaud, b) Norton, c) SAZS 724, d) Schrader, e) McHenry, f) Radanovic (adapted from Ref [2])

search merely describes that the clay content should be sufficiently high to ensure acceptable levels of stiffness and strength while the expansive fraction should remain below 50 % of the total clay content to avoid cracking. Fig. 4.4 shows recommendations for the range in percentage of particle sizes for earth building according to different authors (see also Appendix

B.1). Traditional earth building took soil directly from site with little thought to its composition precision. Soils were selected based on location, visual inspection, smell, feel and taste [5]. Analysis of existing buildings also indicate that PSD curves cannot be used as the only parameter to discriminate between earth materials. Studies by these authors [42]–[44] have shown that PSD should not be a discriminating parameter when selecting the suitability of a soil for rammed earth construction. For buildings based solely on granular properties, no objective rule currently exists to assess the suitability of materials [45].

Plasticity and cohesion

Plasticity of soil is its ability to undergo deformation without cracking or fracturing. Cohesion is the shear strength that binds together soil particles. Sands and gravels are coarse-grained soils. These soils are cohesionless exhibiting zero plasticity. Silts and clays are fine-grained soils. These are cohesive soils with plasticity. This means a lump of soil can have its shape changed or remoulded without the soil changing volume or breaking up. This depends on the amount and mineralogy of the fines and the moisture content. The properties of silt, sand and gravel are totally different from clay. Clays are especially important in earth construction as they bind the other soil particles together, Fig. 4.5.

Clay: Clays have large surface areas, which lead to high intermolecular forces on the surface and edges to attract bipolar water molecules. This property lends soils the plasticity and cohesion when wet and give the material strength and stability when dry. After renewed wetting, it regains plasticity and this mechanism can be repeated an infinite number of times, giving earth as a building material, and clay, its special ecological quality.

Plasticity of clay is influenced by its particle size, particle geometry, chemical composition and water content. Clay particles consist of clay minerals and a clay can incorporate one or more clay minerals. There are 15 types of clay minerals, each with different characteristics and influence on compressive strength. Hygrothermal behaviour is also influenced by the type of clay minerals and the amount of water present. Clay minerals can broadly be categorised by:

- "Two-layer" clay, e.g. kaolinite, are characterised by relatively low specific surface (about $10 \text{ m}^2/\text{g}$), which result in limited swelling/shrinkage characteristics upon wetting/drying. They also result in a weak bonding of the coarse grain soil fraction.
- "Three-layer" clay are characterised by high specific surface (up to $1000 \text{ m}^2/\text{g}$) and are strong binders of the coarse fraction. They are able to generate higher suctions at the same moisture content compared to "two-layer" clays. These clays can be divided into:
 1. non-swelling clays: e.g., micas and illite
 2. swelling clays: e.g., smectite, montmorillonite

Activity: Not only is the amount of clay and type of clay mineral important to describe the behaviour of earthen materials but also the activity of clay. Activity is the ratio of the plasticity index of a soil to the percentage of clay fraction in that soil, and can be described as a measure of the water holding capacity of clayey soils, Skempton (1953). Four groups of activity is defined, ranging from inactive to highly active [38].

High activity means high water adsorption which leads to high volume change. Soils containing kaolinite adsorb less amount of water and therefore have a very low range of plasticity and low value of activity. Soils containing montmorillonite attract a huge amount of water even in a very small quantity. They have a high range of plasticity and high value of activity.

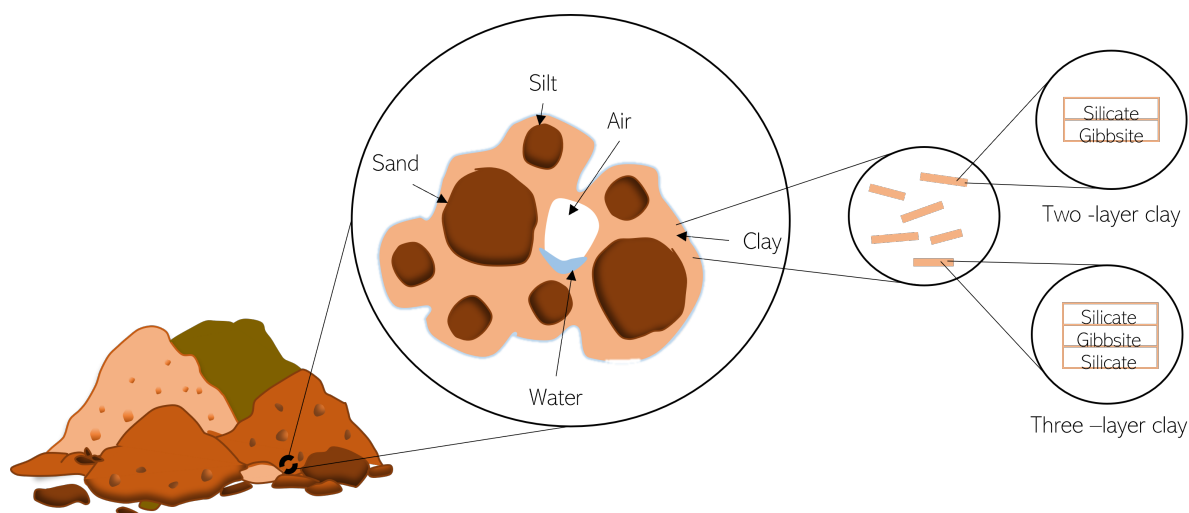


Figure 4.5: Composition of subsoil and clay minerals

It is important to assess clay properties on excavation sites for optimising applications. E.g. two-layer clays are best suited for surface coatings due to limited swelling/shrinkage properties which reduces cracks. Three-layer, non-swelling, clays are most appropriate for structural applications like load-bearing walls because of their powerful binding properties. If locally available clays are not suitable for an envisaged application, fibres can be added to enhance intergranular bonding and/or reduce swelling/shrinkage properties of a mix [2]. To better understand plasticity and cohesion, Atterberg limits are useful in identifying the type of clay mineral present using the plasticity index and liquid limit. See section 4.3.2 Water content in soils.

4.1.3. Materials for modern earth building

Earth building materials, also termed construction soils, suitable for earth building applications are extracted from natural deposits or from recycling/waste products.

Natural construction soils

A natural construction soil suitable for specific applications without much modification is often referred to as unstabilised earth or loam. It is a mixture of clay, silt, sand and sometimes larger aggregates like gravel or stone. It is not a standard building material, as the percentage amounts of its different constituents may differ according to site. Strength is achieved through adding water and compaction [7]. The German DIN standards defines different loam mixtures and their suitability for different earth applications:

- Loess and loess soil: suitable for plasters and light clay application
- Glacial marl and glacial soil (till): suitable for rammed earth
- Eluvial soil: suitable for rammed earth
- Fluvial and slope wash soils: suitable for light clay applications with organic fibres and light weight mineral aggregates and earth block.
- Tropical residual soils: clay rich and commonly used for various applications
- Desert and semidesert soils: has to be modified with other particle sizes or stabilisers

Natural additives: Loam can contain natural additives which can influence properties such as plasticity and strength. Most commonly found natural additives are:

- Lime content. The most common natural addition in loam. The presence of lime in a soil limits the activities of the clay minerals. This leads to a decrease in the water absorption capacity and plasticity of the soil.
- Water-soluble salts. These can occur naturally in soils, particularly sulphates (gypsum), chlorides, and sodium and calcium nitrates. Moisture moves these salts through the building element where they crystallize on the surface when water evaporates. Crystallisation causes a softening of the structure of element surfaces which leads to different types of damages. Few standards define permissible levels of soluble salts (see Appendix B.3). The DIN standard specify that the total percentage of damaging salts should not exceed 0.12 mass in % [19], while other regulations specify permissible contents to be in the range of 1-2 mass in %. The permissible levels differ considerably.
- Organic matter. This consists of living soil organisms, dead plant and animal material and soil-specific conversion products (humic matter, "humus"). Organic matter increases the water absorption capability and plasticity of soils considerably and reduces dry compressive strength.

Generally, lime and organic matter is undesirable in earth applications. However, it has been proven that a certain amount of lime forms a stable lime matrix between the coarser grains after drying, which can improve the strength properties of earth building structures. An example of this is the lime rich soil from the Wadi Hadramaut, Yemen. This soil can reach higher degrees of compressive strength at comparatively low dry bulk densities. More than 8 N/mm²(Shibam) have been measured in specific cubes with an edge length of 8 cm [46]. Lime rich soils have also been used for earth building purposes in southern England [47]. Organogenic and organic soils in the form of cut sod (turf) were traditionally used in Scandinavia, Great Britain, Ireland for the construction of houses. The sod was stacked like masonry units into one-storey load-bearing wall structures. These houses became increasingly stronger as the sod dried [48]. Examples are the turf houses in Iceland.

Processed construction soils

These construction soils are extracted from natural deposits then dried, ground and sold in the form of granulate or powders for further processing into earth building materials. *Dry soil* is used for producing plaster mixes or paints and primers for wood elements. *Powdered clay* is used to increase the plasticity of construction soils. Powdered clay modified with sand or fibres can be used to produce clay panels [19].

Construction soils from recycling and waste

New materials are constantly being developed and researched, making the number of alternative materials that might be used in earth construction infinite. More and more earth construction soils are being obtained by reusing materials from life-expired or redundant constructions. Some of these materials have binding properties to act as a replacement for stabilisation, other the potential to provide hygrothermal effects. The source of these materials mainly come from demolished buildings and elements. Other waste materials are compressed soil, which is a waste product formed during the gravel washing process in gravel pits and mainly contains the finest grains of clay and silt which cannot be used as aggregates by the concrete industry. Generic materials also used in concrete research such as slags, ashes and recycled aggregates can also be found in earth building material research.

4.1.4. Stabilisation

It is rare for a natural soil to be perfectly suitable for earth construction without modification. Houben & Guillaud [40] classified three approaches for stabilisation which can be classified

as physical, mechanical, or binding. The three forms refer to various techniques of controlled modification of soil texture to enhance the physical and/or mechanical properties of a soil for a specific application. Practically all earth construction materials are stabilised in some form, however, the term is commonly applied only to the application of inorganic/ chemical binders. Physical and mechanical stabilisation are already implicit in most modern earth building applications and part of the criteria for material selection for e.g rammed earth.

Physical

Physical stabilisation is the modification of the material's physical properties (texture). Through the addition/subtraction of different soil fractions and fibers, a uniform soil particle size distribution and plasticity can be achieved [8]. Described in section 4.1.2.

Mechanical

Mechanical stabilisation is the modification of soil porosity and interparticle friction by compaction. Compaction of the material results in changes in density, mechanical strength, compressibility and permeability [8], see section 4.3.3.

Chemical binder

The addition of inorganic or chemical binders and additives is general practice in earth construction. The use of stabilizing materials helps achieve particle cohesion, desired moisture content, increase strength and help in the waterproofing (durability) of soils [49]. Table 4.2 shows the most common stabilisation methods of which cement is the most widely used. Other less traditional options incl. liquid polymers, acids, silicates, lignin derivatives, resins, ions, and enzymes. It is uncommon to use admixtures such as plasticisers, set accelerators and retarders for earth. Under special circumstances they can help achieve certain desired properties. At the moment, the effects of these is unclear. The easiest soils to stabilise are coarse grained soils with little or no cohesion. Clayey and silty soils are more difficult to stabilise because they are very sensitive to even the smallest variation in levels of moisture [50]. The Australian Earth Building Handbook HB195 [51] gives a general approach to stabilisation. Non-hydraulic lime should be used to stabilise cohesive soils, cement and bituminous stabilisers should be used for non-plastic and granular soils, Fig. 4.6. Stabilisation should be performed depending on the specific need and should be avoided if possible. There are no rules or consensus on when earth should be stabilised.

Natural binder

Due to the environmental impact of cement and other chemical stabilisers, recent research has focused on the use of natural binders to improve strength and durability. These focus on the use of organic materials from plants or animals. Biopolymers, like clay, ensures cohesion. They are mainly used in plasters (indoor) and render mixtures (outdoor) using animals' excrement, natural extracts from plants, protein from animals' milk or blood. Oils and fats were traditionally used as an external surface layer for render or flooring impermeabilisation. Their hydrophobic properties improve the resistance against water and act as a waterproofing agent. Different fibres used in different earth materials show various benefits, often at a concentration at 1% of the soil. These include increased durability, compressive strength, tensile strength, shear strength, water absorption, thermal properties, reduced shrinkage and formation of cracks, reduced dead weight due to the lighter weight block [53]. Many different types of fibres, both natural and synthetic, are suitable for soil stabilisation. Environmental concerns have also led to increased interest in 'alternative' fibres, which incl. solid waste and by-product materials. By using alternative fibres, the cost of getting rid of this waste is reduced or eliminated. Compared to traditional reinforcement, fibres are both energy and economically

efficient. An overview of different additives and fibres used in current earth building research can be found in Appendix A.

Discussion on stabilisation

Due to the ongoing debate on climate change and especially impact from the construction industry, there are many advantages and disadvantages to chemical stabilisation. In certain construction techniques, such as CEB and rammed earth, "correcting" the soil composition or adding a small fraction of stabiliser is common practice. The act of stabilisation is a very old practice, especially with earth plasters and stuccoes, where tree resins, natural bitumen, arabic gum and various animal products have been used by vernacular builders from around the world. Moreover, soil stabilisation is a widespread technology in road construction. An estimated 5 % of global cement production is used here [54]. The question of whether or not to stabilise a soil is a complicated one. Numerous commercial products have some form of stabilisation that make it easier to assure for quality and strength according to building regulations. For contractors who do not generally understand earth building materials, solutions that use technologies from concrete construction can be an alternative to conventional concrete and easier to scale-up. In wet climates it is beneficial for the durability aspect of load-bearing earthen elements. Apart from the technical benefits, a general argument for stabilisation, is that with modern techniques, it helps bring back this material to our building consciousness and awareness to vernacular building practices, which has lost significance due to modernisation.

On the other hand, stabilisation usually increases the environmental footprint of the material and makes it harder to recycle demolished building components. The material, therefore, loses its ecological qualities. Moreover, earth even after stabilisation remains a mechanically modest construction material and will never compete with concrete, steel or wood. Often the amount of stabilisation added is a poor use of materials and would probably be better served in ie. normal concrete. Furthermore, ancient and some modern construction examples around the world have proven that through knowledge and understanding, it is possible to simply build with earth without modifications.

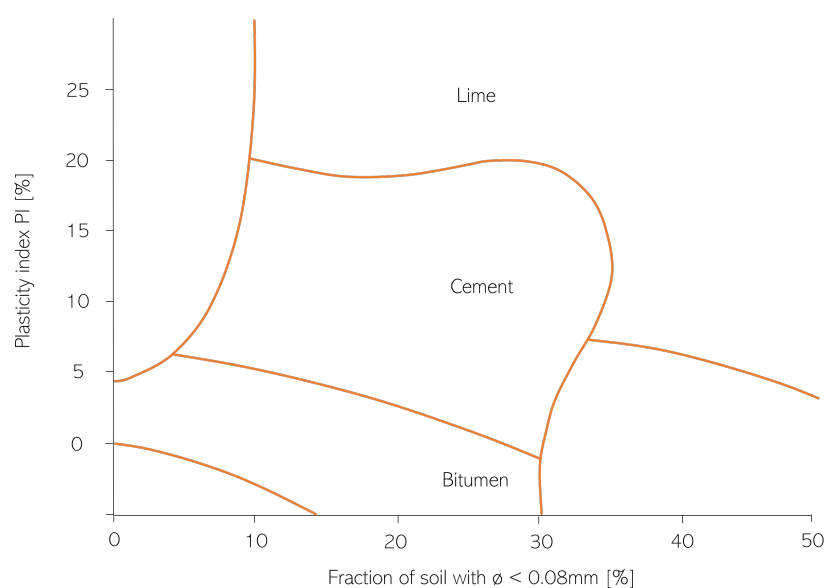


Figure 4.6: Selection criteria for common stabilizers with different soil characteristics, described in Australian Earth Building Handbook HB195 (adapted from Ref [40], [51])

Mechanism	Effects	Suitable soils
Granular (physical stabilization) Blending to poorly graded soils, usually coarse into fine (not clayey) soils	Higher compacted density, more uniform mixing, increased shear strength	Gap-graded or gravel deficient (gravel, sand addition), or harsh ^a FCR (loam addition)
Cement and pozzolans Mixing small amounts (cement modification) or larger proportions (cement binding) into soil	Improve shear strength, reduces moisture sensitivity (modification), greatly increases tensile strength and stiffness (binding)	Most soils, especially granular ones, large amounts of cement needed in clay-rich and poorly graded sands, hence expensive
Lime Mixing hydrated lime or quick lime in small to moderate amounts into soils	Increases bearing capacity, dries wet soil, improves friability, reduces shrinkage	Cohesive soils, especially wet, high – PI clays
Bitumen Agglomeration, coating and binding of granular particles	Waterproofs, imparts cohesion and stiffness	Granular, non-cohesive soils in hot climates
Fly ash Mixing with an activator to form cementitious compounds	Waterproof concrete	Some materials will activate the fly ash; lime or cement may be used to act as an activator by providing the required calcium hydroxide
Fiber Use of different fibers in soil stabilization incl. polypropylene, nylon, poly(vinyl) alcohol (PVA) and natural fibres	Increases the stiffness of soil and also the immediate settlement of soil reduced considerably, the strength and angle of internal friction increase	Tropical soil, clay soil
Other: synthetic binders, polymers, adhesives	Various, mainly reducing permeability and enhancing strength	-

Table 4.2: Common soil stabilisation methods (adapted from Ref [7], [52])

4.2. Earth construction techniques

4.2.1. Construction systems

There are many ways of using soil and earth building materials to make building components and full-scale construction. CRAterre (International Center on Earthen Architecture), Fig. 4.7, identifies twelve ways of using earth for construction, which can be divided into three groups where the first is used to create preliminary load-bearing structures. The second is used as a monolithic mass and the third as smaller masonry elements. Table 4.3 describe the most common construction systems used today.

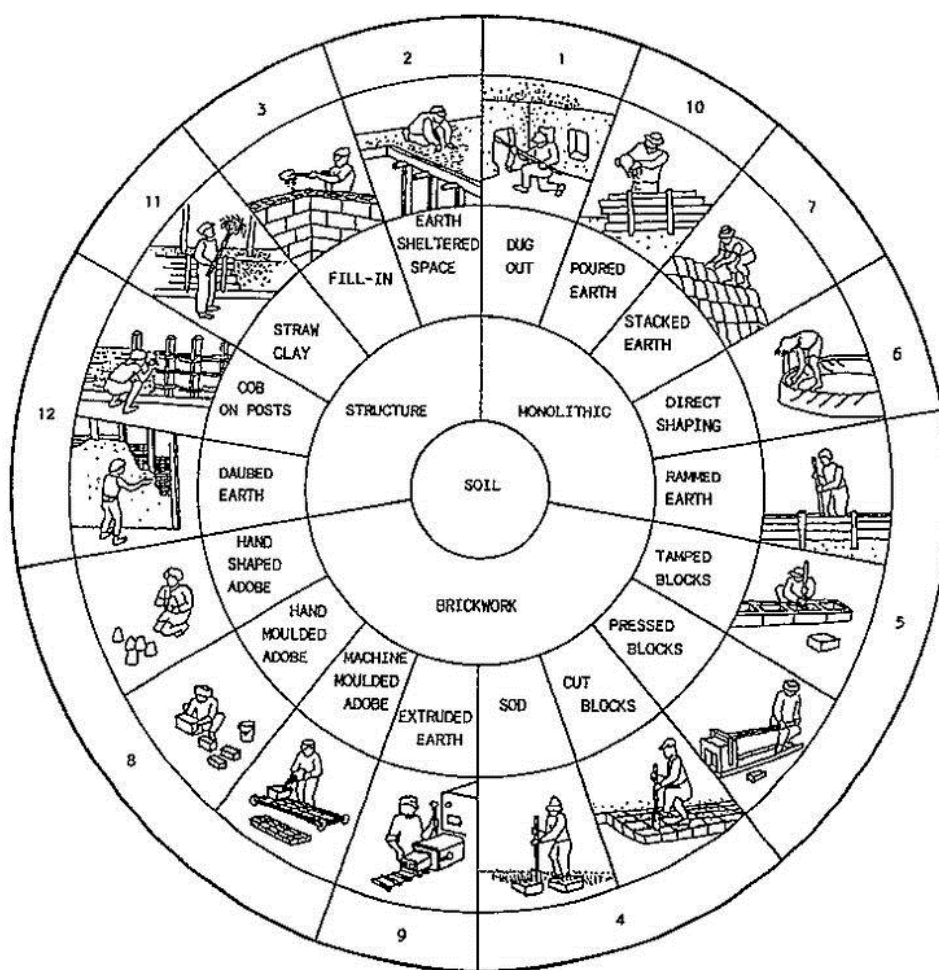


Figure 4.7: Twelve ways of using earth for construction by CRAterre

Technique	Description
Cob	unshaped cob mixture (straw clay) is lightly tamped into place without formwork to form monolithic walls.
Rammed earth	slightly moist unshaped earth is filled into a prepared formwork in layers. Each layer is individually compacted (rammed) which produces the shape of the final structure, usually monolithic walls.
Poured earth	a slurry of earth mortar and artificial binder is sprayed or poured into formwork. Similar to in situ concrete.
Earth plaster	applied to the interior or exterior walls to protect against exposure to water. Helps improve indoor climate.
Earth infill –wattle and daub	used in conjunction with framed or half-timbered constructions that serve as the load-bearing system. The infill between the timber panels can done in a variety of techniques but most known is wattle and daub.
Earth mortars	
Earth plaster mortar	used to apply to surfaces of earth buildings.
Earth masonry mortar	used to construct earth block masonry walls.
Earth spray mortar	used to manufacture earth blocks or parts of building by spraying into or against formwork.
Earth blocks	
Adobe	also sometimes called mud block - air dried block without specific moulding or compaction procedure.
Compressed block	formed in a mould with static or dynamic compaction -compressed stabilised earth block (CSEB) is very popular.
Extruded block	formed by process of extrusion.
Cast block	pouring of spraying a slurry of stabilised earth materials into forms.
Clay panels	used for non-loadbearing partitioning interior walls.
3D printed earth	like 3D printed concrete, layers of flowable earth material is printed and stacked on top of each other to build monolithic elements. It has the potential to more freeform structures but is yet to be proven.

Table 4.3: Earth construction systems and applications (adapted from Ref [19])

At present most earth applications are in internal finishes (plasters boards) and composite insulation materials where the materials' hygrothermal properties is an advantage, see section 4.5. Structural masonry elements (stabilised blocks) with low strength mortars are also commonly found. For load-bearing applications, ancient earth construction mainly consisted of cob, adobe, mud bricks, wattle and daub and rammed earth. Modern earth construction also utilises these but will see more choice due to technological advancements. The main difference between modern and ancient earth construction relates to the building process. Fabrication methods have become more automated, requiring less manual labour and helping speed up construction, making earth a cheaper and more attractive option for architects and builders, see Chapter 5.

4.2.2. Technical standards

All over the world, vernacular traditions and skills, as well as modern contemporary buildings, have shown a large and varied range of technical and architectural possibilities offered by earth building materials. This has resulted in 33 different technical standards and normative documents from 19 countries, see Appendix B.2. They reflect the differing levels of technological development of earth building in different parts of the world which are often derived from local building traditions. As a result, the information they contain varies considerably. The standards and normative documents can be classified into three types with regard to their scope of application [7]:

- Soil, parameters incl. : grading, plasticity, natural constituents content, linear shrinkage.
- Earth building material, parameters incl.: strength/deformation characteristics.
- Earth construction system, parameters incl.: strength/deformation characteristics, aspect ratio, sound and fire performance, thermal characteristics, earthquake resistance.

At present, earth building materials are produced in two ways: (1) manual hand-made production and (2) industrialised factory fabrication. The manual production characterises the traditional way of building with earth. The industrial production changes the traditional, non-engineered into an engineered construction system. The shift means that the material is subject to the same quality standards for testing materials and mechanical parameter, and quality control of the production process. This requires uniform standards for the design, measurement and construction of buildings with earth building materials. The establishment of international standard is essential for the establishment of earthen building materials and other products. Test procedures for earth building products need to be brought to the same level as other "standardised" materials to improve their competitiveness in the building sector. A central reason for this is also to ensure quality control. As earth building becomes more attractive, the number of national standards is expected to increase and become more specific with more research.

4.3. Physical properties

Physical properties are important in determining mechanical properties. Physical properties of earth building materials largely takes principles from existing soil mechanics knowledge.

4.3.1. Determining physical properties

The fundamental difference between soils or earth building materials and conventional civil engineering materials is that it is a multi-phase material, comprising of soil and water (and

air). The changing balance between these components is key to explaining the mechanical behaviour of earth building materials. Since the 1930s, the discipline of soil mechanics developed and the concept of effective stress has proved important in the development of methods for predicting movement and failure of geotechnical structures. The concept considers only saturated soils, soil grains and water, as this is assumed to apply to the majority of geotechnical designs (foundations, retaining walls, tunnels, slope stability assessments). Since the 1990s a subset of soil mechanics, termed unsaturated soil mechanics has grown. Unsaturated soil mechanics recognises that soils have three phases; soil, water and air. This little difference can lead to many different behavioural features. Application of (unsaturated) soil mechanics principles to earth construction is still at an early stage. More information on basic behaviour of soils can be found in soil mechanics textbooks.

As the physical properties of a soil are of major significance when determining strength of unstabilised earthen constructions, soil mechanics knowledge can be used. For modern unstabilised earth constructions, these can also be regarded in part, at least, as manufactured unsaturated soils. For stabilised earth materials, many aspects of the behaviour these are linked to the properties of unstabilised earth. In these constructions, free water may be present and thus they can also be regarded as cemented unsaturated soils. The development of models to understand the behaviour of these is a topic of ongoing research [7].

Dry mass

Due to the infancy of earth building technology and the adoption of principles from soil mechanics, concrete technology and masonry design in determining material behaviour, important physical properties have yet to be standardised for the purpose of earth construction. An example is dry mass, which is important for determining dry density, strength, stiffness, thermal conductivity, heat capacity and adsorption-desorption capacity. However, no consensus exists of how to measure this property [45].

Dry density

Dry density of soil is an important factor for the strength and durability of soil. Therefore, achieving a value as high as possible for dry density is considered important. Dry density is determined by water content and compaction of soils.

4.3.2. Water content in soils

Water plays a crucial role in the strength of soils, both in cases with and without stabiliser. Earth is a cohesive-frictional material, its mechanical behaviour is determined by the combined action of suction and friction. Apart from soils in desert areas, all natural soils contain water. Some soils may be fully saturated (all voids contain water) other partially saturated (voids containing water as well as air). The degree of saturation can be determined by testing. The presence of water activates the binding forces of soils, otherwise it would be a solid. All materials with open porous structures like earth are able to store and transport water within their capillaries [45]. Friction holds soil particles together. Majority of failures in earth materials is due to shear strength and friction is closely related to shear strength. To understand this, it is important to first understand the concept of effective stress.

Saturated soils: Effective stress

Effective stress which applies to saturated soils can be explained by the following equation:

$$\sigma' = \sigma - u \quad (4.1)$$

where σ is the total stress from applied loads, which are stresses that are checked against equilibrium applied to the soil. Within the water, a pressure called pore water pressure μ is also found. Total stresses push the soil grains together while pore water pressure pushes them apart and the difference between them is the effective stress. Effective stress controls the frictional behaviour of a soil. It can be altered by changing water conditions or loads applied. This explains how soils can fail both by increase in load (increase shear stress) but also by water pressure (decrease shear stress) e.g. rainfall-induced landslide.

Shear strength

Shear strength is the most important criteria for soils. The Mohr-Coulomb yield criterion is a model of friction, which is described by the following equation:

$$\tau = \sigma' \tan \phi' \quad (4.2)$$

where ϕ' is the effective angle of friction which can be determined by testing. The relationship is for a 2D case and is expressed in terms of normal stress and shear stress. If actual shear $\sigma' \tan \phi'$ is exceeded, failure will occur.

Unsaturated soils: Suction

Unsaturated soils are stronger than saturated soils and have other behavioural differences. In earth construction, the concept of suction explains why they do not collapse. Although the structures appear dry, small amounts of water inside provides suction to give basic frictional shear strength. Unlike in saturated soils, water will pull soil grains together and not apart. The normal frictional force is greater in the unsaturated case. A greater normal force leads to a greater shear strength. Suction is as the difference between air pressure and pore water pressure.

$$suction = u_a - u_w \quad (4.3)$$

where u_a is the pressure and u_w is the pore water pressure. When a soil is saturated, suction is zero as pore water pressure is zero. As the sample dries, the suction increases as water is lost. This continues until the remaining water is so small that it provides enough grain contact around clay particles.

Pore suction on stiffness and strength

Jaquin et al. [56] showed that strength and stiffness increase with decreasing water content. During axial compression, pore suction increases for specimens at high water content but

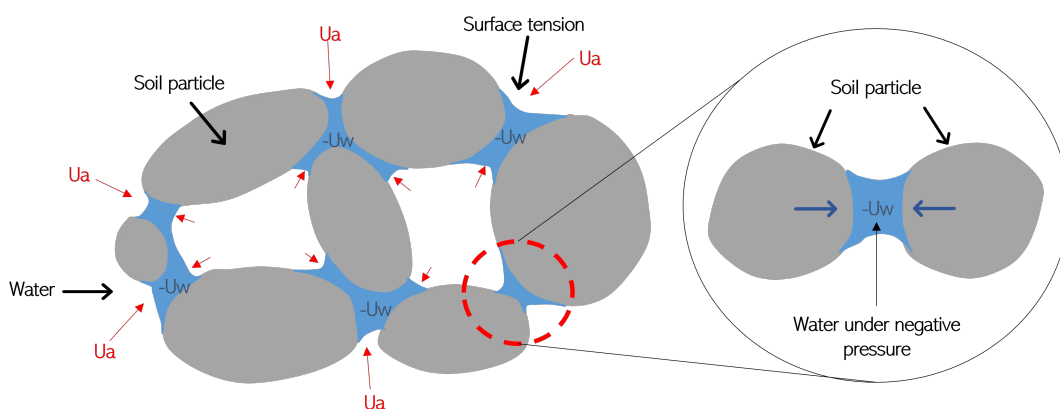


Figure 4.8: The concept of soil suction (adapted from Ref [7], [55])

decreases for specimens at low water content. The material becomes progressively fragile as it becomes drier. Suction was measured using a high capacity tensiometer. Bui et al. [57] also showed that strength and stiffness increase as pore suction grows. Suction was measured by filter paper. Modelling unsaturated soils is an active field of research and there is a lack of consensus as to what stress variables should be used to characterise strength. A highly regarded model for unsaturated soils is the Barcelona Basic Model (Alonso et al. 1990).

Moisture content

The ratio of the mass of water to the mass of solid particles is termed moisture content and is an indicator of the state of the soil and its behaviour. The natural moisture content of a soil is often compared with liquid and plastic limit test results. The difference of moisture content of different soils lead to different earth building applications. Fig. 4.9 shows different earth construction systems differentiated by wet and dry methods. Dry methods are construction systems around the optimum moisture content. Wet methods are construction systems between the plastic and liquid limits.

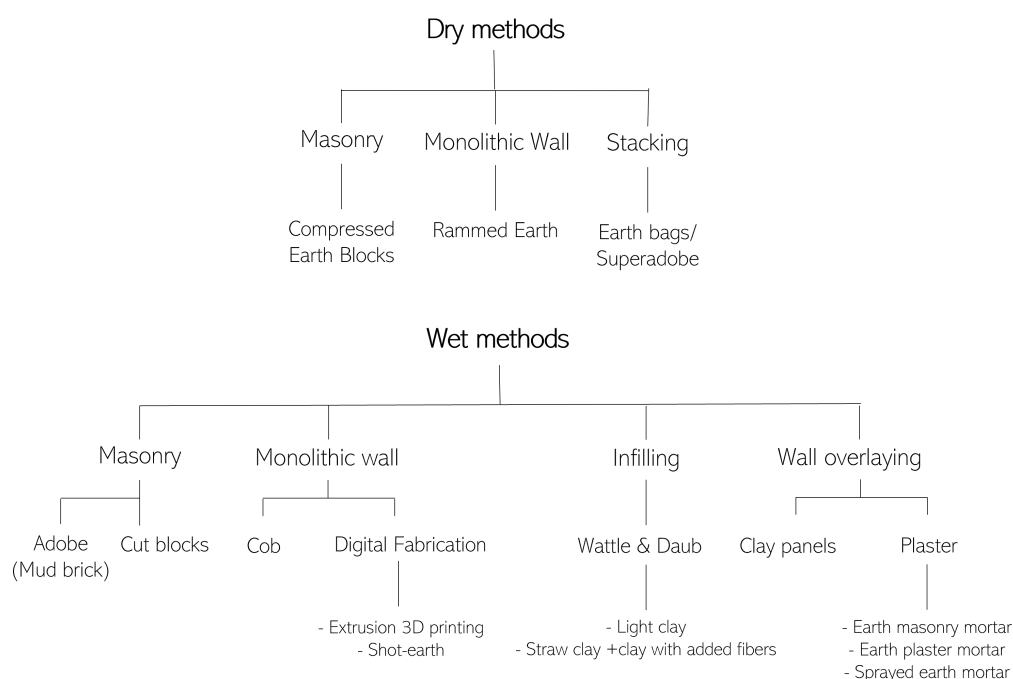


Figure 4.9: Earth construction systems classified as wet and dry methods (partially adapted from Ref [21])

Soil consistency (Atterberg limits)

Soil consistencies also known as Atterberg limits, state the relative ease in which a soil can be deformed. The limits denotes the degree of plasticity of a soil and is indicated by terms: soft, firm, stiff, hard. Depending on water content, four states of consistency is used to describe the behaviour of a soil, and the three limit states, liquid limit, plastic limit, shrinkage limit, mark the boundaries of the states of consistency, as seen in Fig. 4.10. In practice, only clayey soils, for which consistency is related to a large extent, are described using these terms. As moisture content increases, a clayey or silty soil will become softer and stickier until it cannot retain its shape, liquid state. As moisture content decreases, a soil becomes stiffer until there is insufficient moisture to provide cohesiveness. The soil cracks or breaks easily if remoulded. This is the semi-solid state. If moisture content is decreased further, it gets to a stage where the suction forces between soil particles will not permit them to move closer and the soil is

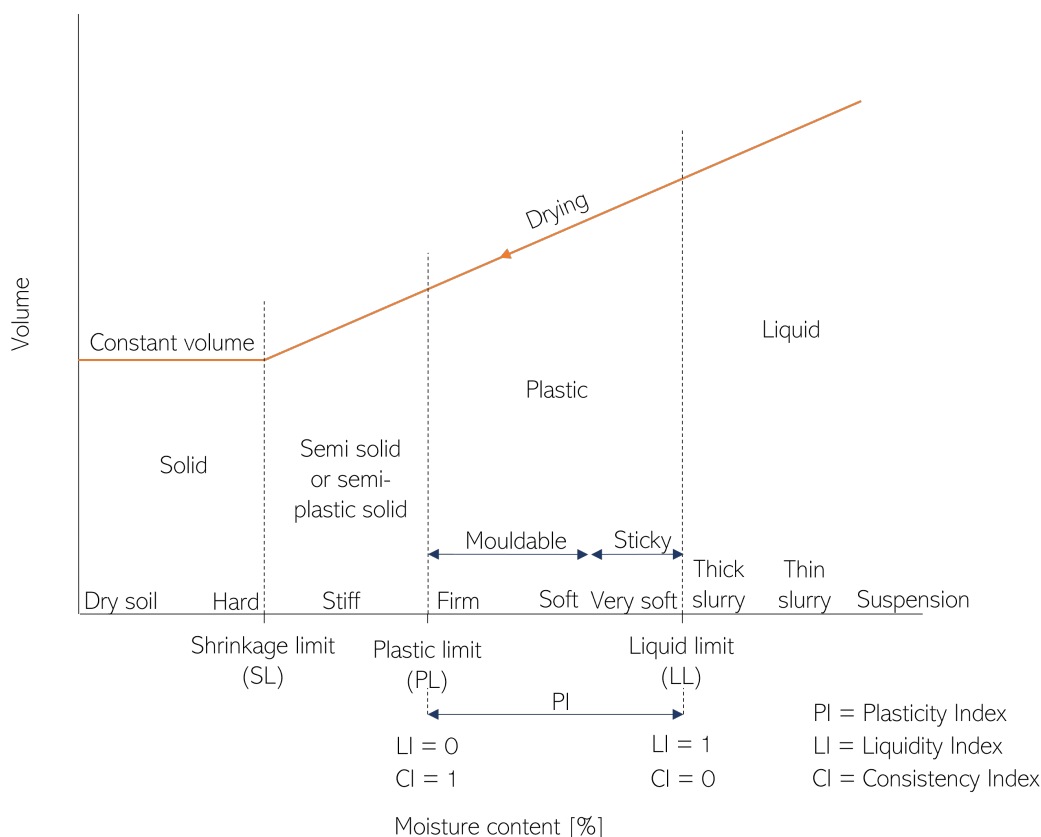


Figure 4.10: Atterberg limits (adapted from Ref [38])

a solid. The transition between the different states is gradual rather than abrupt, depending on the soil. The Atterberg limits are useful to describe moisture contents as it changes and in identifying the type of clay mineral present. Tests for liquid and plastic limits are called Liquidity Index (LI) and Consistency Index (CI). There are standards that define methods and tests in how to measure these limits.

4.3.3. Compaction of soil

Compaction is the process of reducing air voids in a soil by the application of energy. It enables earth building materials reach its desired strength for building applications. This is especially important for e.g. rammed earth. The soil must be moist, ie. have a degree of saturation in order to form suction between the particles. Compaction increases the number of particles per unit volume and dry density is used to indicate the degree of compaction. At maximum dry density (MDD), a soil can derive its greatest compressive strength. Each soil has a moisture content corresponding the MDD, which is known as the optimum moisture content (OMC). Particle size distribution, shape of soil grains, specific gravity of grains, amount and type of clay minerals greatly influences MDD and OMC. Fig. 4.11 shows the MDD and corresponding OMC for a soil. Increasing the moisture content beyond this point will reduce the dry density. At low moisture contents (left of OMC) there is insufficient water to form suction between the particles. At maximum dry density the specimen of compacted soil has a high degree of saturation. Further increase of water (right of OMC) has a dilution effect. In practice, compactive efforts cannot de-air voids completely. Therefore the dry density -moisture content curve is always to the left of the zero air curve ($A_v = 0\%$). The descending part of the compaction curve usually has a minimum air content of 3-5%. It is convenient to plot the air void curves of 5 and

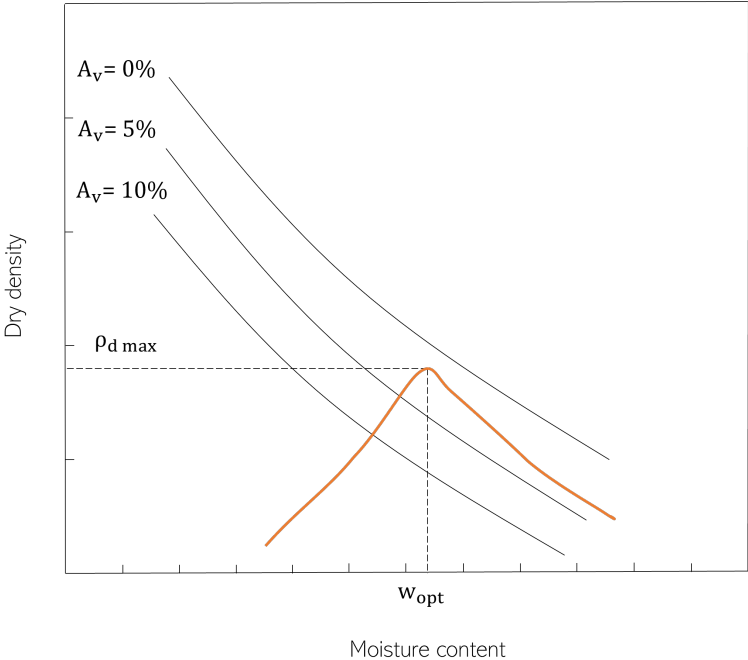


Figure 4.11: Optimum moisture content and maximum dry density of a soil (adapted from Ref [58])

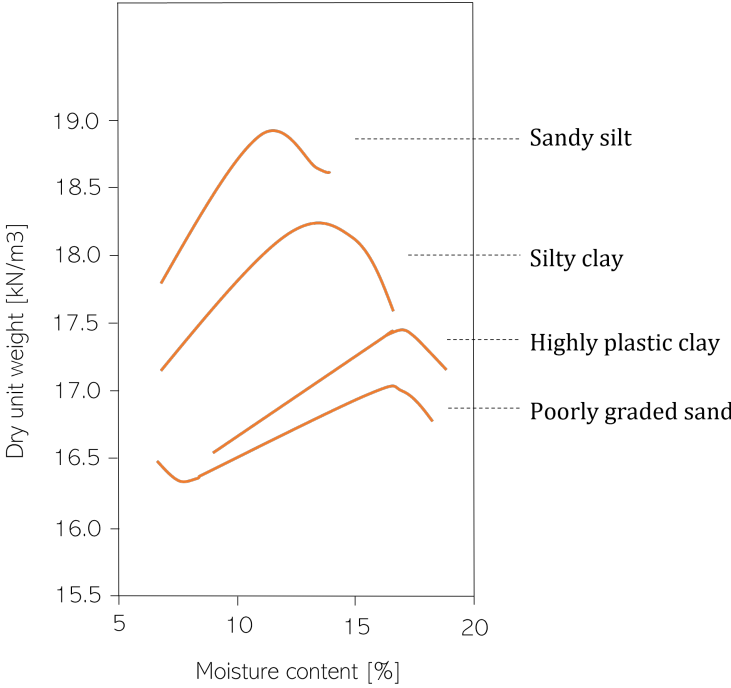


Figure 4.12: Compaction curves from different soils (adapted from Ref [58])

10% to understand the development of compaction. To determine the compaction curve of a soil, the Proctor or modified Proctor test is used. In the Proctor test, standard energy applied to soil specimens is 592 kNm/m^3 of soil. It is important to point that Proctor compaction tests may not apply same energy as the one used in earth construction, which may not result in the same OMC. Nevertheless, they are still a reliable method to assess appropriate manufacturing water content for earth structures [59].

Furthermore, there are different types of compaction, which are dynamic or impact, kneading, static and vibratory. Fig 4.12 shows four different types of soils compacted with the impact method. Different soils have their own OMC for a given compactive effort. Therefore, the MDD that can be obtained for a soil depends on the type of soil. Well-graded coarse-grained soils attain higher density than fine-grained soils. Heavy clays attain low densities due to greater surface area, which require more water and thus higher optimum moisture contents [58].

Compactive effort

The dry density of a soil depends on the soil type, the moisture content during compaction and compactive effort. Increasing compactive effort, energy applied, increases dry density and reduces moisture content. Fig 4.13 shows a higher maximum dry density of the same soil in curve C compared to curve B. The increase in MDD can be explained by the resulting greater orientation of fine particles under the increased compactive effort.

Hypercompaction

Studies by Morel et al.[60], Kouakou and Morel [61], Bruno et al.[62] found that strength increases with increasing density. Especially, Bruno et al. [62] found that the application of higher compaction pressures, "hypercompaction", at 25,50 and 100 MPa (earth blocks are usually compacted at pressures between 2 and 15 MPa), led to higher dry densities. At 100 MPa, the maximum dry density was 2270 kg/m^3 and optimum water content was 5%. This is

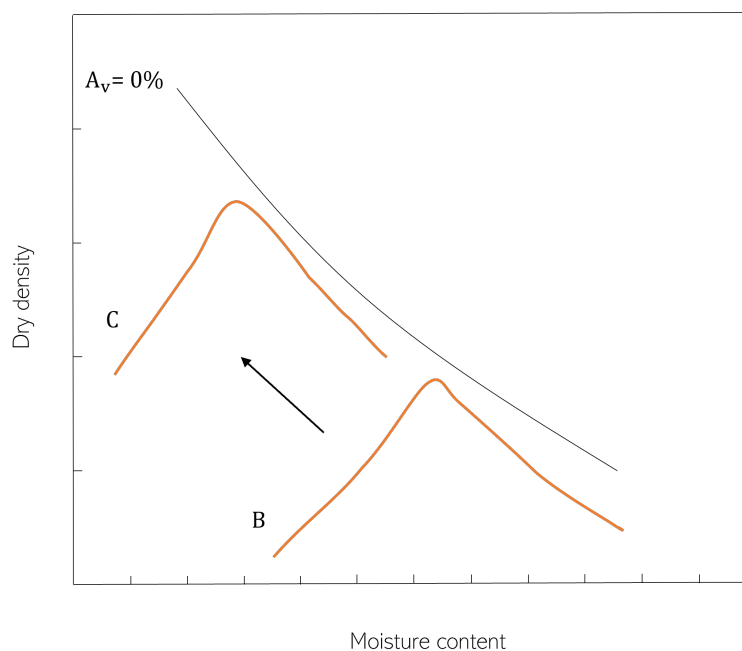


Figure 4.13: Compaction curve of a soil with higher compactive effort, from B to C (adapted from Ref [58])

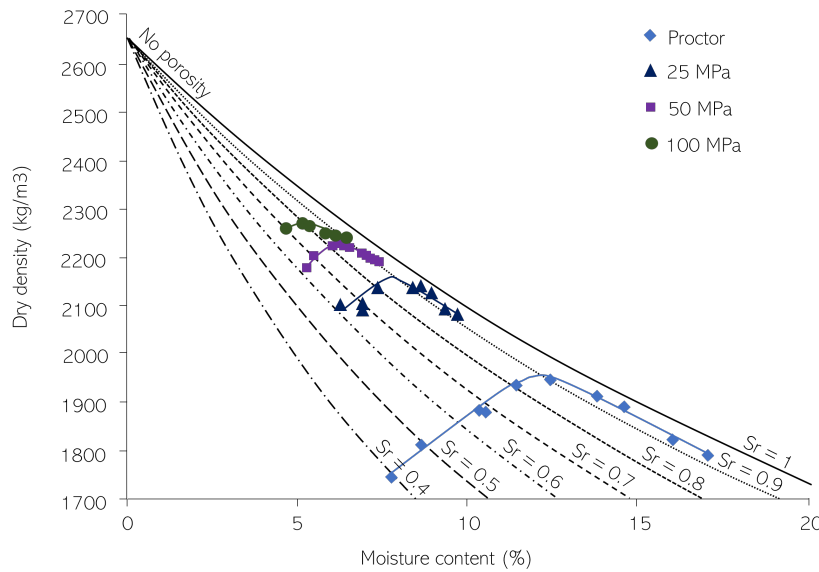


Figure 4.14: Compaction curves at 25, 50, 100 MPa and standard Proctor (adapted from Ref [62])

Material	Compressive strength (MPa)	
	Min.	Max.
Hypercompacted unstabilised earth	4.1	10.2
Compacted stabilised earth	5.2	12.9
Standard masonry bricks	6.9	27.6

Table 4.4: Compressive strength of masonry materials vs. hypercompaction (adapted from Ref [2])

the largest dry density registered in literature for unstabilised earth material. Fig. 4.14 shows the results obtained in the study. As compaction increases, the material shifts towards "no porosity" ($A_v = 0\%$), where dry density is equal to the density of the solid soil particles. Table 4.4 compares the strength of hypercompaction with different masonry materials. The study on compacted stabilised earth used 10% cement which erases environmental benefits of earth material.

4.4. Mechanical properties

Due to the many construction systems with differing moisture contents and applications, this section focuses only on rammed earth, as it is one of the most actively researched construction systems. Therefore, this section forms part of the data gathering to predict shotearth material behaviour in chapter 6. Both unstabilised and cement stabilised properties will be considered, as cement is the most widely used stabiliser.

4.4.1. Determining mechanical properties

Understanding mechanical behaviour of earth materials is important to develop design rules. However, due to the "lack of standard experimental protocols for assessing the engineering performance of earth materials" [45], it is difficult to select appropriate design parameters. There is no consensus on how to measure these. as standards and design principles from

Specimen	Size	Based on standard or principle	ref
<u>CSRE</u>			
Cylinder	Ø150mm x 110 mm	Standards Australia	63
Cylinder and prism	Cylinder: Ø150 mm x 300 mm Prism: 150 x 150 x 300 mm	Concrete and masonry design	64, 65
Walette	600 x 155 x 720	Masonry	64, 65, 66
<u>URE</u>			
Cube	150 mm x 150 mm	New Zealand Standards (1998)	67
Cylinders and prisms	Height to thickness: 2	Concrete and masonry design	68

Table 4.5: Overview of the diversity of testing procedures adopted to measure rammed earth properties

geotechnical engineering, concrete design and technology, and masonry design have been used to determine key mechanical parameters. The applicability of these 'adopted' procedures for earth building materials has not yet been proven.

Unconfined compressive strength (UCS) is the most important parameter in earth building technology but few standards or normative documents distinguish between "design" and "characteristic" values of UCS, see Appendix table B.4. Characteristic strength of a material is often the basis for the structural design of elements using limit-state design principles. For concrete, cube or cylinder strength is used to assess the characteristic compressive strength. In masonry, walleets or prisms are used. For unstabilised rammed earth (URE) and cement stabilised rammed earth (CSRE) a variety of test procedures have been used to obtain UCS, as seen in Table 4.5. The diversity of test procedures makes it difficult to assess mechanical parameters and material performance, which are often tailored to specific materials or external actions. Furthermore, the majority of strength parameters obtained from laboratory tests is on small samples of soils and often different shapes are used, which often result in varied and higher values than the full-scale constructions.

The engineering design of earthen structures is still at an early age. Therefore, from a mechanical point of view, it is still necessary to oversize these structures, allowing to design with simple mechanical parameters. RILEM technical committee TCE 274 is working on defining accurate, repeatable, and reproducible performance oriented-testing protocols that could be adopted as international standards in the future [45].

Basic mechanical behaviour of soils

Soils show very little elasticity, and exhibit plastic deformation almost immediately upon loading. Shear stress leads to failure, therefore, determining the maximum values of shear stress that can be experienced at a material point is of highest concern. Cracking is assumed to occur when a soil is subject to tensile stresses (as soil is often assumed to have no tensile strength). This is of course different with fibers and stabilisation.

4.4.2. Mechanical properties of cement stabilised rammed earth

As cement is the most common form of stabilisation, this section only considers cement stabilised rammed earth (CSRE) and disregards the other types of binders. Cement stabilised

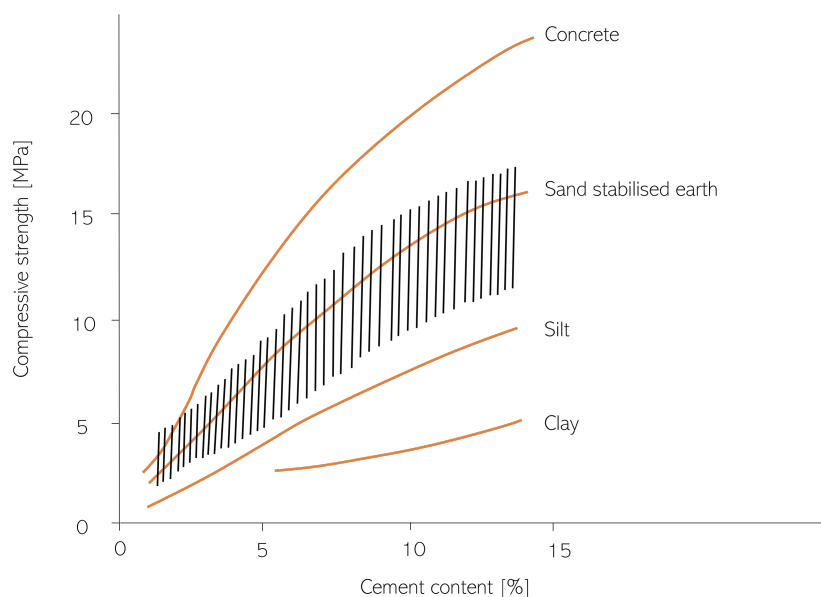


Figure 4.15: Relative increase in compressive strength over % cement content for different soil groups (adapted from Ref [40])

earth has a non-linear increase of compressive strength with the percentage of cement added and also has a wide-range of strength values depending on the soil composition and especially the percentage of the clay fraction. Fig. 4.15 shows the increase of cement stabilised earth compared to concrete, silt and clay. The relative increase in strength with % cement added is greater for soils with lower specific surface area of the clay fraction (e.g. sandy soils). This is likely due to interfacial bonding between cement paste and aggregate [7]. Jayasinghe et al. [66] showed compared three soils in Sri Lanka with varying cement content between 6-10 %. The results showed the sandy soil had higher compressive strengths than hard laterite and clay with increasing cement. The non-homogeneity is less for earth building materials that use washed aggregates. The proportional increase in strength with % cement declines significantly for stabilised earth as the cohesive proportion increases. In other words, the more clay there is in soil, the more cement is required. This presents a problem in interpretation of research data as different soils can exhibit different proportional increases in compressive strength with addition of cement. A solution could be to improve PSD and soil plasticity to make it more compatible with cement stabilisation which can reduce the percentage of stabiliser needed. Further research is required to better understand the behaviour of clay and cement.

Compressive strength

There is a limited number of studies on the strength and behaviour of cement stabilised rammed earth (CSRE). An attempt to summarise these is found in Table 4.6. The literature on CSRE indicates the following:

- soil composition influences strength, a wide range of values for density, thickness, and strength is recorded
- the moisture content of the specimen at the time of testing significantly influences strength. Time lag results in lower strength and difficulty in achieving higher density.
- use of sandy soils and cement content in the range of 6–10% for CSRE construction show higher strength than other types of earthen compositions
- CSRE materials possess good erosion resistance and durability

Sample [cm]	ρ [kg/m ³]	MC [% wt]	Cement [%]	f_c [MPa]	ref
Wall: 75 x 15.2 x 300	1800	6.47	8	3.91	65
Walette: 60 x 15.5 x 72	1800	6.61	8	5.47	65
Prism: 15 x 15 x 30	1800	6.20	8	6.50	65
Cube and cylinders	-	-	11	9.8 -26.85(a)	70
Wall panels according to BS 5628: Part 1:1992	1800 -2000	-	6-10	2-3.7 (b)	66
-	-	-	-	>10	71
-	-	-	8	>2 wet	40
Walette 60 x 15.5 x varying height (40-90)	1700 -1800	1.33-3.18	7	3.44 -4.6	72
Walette 60 x 15.5 x varying height (40-90)	1700 -1800	1.46-4.45	10	5.01-7.40	72
Cylinder	1700 -1800		7	3.46 -4.61	72
-	-	-	10	4.95 -7.44	72
-	-	-	-	3.9-7.9	73

a) For curing duration between 14 and 215 days. Large scatter (150%) in the strength values.

b) Different soils were used (sandy laterite, hard laterite, clayey), sandy laterite soils showed higher compressive strength. Wet compressive strength was 0.45 -0.6 times higher than dry compressive strength. Also depends on cement content. More cement gives higher strength.

Table 4.6: Overview of cement content and compressive strength measured in cement stabilised rammed earth

- CSRE materials should be rammed into a wall within an hour after mixing with water

Measuring CSRE compressive strength

Comprehensive studies to understand the structural behavior of CSRE are limited. Venkatarama et al. [65], points out that in CSRE research, the main focus is on the design of wall elements under concentric or eccentric compression. Compressive strength of CSRE is generally examined through tests on rammed-earth cubes, cylinders, prisms or wallettes. Cube or cylinder strength may not be ideal to arrive at characteristic compressive strength due to them resulting in higher values. It is suggested that square prisms with a height to thickness ratio at a range of 2-6 may be ideal. However, compressive strength of prisms has to be normalised.

Other mechanical properties

Due to the limited number of CSRE studies, it has not been possible to find measurements on other mechanical properties. Tension and shear strength is generally taken as zero in earth building design. However, 10 % may be taken likened to studies found in URE.

4.4.3. Mechanical properties of unstabilised earth

Unconfined compressive strength (UCS)

Unconfined compressive strength is the main parameter in earth construction. It is dependent on moisture content, dry density (compaction energy), and sample size. The relation between these and compressive strength is unclear. Studies in literature have found UCS for rammed earth between 1.0 to 2.5 MPa, see Table 4.7. These values are mostly based on small-size samples with different shapes, with some based on construction-size samples. A study has found UCS up to 10 MPa [69]. Experiments performed by Bui et al. [70] and Maniatidis and Walker [68] found that compressive strength for smaller samples are higher than for bigger samples. The lower strength in bigger and full-scale samples is attributed to the inclusion of

Sample [cm]	ρ [kg/m ³]	MC [% wt]	f_c [MPa]	E [MPa]
30 x 30 x 60	1920	13	0.81	65
40 x 40 x 65	1900	11	1.00	100
Ø4, h=8	1649	21	1.04	103
10 x 10 x 10	1660	-	1.10	1050
25 x 25 x 50	1878	12	1.15	365
55 x 55 x 20	2100	10	1.26	1034
100 x 100 x 30	2000	-	1.30	500
Ø10, h=20	2080	8	1.40	-
Ø7.5, h=15	2043	12	1.77	-
Ø7.5, h=15	2143	7	1.85	34
Ø30, h=60	1850	13	1.90	-
15 x 15 x 15	2020	-	1.90	-
Ø10, h=20	1790	12	2.00	763
Ø7.5, h=15	1946	12	2.23	143
Ø10, h=20	1850	13	2.46	160
Mean	1942	12	1.55	392

Table 4.7: Measured unconfined compressive strength and Young's modulus from different studies (adapted from Ref [41])

bigger aggregates and more variation in PSD. These samples are more representative of the behaviour of real rammed earth walls [41].

Measuring compressive strength

There are no standards for testing UCS of RE samples. Therefore, authors have followed ASTM D1633 [75] for compressive strength of soil-cement cylinders or followed procedures from ASTM for cement mortars [76] or from masonry design rules [77]. The RILEM technical committee suggests that specimens should be tested following the framework of continuum mechanics with specimen sizes which ensures that stress and strain tensors are homogenous within the specimen [45]. Standardised testing procedures are necessary to actually make values obtained from studies comparable.

Young's modulus

There is a big dispersion in the values for young modulus in literature varying from 60-1000 MPa. The dispersion is related to different materials, moisture content, sample size, testing procedures and varying definitions of elastic modulus. This makes it hard to determine a relation between UCS and Young's modulus like in concrete. However, direct relationships have been proved in [68], [78].

Measuring Youngs modulus

Alós Shephard et al. [79] argues that Young's modulus determined following concrete testing standards is higher than the one following geotechnical testing standards due to different techniques used to measure deformation.

Specimen	Strength [N/mm ²]		
	Compression	Tension	Bending tension
Brick A	3.5	0.4	1.1
Brick B	4.4	0.5	1.3
Brick C	6.1	0.6	1.6
Mortar D	2.02	0.21	0.69
Mortar E	2.63	0.35	0.85

Table 4.8: Measured tensile strength of earth bricks and earth mortar (adapted from Ref [82])

Poisson's ratio

Few studies have measured poisson's ratio. The studies that have, found values from 0.22 to 0.30 [59], [80], [81].

Tensile and bending strength

Tensile strength is one of the most relevant parameters in the analysis of rammed earth failure, especially in seismic regions. It has not yet been thoroughly studied and therefore taken as zero in design. Tensile strength can be considered as approximately 10% of its compressive strength [41], [82], leading to values between 0.10 and 0.35MPa. This has been determined using Brazilian tests and pull-off tests [80], [81], [83]. Bui et al. [80] tested the tensile strength in an earth layer and between layers and concluded that it may be acceptable to consider rammed earth as an isotropic material in tension. Reinforcement is necessary if tensile stresses cannot be avoided.

In the absence of direct experimental data, design characteristic bending strength should be taken as zero according to Standards Australia [51]. In cases where design relies on bending resistance from the wall elements, a direct bending strength test should be performed. No data on the tensile and bending strengths of rammed earth is found, however, Table 4.8 shows the results of tensile strength in raw earth bricks and earth mortar. The results of earth mortar are interesting for this research, more in Chapter 6.

Shear strength

In the absence of direct experimental data, design characteristic shear strength should be taken as zero, Australian standards [51], or 0.035MPa, New Zealand standards [84]. Studies measuring shear strength have found values between 0.15 to 0.85 MPa, see Table 4.9. Shear may be assumed to be carried by frictional resistance. Factors that influence shear strength value is moisture content at the testing time. There is a decrease in shear strength with increasing moisture content [85].

Shear behaviour

Shear stress criteria are commonly given by the Mohr-Coulomb theory, which is defined by cohesion, friction angle and normal stress. The relationship between shear and normal stress can be determined by testing, from which cohesion and friction angle can be determined. Some authors suggest a relationship between cohesion and compressive strength $c=(0.10-0.14)f_c$ [80], [86], or cohesion and tension $c=1.5*f_t$ [87], [88]. Further investigation is needed to confirm these relationships.

Sample [cm]	ρ [kg/m ³]	f_s [MPa]	c [kPa]	φ [°]
55 x 55 x 20	2100	0.15	189	37
40 x 40 x 65	1900	0.18	170	51
250 x 250 x 50	1920	0.37	-	-
50 x 50 x 11	2190	0.65 – 0.85	-	39
Ø 7.6 h=14.7	2000	-	13	41
49 x 49 x 36	-	-	30	35
15 x 15 x 18	2143	-	50	65
6 x 6 x 2	2131	-	68	44
100 x 100 x 30	2000	-	130	45
10 x 10 x 3.5	-	-	135 -260	45
50 x 50 x 12	2190	-	561	37
Mean	2064	0.36	157	44

Table 4.9: Measured shear strength from different studies (adapted from Ref [41])

General cohesion values vary from 30 kPa to 560 kPa, while friction angles between 35 and 75 degrees are found. El Nabouch [59] showed that higher density increases cohesion but does not affect friction angle. Small-scale samples were tested. Data reported does not give a clear tendency of these parameters and they have no sound correlations with dry density and/or water content [45].

It has also been suggested by some authors that dilation angle [89] and dissipated energy in shear [90] also affect shear behaviour. Tests to determine shear stress are shear box and triaxial compression test used in geotechnical engineering. Other tests are diagonal compression tests in masonry design.

Fracture energy

Very few studies concern the tensile and compressive fracture energy of RE. Values have been found from 0.002 N/mm to 0.020 N/mm. Tests to obtain fracture energy is with a three-point bending test, wedge splitting test. Miccoli et al. [88] proposed the tensile fracture energy as 0.029 ft and compressive fracture energy as 1.6 fc. Bui et al. [89] proposes to calculate tensile fracture energy according to CEB-FIP Model Code 90 [91]. Based on the existing studies, no conclusions can yet be drawn on this property and further investigations are needed [41].

4.5. Hygrothermal properties

The term 'hygrothermal' refers to the movement of heat and moisture through buildings. Earth building materials are well known for their hygrothermal properties and they have shown to be beneficial for the health and well-being of their occupants. Occupants in earth buildings report that their home is warm in the winter and cool in the summer as earth materials have excellent hygroscopicity (ability to adsorb and absorb water from the surrounding environment) enabling them to balance indoor climate. Therefore, RE walls, earth plasters and other earth

buildings, when designed properly, can be used as a building-integrated form of "passive air conditioning".

4.5.1. Determining hygrothermal properties

Moisture buffering

Hygroscopic behaviour is often described by moisture adsorption and most commonly the Moisture Buffer Value (MBV). Moisture adsorption is the amount of water uptake in $g/(m^2)$. MBV indicates the amount of moisture uptake or release by a material when it is subject to change in environmental conditions, typically relative humidity (RH), and the response is measured as mass change with change in RH, presented in $g/(m^2 \cdot \%RH)$. The limitation of the MBV is that testing methods generally follow the principle of the step-response method. This test method does not represent an intrinsic material property and the results are dependent on the chosen RH and time cycles as well as experimental set-up. This makes comparison between different studies difficult. Moreover, existing tests on hygroscopic materials only focus on the adsorption of water, where indoor pollutants have not been considered in relation to thermal properties of earth materials [92].

Thermal insulation

In countries with cold and temperate climates, buildings in regular use have to be heated during the winter. Building standards in these countries require appropriate thermal insulation. According to these standards, earth building materials are not good thermal insulators and generally do not fulfil the thermal insulation requirements for exterior walls in new buildings. This is due to limited knowledge on the thermal conductivity of earth materials, which is related to its density and water content. Therefore, more research is required to define new standards. At present, earth products in new buildings can be used in exterior or interior walls in combination with other thermal insulating materials [7].

The parameters that define thermal insulation is thermal conductivity and thermal resistance. The lower the thermal conductivity coefficient, the higher the insulation will be. Thermal resistance is the ratio between the thickness of the element and its thermal conductivity. Table 4.10 shows the comparison of thermal conductivity and resistance of earth materials, concrete and stone. It can be seen that thermal conductivity and resistance of earth is lower than the others. The Australian earth standard defines a minimum value of $1.3 \text{ m}^2\text{K/W}$ for thermal resistance. This leads to conclude that the resistance value might not be representative enough to characterise thermal behaviour of rammed earth [41].

4.5.2. Moisture buffering capacity

Studies have shown that earth materials have higher moisture adsorption values than conventional materials. Lustig-Rössler [93] found that the average moisture uptake for 10 mm thick

Material	Thermal conductivity $[Wm^{-1} \cdot K^{-1}]$	Thermal resistance $[m^2K/W]$
Earth	1.0 -1.4	0.2 -0.6
Concrete	1.5 -2.5	0.8 -1.3
Stone	1.1 -3.5	0.11 -0.12

Table 4.10: Thermal conductivity and thermal resistance of earth compared to other materials

earth materials varied between 45 and 65 g/m², compared to fired bricks and plasterboard at 1 g/m², and wood at 25 g/m². A study based on newly constructed URE walls, in an environment where RH fluctuated by 5 to 10% throughout the year, found MBV values between 1.0 and 3.7 g/(m².%RH) which is considered good and excellent defined in [94].

McGregor et al. [95] measured the MBVs on five samples of stabilised and unstabilised earth and found that unstabilised earth exhibited the highest MBVs and the addition of any stabiliser reduces it. The reduction of MBV with the cement and lime samples increased as the percentage amount grew, Fig. 4.16. Although the addition of stabilisation affects the moisture buffering abilities of earth materials, both SRE and URE walls have higher moisture adsorption values compared to conventional materials. Allinson and Hall [96] found MBVs between 29 and 54 g/m² for cement stabilised rammed earth walls. The mixes were stabilised with 10% per dry mass of cement. Fig. 4.17 shows different studies on the moisture adsorption of different earth materials.

4.5.3. Thermal performance

The passive temperature and moisture buffering behaviour of earth materials have been monitored (and exploited), in several modern earth buildings before. In Sydney, Australia, a SRE house was left unoccupied for a year. Over a period, internal sensor readings recorded an average indoor temperature between 18°C and 27°C, compared with outdoor temperature between 7°C and 42°C. Another study in New South Wales, Australia, a two storey SRE office building also showed that indoor temperature was reduced by passive cooling and dehumidification throughout a hot summer period. A case study in Southern Portugal [43] also showed that URE can provide satisfactory thermal comfort almost the whole year. A heating system could be necessary for some periods of thermal discomfort during winter. All these studies show that the amount of energy required to meet heating and cooling loads is significantly lower than that in conventional buildings.

Effect of humidity and temperature on strength and stiffness

Along the thickness of earth walls, large gradients of temperature, humidity and pore suction can be found due to different ambient conditions on the inside and outside faces of the wall. The impact of these gradients on structural performance has been subject to investigation by [97]. The main conclusion from this study was that strength reduces when humidity increases and water condenses which produces a decrease in suction. This leads to conclude that the design of earth buildings have to take into account change of environmental conditions that can occur over the lifetime of the building.

Acoustic performance

Acoustic insulation has not been thoroughly studied in literature. The few studies and guides [51], [72], [98]–[100] on this parameter have found on average R and STC values of 57 dB. Therefore, it can be concluded that RE have good acoustic behaviour. There are not enough studies to validate its acoustic performance but some authors [98], [101], [102] indicate that due to its porosity, rammed earth has excellent reverberation properties, generating far fewer echoes than conventional materials.

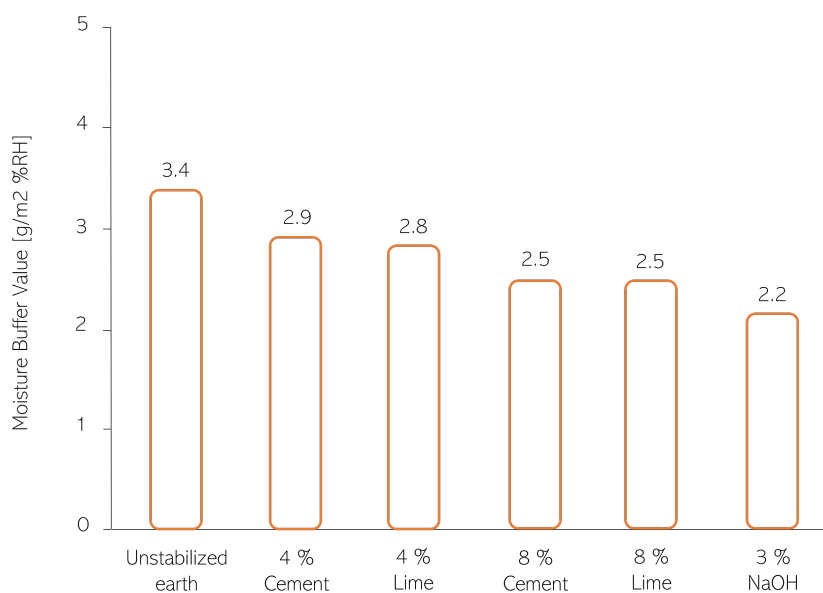


Figure 4.16: MBV of stabilised and unstabilised earth samples (adapted from Ref [95])

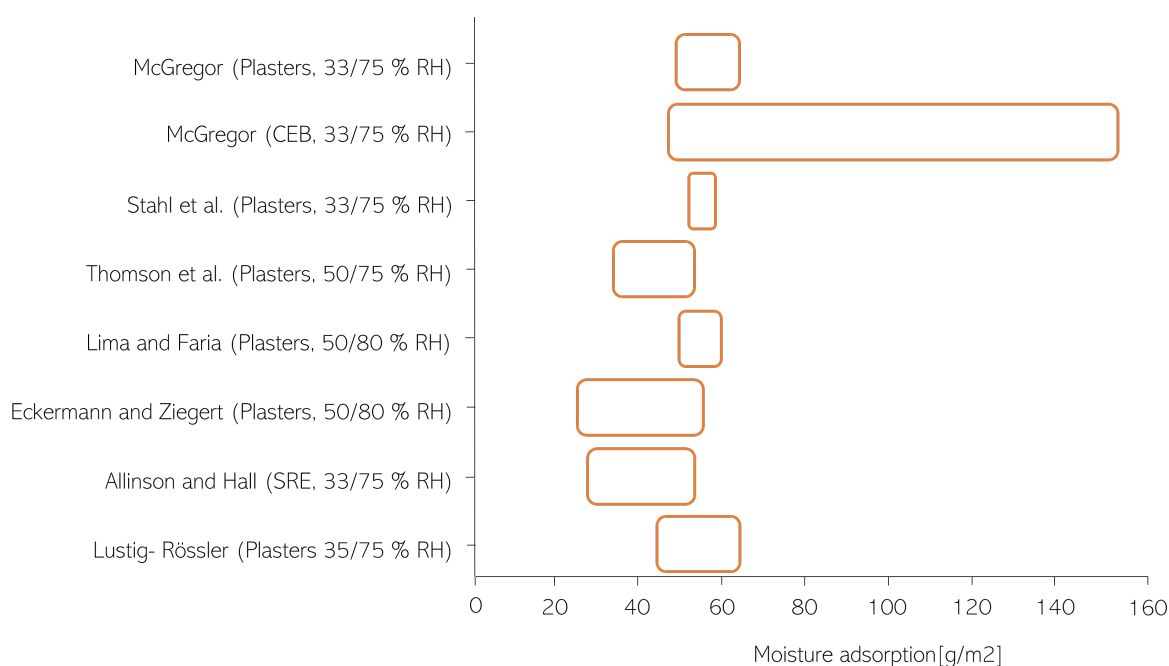


Figure 4.17: Measured moisture adsorption in g/m² at 8 hours for different earth products (adapted from Ref [92])

4.6. Durability

In the context of earth construction, durability means the resistance and ability of a structure to withstand the action of weathering and functional deterioration over time without degradation to the expected service life.

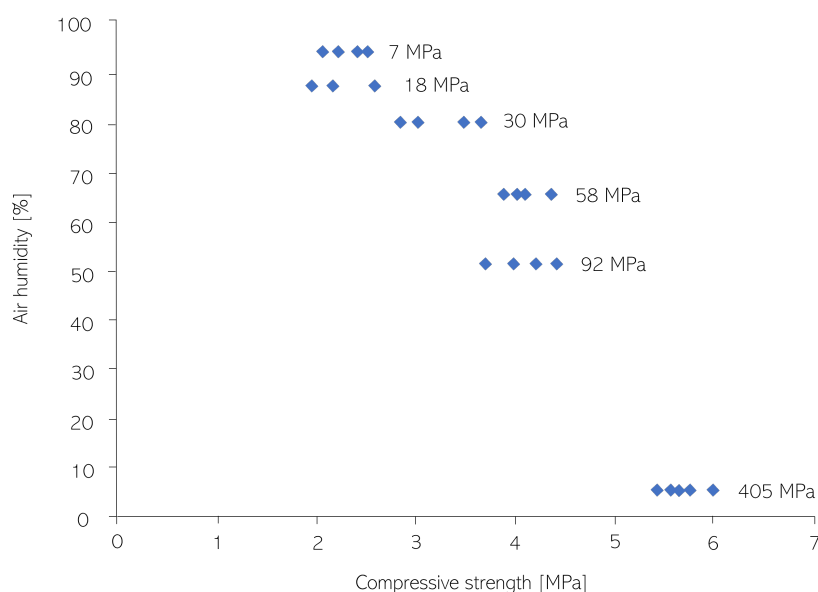


Figure 4.18: Effect of humidity on strength (adapted from Ref [97])

Effect of water on durability

Water penetration into walls can be caused by different mechanisms but mainly from absorption from the surrounding ground, and rainfall, which causes erosion. Rain and frost are the most destructive natural actions causing deterioration. Apart from erosion, the effects of water penetration can lead to decrease in mechanical strength, increase in freeze-thaw effects as well as increase in swelling/shrinkage. The degree of deterioration caused by these effects depend on the soil composition, clay mineralogy and existing moisture content of the structure.

Another effect caused by water penetration is efflorescence. Efflorescence shows as white streaks on a wall surface and is caused by cycles of wetting and drying of an earthen material containing cement or lime. It can also be caused by the transport of soluble salts from the subsoil aggregates or ground water, which re-crystallise at the surface after water evaporation. Efflorescence is detrimental to the appearance of wall. Other similar effects of water penetration are surface soiling or deposits of other staining material as well as damages to thermal insulation properties. This can be caused by cold earth walls in winter being heated.

Erosion is caused by incident rainfall and rain splash at the foot of walls. With significant water content, internal cohesion of the material decreases. For the same amount of water, strong but short rainfall is less erosive than prolonged rainfall as the water has more time to penetrate the material. The angle of the rain, which is determined by the wind speed (kinetic energy), is also a factor on the degree of erosion. It has been found that lower impact angles leads to more erosion. Long term studies on erosion are rare and expensive and therefore, not much literature is on it. Bui et al.[103] investigated stabilised and unstabilised RE walls exposed to natural weathering for 20 years in a wet continental climate. For SRE walls (5% by dry weight of hydraulic lime), the mean erosion depth was about 2 mm (0.5% wall thickness). For URE walls, about 6.4mm (1.6% wall thickness). The results concluded that erosion of RE walls is not a linear function over time and that the walls initially showed more erosion on the surface, due to the loss of compaction energy caused by friction on the formwork, but over time the erosion stabilises. Earth material in contact with formwork is less compacted and therefore more eroded. Two functions, a linear and a non-linear, were used to assess the durability of

URE and SRE walls, Fig. 4.19. Using the linear function, URE walls take 63 years before these walls are eroded to 5% thickness. For SRE walls it is 204 years. Using the non-linear function, the lifetimes of URE and SRE may be much longer. There is no scientific data giving an exact function and therefore it is currently impossible to estimate the lifetime of these walls using non-linear functions. The data is also only valid for the climate zone studied and it is hard to ‘extrapolate’ for other climatic zones.

Another study in Massachusetts, USA [104], exposed an unstabilised, uncoated rammed earth wall for 9 years. It showed an erosion depth between 5 and 7 mm, which corresponds to an annual rate between 0.55 mm/year and 0.77 mm/year. The difference in erosion rates between the two studies are likely due to different earth materials, construction methods and measurement techniques rather than climate. The climate at the two sites are rather similar with average annual precipitation at 1000 mm, average temperature in august a bit above 20°C, January 0°C and frost commonly occurring during winter. Erosion can be limited by regular maintenance of the building envelope. Taos Pueblo in New Mexico, USA is an example of this. It is a complex of adobe houses dating back almost 1000 years and still inhabited by around 150 people. The houses need regular maintenance to prevent progressive erosion. This consists of application of a fresh sacrificial layer of mud over the external wall surface every year [45].

Effect of fire, wind and solar on durability

Other aspects that effect durability of earth constructions are fire, wind and solar radiation. Stabilised earth buildings are particularly vulnerable to fire as high temperatures can produce a loss of inter-granular cementation and can therefore rapidly damage them. Wind is a moderate threat to earth structures that may be sensitive to surface mechanisms (erosion and abrasion). Solar radiation is limited to an unaesthetic discoloration of photosensitive binders like polymer-stabilised earth. Damages caused by wind and solar radiation progress slowly and can be counteracted by regular maintenance of the building envelope.

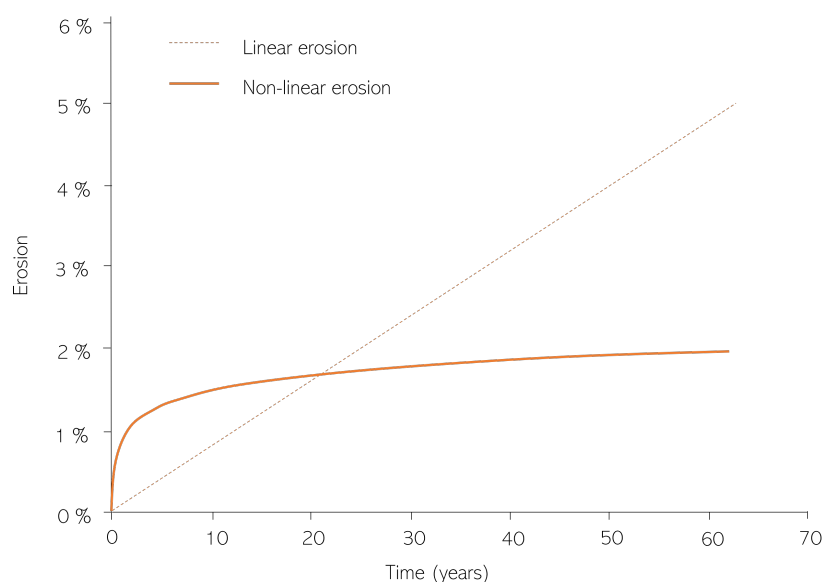


Figure 4.19: Linear and non-linear erosion over time (adapted from Ref [103])

The impact of water, fire, solar, wind on durability of earthen structures and chemical agents or other methods to prevent the impact of these is still unclear due to absence of detailed investigations at field scale. Durability can be increased through design by making sure good foundations are designed to prevent capillary flow and roof design such as overhangs to prevent exposed walls to directly impacted by rain. Lastly, the most popular option is to apply surface treatments on earth walls.

Admixtures and post-surface treatments to improve durability

To increase durability, post-surface treatments are used to provide protection against natural weathering to improve the quality of the construction and impart more functions to earth buildings. The most popular surface treatments are silicone-based water repellents, which can provide long-term protection against natural weathering. Kebao and Kagi [105] found that addition of 0.05% of a silicone-based water-repellent admixture to a cement SRE reduced water absorption by 80% in comparison with untreated material. For internal surface treatments, surface sealings or renderings can be done. Oil-repellent (stain resistant) sealers can be ideal for areas like kitchens, bathrooms, or public areas where repeated cleaning is required. Repeated cleaning of an earthen surface is not recommended as they are not strong enough for repeated harsh cleaning. Other surface treatments are coatings on the interior and exterior surfaces.

4.7. Challenges in current earth building technology

Earth materials, while they have many benefits for their ecological quality and indoor climate regulation, are not widely employed in mainstream construction due to the following limitations:

- limited durability against weathering, erosion due to exposure to rainfall
- frequent need of earth stabilisation via chemical, biological or physical methods, which can increase the carbon footprint of the material.
- uncertainty related to the mechanical performance of the unstabilised and stabilised earth. Due to the fact that each earth material has a specific mineralogy and chemical composition which has a direct influence on the mechanical properties. For stabilised earth, it is difficult to define a stabilisation method that works for all types of soils. It is more common that a stabilisation method is tailored on the specific earth material, due to a variety of reasons i.e. local availability of the stabiliser to its chemical affinity with the earth, costs, environmental impact. A broad diversity of stabilisation methods exist and is being developed making it difficult for potentially standardising earth materials. It is difficult to predict the influence that the various types of stabilisation have on the mechanical behaviour of earth materials. Which may require numerous and expensive laboratory testing before reaching an appropriate understanding of the mechanical performance of stabilised earth.
- uncertainty related to the measurement of properties due to lack of standardised ways for testing and measuring.
- construction techniques relying heavily on manual labour.

Despite these limitations building and research in earth building materials has gained a lot of interest in the last decades and will continue to do so. Efforts are being made into understanding the material, building guides and faster construction methods.

5

Additive Manufacturing for Earth Construction

This chapter aims to describe the state of the art of additive manufacturing (AM) in the context of earthen structures. An introduction to AM technologies and processes will be given, especially that in 3D concrete printing (3DCP), followed by potentials in the new shotcrete 3D printing (SC3DP). Thereafter, highlighted studies and demonstrations of digitally fabricated earth structures will be presented. The chapter also aims to highlight the inter-dependencies of material, manufacturing and design process in the world of digitally fabricated structures.

5.1. Additive manufacturing and 3D printing

For a few decades now, the construction industry has been slowly shifting towards digitalisation and automation. AM techniques and 3D printing are set to revolutionise the industry, as they enable the fabrication of complex geometrical elements directly from a 3D computer model, through the process of a layer upon layer build-up [106]–[108]. The advantages, which include increased geometric freedom, reduction in human labour, cost and time, reduction of materials, lower risks and increased safety, has the potential to create custom products with high precision and accuracy [76], [109], [110]. The potentials have led to extensive research in the areas on understanding materials and properties that suit these methods, creating numerical models that simulate these techniques, and printing prototypes from connection elements, to components, to full-scale buildings to better understand these processes [111]–[115].

3D concrete printing

In the context of the building and construction sector, the term AM, now mostly refer to three-dimensional concrete printing (3DCP) with an extrusion-based manufacturing process and it is one of the areas in construction being rapidly developed [116]. Some research have also focused on metals and polymers, an overview of these can be found in [25], [117], and new materials pop up all the time. 3DCP uses cementitious material which gets extruded through a nozzle as a continuous filament in a layer-by-layer build-up

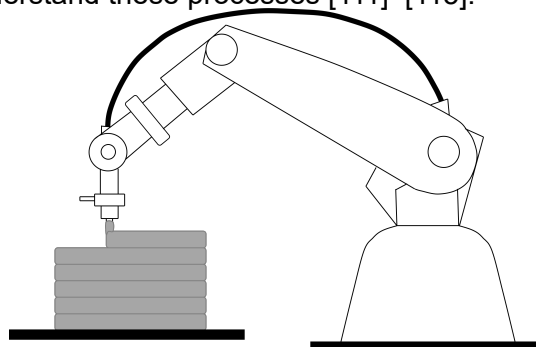


Figure 5.1: Process of 3D concrete printing



Figure 5.2: First 3D printed office in Dubai [122]



Figure 5.3: First 3D printed bridge, Netherlands [123]



Figure 5.4: "The Bridge Project", Netherlands [124]



Figure 5.5: Project Milestone, Netherlands [125]

[118]. It was inspired by Koshnevis et al.[119] contour crafting method, originally conceived as a method to construct molds, but the first studies on 3DCP were at the University of Loughborough. Since then numerous research and academic institutions have reported findings on various aspects of 3DCP, most notably from the Technical University of Eindhoven [115]. Noteworthy 3DCP construction projects incl. 10 houses fabricated in less than 24 hours performed by Chinese company, WinSun, in 2014 [120], [121]. The first 3D printed office, in Dubai 2016 [122]. A bicycle bridge in the Netherlands, opened in October 2017 [123]. "The Bridge Project", aka. the world's longest 3DCP cycle and pedestrian bridge in Nijmegen, Netherlands, opened in 2021 [124]. Project Milestone, Eindhoven, Netherlands which is currently being tested for living [125]. More examples of successful 3DCP is found in [126]–[130].

Shotcrete 3D printing

Shotcrete 3D printing (SC3DP) is a new AM method with sprayed concrete based on conventional shotcrete technology. SC3DP is a robot-controlled process that builds up concrete components layer by layer through the controlled addition of compressed air. Compared to extrusion-based methods, sprayed concrete has several different advantages. It is fast, easy to apply on all kinds of surfaces and allows the integration of reinforcement even with non-standard geometries. It is possible to spray not only as horizontal layers but possible to be placed laminar on surfaces with altering orientations, Fig. 5.6. The method has the potential to produce large scale structural free form concrete elements with large overhangs and reinforced concrete elements with a high surface accuracy and quality. Table 5.1 shows how SC3DP can overcome some of the current technical challenges in 3DCP. The method takes inspiration from conventional shotcrete, which has been used for around 100 years, mainly in tunnel construction and the mining industry [131]. Fig. 5.7, 5.8 demonstrate the potentials of SC3DP so far.

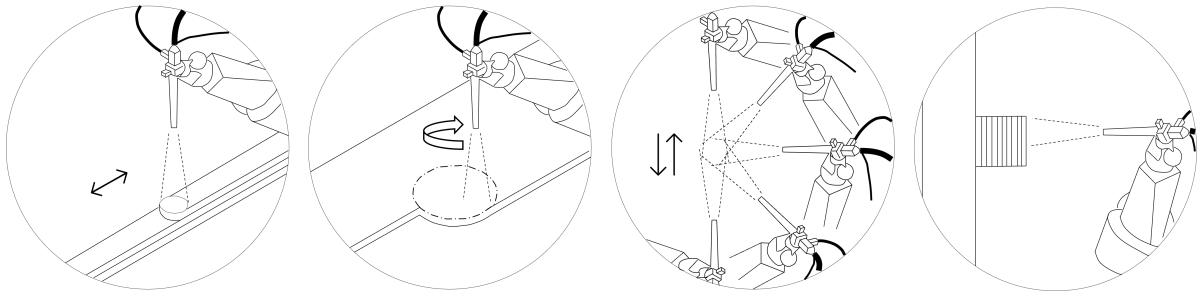


Figure 5.6: Opportunities of SC3DP (adapted from Ref [131])



Figure 5.7: Reinforced curved wall using SC3DP [131]



Figure 5.8: Cylinder with overhang using SC3DP [132]

Technical challenges in 3DCP	Solutions investigating	SC3DP
Interlayer bonding	Layer bonding through gluing, material research	Intense layer bond through the projection of material which creates layer intermixing
Integration of tensile reinforcement	Post tensioning	Sprayed material can flow around the structural reinforcement and embed it
Creation of pronounced overhangs	Hybrid printing through support material	Creation of pronounced overhangs can be realised by gradually transitioning from horizontal to vertical printing plane
Surface quality	Simultaneous troweling during printing	Second layer of concrete can be sprayed and subsequently smoothed

Table 5.1: Advantages of SC3DP over 3DCP (partially adapted from (Ref [25], [117], [131]))

5.2. AM in the context of earthen construction and architecture

AM processes are especially interesting in the context of earth construction, as it can help revive the interest and knowledge in earth material and building techniques as well as open up new opportunities for earthen architecture. Existing fabrication methods in earth construction are based on tradition, transferred orally and include manual labour [5]. New fabrication methods in earth construction include robotic rammed earth, 3D printing extruded earth, and sprayed earth [133]. Some demonstrations show the potential of this new direction in modern earth architecture but very few studies have looked into the mechanical properties and structural feasibility. The results are few and scattered.

5.2.1. Robotic rammed earth

Robotic rammed earth is a semi-automated system for the production of standardised rammed earth components. Layers of earth is compacted by a pneumatic rammer or heavy vibratory plate in a robot guided slipform. This fabrication method minimises material and labour requirements [133].

5.2.2. 3D printing earth and clay materials

Following the rapid growth of 3DCP, the method has in recent years also been studied and implemented for clay and earth building materials due to environmental potentials. One prospect is with 3D printed clay formworks for concrete construction. With the rise of 3D concrete printing and the search for new geometric possibilities. 3D printed formworks has been under investigation for structural and nonstructural applications and their potential for making concrete construction more sustainable. 3D printed clay formworks have been demonstrated as a solution to create more freeform 3D printed concrete structures. Due to the plastic properties of the material, it can easily be washed away for demolding, then shaped and reused for other projects [134].

Studies involving 3D printed clay for the design and construction of building components have been demonstrated by Kontovourkis and Tryfonos in [135], [136]. The studies look into the influence of 3D printing parameters in the early age design of clay components to assess their impact on 3D printing performance, focusing on geometric conformity aspects. Influence of parameters included layer height, wall thickness, infill density, extrusion velocity and nozzle diameter. In [135], overall printing time was evaluated for a conventional and non-conventional wall in a comprehensive parametric investigation.

3D printing of earthen material has been studied by Perrot et al. [137] and Gomaa et al. [17]. Perrot et al. looked at the early age yield stress and Young's modulus development over time. Two earthen mixes, one with alginate (stabilised) and one without (unstabilised) were compared for their strength and buildability. The addition of alginate proved to give higher and faster strength gain and less deformation, which allowed for faster fabrication time compared to the mix without alginate. For the mix without alginate, the only mechanism that induced strengthening of earth was drying. This slow hardening process can be an explanation for why unstabilised earth is not widely used in industrial applications. The study proved that a binder is required for faster fabrication time and better strength. A high water-content in mixes are required for extrudability. Both mixes had a consistency close to the liquid limit of the soil. This study is the only study so far about early age printed earth properties.

Gomaa et al. [17] examined the structural feasibility of a 3D printed earthen wall for low-rise construction. The material mix developed is likened to traditional cob due to the inclusion of straw fibers. The investigation first tested 3D printed earth cylinder specimens for compression to obtain key mechanical parameters, compressive strength and Young's modulus. These properties were then used to examine three wall patterns and their load carrying capacity based on limit state design. The results were then implemented in an idealised case study considering a 1 -and 2-storey building. The case study showed that 3D printed earthen walls have the potential to sustain the typical loads of a low-rise residential building. It also has the potential to emerge as a strong competitor to conventional concrete and 3D printed concrete for low-rise construction.

5.2.3. Sprayed earth

Sprayed earth also known as shotearth or PISE (Pneumatically Impacted Stabilised Earth) is a process that comes from conventional shotcrete. PISE, first invented in the 1970s by David Easton, is a dry cement-earth mix which is conveyed by air pressure to a spray nozzle where water is added at the nozzle. The mixture is sprayed with a high pressure against a single sided formwork where thicknesses of 60 cm can be obtained. Conventional steel reinforcement cages can be integrated with this method [7], similar to the mesh mould method developed at ETH Zürich, see Fig. 5.13. Not many projects have been demonstrated with sprayed earth. Easton implemented the technology on a few small projects in the 80s in California, USA, before deeming it too expensive. A similar concept to PISE developed by French architect Stéphanie Chaltiel together with Summum Engineering, involves a flying drone spraying soil onto a lightweight textile membrane structure. The goal of this project was to demonstrate a way to build emergency shelters in disaster areas [138]. Aside from these demonstrations, sprayed earth materials have mainly been used for internal plastering where clay plaster is most commonly used [19].

Studies that quantify sprayed earth have largely been non-existent until recently when Curto et al.[139] studied the mechanical properties of a sprayed earth mix with cement and found compressive strengths up to 9.5 MPa. The results of this study can be likened to a low strength concrete and highlights the benefits of locally excavated earth as a potential sustainable construction material, albeit with cement. Experiments are currently being performed in Eindhoven with Jelle Feringa and in TU Braunschweig, one of the universities that also started SC3DP.

5.3. Material and processing requirements for digital earth

The material and processing requirements of earth materials can be drawn from research in concrete extrusion and spraying. It is assumed that these requirements are the same.

5.3.1. Material requirements

Most research into material requirements for AM have been in 3DCP. A few have looked into SC3DP where requirements are taken from conventional shotcrete. However, due to the novelty of the method very little research has been published on it.

Fresh properties

In 3DCP, workability, extrudability, flowability, buildability, pumpability, and open time are defined parameters of concern [140]–[143], Table 5.2 describes these terms in detail. 3DCP mix design is based on wet mixed mortars used in spraying applications. Fresh state of printed concrete is important to understand its buildability, which is the ability to obtain the desirable shape with minimal deformation and avoiding collapse. The extruded material should be able retain its shape under its self-weight, weight of subsequent layers and resist the stresses generated by self-weight. This is known as thixotropy. Workability and extrudability depend on the thixotropic behaviour of the material where high thixotropy means better shape stability [144]. Flowability and buildability depend on the rheological requirements. This demands for a pasty consistency of the material.

Fresh state concrete can be assumed as a visco-plastic Bingham material that presents a viscous behaviour. It usually flows when the stresses surpass its yield stress. Properties relevant for determining the ability to print of concrete materials are:

Terminology	Definition
Workability	The ease of placement and easy compaction without segregation
Extrudability	Ability of a material to be extruded through a nozzle with minimal energy required
Flowability	Characterised by the Bingham model where dynamic yield stress and plastic viscosity are obtained. The steady state after strong continuous shear.
Buildability	The ability to 3D print layer by layer to reach a target height without significant deformation and collapse.
Pumpability	Ease of transporting the material from the reservoir to the nozzle
Open time	An aspect that determines workability. The time that the material is dispensed continuously through the nozzle without stopping or clogging.

Table 5.2: Key terminology used in 3D concrete printing

- Rheology
- Stress-strain behaviour
- Time-dependent behaviour

Elements can fail in one of two ways:

1. Strength based failure criterion, also known as plastic collapse is based on yield stress. An adequate yield stress is crucial to assure stability after deposition of the printed layer, to resist gravity load from the layers above.
2. Stability based criterion, also known as elastic buckling is based on the maximum printable height, which depends on Young's modulus. Buckling failure is related to successive lateral deformation and second order effects.

Determining stiffness and yield stress is required to develop models that predict failure by buckling or plastic collapse, respectively. These models are validated by comparing results from FE analysis with printing experiments. Stiffness is tested and monitored based on deformation, which depends on Young's modulus and is quantified by either stress-strain relation using the unconfined compression test for cylindrical specimens (ASTM D4648), optical metrology, or PZT (piezoelectrical transducers) that assess stiffness gain and damage evolution, thereby ensuring stability of the stacking process. Time-dependent yield stress depends on cohesiveness of cement paste, which is suggested by authors to resemble the behaviour of a cohesive soil, as failure in compression result from relative movement of particles. Strength is attributed to a combination of inter-particle friction and cohesion, which can be translated by a Mohr-Coulomb yield criterion, similar to cohesive soils. An alternative way to perform yield stress analysis is through the dynamic stress sweep method using an oscillatory rheometer, which allows proper reproducibility of results and minimizes wall slippage problems in high-viscosity mortars [145].

Clay extrusion is essentially similar to concrete extrusion. A ceramic slurry or paste is pushed through a numerically controlled deposition tool. The structural buildup is achieved due to the non-Newtonian shear-thinning rheology of the extruded paste: once the shear-inducing extrusion process ceases, the viscosity of the material increases. The printed parts are typically very fragile and soft and usually rely on a postprocessing stage like drying or sintering to achieve the necessary mechanical properties [134].

Fresh properties in SC3DP

The material requirements of SC3DP are similar to those of 3DCP in terms of rheology, stress-strain behaviour and time-dependent behaviour. The main difference is the addition of admixtures and accelerators at the spray nozzle where setting behaviour and load-bearing capacity of layers can be better controlled [146].

Hardened properties

It is possible, in printed material, to achieve greater material density and strength similar to cast materials. This is yet to be proven on a commercial scale. Due to the printing direction of 3DCP objects, the material exhibits anisotropy. To minimise this effect research is currently performed on the following: improving layer adhesion, bulk-density and underfilling, tensile reinforcement, shrinkage and durability. Measuring hardened material properties is also not standardised.

Tensile strength and ductility

One of the biggest challenges in 3DCP is the inability to introduce steel reinforcement. Many concepts to integrate steel reinforcement have been proposed as well as printable concretes with fibre reinforcements and textiles have been developed but better integration and automated processes are still being investigated. An comprehensive overview of solutions for integrating reinforcement AM for concrete can be found here [147]. A limitation of fibre reinforced concrete is that improvement in tensile strength is mainly observed when tested parallel to the direction of printing, as fibres orient themselves in the print direction due to the extrusion process [148]–[151].

Hardened properties in SC3DP

SC3DP seems to be able to overcome the challenges of layer adhesion, bulk density due to the spraying that increases particle interlocking. The acceleration of material caused by compressed air gives higher compaction of concrete as well as good mechanical bond between successive layers, reducing cold joints. High bulk density or low porosity can be achieved which results in good strength and durability properties of the manufactured components. The versatility of the nozzle and spray directions means that tensile reinforcement can easily be integrated. These aspects give the possibility to print complex 3D concrete components. There is no published research on the shrinkage and durability of SC3DP structures yet but these are highly dependent on the mix design [131], [146].

5.3.2. Processing requirements

The mechanical behaviour of the material is also dependent on the processing parameters as well as the geometry being printed (geometrical effects will be discussed in chapter 7). The variation of the process parameters influences the target values to be achieved.

Overview of robotic systems

There are a number of 3D concrete extrusion or spray based systems adopted in both research and industrial applications. These are (adapted from [145]):

- Gantry system. A large frame structure that mimics smaller printing systems. Only three main movements, translation in x, y, z directions are allowed.
- Delta system. A nozzle hangs from cables that can be raised and lowered enabling non-linear motion, so a larger printing area can be reached.
- Stationary industrial robotic arm system. Three translation and rotation movements are permitted increasing printing flexibility.

- Cooperative small mobile robots. Each robot is able to move on a defined region in a shared environment with other robots and contribute as a whole to a larger task.
- Mesh mold system. Spraying concrete over a printed mesh. The mesh works as host formwork to receive shotcrete, which allows curvatures that could not be possible to obtain using a layer-by-layer extrusion process without formwork.



Figure 5.9: Gantry system [152]



Figure 5.10: Delta system [153]

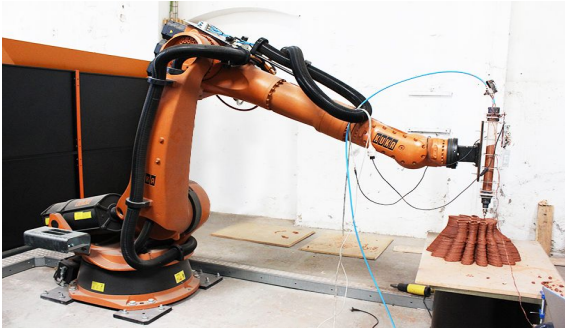


Figure 5.11: Industrial robot arm system [154]



Figure 5.12: Cooperative robot [155]

Processing parameters in 3DCP vs. SC3DP

Fig. 5.14 shows the different processing parameters involved in 3DCP and SC3DP processes. In SC3DP, there are more process parameters to consider compared to 3DCP. A large number of these have to be kept in a constant ratio in order to achieve a homogeneous concrete application and acceptable accuracy.

Little is currently known on how much processing parameters influence the mechanical strength of a printed object. Chen et al. [157] showed that time between printed layers and nozzle distance to target plays has an influence on the resulting interlayer bond strength in 3DCP. For the printing of overhangs Carneau et al. [158] showed how maximising these two processing parameters can give bigger overhangs. A dome and a Nubian vault was created as proof. In SC3DP, Dressler et al. [159] showed that deposition rate and printing speed have nearly linear dependencies on the layer thickness. Spraying distance has a linear influence



Figure 5.13: Mesh mould system at ETH Zürich [156]

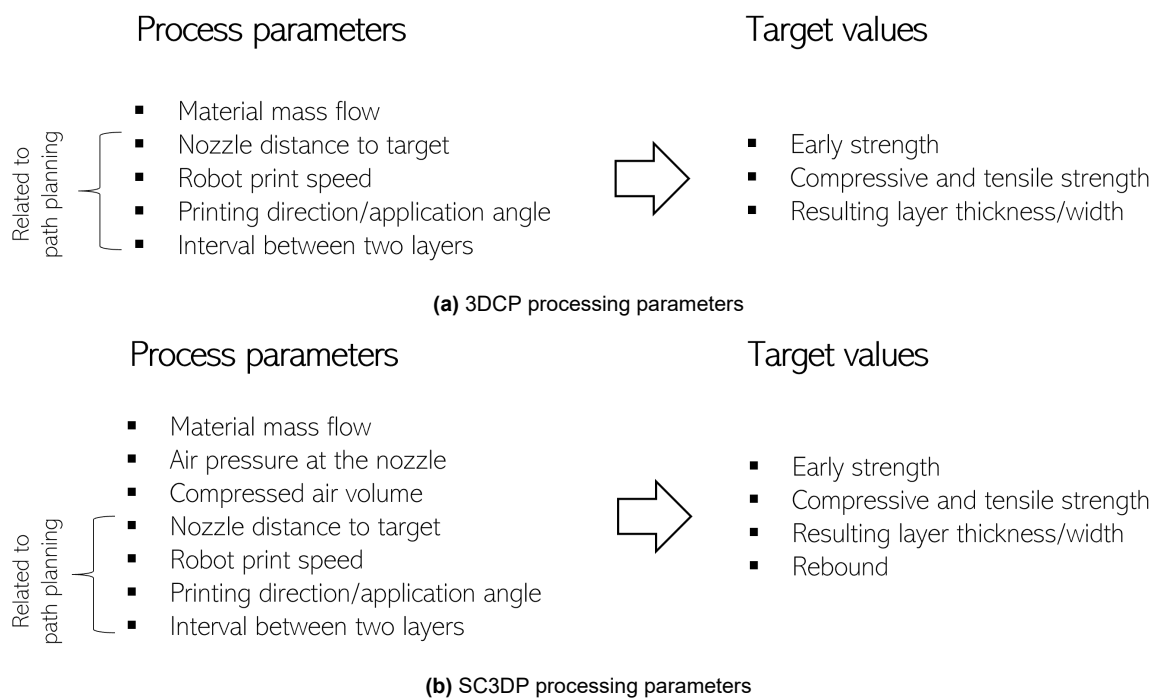


Figure 5.14: Comparison of processing parameters in 3DCP and SC3DP and their target values

on the layer width and height. Air flow also has a major influence on the material distribution and therefore the resulting layer geometry and rebound. No full-size structure has yet been printed to fully understand these effects on a geometry.

Printing resolution, direction and toolpath planning

Other effects that affect a resulting geometry are printing resolution, the direction and toolpath planning. Little research has studied these in depth. In 3DCP, several different processes have been developed, which can be divided into three types depending on filament size [160].

- Fine filaments are less than 1 cm in diameter
- Medium fine filaments are in the range of several cm
- Coarse filaments are in the range of several dm

The printing resolution depends on the size of nozzle which in turn depends on the maximum aggregate size in the mix design as well as project requirements. Fine filaments allow for higher printing resolution, greater precision and geometric complexity. Larger filaments allow for higher productivity and use of coarser-grained concrete which reduces the need for cement and less shrinkage. Three-axis printing devices with filament size of several cm are most commonly found in research.

Also in 3DCP, the printing direction affects the compressive and flexural strength due to the anisotropic behaviour of the material. For the toolpath planning, geometry plays a key role in the development of an efficient 3D printing process. In 3D concrete printing of architectural elements, interior of structural elements are filled with "space-filling" or "hatching" material which aims at giving structural stiffness but also material minimisation. Thus different infill geometries and strategies can be found in research. This is related to the toolpath generation which have potential for further material optimisation. The toolpath is dependent on the fresh material properties, the desired hardened properties, processing parameters as described above, and geometry [135].

5.4. Design and computational modelling

Numerical models in 3DCP are actively being developed but are at their infancy. There are currently three known methods developed in 3DCP to model buildability. The first is the method by Suiker [161] who developed a mechanistic model which considers elastic and plastic buckling. The model was verified by experiments which underestimated the number of layers by 10%. The model is limited to straight wall geometries. An open source tool based on Suiker's methodology has been created by Witteveen +Bos using Karamba3D for the FEM analysis. This method requires data of compressive strength and Young's modulus over time. The second method is by Wolfs et al. [116]. This method is based on the Mohr-Coulomb failure criterion, parameterising the cohesion and angle of internal friction of the material. Mechanical properties for the numerical model was developed through compression test and direct shear test. The model and analysis was performed using ABAQUS. The model was verified with experiments and showed to overestimate the number of layers by 25%. However, the model was able to predict the failure modes of the experiment, elastic buckling and plastic collapse. An open source tool based on Wolfs et al. is Voxelprint, a plugin for Grasshopper, with FEM output to ABAQUS. The third method is the extended lattice model by Chang, Schlangen, Savija [162]. This model is based on the discontinuous formulation, which avoids singularity related issues in continuum-based numerical methods. The model can be used to simulate green strength and printing process and it takes geometric and material nonlinearity into account. Imperfections during printing can be implemented in the lattice model. Comparison of numerical model to experiments has not been performed to verify the model. It is important to note that the current numerical models evaluates buildability, while factors such as imperfections, plastic shrinkage, creep and other material factors are not considered.

Computational modelling for SC3DP

There are currently no developed computational models for SC3DP. Computational models developed in 3DCP can be used and extended to SC3DP. Modelling parameters such as flow rate, air pressure, nozzle distance to target would require computational fluid dynamics and DEM modelling.

5.5. Challenges of AM technologies with earth building materials

Research into both AM technologies and earth building materials are at their initial stages. Although there have been successful demonstrations combining the material with the fabrication method. Many challenges need to be overcome for this to become widely implemented in the future. The main challenge surrounding current earth construction with AM processes is the lack of material research. Earthen materials when going through an AM fabrication process requires high water content but little is known about its shrinkage behaviour which will influence the precision of and quality of the resulting construction. More research into shrinkage behaviour can allow for higher print accuracy. Due to this, tolerances between -20/+40 mm is advised for the design of walls. This also leads to difficulties in detailing. Furthermore, 3D printing of granular materials generally lack larger aggregate sizes. This has an impact on the durability and erosion of a structure, which needs to be addressed either in the mix design or post processing of elements.

As construction continues to move toward digital fabrication, traditional design strategies and geometries need to be reevaluated for the material and process constraints related to the

fabrication. The challenges here can also be applied for earth materials. In 3DCP, the main material constraints are the low yield strength of early age concrete and the lack of tensile strength, which limits the production of non-supported structures i.e. slabs and overhanging elements. Tensile strength requirements can be enhanced by incorporating reinforcement or fibres and different strategies has been proposed and is currently researched. Another way of overcoming this challenge is to optimise the design of a structure to maximise its reliance on compressive strengths. This requires a fabrication strategy that can enable this, which are currently being developed and refined [25].

Other current challenges is the development of analysis tools that can integrate both the material and process limitations to can enable accurate predictions of fabrication and structural behaviour of components. These tools will have the potential to expand design flexibilities even further [25]. Strategies to transition from computer models and small prototypes to full-scale construction is also being developed. As scale and complexity of structures increase, appropriate toolpath generation strategies are required. For the printing process, the transition to large scale construction brings about challenges where Gantry and Delta systems need to be larger than the structure. Robotic arms might involve large operational costs due to acquisition of several robots and complex operations to move them around the construction site. Although 3DCP and SC3DP methods have different processes, similarities can be drawn between the two techniques. Therefore challenges in 3DCP can be applied to SC3DP and shotearth 3D printing.

6

Design and Model Part 1: Defining material models

This chapter aims to define shotearth material for exploring the design space of shotearth structures. It aims to combine the theory regarding earth material properties with the SC3DP fabrication method, which can be termed shotearth 3D printing, SE3DP. The process and assumptions used for the prediction of material models are described and discussed.

6.1. Material and processing requirements for SE3DP

From the previous chapter, it was learnt that both material and processing requirements need to be taken into account for the definition of shotearth material. Therefore, it will be assumed that shotearth 3D printed structures take the same material requirements as 3DCP but for earthen materials, which was researched in depth in Chapter 4, and the same processing requirements as SC3DP, here termed SE3DP.

Computational modelling of SE3DP

Due to the infancy of current numerical methods to model printed structures, to determine shotearth structures, the numerical method chosen for this study will follow the Suiker model where early stress and stiffness development governs the stability of the structure. This is due to the readily defined tool in Karamba by Witteveen+Bos and the parametric opportunities within the Grasshopper environment. The Wolfs method using Voxelprint requires access to Abaqus. Due to the limited access given to students at the TU this option has not been further investigated. As a result the material prediction will follow the requirements from this modelling tool.

Knowledge of fresh properties from literature

The studies found on unstabilised 3D printed earth and clay materials suggest that the material when going through a 3D printer resembles traditional cob, adobe, earthen mortar or poured earth. Both Perrot [137] and Gomaa [17] compared the rheology and properties of their 3D printed earth-based material to traditional cob due to the high water content in both mixes. This ensured extrudability when passing through a robotic nozzle. Therefore, printed earthen materials can be assumed to be close to the liquid limit on the water content scale and shotearth can be assumed to be the same. Fig. 6.1 shows common earth building techniques according

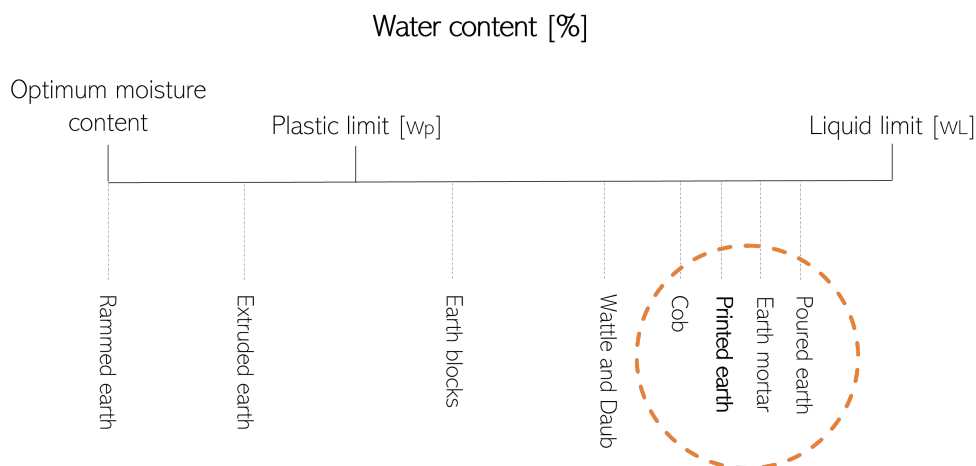


Figure 6.1: Water content of different earth building applications and where printed earth is assumed to be

Type of test	Perrot & Gomaa	Curto	Unit
Compressive strength	0.87 -2.25	9.50	MPa
Youngs modulus	20 -22.9	9707	MPa
Poisson ratio	0.22	0.15	
Direct tensile strength	N/A	1.16	MPa
Flexural strength	N/A	2.04	MPa
Shear strength	0.15 -0.85	2.45	MPa

Table 6.1: Mechanical properties of unstabilised (Perrot and Gomaa) and cement stabilised printed earth (Curto)

to their water content and where printed earth is assumed to be. The figure assumes that all building techniques has the same soil composition. For time-dependent behaviour, Perrot is the only study found that measured the stress and stiffness over time.

Cement is the most common stabiliser in earth building materials and is most effective when the clay fraction is at a minimum. The one study on sprayed earth has been stabilised with cement and is the only study that gives any indication of shotearth material properties. However, no information is given on its fresh properties. Given that the material requires a similar consistency to 3DCP, cement stabilised poured earth is the closest in this aspect. There are no studies that describe its time-dependent behaviour and also no studies on 3D printed extruded earth material with cement stabilisation. The latest progress in the study of early age material behaviour of 3DCP can be taken as an informed assumption for possible early age behaviour of shotearth with cement stabilisation.

Knowledge of hardened properties from literature

Hardened properties have been measured by Perrot and Gomaa for the unstabilised earth based on the extrusion method after at least 1 day and by Curto based on the spraying method after 28 days, see summary of these in Table 6.1. Integration of fibers and reinforcement to enhance tensile properties will not be considered in this work.

Knowledge of processing parameters from literature

The processing parameters of SC3DP may be applied to SE3DP. The projection of the material via compressed air ensures a high degree of compaction of earth materials. When comparing the three digital fabrication methods for earth materials, robotic rammed earth, earth extrusion and sprayed earth, it can be assumed that in terms of compressive strength, SE3DP will be higher than the extrusion method but lower than the robotic rammed earth method. In terms of geometric freedom, SE3DP is more controlled than the earth extrusion method but more free than robotic rammed earth, potentially resulting in more geometrically complex elements compared to both [133].

6.2. Defining material models for Shotearth 3D printing

6.2.1. Stress and stiffness over time development

In AM, analysis of material development data for the adaptation to a fabrication process is needed but not always available. In this regard, the stress and stiffness development of two forms of shotearth; unstabilised shotearth and cement stabilised shotearth will be predicted and assumed based on the information presented previously on the fresh and hardened properties. The unstabilised shotearth will be based on the data from Perrot and properties gathered for unstabilised rammed earth (URE) from Chapter 4, section 4.4. The cement stabilised shotearth will use the hardened properties from Curto as the target values for a mathematical function that can describe its time-dependent behaviour. The mathematical functions will come from existing models developed in conventional shotcrete and concrete standards. The results will show a lower and an upper boundary prediction of these materials.

6.2.2. Unstabilised robotic shotearth

The assumption for unstabilised shotearth is that its compressive strength lies between 3D extruded earth and URE. This stems from the prescribed influence of the processing parameters.

3D printed earth < Shotearth < Rammed earth

Assumed physical properties

Dry density of 3DP earth measured in Perrot was 1750 kg/m^3 and in Gomaa 1835 kg/m^3 . Average dry density in URE is 2200 kg/m^3 according to the review by Avila et al. [41]. Therefore, dry density for shotearth is assumed to lie between these bounds which also results in the compressive strength to lie between these bounds. Fig. 6.2 shows the assumed water content range of shotearth material in relation to the plasticity index. Fig. 6.3 shows a proctor curve that assumes dry density and moisture content of shotearth relative to URE and 3D printed earth. Assuming same soil composition, shotearth is thought to be close to 3D printed earth mainly based on water content.

Defining the boundaries

As shotearths dry density and compressive strength is between the bounds of 3D printed earth and rammed earth, the strength and stiffness developments over time of these two construction methods have been found. Fig 6.4 and 6.5 show the actual data points from Perrots study,

where yield stress and stiffness, for a mix with alginate and one without, over a time period of 20 and 10 days respectively have been plotted. Only the mix without alginate, unstabilised, is of interest for the lower boundary definition.

For the upper boundary definition, which is assumed to be URE, Fig 6.6 and 6.7 shows the assumed strength and stiffness gain of URE together with Perrots unstabilised data. No actual data exists on the stress and stiffness developments over time for URE, so the curves are based on assumptions. For the strength development, assuming that the URE soil composition is similar to Perrots, through comparison of the water contents known, Perrot measured a water content of 45 %, while from Avila et al. [41] overview of URE properties, it was found that URE water contents typically range between 8- 13 %. This means that URE has less than a third of the water content as 3D printed earth, and also means that URE is going to gain strength quicker than 3D printed earth. Now assuming that both mixes have been exposed to the same environmental conditions during drying, usually at 50% RH and 20°C. The data from Perrot suggests that the material has gained most of its strength at around 166 hours, 7 days, after printing as the curve plateaus afterwards. URE is then assumed to have gained most of its strength at around a third of that time, which results in 2 -2.5 days. Comparing the strength overview from Avila in Table. 4.7 and a few earth construction guides, mainly the German Lehmbau Regeln, whose standard limit is between 2 -3 MPa, URE can be assumed to reach a target strength of 2.5 MPa. The strength at the beginning of ramming is assumed to be at 0.5 MPa.

For the stiffness development of URE, it is assumed to develop the same way as the strength, a linear increase until it plateaus, as Perrots data suggests a similar development. Perrot and Goma measured values between 15-22.9 MPa, while Avila found values ranging from 60 - 1000 MPa, Table 4.7. The big scatter in these numbers can be due to varying soil compositions and testing procedures. It is therefore unknown or impossible to know the stiffness of URE. As a result, the upper bound target stiffness was taken as 60 MPa as it is the closest one to Perrot and Goma's measured range. It has not been possible to find a value for stiffness at the beginning of ramming earth. Therefore the curve starts at the same value as Perrots.

Proposing shotearth strength and stiffness development

Now that the upper and lower bound limits have been defined based on the information available from literature, a curve is proposed for the unstabilised shotearth within these limits. For strength, the shotearth target strength is set at 2.4 MPa as the upper and lower bound limits are quite close. Just above 2.25 MPa reached by Perrot and just below 2.5 MPa assumed for URE. A linear interpolation was reached through the assumption that 95 % of strength will be reached at 7 days, roughly the same time as Perrots. The starting strength is assumed to the same of as Perrots.

For the proposed stiffness curve, as shotearth is assumed to have a similar water content as Perrot, but higher compaction due to the high compaction energy from the compressed air of the spraying mechanism, the stiffness is set at a target at 25 MPa. This is an arbitrary target as stiffness is not widely understood in earth materials. Therefore, a lot of uncertainty is involved in the assumed URE and proposed shotearth stiffness developments. Fig. 6.8 and 6.9 show the result of the proposed strength and stiffness developments of unstabilised shotearth. For detailed calculations of all curves, see Appendix C.

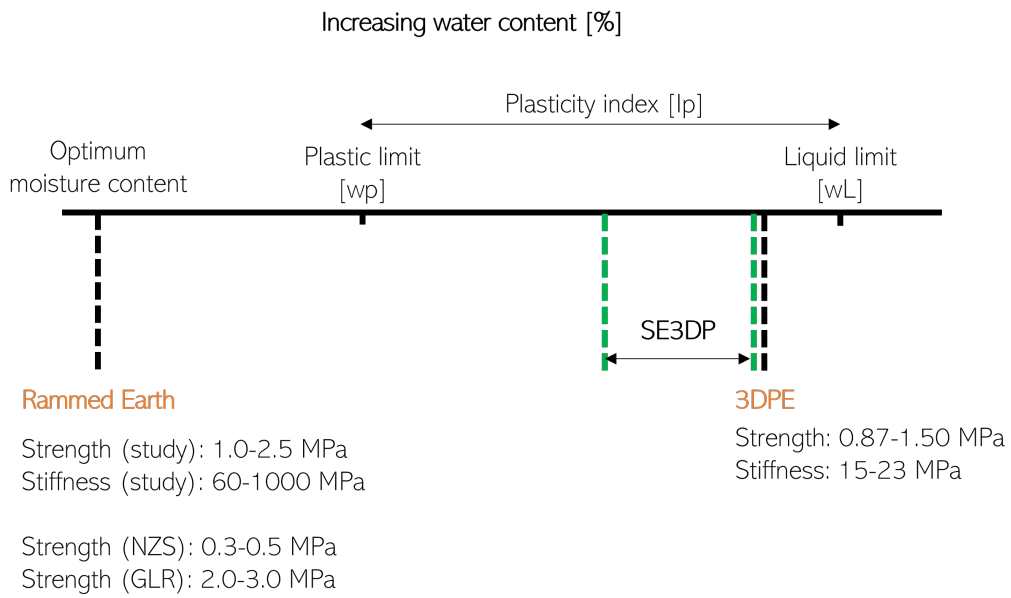


Figure 6.2: Assumed range of SE3DP relative to plasticity index based on data gathered

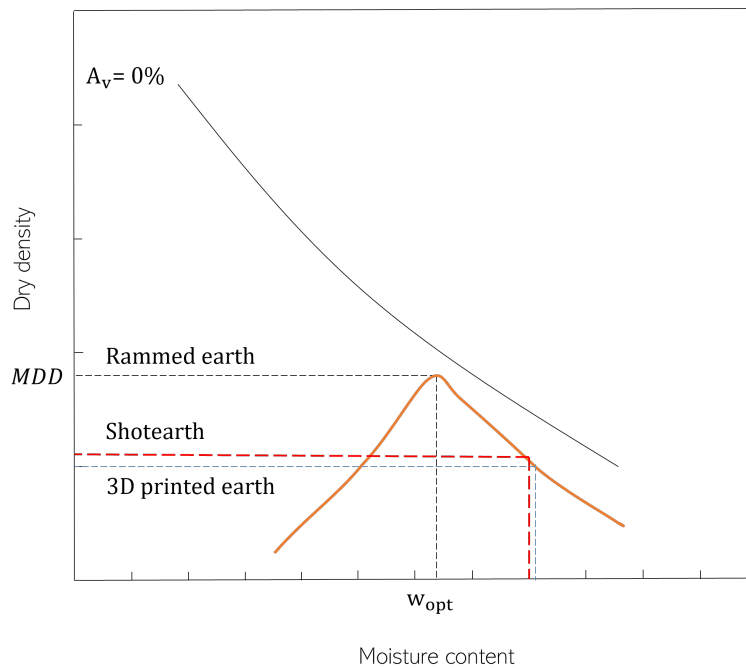


Figure 6.3: Assumed maximum dry density (MDD) and moisture content (W_{opt}) of unstabilised robotic shotearth relative to rammed earth and 3DP earth, assumed same soil composition.

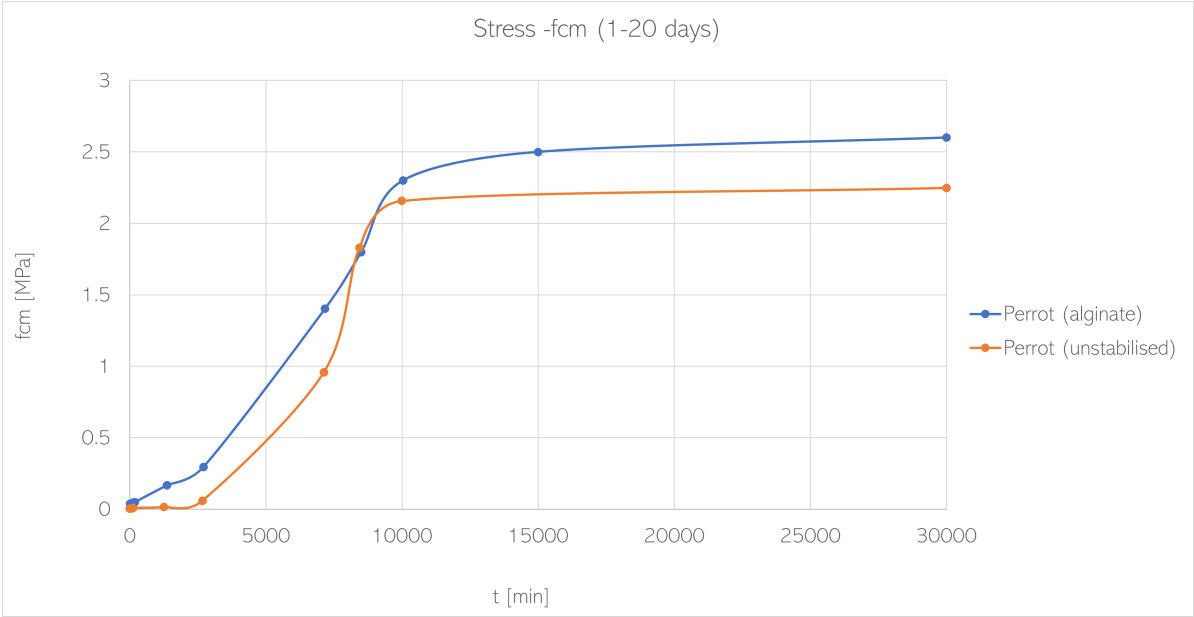


Figure 6.4: Yield stress data from Perrot (adapted from Ref [137])

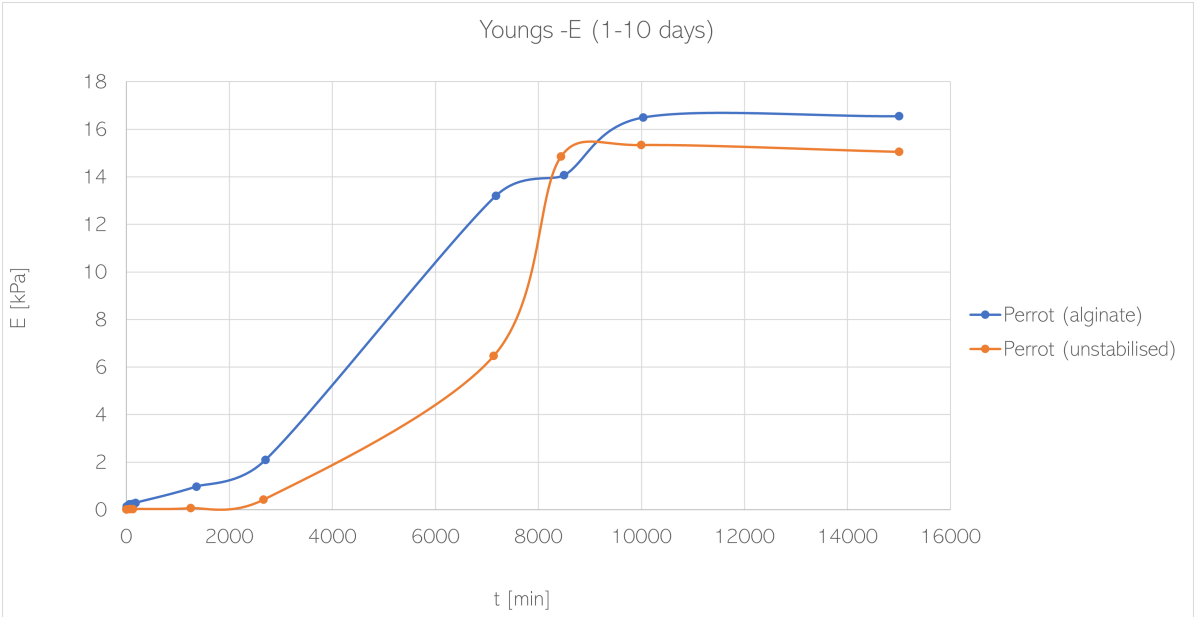


Figure 6.5: Stiffness data from Perrot (adapted from Ref [137])

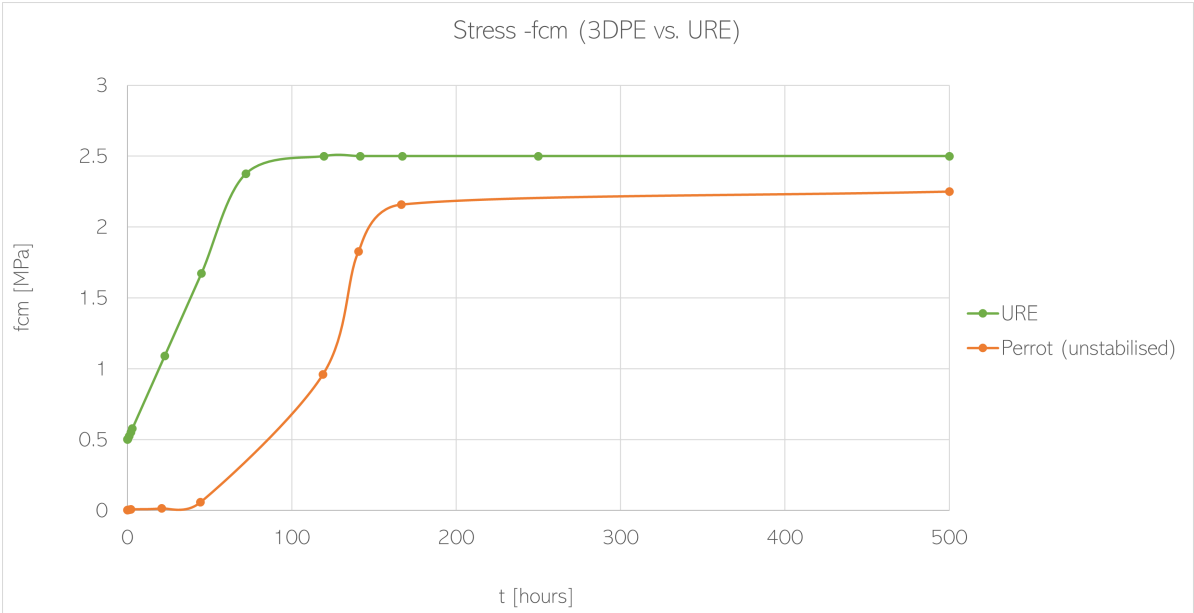


Figure 6.6: Strength: upper and lower limits of unstabilised shotearth

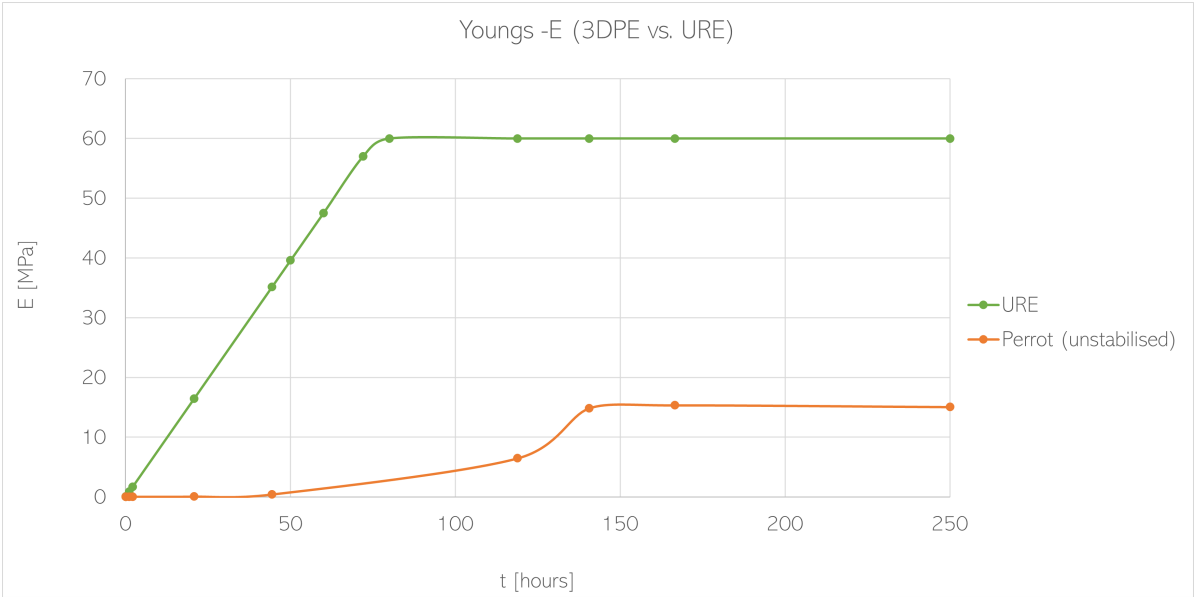


Figure 6.7: Stiffness: upper and lower limits of unstabilised shotearth

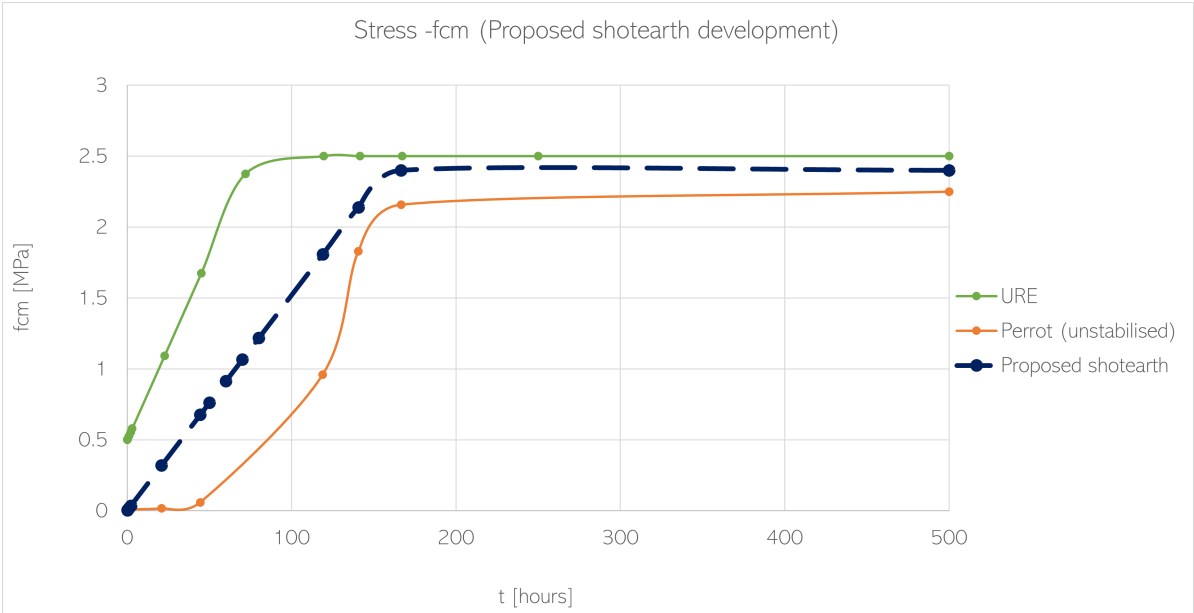


Figure 6.8: Stress: Proposed shotearth relative to the bounds

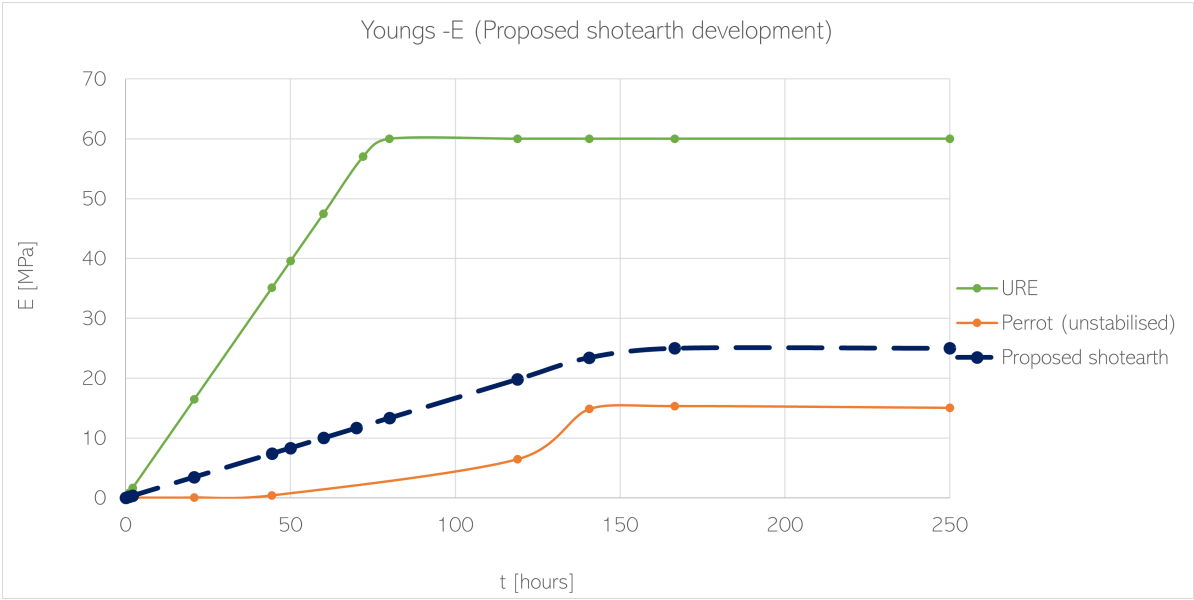


Figure 6.9: Stiffness: Proposed shotearth relative to the bounds

6.2.3. Cement stabilised robotic shotearth

The assumption for cement stabilised shotearth, also termed shotearthcrete, is that its strength and stiffness development is between 3D concrete extrusion and 3D concrete spraying.

3D printed concrete < Shotearthcrete < Shotcrete 3D printing

Prediction of early age development

As described earlier, the study of Curto et al. is the only published paper on sprayed earth which gives some indication on its mechanical properties. However, the measured values are tested after 28 days of casting cube specimens. Therefore, the approach to predict shotearthcrete is different from the approach for the unstabilised shotearth. Rather than finding a range of values where shotearthcrete may be, it is assumed that the values of Curto are the target values that can be achieved. The mix design used in the study contains 7 parts soil, 7 parts sand and 2 parts cement, which results in the mix containing 14 % cement by weight. This is within the range of normal concrete which usually contains between 10 -15 % cement. Therefore, the mix can be partly regarded as concrete.

The attempt to predict the early strength of this mixture has been made through looking into existing conventional concrete codes and shotcrete models used in tunnelling as well as geotechnical models. The inspiration to do this comes from the fact that shotcrete strength development for tunnelling is an active field of research. Soil stabilisation in geotechnical engineering is common practice and well documented. Fig. 6.10 and 6.11 show the results of the strength and stiffness development prediction from two concrete models defined in Eurocode 2, American Concrete Institute (ACI) and four shotcrete models defined in the CEB-FIP code and authors, Aldrian (1991), Weber (1979), Chang (1994). From the two figures it can be seen that the ACI model vastly overestimates both the target strength and stiffness while the other models are more accurate in reaching the target of 9.5 MPa strength and 9707 MPa stiffness. Therefore, the ACI model is not considered any further. Two other shotcrete models by Golser (1990) and Aydan (1992) were also calculated but given that these models vastly underestimated the 28 strength and stiffness, they are not plotted. Other shotcrete models found required data measurements after 1 day, and therefore not used. If more data is known it could be interesting to plot these as well. The equations that describe these developments can be found in Appendix D.1 along with the ones that could be interesting for further work.

No relevant geotechnical models or research in soil stabilisation, soil reinforcement, soil-cement, and cement treated soils (keywords searched) were found due to a large variation in the materials studied. Strength models are most important and more commonly measured over a long period of time, up to 200 days, due to interest in foundation and road construction design.

Fig. 6.12 and 6.13 shows all models zoomed in to early ages between 0 -120 min. It can be seen that a big scatter of developments are found. For the strength development the prediction scatter is between 0.0022 MPa (Weber) and 0.61 MPa (Aldrian & Müller). For the stiffness it is between 228.46 MPa (Weber) and 3582.91 MPa (Eurocode 2). The scatter in developments can be explained by the fact that these models were not designed to describe early age concrete but rather concrete age between 3 and 28 days. Moreover, they are formulated to describe normal strength concrete which is usually between 20 -60 MPa.

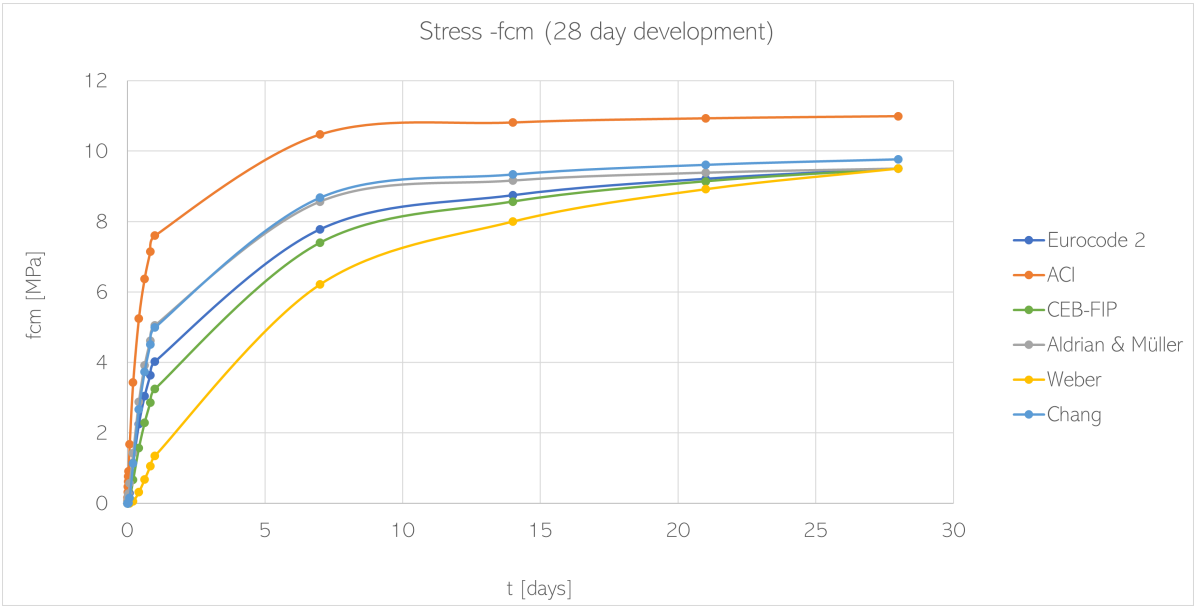


Figure 6.10: Assumed strength of cement stabilised robotic shotearth

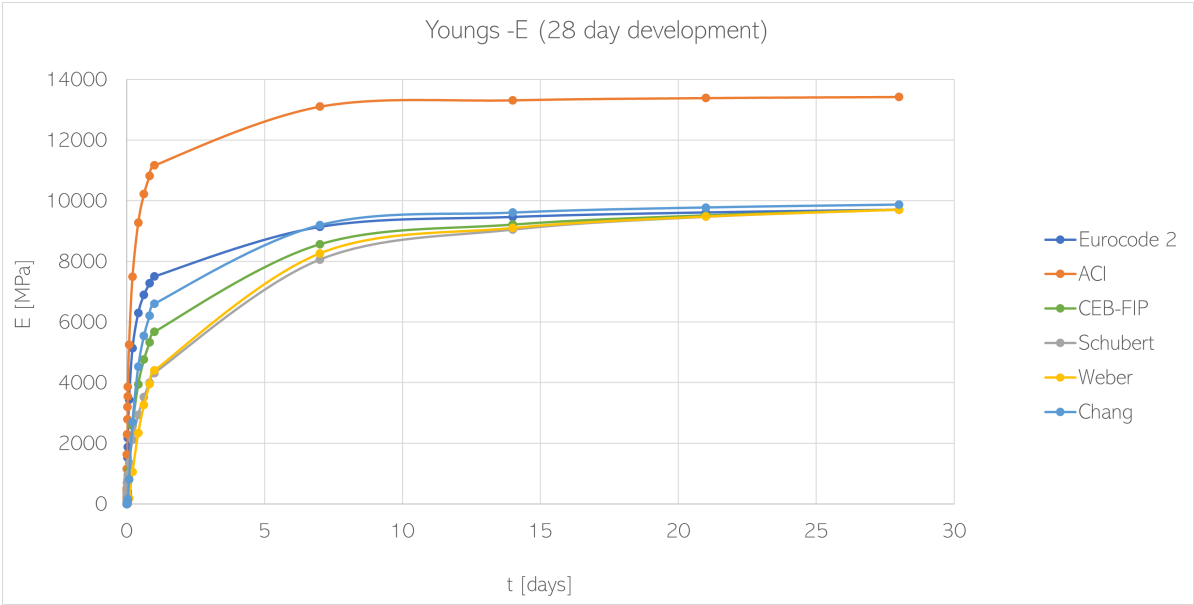


Figure 6.11: Assumed stiffness of cement stabilised robotic shotearth

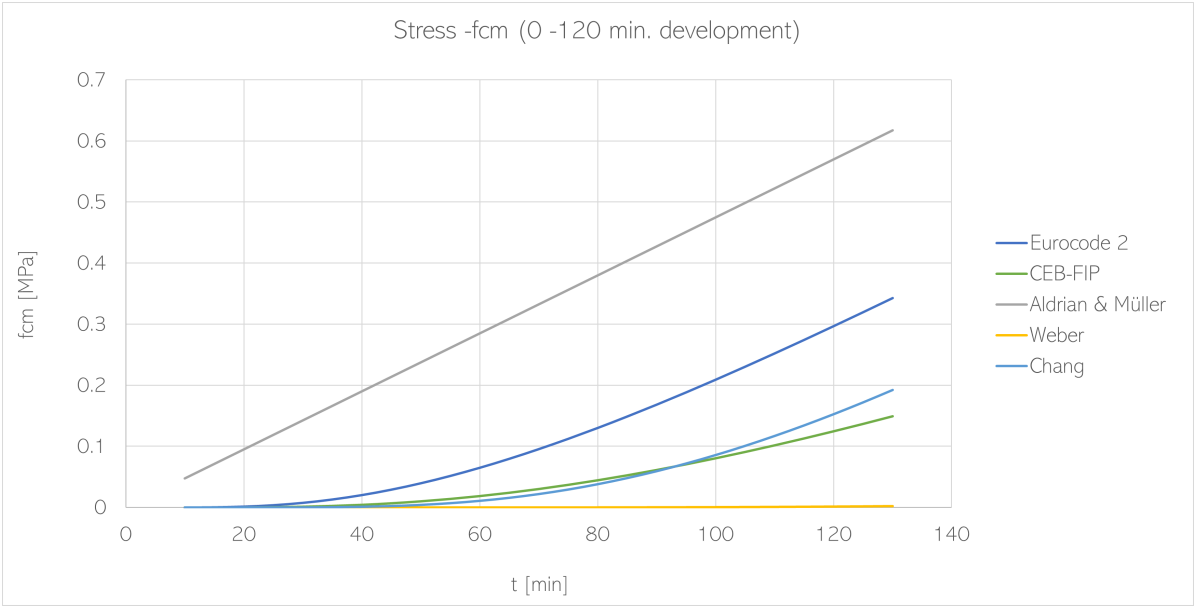


Figure 6.12: Strength predictions from concrete and shotcrete models

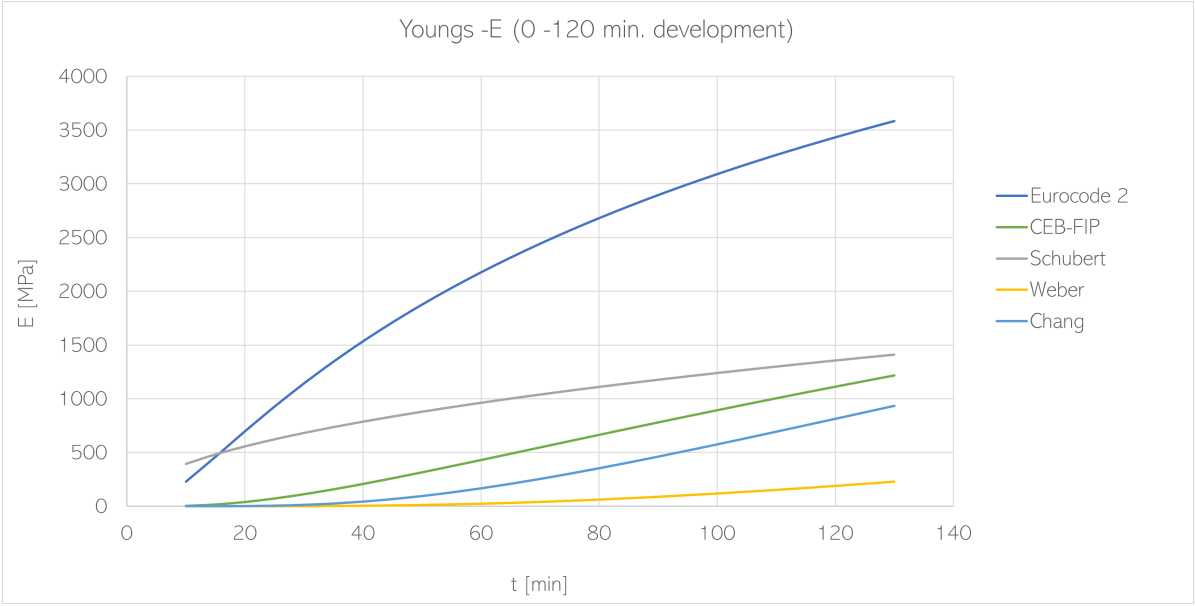


Figure 6.13: Stiffness predictions from concrete and shotcrete models

Fig. 6.14 shows the original stress data from Suiker measured for 3DCP [161] and Dressler measured for SC3DP [163]. Fig. 6.15 shows the stiffness data from Suiker and assumed stiffness development from Dressler's stress data. Dressler did not have this data and therefore the stiffness has been assumed by multiplying the stress with the difference of Suiker's data, using the following:

$$E_{\text{Dressler}} = \sigma_{\text{Dressler}} * \frac{\sigma_{\text{Suiker}}}{E_{\text{Suiker}}} \quad (6.1)$$

From this data it can be seen that for 3D printed concrete and shotcrete have strength is between 0.02 and 0.11 MPa and stiffness is between 0.2 and 1.1 MPa in the early age. See Appendix D.2 for calculation details.

Fig. 6.17, 6.18 shows the all the models found in literature compared to the early age data of Suiker and Dressler. It can be seen that for stress, the CEB-FIP and Chang models fall within the two early age developments and that Weber's model is very close to Suiker's. However, for stiffness, all models predict too high values. The "best" prediction is the one by Weber but the value is a magnitude of 10^3 higher than both Suiker and Dressler's data. From this, it can be concluded that the formulas from conventional concrete and shotcrete codes cannot be used to describe the early-age developments that are required.

This conclusion is further backed up in Fig. 6.16. In shotcrete for tunnel lining, ASCCT (2004) defines three early strength classes J1, J2, J3 for early-age shotcrete, where [164]:

- J1: for application of thin layers on dry surfaces. Not meant for structural use.
- J2: for application of thick layers on vertical or overhead surfaces with structural use.
- J3: only used when absolutely necessary due to high dust production and rebound

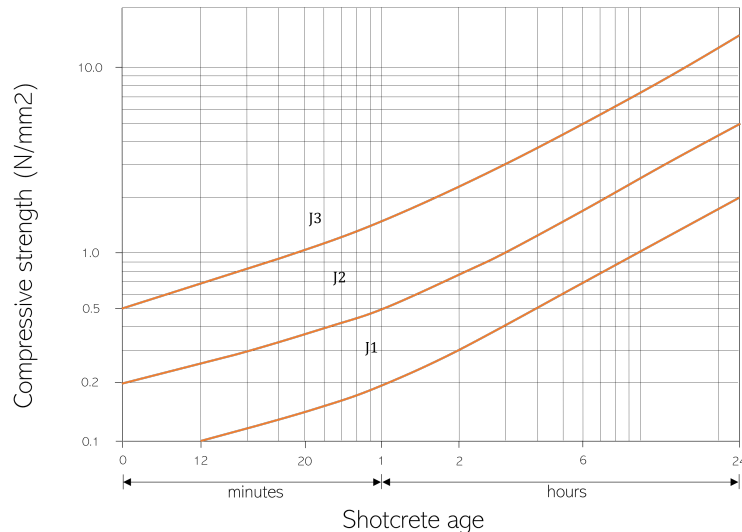


Figure 6.16: Shotcrete in tunnelling compressive strength development

Fig. 6.16 shows the minimum strengths for each class. By comparing J2 to the data presented in Fig. 6.14 and 6.15, it is seen that the shotcrete overestimates the strength.

Due to the too high predictions of these models in the early age, another approach had to be taken to give a better prediction of the development. In Fig. 6.19 and 6.20, it can be seen that

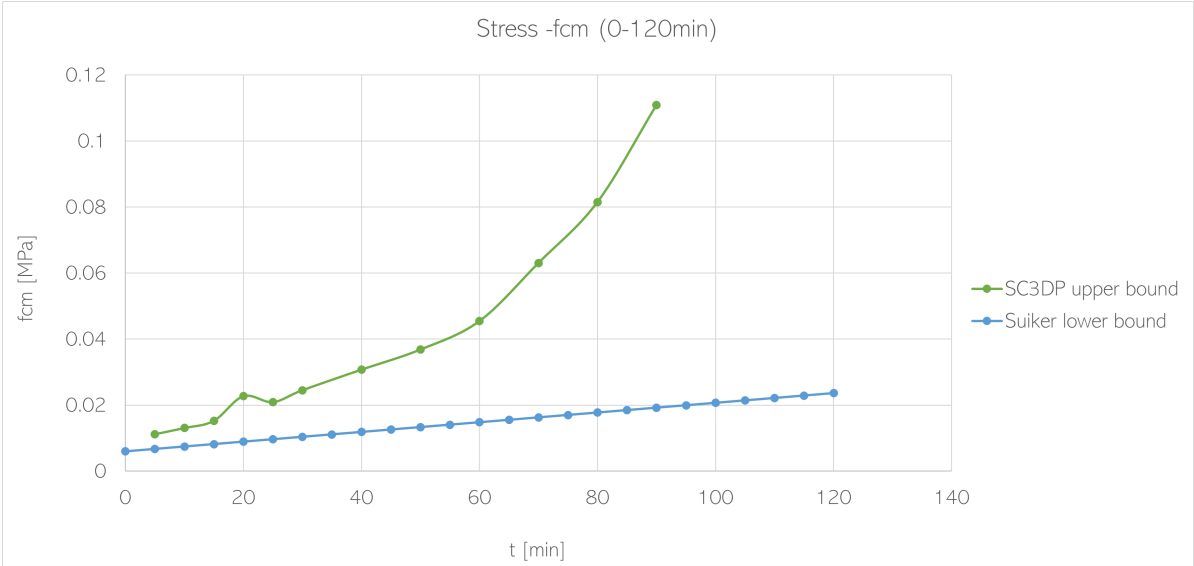


Figure 6.14: Stress data from SC3DP and 3DCP

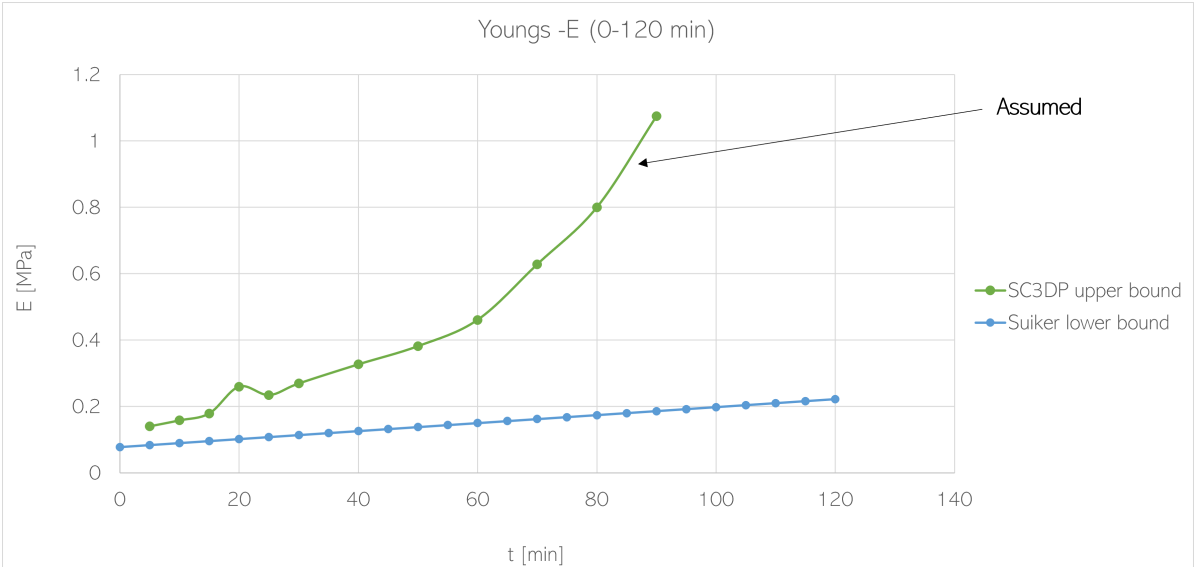


Figure 6.15: Stiffness data from SC3DP and 3DCP

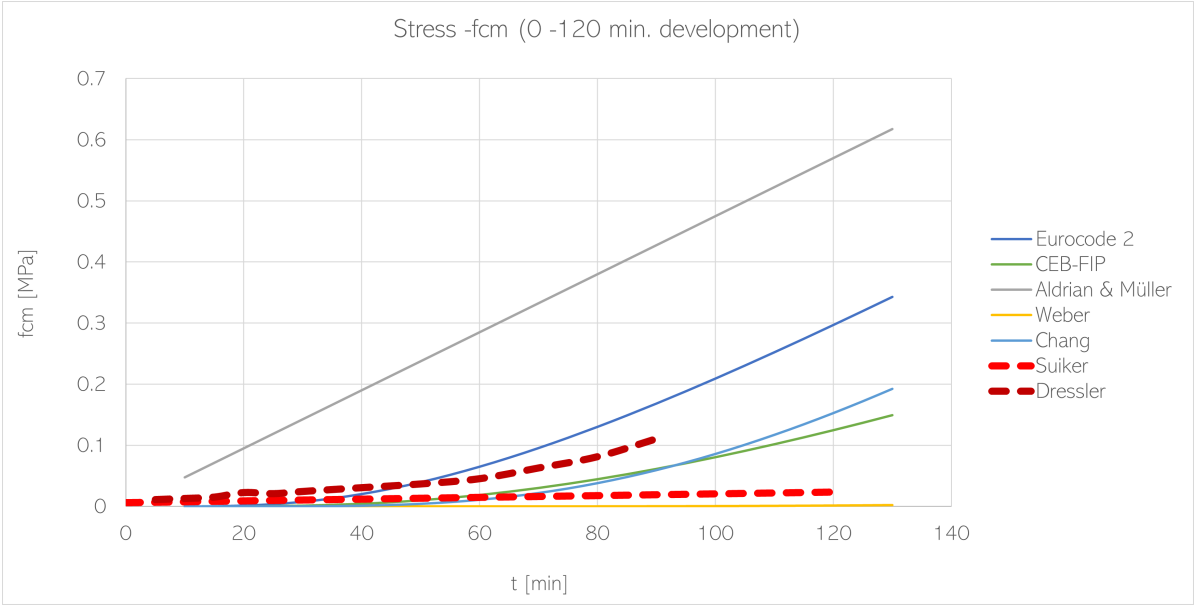


Figure 6.17: Comparison of strength development

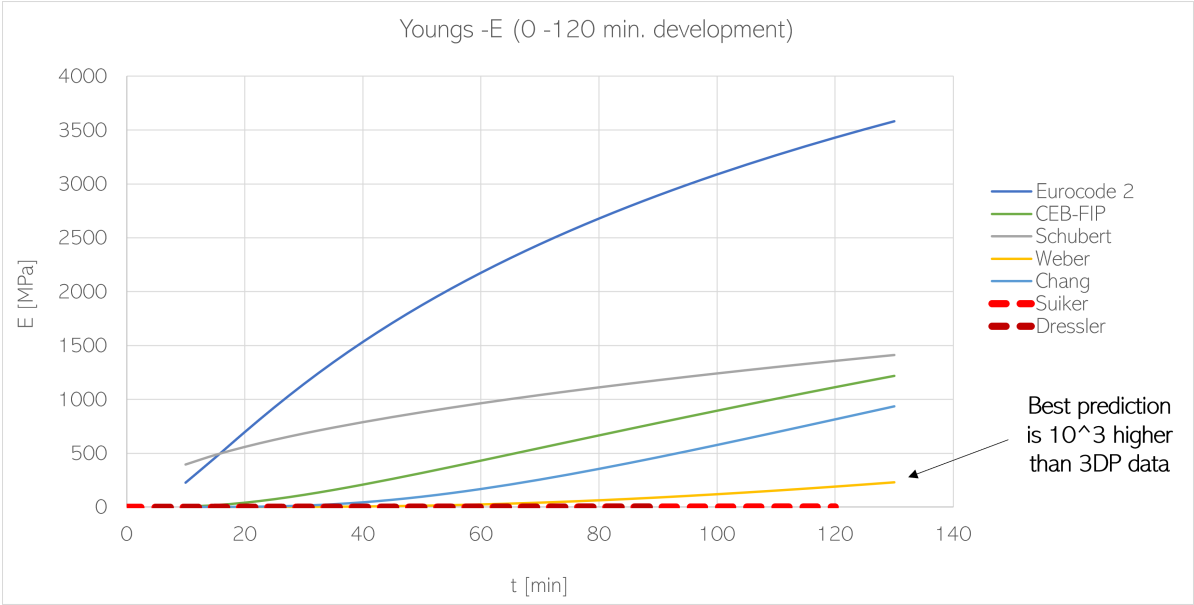


Figure 6.18: Comparison of stiffness development

Perrots alginate stabilised mix lies between both Suikers and Dresslers measurements. Originally it was intended to assess alginate stabilisation seperately. However, very little literature on alginate stabilisation exist. One of the few by Galan-Martin [165] suggests that the mechanical characteristics of alginate and cement stabilisation are similar. Based on this statement and comparing the alginate data from Perrot with Suiker’s and Dressler’s in the early ages 0-120 min. It is seen that the strength development of alginate earth is higher than Suiker’s but lower than Dressler’s. Therefore, shotearthcrete can be regarded as close to or follow the same development as Perrot’s with alginate. The strength and stiffnes development of Curto’s shotearthcrete is assumed to be between Suiker’s and Dressler’s in the early ages.

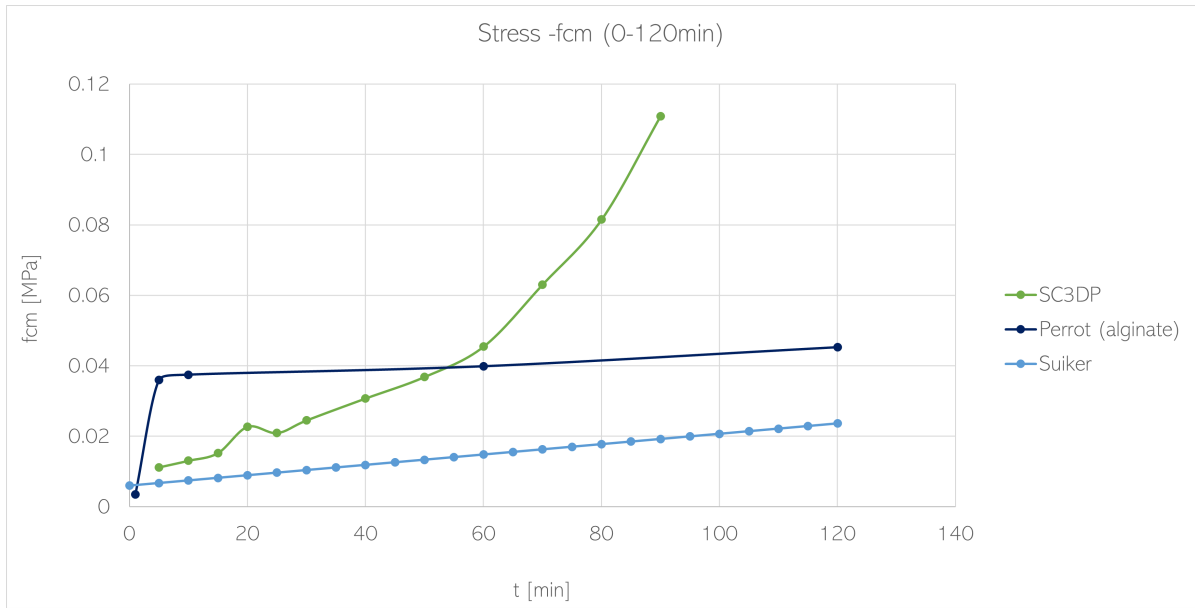


Figure 6.19: Stress data from SC3DP and 3DCP compared to alginate stabilised earth

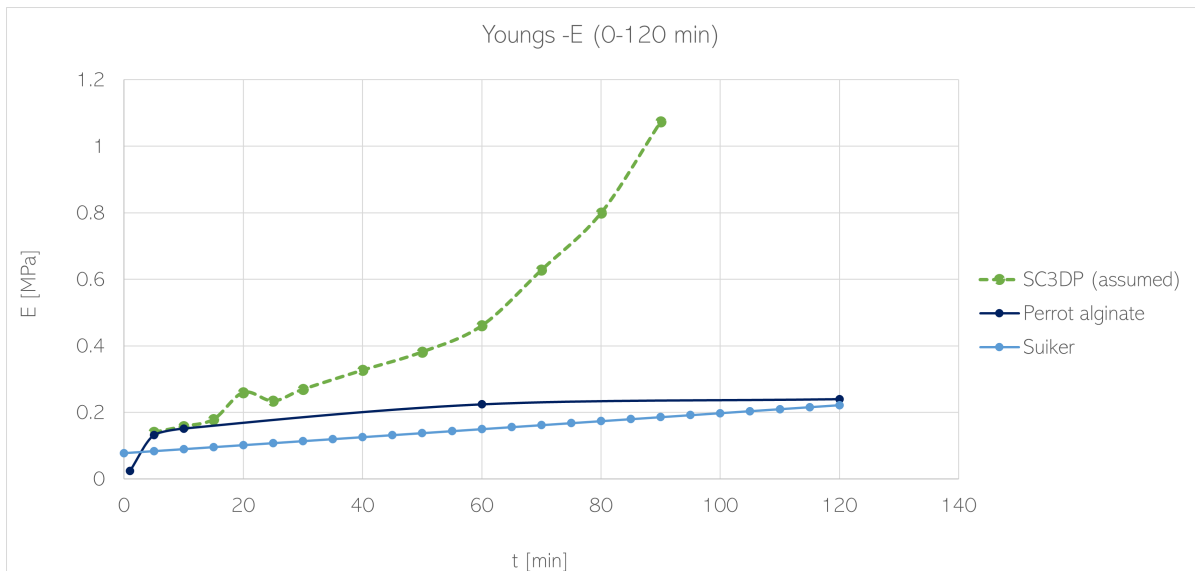


Figure 6.20: Stiffness data from SC3DP and 3DCP compared to alginate stabilised earth

Curvefitting

As the early-age strength is now assumed to be between these two boundaries, and the conclusion for the conventional concrete models are that they are more appropriate to predict strength and stiffness gain between 3 and 28 days, as they are usually intended for. This results in a "gap" in the development in the time between 2 hours and 3 days. A proposed method to fill this gap is through the use of a first order differential equation. This function has a curve found in Fig. 6.21 and the following equation:

$$y(t) = K \left(1 - e^{-\frac{t-\theta}{\tau}} \right) \quad (6.2)$$

where:

K –the value the function approaches

θ –the value that crosses the x-axis

τ –the value that describes how quickly it approaches the asymptote, K

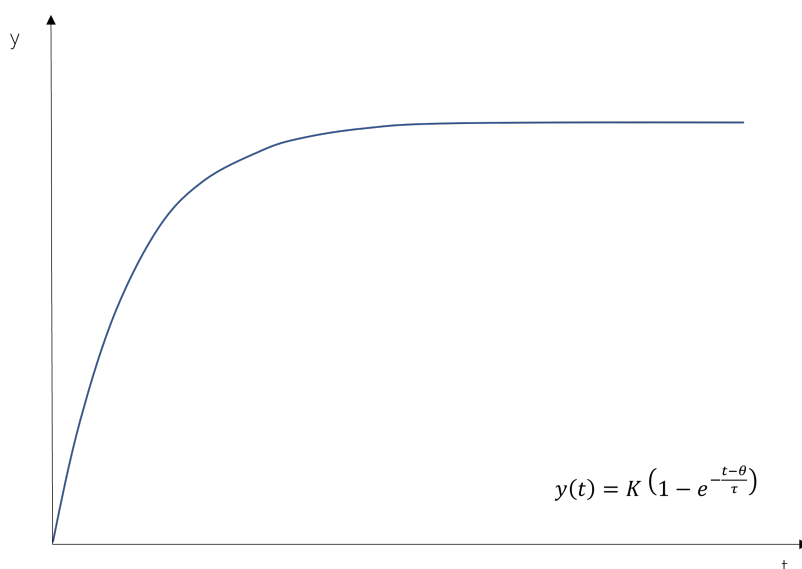


Figure 6.21: Shape of the first order differential function

This first order differential equation is proposed due to the fact that it follows the form of conventional concrete strength development over 28 days. As data for early-age strength between 0 -2 hours and later age strength between 3 -28 days is known, the function can easily be applied to predict the strength development between 2 hours and 3 days. Fig. 6.22 -6.25 shows the prediction of strength and stiffness in this time gap, visualised logarithmically by the orange dots. The lower bound strength and stiffness comprise of Suiker's early age development and the prediction model by Weber (1979) for the later age. The upper bound strength and stiffness comprise of Dressler's early age development and the prediction model by CEB-FIP for the later age. To find the best fit for e.g. the upper bound stress development, first, time steps were added between 90 min. and 4320 min., representing 3 days. Then the values of K , θ and τ was determined. K was set to 9.5, as this is the target strength the function needs to approach, 9.5 MPa. θ was set to 80, as in the time step 80 min. As Dressler's data only goes to 90 min., the time step could start at 90 min. but it was found that a better fit curve was found at $\theta = 80$. τ was varied between 1000 -6000. The value is varied to see how quickly it would approach the stress at time 4320 min., 3 days. $\tau = 3500$ was determined resulting in the best

fit. The same procedure was taken for the other models, see Appendix D.3 for calculation details. The final equations found to fit between early age and later age strength and stiffness are the following:

Equation for stress upper bound:

$$y(t) = 9.5 \left(1 - e^{-\frac{t-80}{3500}} \right) \quad (6.3)$$

Equation for stress lower bound:

$$y(t) = 9.5 \left(1 - e^{-\frac{t-120}{6000}} \right) \quad (6.4)$$

Equation for stiffness upper bound:

$$y(t) = 9707 \left(1 - e^{-\frac{t-80}{3500}} \right) \quad (6.5)$$

Equation for stiffness lower bound:

$$y(t) = 9707 \left(1 - e^{-\frac{t-120}{4000}} \right) \quad (6.6)$$

Result of shotearthcrete material prediction over 28 days

The final results with the curvefitting are shown in Fig. 6.26, 6.27, where the full 28 day model for upper and lower bound developments are visualised.

6.2.4. Discussion on results

Only the properties of strength and stiffness were considered. Other material parameters such as shear, tension, bending and effects such as shrinkage and fracture mechanics is not considered. 3D printed simulation tools are not yet developed to consider further material effects.

Unstabilised shotearth

From chapter 4, it was determined that the strength of raw earth materials depend on the type of soil, its composition; percentage of clay, silt, sand/gravel, its water content and the compactive energy applied. The mineralogical makeup and activity of the clay fraction along with its interaction with water is especially important to understand when determining mechanical strength and stiffness. In the procedure to predict strength and stiffness, soil composition was not taken into account as this was impossible to do. The statistical data gathered for 3D printed earth is only based on Perrot and Goma as these were the only two published papers with measured mechanical properties. The two papers uses two different earth mixes, Goma even included fibers, which changes the requirements for water content. Goma's mix is composed of 20 % clay, 80 % sand/gravel, 20 -25 % water, 2 % fiber (30 -50 mm wheat straw) by weight. Perrot offers more details in the mix, a fine soil from Saint-Sulpice-La-Forêt with a particle distribution showing 60 % of particles finer than 10 μm , the clay fraction consists of quartz, kaolinite, illite and smectite minerals. Plasticity index of the soil was 21 with 45 % water content. Data gathered for URE by Avila was even more varied. Densities were found between 1650 and 2150 kg/m^3 and clay content between 4 -20 %. Due to this wide range of soil compositions, the only solid parameter to base the assumption of URE and shotearth on was water content. Average compressive strength and stiffness values for both 3D printed

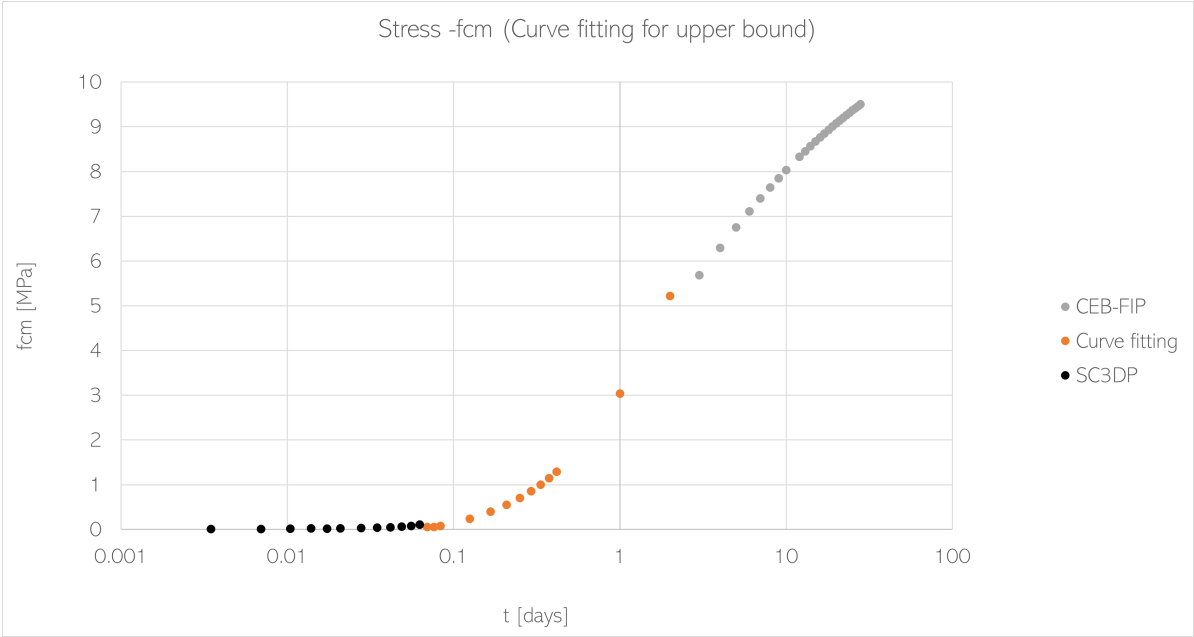


Figure 6.22: Curvefitting for upper bound strength

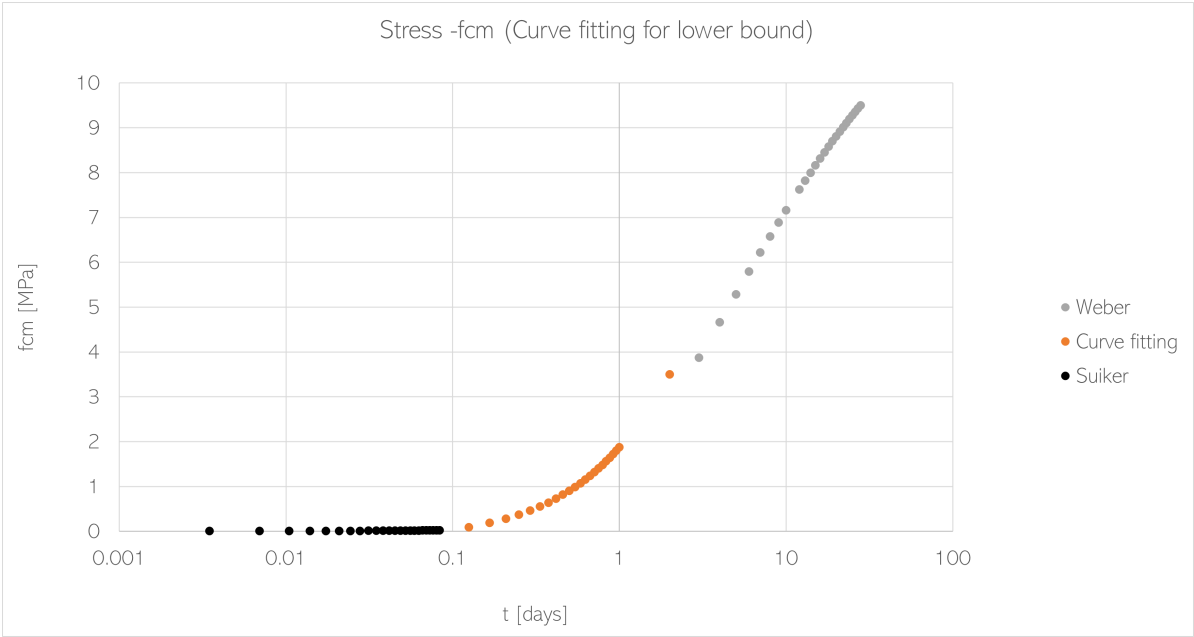


Figure 6.23: Curvefitting for lower bound strength

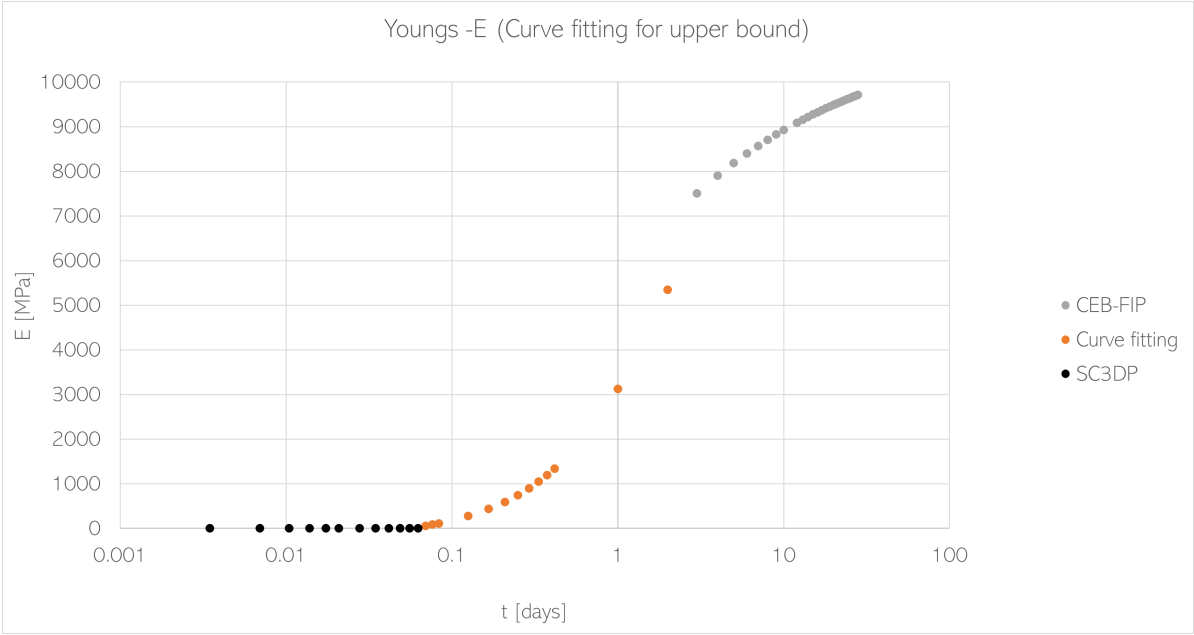


Figure 6.24: Curvefitting for upper bound stiffness

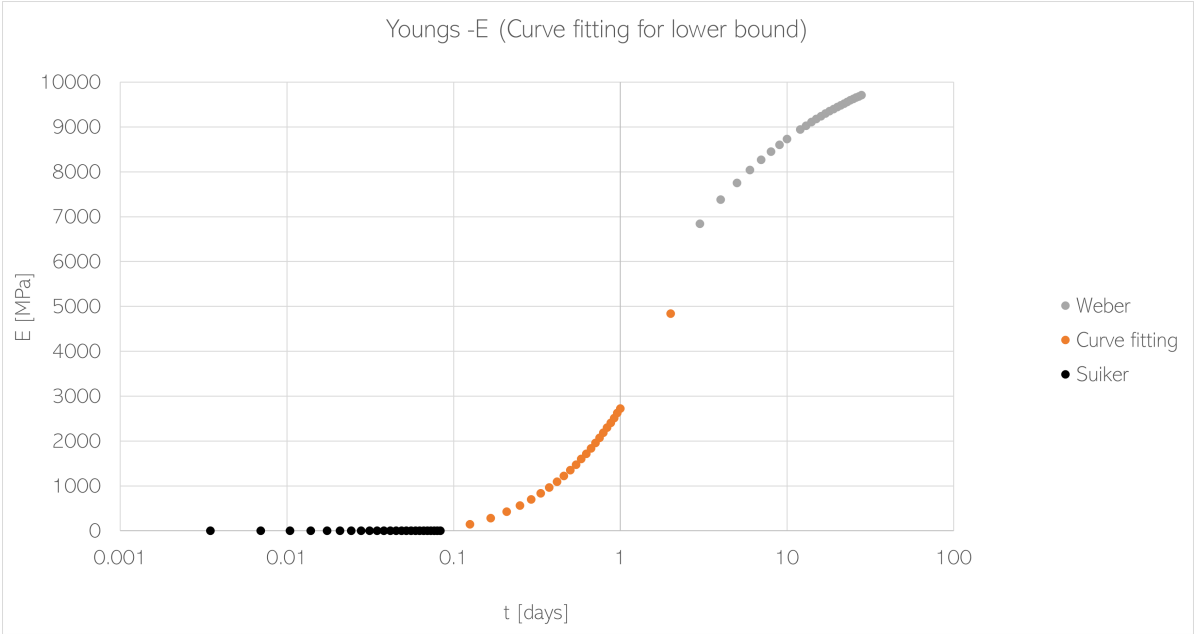


Figure 6.25: Curvefitting for lower bound stiffness

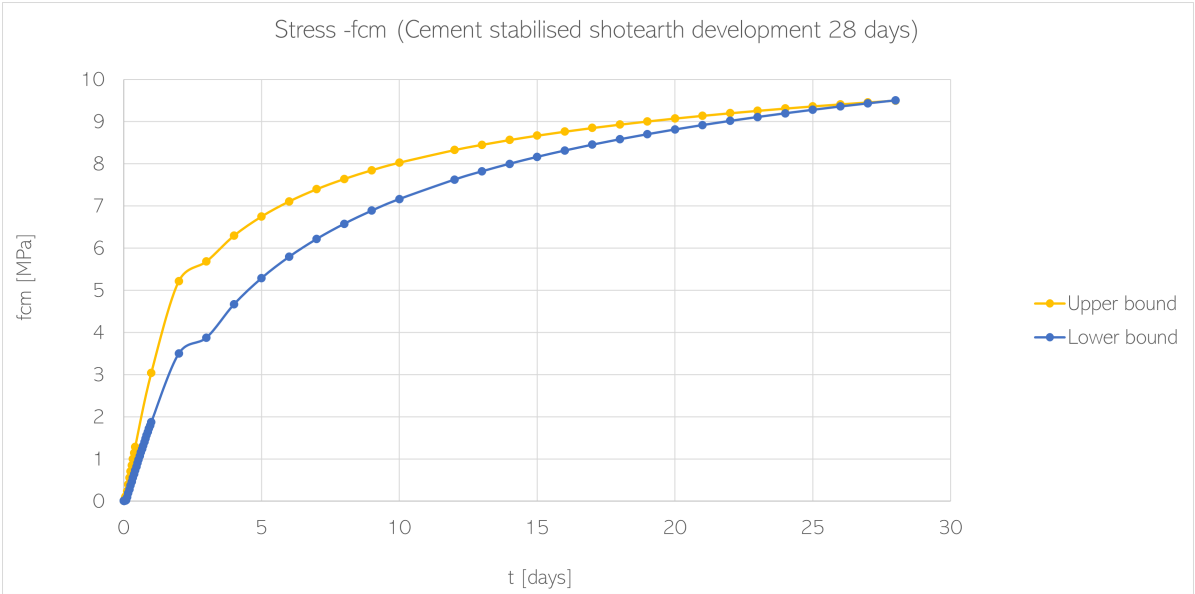


Figure 6.26: Results of the strength development over 28 days

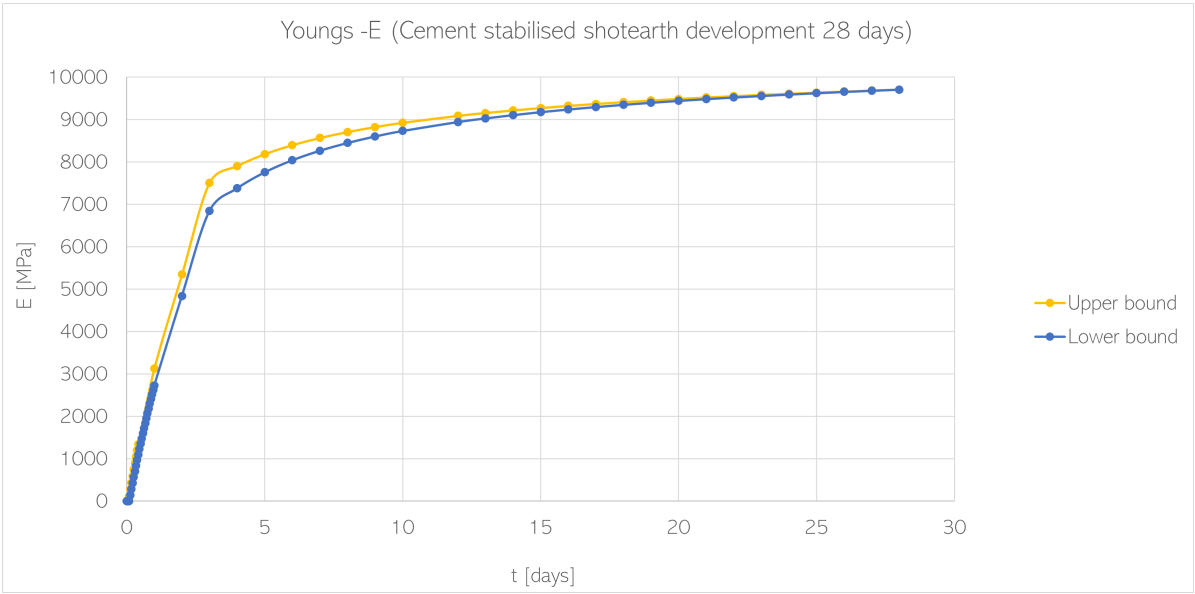


Figure 6.27: Results of the stiffness development over 28 days

earth and URE were set as targets. All soil compositions were assumed to be the same. However, the limitation of this approach is that different soils have different natural water contents and will also require different amounts of water to reach a consistency that satisfied a robotic fabrication process. Therefore, in order to validate the proposed shotearth material, the same soil from Perrot will have to be used and tested. This is tedious and unpractical.

A big uncertainty in the results is the stiffness development. No information is available that can solidly describe the stiffness behaviour of earth materials as compressive strength is usually the most important parameter. Stiffness' measured from Perrot and Gomaa are relatively similar, 15 -20 MPa, despite their different soil compositions and water content. Stiffness' measured in Avila show a big range between 60 -1000 MPa making it impossible to predict where stiffness for shotearth could be. This is made even more uncertain due to the large variation of testing procedures when measuring earth mechanical properties. The only solid assumption is that both strength and stiffness is higher than that of 3D printed earth simply due to the higher compaction energy from air pressure used in the shotearth fabrication process. Therefore, the proposed stiffness for shotearth was targeted at 25 MPa, higher than 15 -20 MPa for 3DPE but this is largely an arbitrary value. The proposed strength for shotearth is more certain and targeted at 2.4 MPa just inbetween URE and 3DPE as the boundaries were found to be closer together. Based on existing literature and understanding, the results are the best attempt at quantifying unstabilised shotearth strength and stiffness development from early-age to 20 days. For better predictions, more testing and validation is strictly necessary to get a better understanding of both parameters. Especially a correlation between stiffness development and water content or density is desirable.

Cement stabilised shotearth

The prediction of early-age shotearthcrete is based on data from concrete printing as nothing on cement stabilised earth printing can be found. The results are therefore based on the gross assumption that shotearthcrete will develop in the same manner. The target strength and stiffness of the concrete printing data is unknown as this was not the goal of the original studies. However, given that printed concrete structures can reach hardened properties similar to casted concrete, the target strengths are likely around 20 -40 MPa. This perhaps suggests that the early-age data used overestimates actual cement stabilised printed earth. This can only be verified through testing.

Furthermore, looking closer at the results of Curto, the actual soil profile is unknown and is vaguely described as containing 7 parts sand, 7 parts soil and 2 parts cements, resulting in 14 % cement content by weight. Therefore, replicating this fabrication procedure with a similar soil will not guarantee the same mechanical properties. As cement stabilisation is mostly used in rammed earth, which can be regarded as a low strength concrete, as can Curto's shotearthcrete, comparing the mechanical properties of Curto to existing CSRE data can be done, see Table 4.6. When comparing this data, two observations were made. First, CSRE studies rarely uses up to 14 % cement, most CSRE experiments contain 5 -12 %. Second, a big variation of results can be found. The closest comparisons found of compressive strengths are measured at 9.80 to 26.85 MPa for 11 % cement by King [71] and 4.95 -7.44 MPa for 10 % cement by Reddy [73]. Reddy's results are perhaps the most reliable for this comparison as Reddy is one of few people currently researching cement stabilisation. King's results are from 1996 and in the past different practices were used. Curto's results are within these ranges but shows that it cannot be guaranteed that shotearth will reach the target values predicted due to uncertainty in the material. Replicating the same procedure might give very different results. As previously seen in chapter 4, mechanical properties, depending on cement content

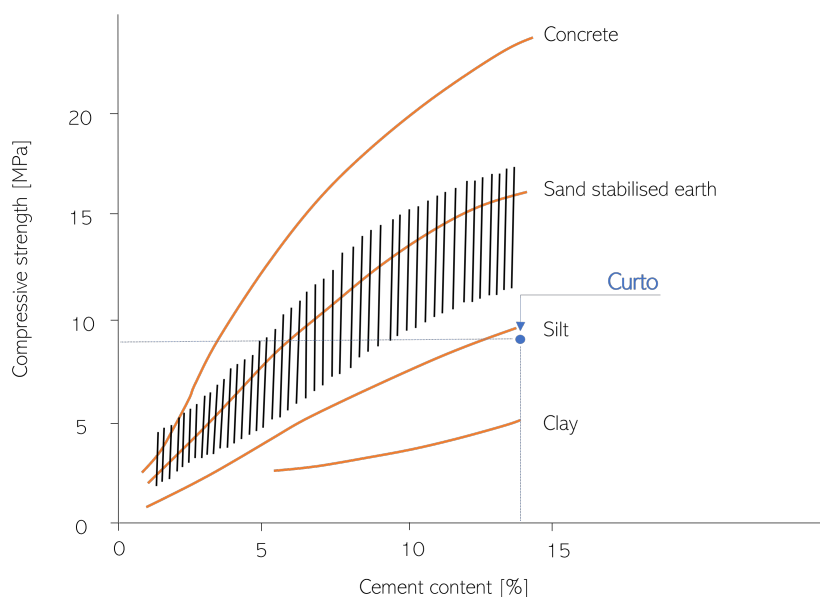


Figure 6.28: Comparison of Curto's results to Houben & Guillaud.

and soil composition, compressive strength varies. Fig. 4.15 shows Curto's results compared to Houben & Guillaud's graph showing the relationship between compressive strength and cement. It can be seen that depending on the soil and especially clay content, compressive strengths can vary between 4 and 17 MPa. Cement and clay don't work well together and there is currently not much knowledge in how these interact and how it will affect the overall behaviour. An assumption of Curto's soil profile can be that the clay content is about 4%. This is based on the fact that the 7 parts soil contains about 10% clay, which has been diluted with the same amount of sand and then added some cement. However, this will have to be tested.

6.2.5. Discussion on procedure

The results reached for the unstabilised and the cement stabilised shotearth models show a 20 and 28 day development respectively. Really only the early-ages between 0-2 hours is necessary as this is the most critical time frame for printed structures. The developments beyond 2 hours can be useful for construction planning but this is not considered in this work. Moreover, the results were obtained following two different approaches. The first one is largely based on the theory of earth materials and soil mechanics where the prediction is kept at a range of where strength and stiffness could be. The second one follows theory in concrete science where the prediction is aimed at reaching one target strength and one target stiffness. This makes it perhaps unreasonable to compare the resulting constructions. A better approach would be to also vary the cement stabilised shotearth to predict a lower bound target and an upper bound target. From chapter 4, mechanical properties, it was found that cement stabilised rammed earth strength varies between about 2 MPa to 27 MPa. Taking this approach would become challenging when assuming targets for stiffness as many studies in cement stabilisation have not measured this property. Performing this prediction without testing would be almost impossible to do with the limited information available.

7

Design and Model Part 2: Assessment of shotearth structures

This chapter describes the fabrication and structural performance of a monolithic earthen wall and two arched structures using the material models found in the previous chapter. The chapter aims to explore the possibilities of creating a compression-only structures with sprayed earth and describes the considerations taken during the design process. An assessment of suggested dimensions and fabrication time of the structures are given. Finally, a discussion on the structural safety, material models and modelling method is provided.

7.1. Structural design of earthen wall structures

3DCP has been related to masonry structures for structural design, as suggested by Duarte et al. [145]. Other who have referred to this are Pegna [167], "3D printing is a new approach to masonry," and Khoshnevis [119], "possibility of 3D printing for construction of barrel vaults without external supports." Therefore, it can be assumed that the shotearth construction method is linked to unreinforced masonry.

SE3DP as unreinforced masonry shells

Unreinforced masonry elements were the first building components to create shell structures. They have evolved from sun-dried bricks and mud to fired bricks and cement mortar. They were used to create different structural and architectural forms and the analysis of these can be termed masonry shells. From a structural point of view masonry is a homogenous and isotropic material. The strength is limited by its weakest joints, therefore the load-bearing capacity largely depends on the mortar strength. Unreinforced masonry is a compression material where tension may lead to cracking and accelerates the deterioration of the walls. Compressive strength is generally far stronger than the loads placed on it. Unbaked bricks can achieve 5 MPa in compressive strength which would allow a hypothetical 200 m high tower in earth before the bricks at the bottom begin to crush. Applying a safety factor of 10 against crushing would allow for 20 m high earthen walls. Stiffness is rarely an issue in masonry structures as the low stresses account for very small displacements due to elastic deformation of the material. Strength and stiffness are of negligible importance in the design of masonry structures but stability is of paramount importance.

Existing earth wall design guidelines from different countries have recommendations for dimensions and slenderness requirements for earthen walls. However, these all consider dry method constructions e.g. rammed earth and earth masonry, see Appendix E.1. In 3D printing, no design guidelines exist as experimental research focus on optimising material and printing parameters to maximise buildability, maximum dimensions able to be printed.

7.2. Structural design of earthen arch structures

The construction of compression-only structures such as arches, vaults and domes using earthen materials as masonry elements can be traced back to ancient times. Much can be learnt from traditional methods of brick layering with the newest methods of 3D printing either by extrusion or spraying. Existing earth masonry structures of these shapes prove that earth construction is capable of creating architectural spaces that match the longevity and durability of any contemporary building material when properly designed.

Why design earthen vaults and domes?

The majority of structures are linear box-like structures with a flat or pitched roof. These structures are functional and appealing but wasteful of materials and do not optimise for stresses. Optimal structures are curved and comprise of shells, tubes and arches. Earthen materials are strongest in compression and weakest in tension. This makes earthen arches, vaults and domes particularly interesting shapes to explore with this material.

However, earthen arches, vaults and domes also present unique challenges. Designers must accept the limitations inherent to the material, which include low strength and low durability compared to contemporary materials. Methods to design structurally efficient shapes for earthen arches, vaults and domes are largely unknown in the contemporary structural engineering community as building codes do not accept earthen vaults as a viable structural system.

Shells

Shells are structures that enclose spaces with a smooth continuous surface (vaults and domes). The definition of a shell is "a thin, curved plate structure shaped to transmit applied forces by compressive, tensile, and shear stresses that act in the plane of the surface." Due to their curvature, they have the advantage of being efficient load carrying structures, have high strength to weight ratio and have high stiffness.

In masonry earthen arches, compressive force resultants should remain in the middle third of the masonry at the base of the structure. Safety factors should account for variable soil composition. Elements should be designed to resist loads during construction and the finished structure. As arches, vaults and domes derive strength from their geometry, individual elements often experience greater loads during construction than when complete. The finished project must be protected from moisture. Due to high self-weight and low compressive stresses, unreinforced masonry vaults are typically a problem of stability rather than strength. When analysing these types of structures, three criteria needs to be fulfilled.

- Strength: comparison of applied stress to the capacity of the construction materials.
- Stiffness: limitation of deflection.
- Stability: prevention of buckling.

The type of forces applied to the structure produce different levels of stress. Expensive forces are bending moments and shear forces. These produce high concentrations of stress along the member surface and more material is required to resist these forces. The most economical forces are the in-plane forces, forces that travel along its axis. Depending on support fixity and type of load, the level of stress can be reduced by as much as 90 % if bending is avoided. The most economical way of resisting stress is to avoid bending and shear forces. In shell structures, the stress flow is graphically represented by a thrust-line, which is the centre of the stress flow and can be compared to the centroidal axis of the shell. Most efficient structures are those in which the thrust-line matches the axis of the structure. A mismatch can cause bending and tension in the shell. The only shell that is free of bending is the catenary [166].

For shotearth, only main difference is the consideration of the time-dependent behaviour where the early age material and construction method is crucial for both stability and strength of the geometry. Constazi et al. [168] and Carneau et al. [158] have demonstrated the ability and material limitations of printing overhangs and compression only structures in 3DCP. Printing overhangs using SC3DP have been demonstrated in [132]. However, the angle of overhang has not been quantified.

7.2.1. Roman, Nubian and Corbelling techniques

There are different layering techniques to different types of vault structures. These are can be termed roman, nubian and corbelling. Roman is laying each brick vertically such that they eventually meet the top. Nubian is laying the bricks at an incline such that each brick layer supports the next brick layer. Corbelling is laying the bricks horizontally such that the center of gravity is always at the center and they eventually meet at the top. A schematic of the three most common brick laying techniques can be found in Fig. 7.1.

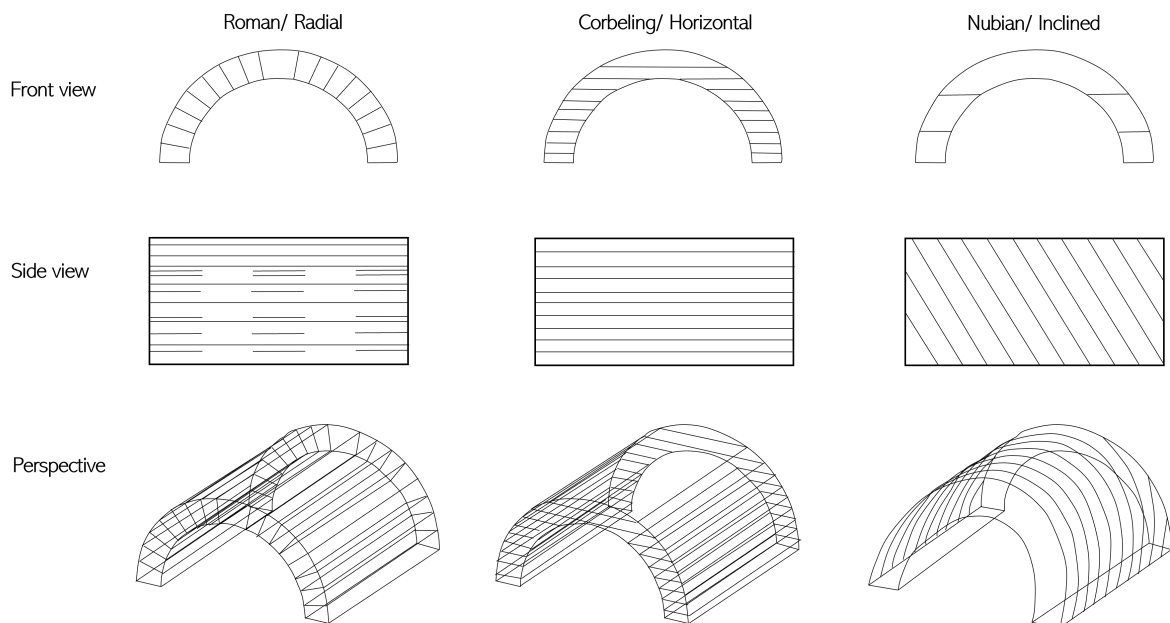


Figure 7.1: Roman, Nubian and Corbelling layering techniques used in masonry structures (adapted from Ref [145])

Formwork

The construction of vaults and domes in masonry traditionally involved temporary supports during construction to maintain stability until the final shape was formed. With the viscous behaviour of 3D printed materials this poses a challenge to the fabrication of overhanging elements. Some methods to overcome this has been to implement flexible moulds for 3D printed shells to act as formwork, as previously mentioned the 3D printed clay shells. Another solution to avoid formwork is to optimise the fabrication process.

7.3. Design of shotearth structures with shotearth 3D printing

The previous chapter showed the development of the material models with the consideration of the SE3DP fabrication method. As mentioned, due to the novelty of the method, the computational design tool developed by Witteveen +Bos for 3DCP, which is based on Suiker's method, will be used and extended for SE3DP to assess the structural build-up.

7.3.1. Model setup

The Witteveen +Bos model uses the parametric modelling programme Rhino with Grasshopper and the structural analysis plug-in Karamba to analyse for its stresses. The full model setup can be found in Fig. 7.2.

Karamba3D structural analysis

Karamba3D is a parametric structural engineering tool integrated into the Grasshopper environment. The tool can perform structural analysis of spatial trusses, frames and shells. The tool is geared towards architects and engineers in the early design phases and works interactively with Rhino and other plug-ins for Grasshopper. Karamba provides a basic finite element package and Fig. 7.3 shows the type of analyses available. The tool is confined to linear elastic calculations where the calculation of element stiffness matrices can be done without the need for numeric integration which greatly reduces computation time. In this work, a stress analysis and a buckling analysis will be performed on structures modelled as a shell. The shell

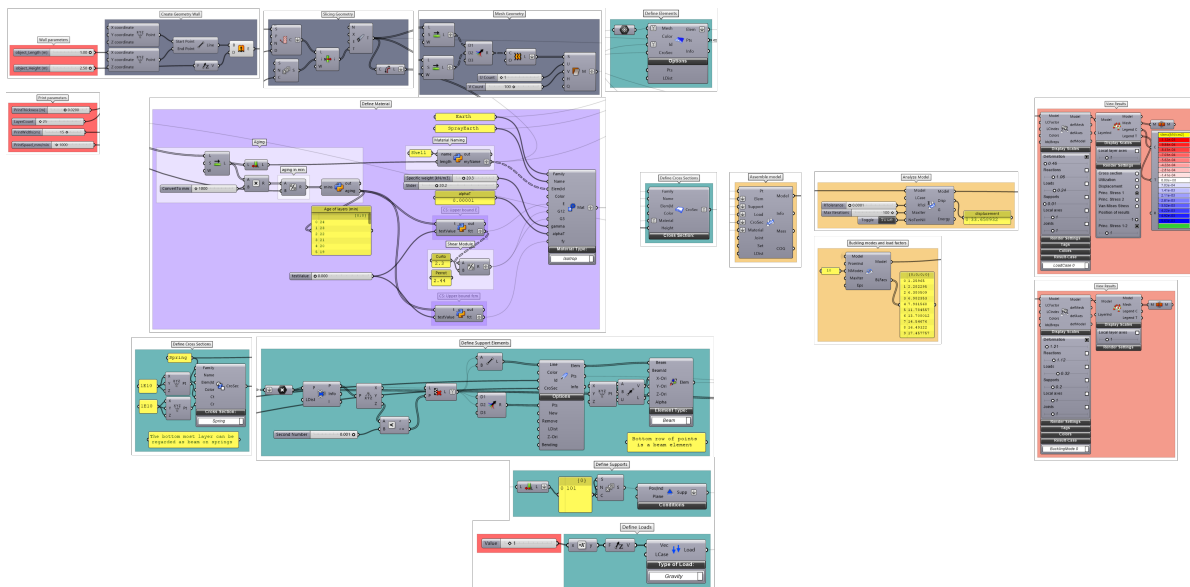


Figure 7.2: Model setup for wall structure

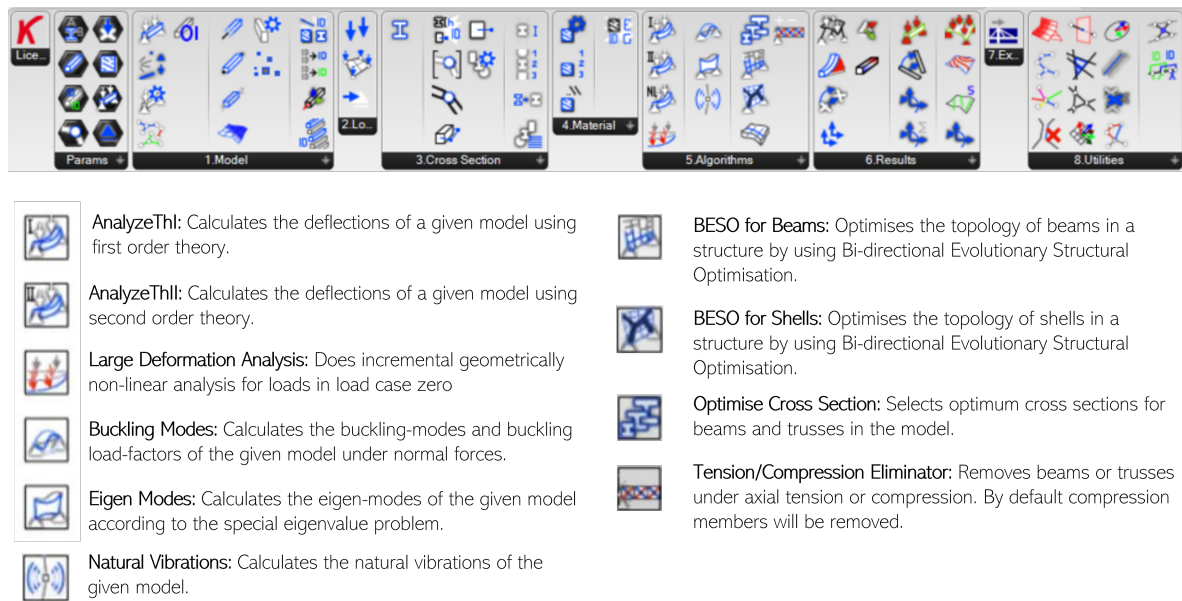


Figure 7.3: Functions and types of analysis of Karamba

element formulation in Karamba is based on the TRIC element with 6 DOFS per node and a constant strain state is assumed for each layer. No in-plane rotational stiffness is added as it is based on Kirchhoff theory.

7.3.2. Processing parameters considered

The table in Fig. 7.4 shows the processing parameters involved in SC3DP (assumed to be the same in SE3DP). The corresponding value for each parameter have previously been applied in the reinforced curved wall study by [131], seen previously in Fig. 5.7. Due to the limitation of the computational tool used only the highlighted ones from the table in Fig. 7.4 will be considered in this study, as seen on the right with the number sliders. It will not consider the variation of the other print parameters, aside from the printing speed, which will vary between 1000 and 6000 mm/min. The influence of this parameter on the resulting structures possible to be constructed will be evaluated. Thus the layer height and width will be kept constant at 0.02 m and 0.15 m respectively.

Parameter	SC3DP
Material mass flow (kg/h)	1829
Air pressure at the nozzle (bar)	1.8-2.2
Compressed air volume (m ³ /h)	55
Robot speed (mm/min)	6000
Standard time interval between two layers (s)	1-20
Nozzle distance to target (mm)	200
Resulting layer height h_L, average (mm)	18.6
Resulting layer width w_L (mm)	140-149

Figure 7.4: Left: Processing parameters assumed and applied for SE3DP, only rows marked in yellow is considered in the design tool. Right: Printing parameters considered in the tool where only layer count and printing speed is varied

Other simulation assumptions

Other simulation assumptions considered in the analysis is a continuous print without formwork. This means a short interlayer time between layers is considered, however not quantified. Printing of layers will continue once the printing of the previous one is complete. Maximum structural dimensions will be evaluated with minimal or no formwork.

7.3.3. Material models

The results of the material models have been input into the material definition component in Karamba through equations. From the results found in Chapter 6, a linear or polynomial regression, depending on which was the better fit (returned the highest R value), in Excel was performed to find an equation that described the strength and stiffness developments. The resulting equations have then been scripted as if -else statements in the GHPython script component. This means that depending on the time it takes to print, the model will use the appropriate equation to determine the aging of the material. An example is found in Fig. 7.5. Units in Karamba is kN/cm², therefore all the equations found have been converted to fit these units. See Appendix E.2 for functions and python conditionals for all material models.

The other parameters required for the material definition are specific weight (gamma), which is defined at 20.3 kN/m³. This is the general specific weight for soils, and is similar to that of concrete. The coefficient of thermal expansion (alphaT) is kept at 0.00001, same as for normal concrete, as there is no information that could be found for this value for soils. However, thermal effects are also not considered in this analysis. These specific weight and coefficient of thermal expansion are kept constant in all the following experiments. The only variables input

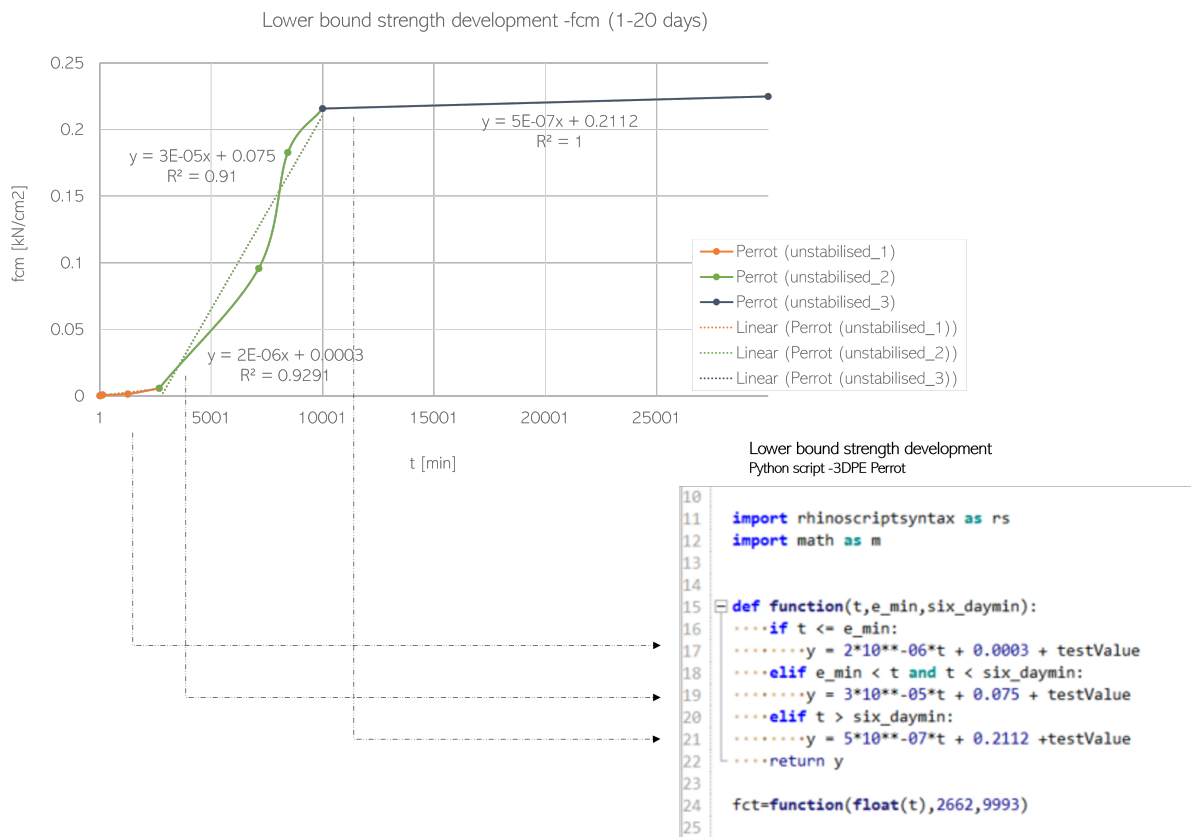


Figure 7.5: Linear regression in Excel to GHPython conditionals

into the component are yield strength (f_y), Young's modulus (E) and shear modulus G_{12} for in-plane and G_{33} for transverse. As a result, each layer will get a different, strength, Young's and shear modulus depending on the time it takes to print this layer.

For shear modulus, a Poisson's ratio of 0.22 is used for the unstabilised cases, found in Perrot, and 0.1546 for the stabilised cases, found in Curto. The shear modulus (both transverse and in-plane) has been found with the following relationship:

$$G = \frac{E}{2(1 + \nu)} \quad (7.1)$$

As a result the Young's modulus has been divided by 2.44 when assessing the cement stabilised cases and 2.3 when assessing the unstabilised cases for the shear modulus values. For the proposed shotearth model in Fig. 6.8 and 6.9, no analysis has been performed as it has been made to fit within the bounds of 3DPE and URE and therefore obviously will result in wall heights that fit within the boundaries.

7.3.4. Analysis

In this work, geometries defined will be analysed as shell structures. A stress analysis will be performed utilising the Analyze THII component. A buckling analysis will be performed utilising the Buckling Modes component. The stress analysis method utilises second order theory based on small deformations. Compared to first order theory, second order theory counts the influence of in-plane forces in shells which influences the structures stiffness and redistributes stresses in a section. In small deformations or small strain theory, strains and rotations are both small, which means the undeformed and deformed configurations of the body can be assumed identical. This theory is often used in the analysis of deformations of materials exhibiting elastic behaviour e.g. concrete and steel. Although both concrete and steel fail in a non-linear way, they are usually designed considering linear elastic properties. In other words, the analysis performed will consider geometrical non-linearities but the material models defined are linear.

Stress and buckling check

Stresses of a 3D printed, extruded or sprayed, component requires evaluation of its elements (each layer) under combined axial load and imperfections caused by the printing. The geometries defined will increase as a result of growing dead weight loading. The initial low strength and stiffness properties of printed material is critical during manufacturing and needs to be ensured against failure. This means that the section capacity of each layer can be governed by either material yielding or local buckling of the shell structure. The compressive stress capacity of a layer can be evaluated as:

$$\sigma_{c,max} > \min(\sigma_{mat}, \sigma_{buck, loc}) \quad (7.2)$$

Stresses at the first layer are governing for material yielding while stresses in subsequent layers govern local buckling. In this analysis, structures were checked against ultimate limit states. For each printing time (1000 -6000 mm/min), the time it takes to print e.g. 10 layers has been checked against each respective yield strength equation from the material models to determine the maximum allowable stress. This maximum allowable stress has been checked against the principal stresses 1 and 2 from the shell view component in Karamba. Principal stress 1 is the larger of the two and the maximum value has been taken into account (tension), while principal stress 2 is the smaller of the two and the minimum value has been taken into account (compression). For the buckling check, when the buckling load factor (BLF) is above 1, it has passed the check.

Influences on the analysis

Processing parameters that affect these failure mechanisms are the curing properties of the printed material, the printing velocity, the geometrical features of the object, the strength and stiffness characteristics, the non-uniform dead weight loading, and the presence of imperfections. Only the influence of the printing velocity has been considered in this analysis. The influence of the other parameters will be discussed in Section 7.4.4 and 7.5.4.

7.4. Monolithic shotearth wall structure

For the evaluation of a monolithic shotearth wall structure, the different material models at varying printing speeds will be simulated. The reason for modelling the wall first is to get an idea of the wall heights that can be achieved from the different material models and the influence of printing speed on the geometry. The wall model is also certain to only contain in-plane stresses and axial forces which can be verified against existing literature to see how accurate the model is.

7.4.1. Wall geometry and element definition

A wall geometry of 1.0 m in width and 1.0 m in height is defined. Each printed layer is set to be 0.020 m in height and 0.15 m in width as seen in Fig. 7.6. The geometry is then converted from a surface to a mesh, where the UV count in the mesh component is set at 1 and 100 respectively. The UV count determines the resolution of the mesh in the x,y directions. This means each layer ($U = 1$) is divided into 100 triangular elements ($V = 100$). For the analysis, the mesh is defined as shell elements, where it is only possible to get the stresses and moments in the centre of each element in the principal directions as this is how Karamba is built.

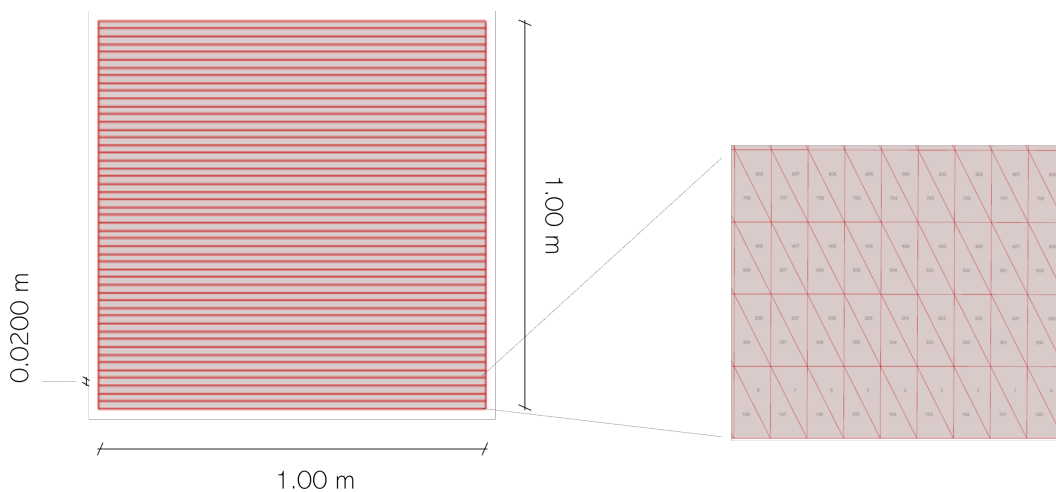


Figure 7.6: Left: Wall geometry and dimensions. Right: triangular shell elements

Boundary conditions and loads

All translations and rotations are fixed at the bottom of the wall, the interface between print surface and first print layer. An initial stress state corresponding to the gravity load has been applied to the structure. This will be the only load considered as this is the same as printing in an enclosed lab facility.

7.4.2. Analysis check

First order analysis check

A simple hand calculation has been done to check the outputs of Karamba. To verify this, the Analyze component which utilises first order theory has been used in the model analysis and checked against the following equations.

$$F := \rho \cdot l \cdot h \cdot w \quad (7.3)$$

$$\sigma_c := \left(-\frac{F}{l \cdot w} \right) \quad (7.4)$$

Where $\rho = 20.3 \text{ kN/m}^3$, $l = 1 \text{ m}$, $w = 0.15 \text{ m}$, $h = t \cdot n \text{ [m]}$, where $t = 0.02 \text{ m}$ and n is number of layers.

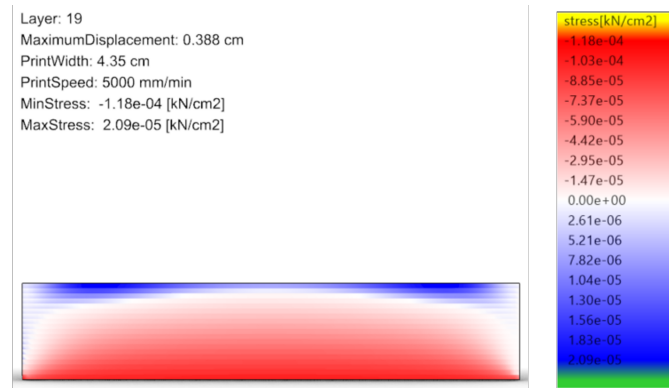
By inserting $n = 39$, $F = 2.37 \text{ kN}$ resulting in σ_c to be -0.016 MPa . The Karamba output gives a maximum compression stress at -0.022 MPa , which equals a 27 % difference between the hand check and the output of the programme. Tension stresses are not expected at the bottom of the wall due to the geometry being a straight wall element. However, Karamba also gives a maximum tension stress at 0.000113 MPa . This stress is found at the edges or top of the geometry due to deformations. This can also be found in the results in the following section.

Second order analysis check

The model has been verified against the numerical and experimental results of Suiker and show a good prediction for a free standing wall found at 0.175 m before failure by buckling. This is a 2.23 % difference compared to Suiker's study. Fig. 7.7 show the numerical results from the Karamba model using the same dimensions, printing parameters and material models as Suiker's study. Tables 7.1 show the printing parameters considered and the resulting experimental and numerical results from Suiker. Suiker's model prediction was found at 0.179 m and 0.184 m due to different material curing rates considered. This resulted in about a 10 % difference from the experimental results.

Parameter	Value	Description	Value
Layer thickness	43.5 mm	Geometry	Free wall
Layer height	9.2 mm	Experiment	0.202 [m]
Concrete density	2020 kg/m ³	Model prediction	0.179 (0.184) [m]
Printing speed	83.3 mm/s	Relative difference	13 (10) %

Table 7.1: Printing parameters (left) and results for a free standing 3DCP wall (right) (adapted from Ref [161])



Gravity load	1							
Position	0 center of elements							
		From shellview component				Allowable		
		Principal 1	Principal 2					
Print speed [mm/min]	Max layer height	Max stress tensi	Min stress compress	BLF (first)	Time to print	Max compression	Max tension [MPa]	
5000	19 (0.175 m)	0.000209	-0.00557	1.003	3.42	-0.0064628	-0.00064628	

Figure 7.7: Karamba model verification of Suiker's results where red is compression stress and blue is tension stress. The table shows resulting maximum compression and tension stresses of the model compared to those allowed and the buckling load factor. The highlighted yellow cell is the governing failure mode.

7.4.3. Results

Fig. 7.8 and 7.9 shows the visualisation of the maximum wall heights achieved with the different material models at a printing speed of 6000 mm/min, checked against maximum stresses and BLF above 1. See full calculation details in Appendix E.3.

Maximum layers for unstabilised models

For the unstabilised material models it can be found that the number of layers for shotearth is assumed to be between 5 and 16 layers, which results in 0.1 m and 0.32 m wall height respectively. This is the case when comparing the walls printed at 6000 mm/min. At lower speeds more layers and therefore more wall height can be printed, the model predicts layers between 6 -31 layers (0.12 -0.62 m) for the lower and upper bounds models at 1000 mm/min, respectively. Fig. 7.11 show the allowable wall layers for the upper and lower bound models at different printing speeds. The results show that for the lower bound material, the model is governed by compressive stress for all printing speeds and for the upper bound material, the material is governed by buckling for all printing speeds.

Maximum layers for stabilised models

For the cement stabilised material models it can be found that the number of layers for shotearth is assumed to lie between 13 and 14, which results in 0.26 m and 0.28 m wall height respectively at printing speed 6000 mm/min. At lower speeds more layers and therefore more wall height can be printed, which vary between 16 -27 layers (0.32 -0.54 m), lower and upper bound models respectively at 1000 mm/min. Fig. 7.12 show the allowable wall layers for the upper and lower bound models at different printing speeds. Here as well, the results show that for the lower bound material, the model is governed by compressive stress for all printing speeds and for the upper bound material, the material is governed by buckling for all printing speeds.

Buckling analysis

For both the unstabilised and cement stabilised material models, the walls were governed by buckling regardless of their printing speeds. The buckling modes component in Karamba

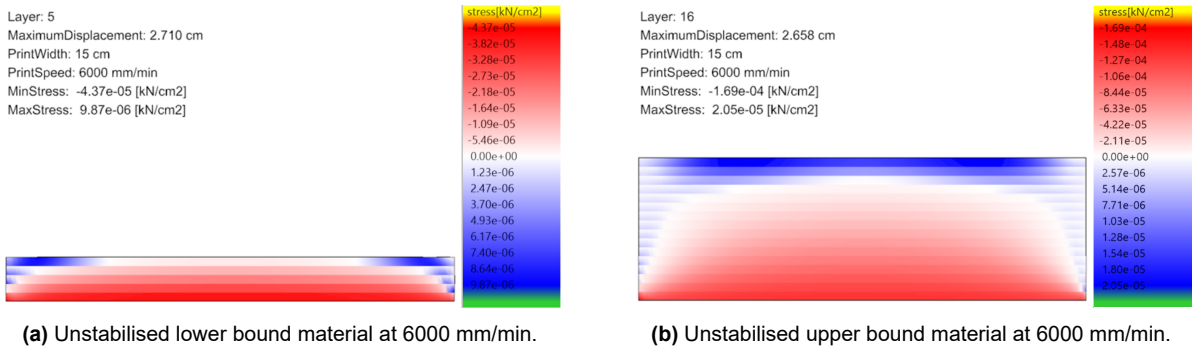


Figure 7.8: Visualisation of maximum wall height that can be printed before failure either through material crushing or buckling for the unstabilised material models at speed 6000 mm/min. Red =compression stress. Blue =tension stress.

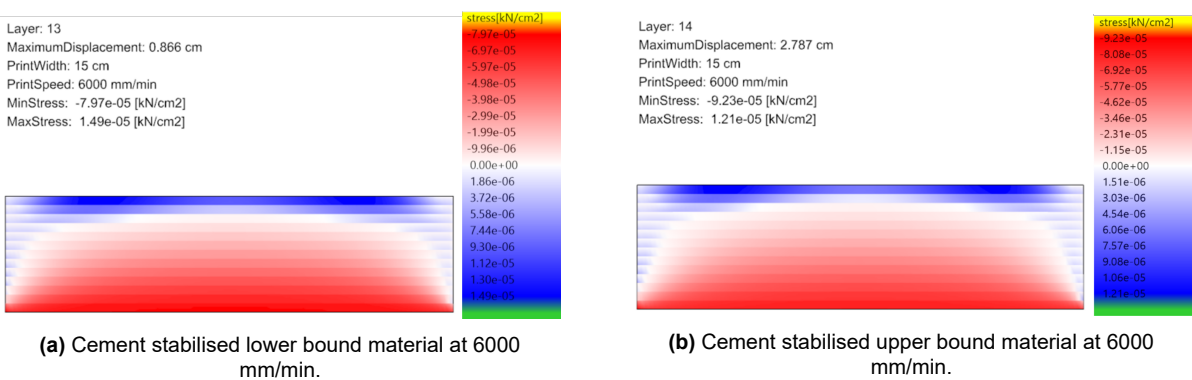


Figure 7.9: Visualisation of maximum wall height that can be printed before failure either through material crushing or buckling for the cement stabilised material models at speed 6000 mm/min. Red =compression stress. Blue =tension stress.



Figure 7.10: The first four buckling modes for the wall upper bound models unstabilised and cement stabilised

calculates the buckling load factors and visualises the buckling modes. Fig. 7.10 shows the first four buckling modes for the wall model. These buckling modes are the same for both the upper bound material models. The first buckling mode is of highest interest as it is most likely the model will fail this way during printing.

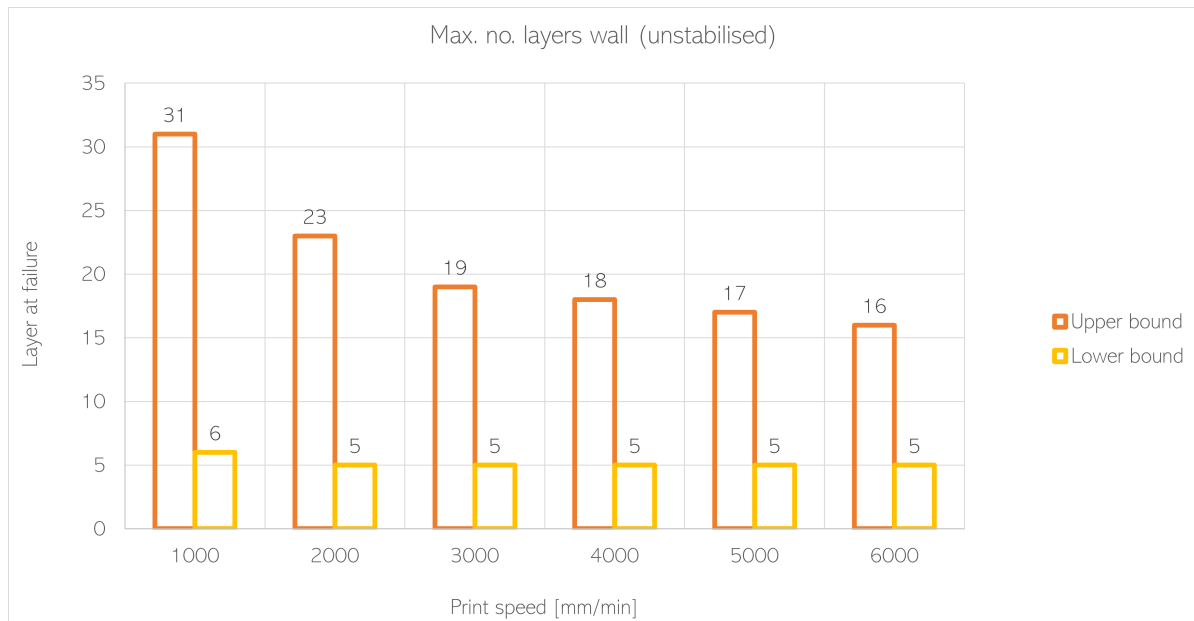


Figure 7.11: Maximum number layers for the unstabilised material models

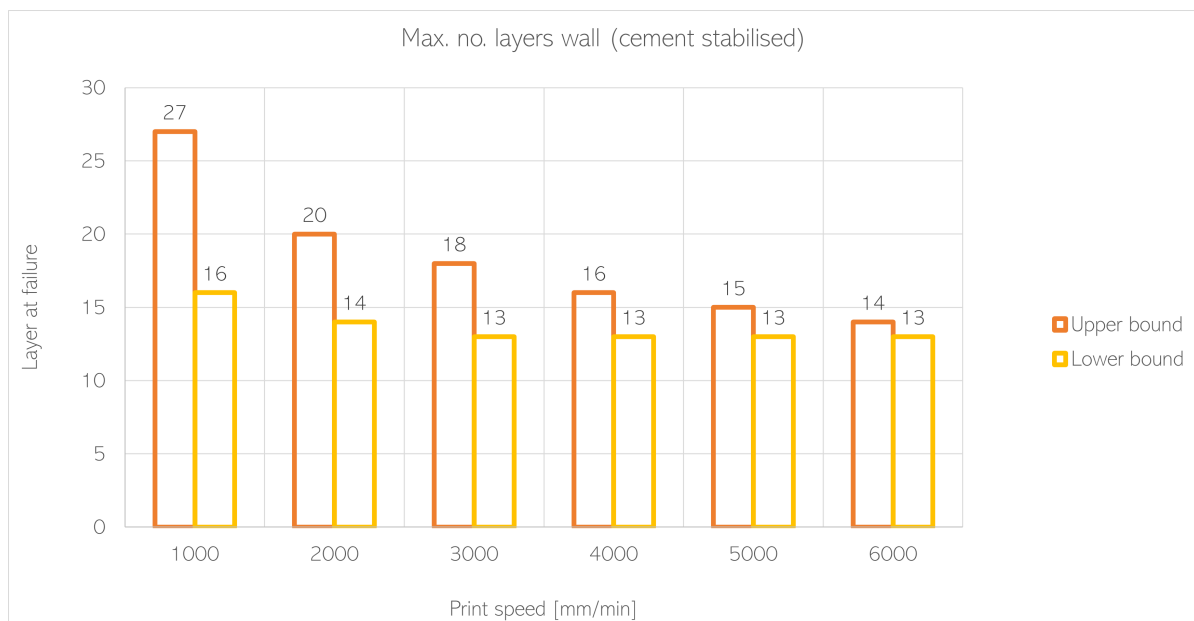


Figure 7.12: Maximum number layers for the stabilised material models

7.4.4. Discussion

Influence of model setup

The wall has been modelled as a shell where a gravity load of 1 was considered. As long as the average compressive stresses did not exceed the maximum stress and a buckling load factor of above 1 was fulfilled, the structure was deemed good. No imperfections have been considered in this analysis. Therefore the limit load and resulting maximum wall heights are probably lower in an experimental test than what is seen in Fig. 7.11 and 7.12.

A limitation of this type of analysis is that it overestimates the BLF due to imperfections. Dur-

ing fabrication a geometry will not be perfect, loading distribution will not be perfect and the same properties across each layer cannot be ensured. All these factors will lead to a reduced capacity, and is not considered in ordinary Euler buckling, which is considered in this analysis. Imperfection has not been included in the model due to the small number of layers that can be printed for the lower bound unstabilised model. Including imperfections will give a more realistic model and is further discussed in section 7.5.4.

Influence of mesh on results

For the wall model, the U count has been kept at constant 1. This represents the vertical distance of elements. Each layer is one element in the vertical direction. The V count is the number of horizontal elements. This has been varied between 10 and 110 to check how the results change with changing mesh. As seen in Fig. 7.13, a V count of 50 and above does not significantly change the results. A V count of 100 has been applied in this analysis.

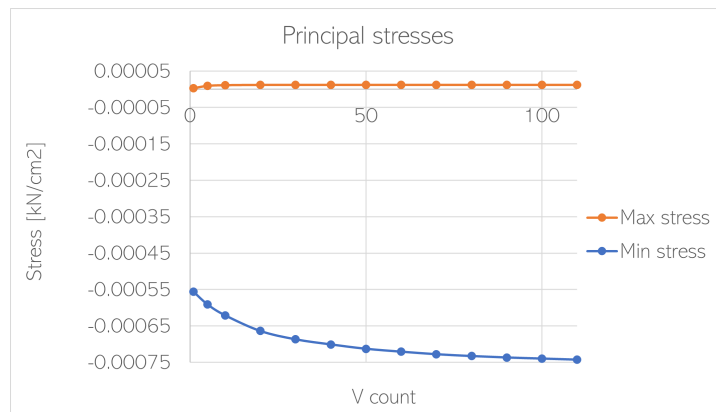


Figure 7.13: Mesh resolution influence on results, U count =1, V count =1 -110 where max. stress = maximum tension stress and min. stress = maximum compression stress

Influence of material models

The materials models have resulted in wall heights within the expected. All upper bound models give more layers than lower bound models with the variation of printing speed. With the lower bound models it is observed that maximum wall heights do not change much when varying the speed. Also both lower bound model failures are governed by maximum stress, while the upper bound model failures are governed by buckling.

A specific weight of 20.3 kN/m³ has been used for all the material models. This differs from what has been specified previously. 20.3 kN/m³ is the value from Curto but since density of natural earth varies between 17.5 to 22.0 kN/m³, it was deemed reasonable to keep the same value for all, although density from Gomaa's study on 3D printed earth was found to be 18.3 kN/m³.

Comparison of results

Fig. 7.14 and 7.15 compares the upper bound and lower bound models together. Especially for the upper bound models, it can be seen that around the same number of layers can be achieved which means that the unstabilised earth may work as well as the cement stabilised earth. This brings back the discussion on when to stabilise earth materials for construction, section 4.1.4.

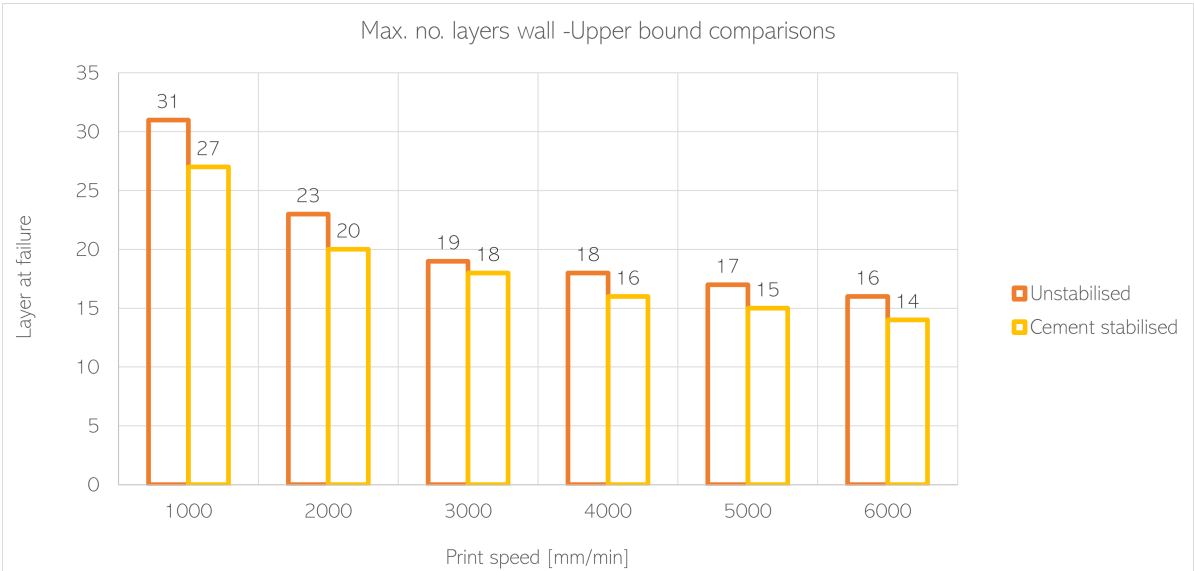


Figure 7.14: Comparison of maximum wall height for upper bound material models

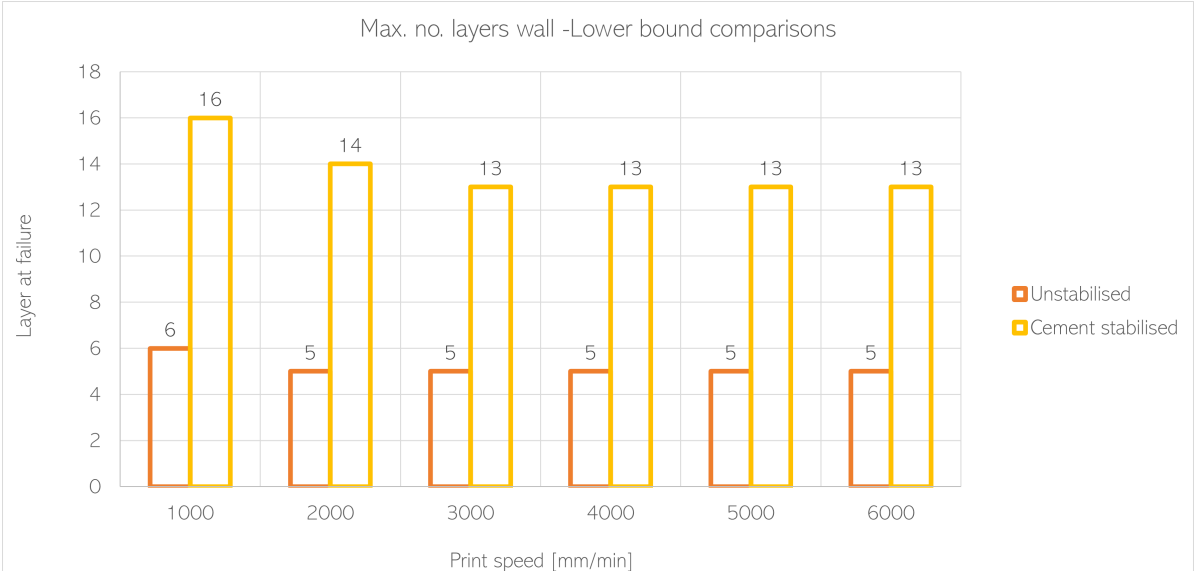


Figure 7.15: Comparison of maximum wall height for lower bound material models

7.5. Barrel vault and half dome structures

To determine the fabrication feasibility of shotearth compression-only structures, the next geometries assessed are a barrel vault and a half dome. The goal is to find the maximal overhang that can be achieved with no or minimal formwork. This gives opportunity to a more fully automated construction process that uses the least amount of material. To evaluate the maximum dimensions that can be achieved, both the roman and nubian layering techniques is applied. Corbelling is not considered due to the difficulty of modelling. For this work, the hypothesis is that the nubian method will result in a bigger overhang compared to the roman method, as the inclined layer stacking is expected to result in greater stability of the structure during printing.

7.5.1. Geometry, element definition and loads

The model setup for the barrel vault and the half dome is the same as previously for the monolithic wall, the only difference being the input geometries. The elements, material definitions and loads are the same as described earlier. Both geometries analysed will have target dimensions of 1 m rise, 1 m span and 1 m depth. Section width is again 0.15 m and layer thickness is 0.02 m. The curvature of the vault and dome follows a bezier curve, see Fig. 7.16. Fig. 7.17 shows the scripted definition in GH.

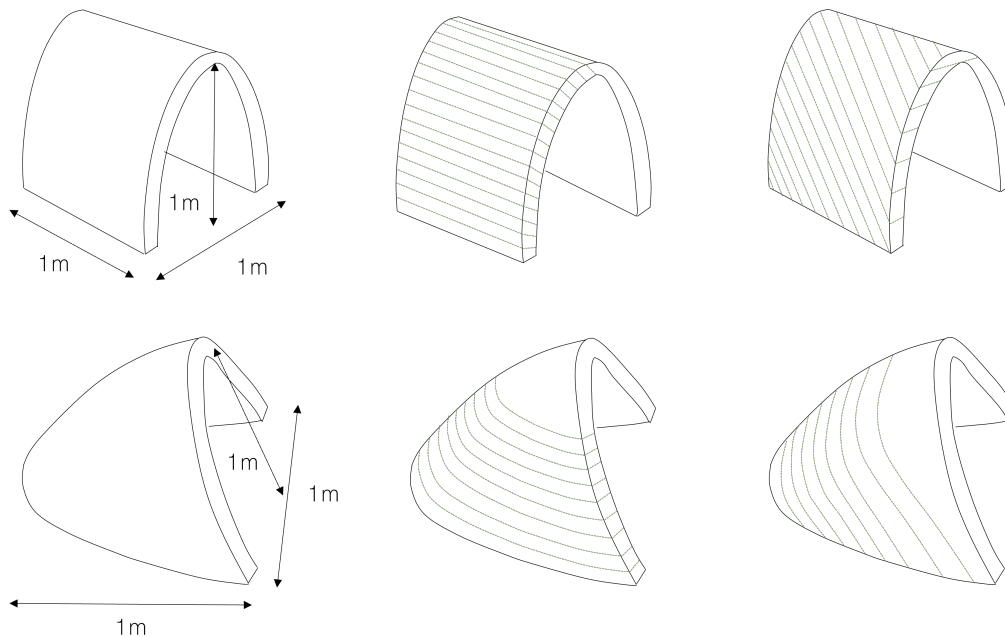


Figure 7.16: Top: geometric setup of the barrel vault. Bottom: geometric setup of the half dome. Middle: Roman layering for both geometries. Right: Nubian layering for both geometries.

Boundary conditions and slicing direction

All translations and rotations are fixed at the interface between printing plane and first print layer. For the barrel vault, when modelling the nubian layering technique, the edge in z direction is also fixed, assuming that the structure is printed against a support wall. For the nubian vaulting technique, the slicing direction applied can be seen in Fig. 7.18, resulting in an angle of 35 degrees. This has been applied to both geometries.

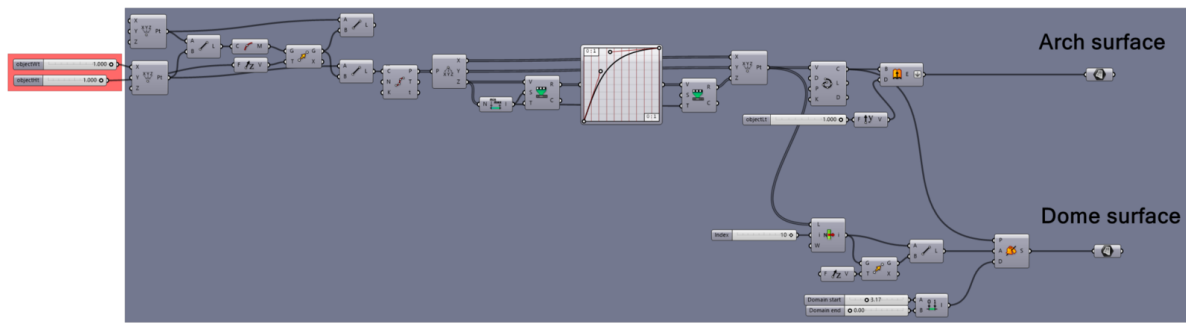


Figure 7.17: Grasshopper definition for both the barrel vault, labelled arch surface, and the half dome, labelled dome surface, geometries.

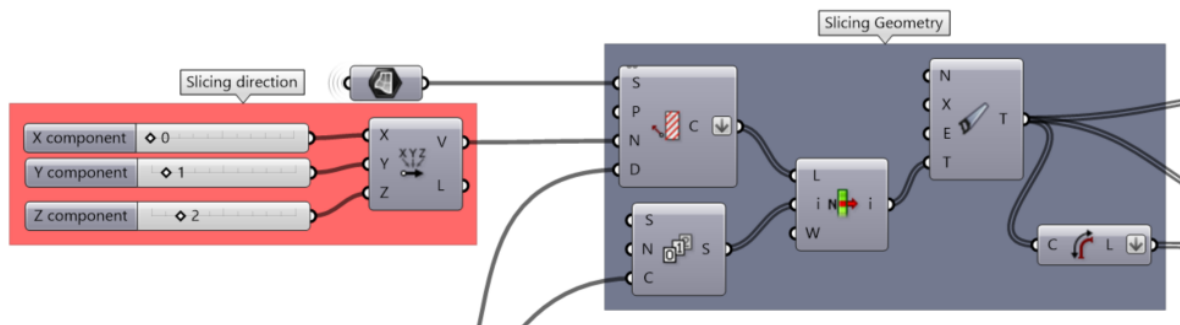


Figure 7.18: Setup of the slicing direction for the geometries

7.5.2. Analysis check

Stress and buckling check

To evaluate the maximum overhang angle and the maximum number of layers that can be printed not only compression stresses and buckling will govern the failure but also tension stresses can cause failure due to bending caused by the geometry of the structures. For the compression and buckling check, the same requirements as before applies. Maximum compression is governed by the equations defined for the material model in question. For maximum tension, if it is within 10 % of the compression strength it is okay. For the buckling check, a buckling load factor (BLF) above 1 is considered good. Excessive deformations can be a governing factor but they are not considered in this analysis. More on this will be discussed in section 7.5.4. In summary the ultimate limit states checked in this analysis are:

- principal compressive stress < compressive strength of material model
- principal tensile stress < tensile strength = 10% of compressive strength
- buckling load factor > 1

First order analysis check

Again, to verify the outputs of Karamba, a simple linear stress analysis was performed for the barrel vault using the following equations. First the resulting force (self-weight) of the geometry was found. Then the moment was calculated and from this these the equivalent compression and tension stresses found in the first layer of the structure.

$$F := \rho \cdot l \cdot h \cdot w \quad (7.5)$$

Where $\rho = 20.3 \text{ kN/m}^3$, $l = 1 \text{ m}$, $w = 0.15 \text{ m}$, $h = t \cdot n \text{ [m]}$, where $t = 0.02 \text{ m}$ and n is number of layers.

$$M := F \cdot e \quad (7.6)$$

Where e is the distance between the center of gravity of the whole geometry to its fixed boundary. This value is measured in the model as it changes with layer height.

$$\sigma_c := \left(-\frac{M}{\frac{1}{6} \cdot l \cdot w^2} - \frac{F}{l \cdot w} \right) \quad (7.7)$$

$$\sigma_t := \left(\frac{M}{\frac{1}{6} \cdot l \cdot w^2} - \frac{F}{l \cdot w} \right) \quad (7.8)$$

Inputting $n = 21$, e is 0.037, which results in σ_c is -0.2139 MPa and σ_t is 0.0043 MPa. The Karamba first order analysis output shows $\sigma_c = -0.2100$ MPa and $\sigma_t = 0.00389$ MPa. The difference between the hand check and the computational output is about 1.8 % for σ_c and 9.30 % for σ_t . The hand check and the first order stress outputs from Karamba is shown to correspond very well.

7.5.3. Results

The results shown are outputs of the second order analysis in Karamba. For the roman layering only printing speeds at 1000 and 6000 mm/min. have been analysed, as from the wall structure, it is evident that taller structures can be printed at lower print speeds. For the nubian layering only printing speeds at 1000 mm/min. have been analysed to assess maximum dimensions compared to the roman layering. Table 7.2 provides an overview of all the results. For detailed calculations see Appendix E.4, E.5.

Barrel vault -roman method

Unstabilised material: For the lower bound material, the maximum layer height across all printing speeds is 5. This results in an overhang angle of 8.92 degrees compared to the monolithic wall. For the upper bound material the maximum layer height for a 1000 mm/min. printing speed is 26 layers and for a 6000 mm/min speed is 15 layers. Resulting in an angle of overhang between 10.18 to 9.67 degrees respectively compared to the monolithic wall. Fig 7.19 and 7.20, show the visualisation of the results.

Cement stabilised material: For the lower bound material, the maximum layer height varies from 10 layers at 1000 mm/min to 9 layers at 6000 mm/min. The angle of overhang is 9.36 and 9.28 degrees respectively. For the upper bound material, the maximum layer height varies from 21 layers at 1000 mm/min to 11 layers at 6000 mm/min. The angle of overhang is 9.44 to 10.02 degrees respectively. Fig 7.21 and 7.22, show the visualisation of the results.

Barrel vault -nubian method

Unstabilised material: For the nubian method, a layering angle of 35 degrees has been set. This is in correspondence with the angle used in Carneau et. al. [158], which varies but is at maximum 40 degrees. Fig. 7.23 show the results for the unstabilised models (a) lower bound and (b) upper bound for a printing speed at 1000 mm/min. The number of layers that can be printed are 3 and 9 respectively before failure by buckling occurs.

Cement stabilised material: Fig. 7.24 show the same for the cement stabilised models. Interestingly in (a) lower bound shows more layers, 13, than (b) upper bound model with 8 layers. The lower bound model also fails by compression rather than buckling for the upper bound. An overhang angle has not been obtained due to fact that only a corner of the model is printed.

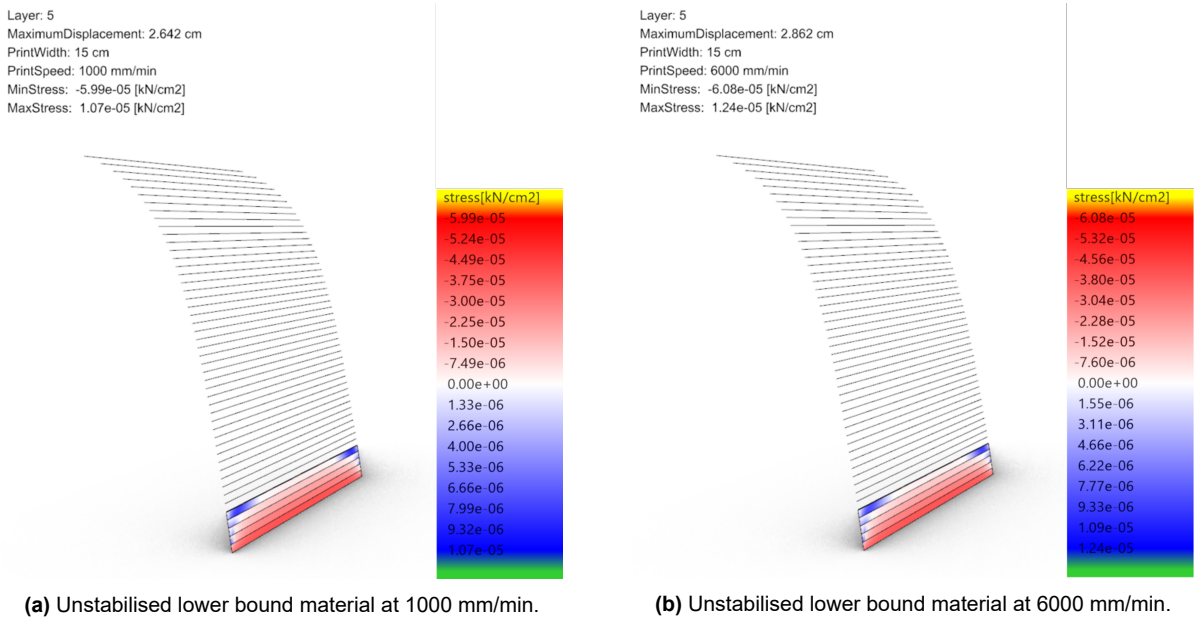


Figure 7.19: Half of the barrel vault with roman layering technique using unstabilised lower bound material model at printing speed 1000 and 6000 mm/min. The horizontal lines show the expected printing path. Red =compression stress. Blue =tension stress.

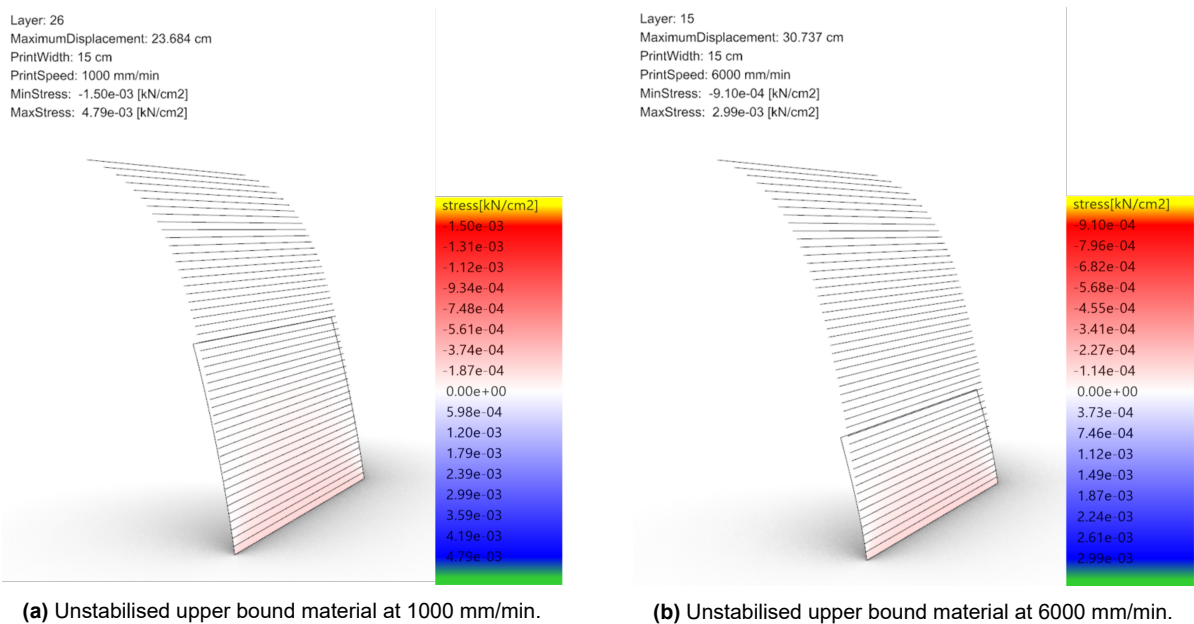


Figure 7.20: Half of the barrel vault with roman layering technique using unstabilised upper bound material model at printing speed 1000 and 6000 mm/min. The horizontal lines show the expected printing path. Red =compression stress. Blue =tension stress.

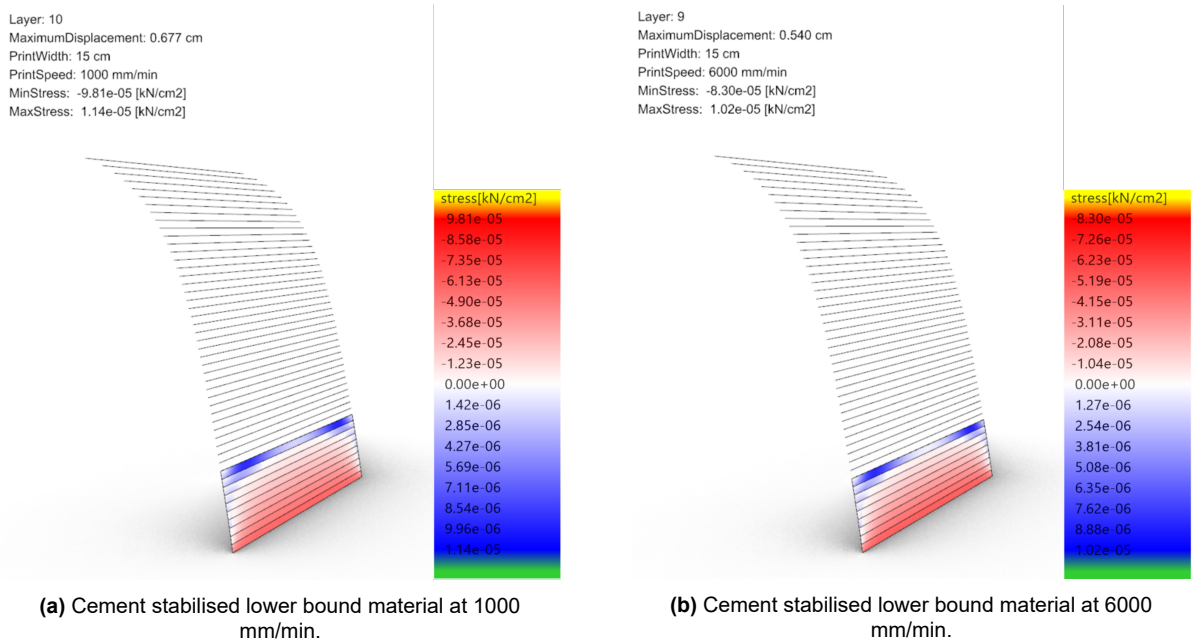


Figure 7.21: Half of the barrel vault with roman layering technique using cement stabilised lower bound material model at printing speed 1000 and 6000 mm/min. The horizontal lines show the expected printing path. Red =compression stress. Blue =tension stress.

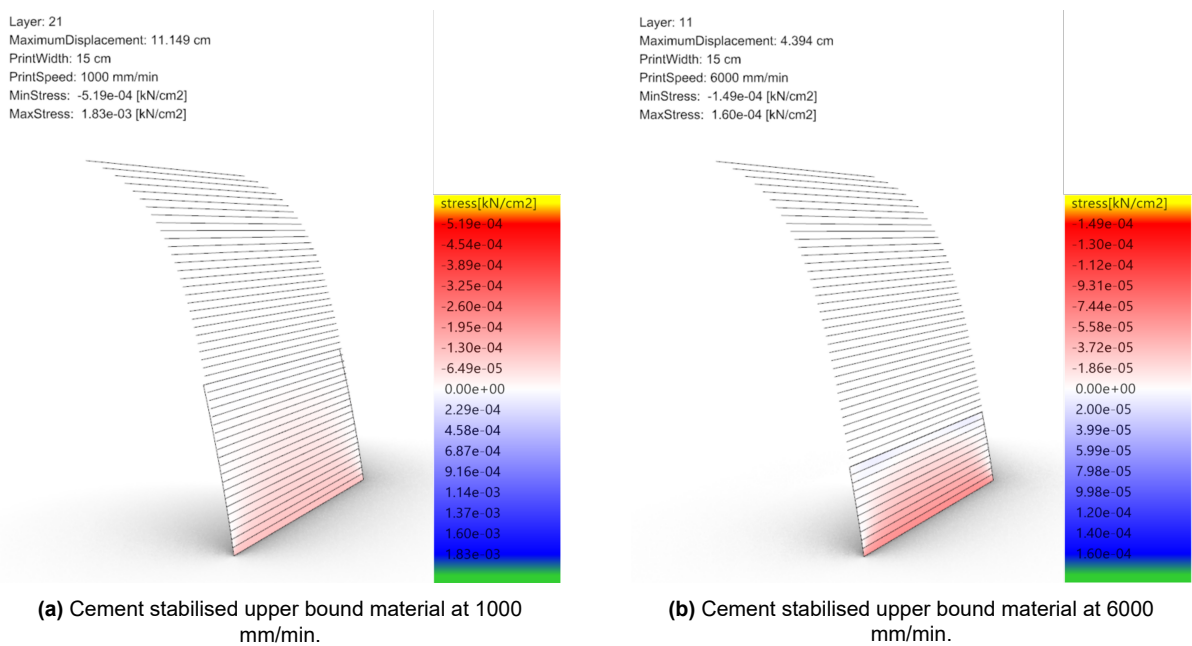


Figure 7.22: Half of the barrel vault with roman layering technique using cement stabilised upper bound material model at printing speed 1000 and 6000 mm/min. The horizontal lines show the expected printing path. Red =compression stress. Blue =tension stress.

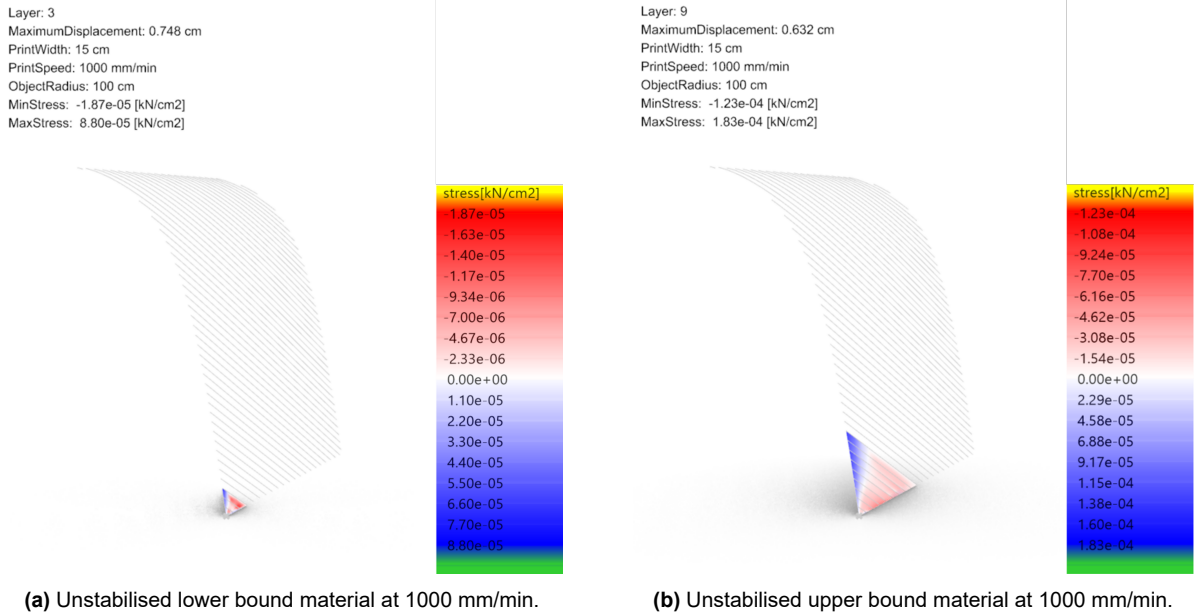


Figure 7.23: Half of the barrel vault with nubian layering technique using unstabilised material models at printing speed 1000 mm/min. The inclined lines show the expected printing path. Red =compression stress. Blue =tension stress.

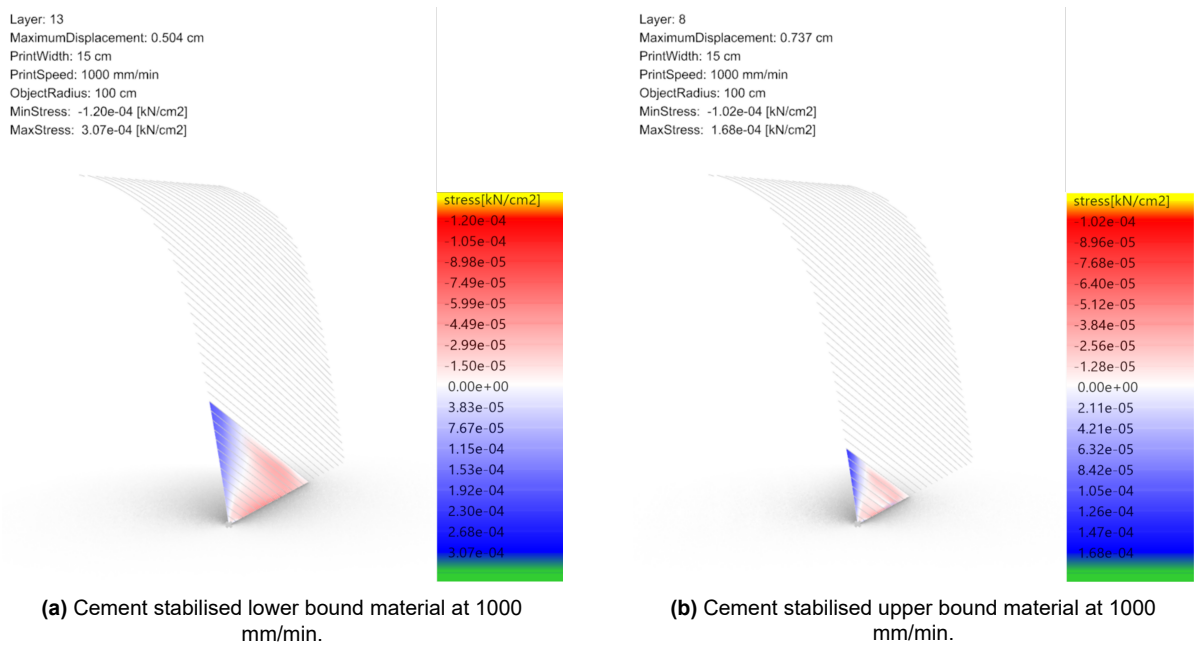


Figure 7.24: Half of the barrel vault with nubian layering technique using cement stabilised material models at printing speed 1000 mm/min. The inclined lines show the expected printing path. Red =compression stress. Blue =tension stress.

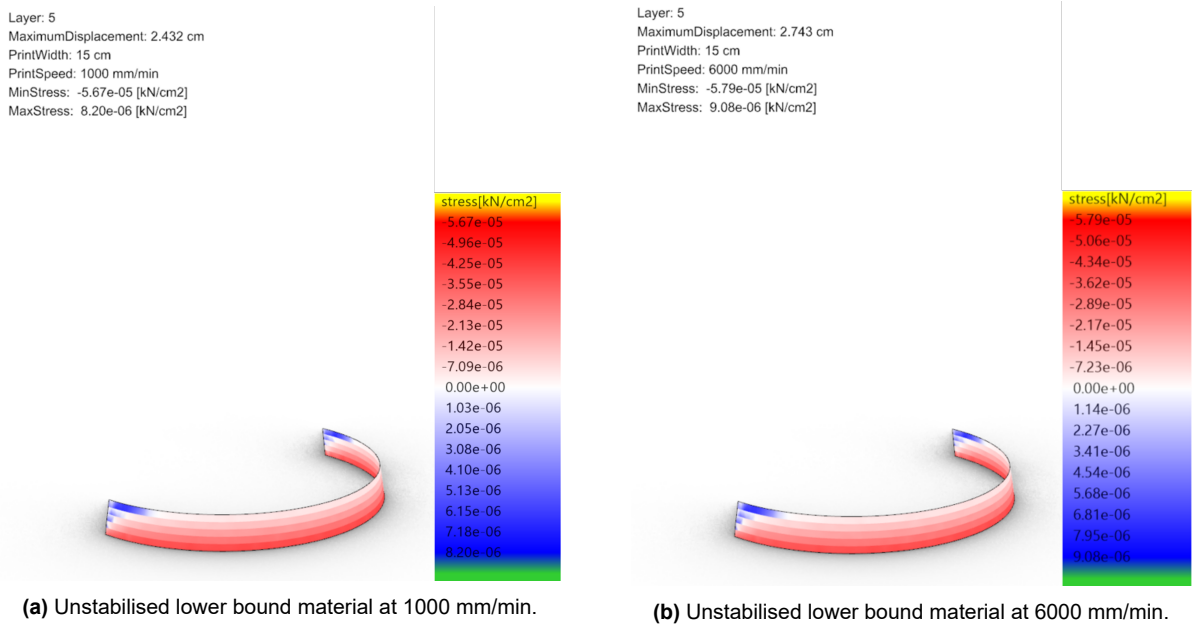


Figure 7.25: Half dome with roman layering technique using unstabilised lower bound material model at printing speed 1000 and 6000 mm/min. Red =compression stress. Blue =tension stress

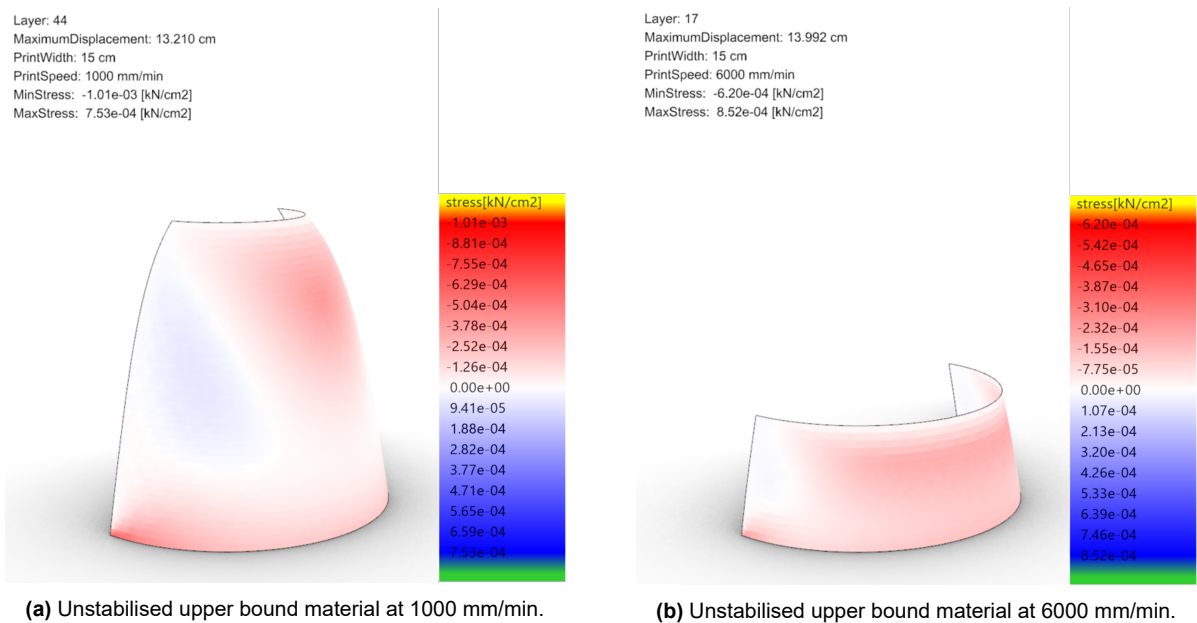


Figure 7.26: Half dome with roman layering technique using unstabilised upper bound material model at printing speed 1000 and 6000 mm/min. Red =compression stress. Blue =tension stress

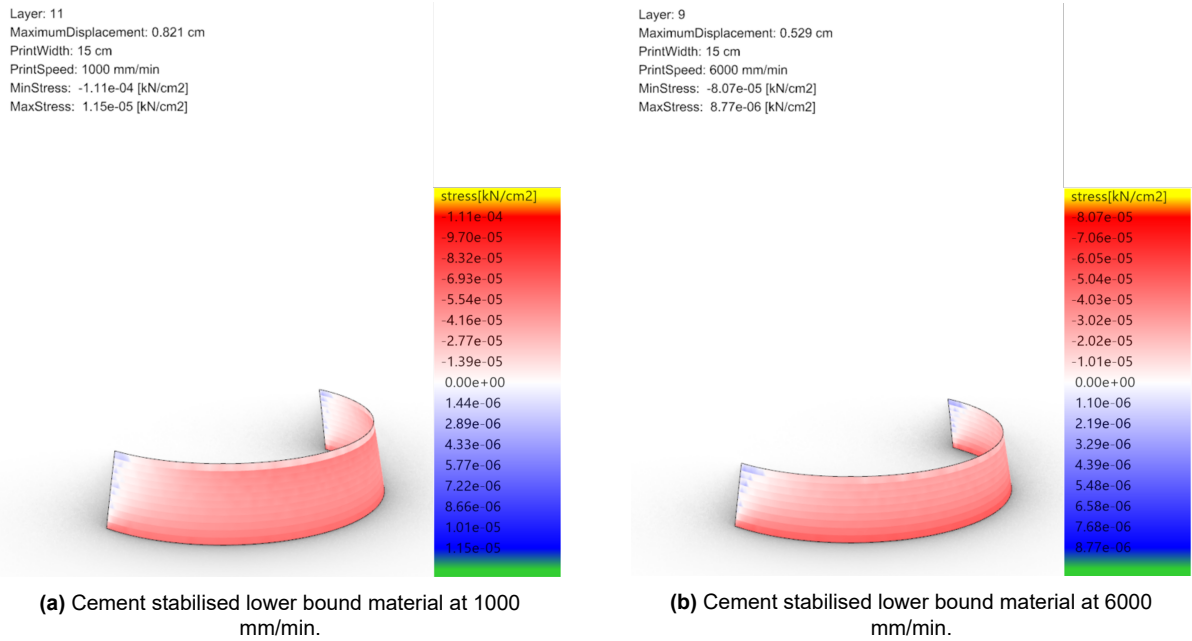


Figure 7.27: Half dome with roman layering technique using cement stabilised lower bound material model at printing speed 1000 and 6000 mm/min. Red =compression stress. Blue =tension stress

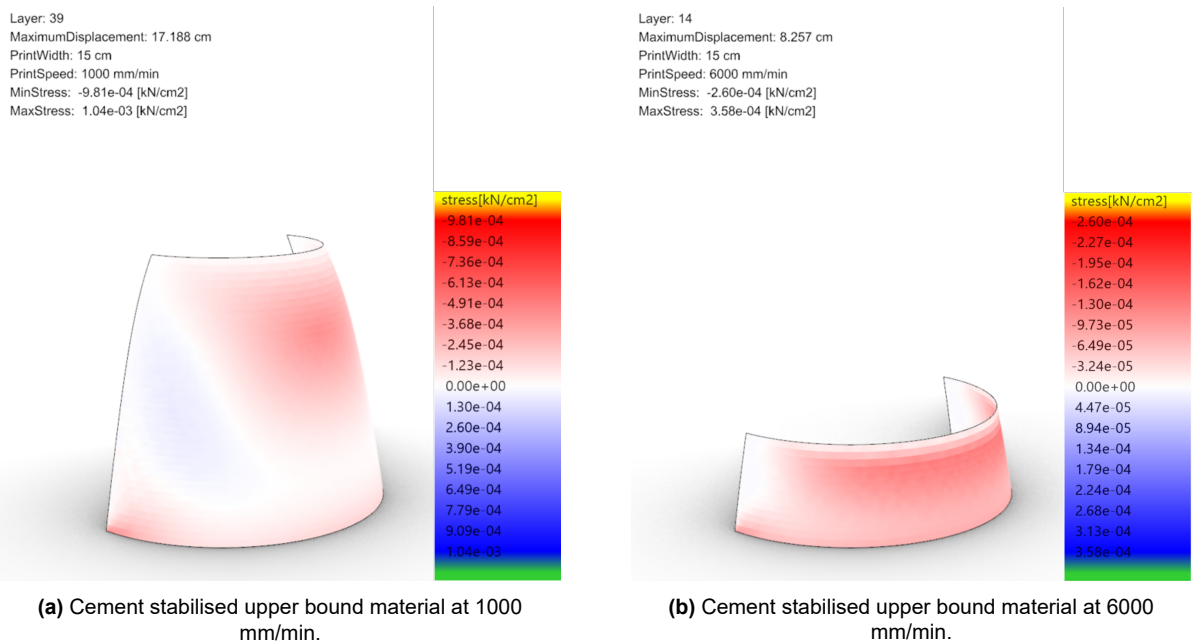


Figure 7.28: Half dome with roman layering technique using cement stabilised upper bound material model at printing speed 1000 and 6000 mm/min. Red =compression stress. Blue =tension stress.

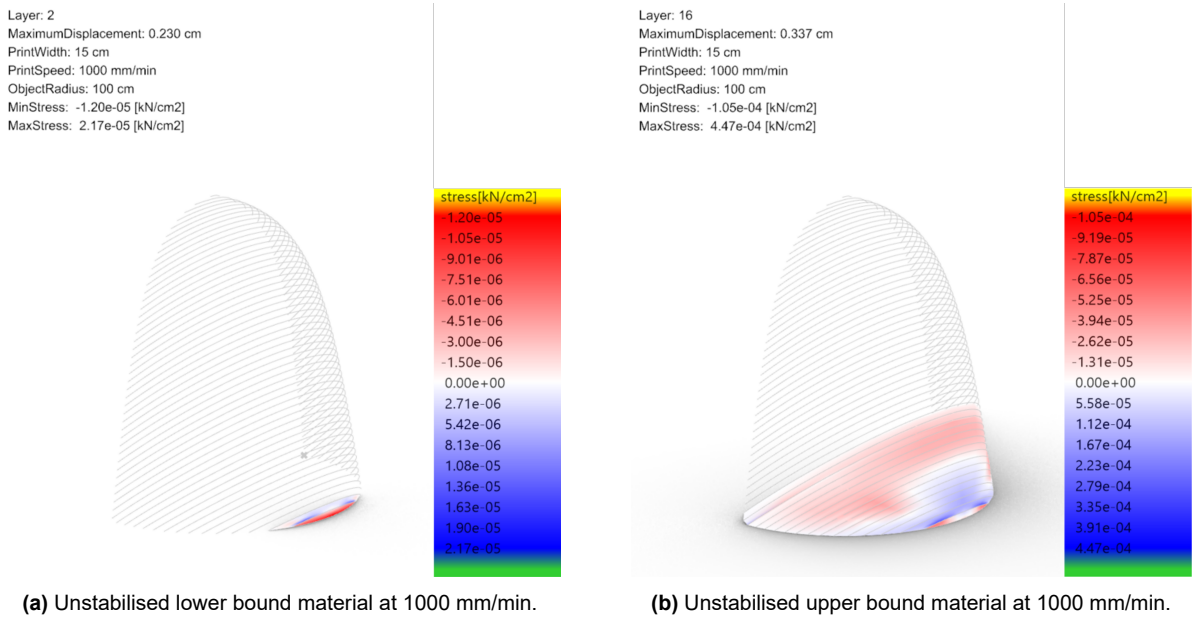


Figure 7.29: Half dome with nubian layering technique using unstabilised material models at printing speed 1000 mm/min. The inclined lines show the expected printing path. Red =compression stress. Blue =tension stress.

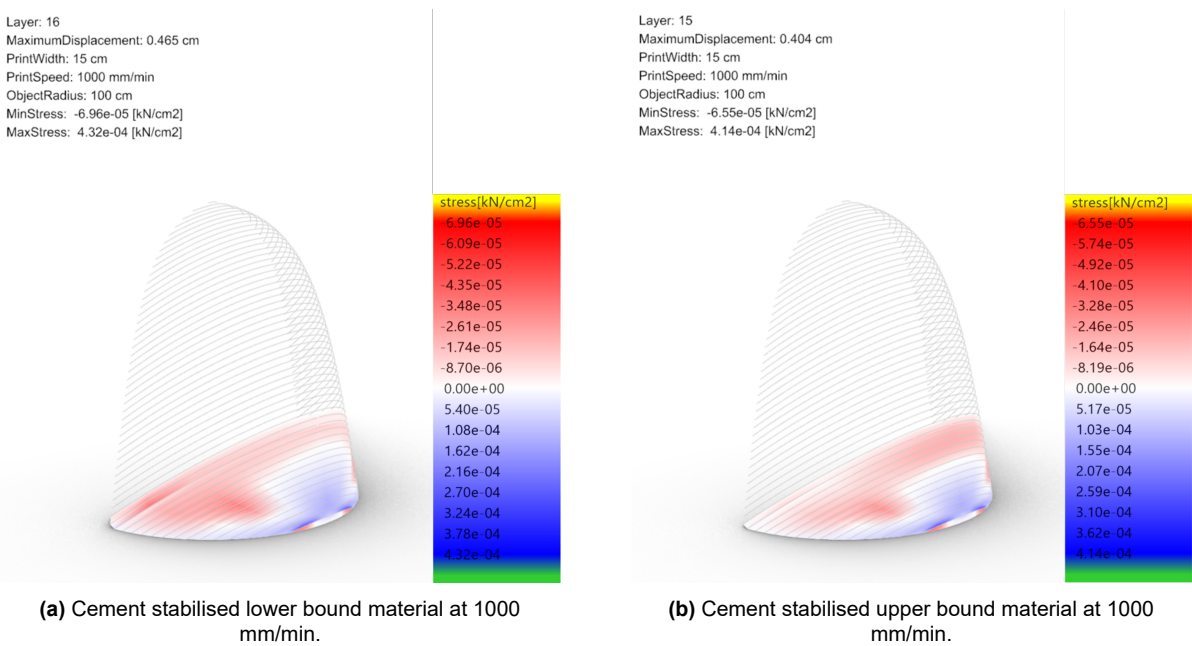


Figure 7.30: Half dome with nubian layering technique using cement stabilised material models at printing speed 1000 mm/min. The inclined lines show the expected printing path. Red =compression stress. Blue =tension stress.

Half dome -roman method

Unstabilised material model For the lower bound model, a maximum of 5 layers regardless of printing speed is possible. This results in a maximum angle of 8.92 degrees compared to the vertical wall. For the upper bound model, a big variation in the maximum number of layers that can be printed is found. At 1000 mm/min. the maximum number of layers is 44, and almost the full geometry can be printed, however, tension stresses then start to become too high. At 6000 mm/min, the number of layers is 17 where buckling is governing. Fig. 7.25, 7.26 show the visualisation of the results.

Cement stabilised material model For the lower bound model the maximum number of layers varies between 11 and 9 at the lowest and highest printing speeds. The governing failure is compression stresses being exceeded. The upper bound model also shows a big variation in maximum number of layers that can be printed, when comparing the lowest and highest printing speeds, at 39 and 14 layers respectively. Fig. 7.27, 7.28 show the visualisation of the results.

<u>Barrel vault</u>				
	Max. no of layers	Height of structure [m]	Overhang angle [degree]	Governing failure
Roman				
Unstabilised				
-1000 mm/min	5 -26	0.1 -0.42	8.92 -10.18	C -T
-6000 mm/min	5 -15	0.1 -0.28	8.92 -9.67	C -B
Cement stabilised				
-1000 mm/min	10 -21	0.2 -0.42	9.36 -9.44	C -T
-6000 mm/min	9 -11	0.18 -0.22	9.28 -10.02	C -T
Nubian				
Unstabilised				
-1000 mm/min	3 -9	Only prints a corner	N/A	B -B
Cement stabilised				
-1000 mm/min	13 -8*	Only prints a corner	N/A	C -B
<u>Half dome</u>				
	Max. no of layers	Height of structure [m]	Overhang angle [degree]	Governing failure
Roman				
Unstabilised				
-1000 mm/min	5 -44	0.1 -0.88	8.92 -9.95	C -B
-6000 mm/min	5 -17	0.1 -0.34	8.92 -9.73	C -B
Cement stabilised				
-1000 mm/min	11 -39	0.22 -0.78	9.44 -10.01	C -B
-6000 mm/min	9 -14	0.18 -0.28	9.28 -9.67	C -T
Nubian				
Unstabilised				
-1000 mm/min	2 -16	0.04 -0.33	8.63 -10.02	T -B
Cement stabilised				
-1000 mm/min	16 -15*	0.33 -0.35	10.02 -9.96	B -B

*lower bound model results in more layers than the upper bound model

C: compression, T: tension, B: buckling

Table 7.2: Overview of results from the both barrel vault and half dome roman and nubian layering techniques

Half dome -nubian method

Unstabilised material model: Fig. 7.29 show maximum number of layers that can be printed for the lower bound material model (a) and upper bound model (b) at a printing speed of 1000 mm/min, which is 2 and 16 layers respectively.

Cement stabilised material model: Fig. 7.30 show that 16 and 15 layers can be printed respectively for the lower bound (a) and upper bound (b) material models before they both fail by buckling. The governing failure is buckling and due to the geometrical shape, as the free edge of the shape has not been restrained in the model.

7.5.4. Discussion

Barrel vault

For the barrel vault, the results show that the roman technique yields more layers compared to the nubian technique. This applies for all the material models assessed and therefore disproves the hypothesis set at the beginning of this chapter. The few number of layers that can be printed from the nubian technique can be caused by the fact that the first layer in the corner is really short or small. The time required to print this is so short that it can simply not support the next layer, which is bigger, and the next layer again which is even bigger. Karamba reads the material development linearly, therefore, it is likely that the small layers in the corner are simply not strong enough to support the rest of the print. The governing failure mode for the nubian technique is buckling. The buckling modes show the material sliding down towards the bottom edge. Again, this can be attributed to the material not being stable enough. Varying the printing time for the first few layers, giving more time between the first 5 layers and then fully printing the subsequent ones can give more stability and more structure to be fabricated.

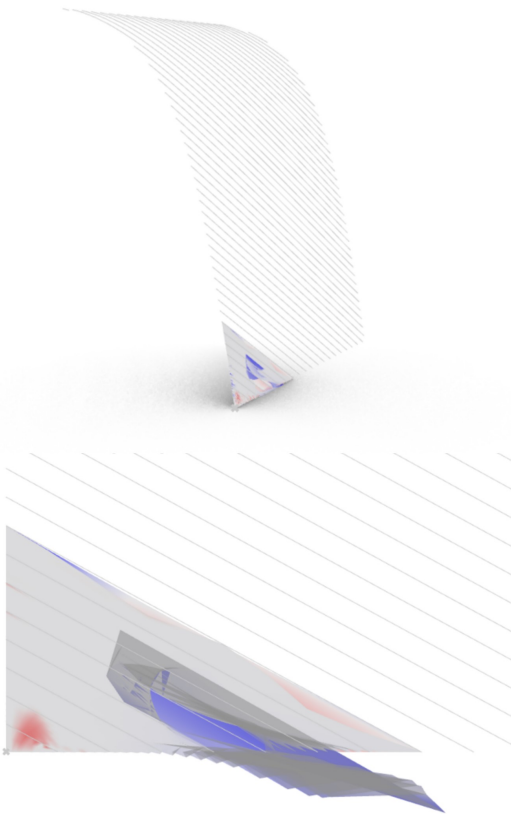
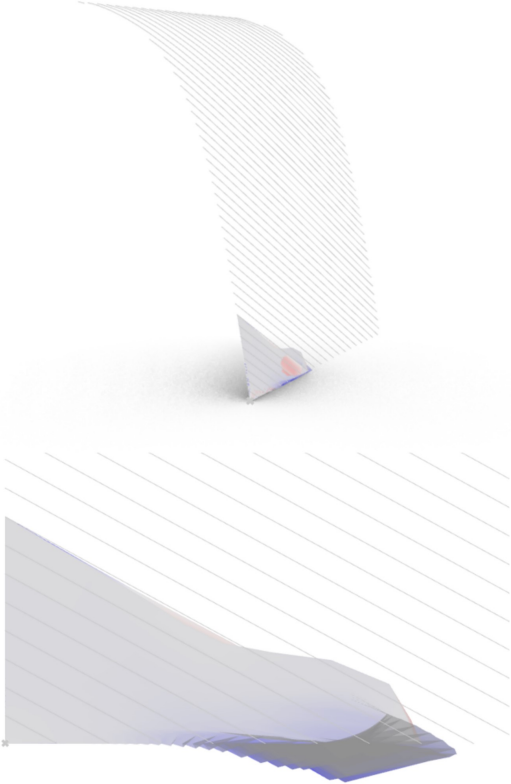
Buckling modes The buckling modes of the inclined layering sees the layers collapsing onto itself in the same direction as the printing (in-plane) as opposed to out of plane which is seen for the other models, Fig. 7.31. This may suggest a modelling issue, where a redefinition of either mesh or different take on nubian layering is required.

Model setup The main problem when modelling the barrel vault with the nubian technique is the inclination of layers where the definition of support points along the vertical z-direction and the horizontal x-direction proved to be tricky. This in combination with finding an appropriate mesh resolution. For both the barrel vault and half dome, the mesh UV count has been set at $U = 10$ and $V = 10$ as higher resolutions resulted in convergence problems. The way Karamba read the inclination of layers is that it omitted the first layer surface of both geometries. For the barrel vault, this concerned the corner, for the half dome, the layers were arched hanging in the air unsupported. This first layer surface had to be redefined and then added to the other surfaces, in order to create one uniform mesh. As a result the mesh resolution here is slightly different from the rest. The definition of support points also follow the mesh resolution as points can only be created along the mesh edges. Again, a redefinition of either mesh or a different take on nubian layering can be done to resolve this issue, Fig. 7.32.

Layering angle The layer angle and supporting points are not always parametric. Meaning changing the layering angle does not always capture all the supporting points required, this is also related to the mesh resolution, where changing of the layering angle requires redefining support points and mesh.

Layer: 8
 MaximumDisplacement: 0.737 cm
 PrintWidth: 15 cm
 PrintSpeed: 1000 mm/min
 ObjectRadius: 100 cm
 MinStress: -1.02e-04 [kN/cm2]
 MaxStress: 1.68e-04 [kN/cm2]

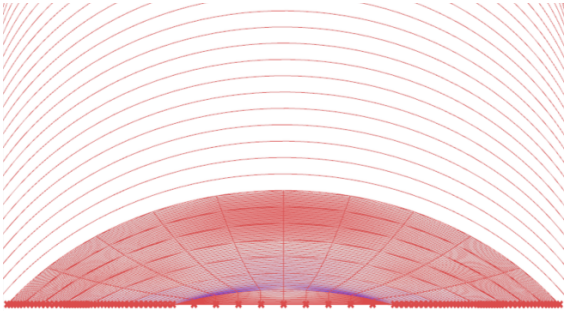
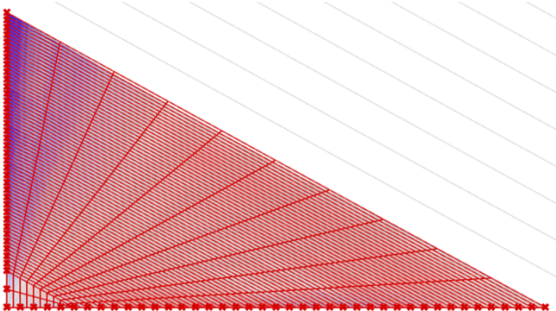
Layer: 8
 MaximumDisplacement: 0.737 cm
 PrintWidth: 15 cm
 PrintSpeed: 1000 mm/min
 ObjectRadius: 100 cm
 MinStress: -1.02e-04 [kN/cm2]
 MaxStress: 1.68e-04 [kN/cm2]



(a) Barrel vault with nubian layering where the lines show printing path. Buckling mode 1, BLF =1.24

(b) Barrel vault with nubian layering where the lines show printing path. Buckling mode 2, BLF =1.35

Figure 7.31: Barrel vault with nubian layering buckling modes 1 and 2



(a) Mesh and support points for the barrel vault nubian technique

(b) Mesh and support points for the half dome nubian technique

Figure 7.32: Barrel vault and half dome mesh and support definitions

Half dome

For the half dome, when comparing it to the free standing wall and the barrel vault, it shows that for the upper bound material models (both unstabilised and cement stabilised), a lot more layers can be printed at the same printing speeds. This can be explained by the fact that the half dome has more stability than the wall and the vault. The curvature of the dome also results in longer print times, which gives more time for the material to harden. When comparing the roman and nubian methods, it is seen that the nubian models can only reach layer 15 or 16 which is the corner of the geometry. The edge of the geometry is not fixed and hence, the models will fail by buckling, due to sliding of the material. However, the results show that it is possible to model a vault with the nubian technique and if the free edge was fixed it could probably give more layers. Therefore, again the hypothesis set at the beginning of this chapter is disproved. More consideration to the geometry and layer transition of printing angle could give a better result.

Carneau et al. [158] obtained a dome structure and a nubian vault structure without formwork by optimising the printing parameters such as inter-layer time for every layer and distance of nozzle to target. The main part of the vault here was obtained with a 40 degree angle, and the transition region with an inclination ranging from 0 to 40 degrees. This highlights the importance in developing parametric algorithms for toolpath generation to push the boundaries of what can be achieved. The ability to print overhangs depend on shape (geometry), thixotropy, interface adhesion (material), inter-layer time, and nozzle distance to target (processing).

Barrel vault and half dome

The results also show that the nubian method is more favourable for printing a half dome as opposed to a barrel vault starting in the corner. This can be improved by optimising printing parameters. Here it is seen the importance the printing parameters play a role in the fabrication feasibility of a structure. This aspect is out of scope for this thesis.

The analysis of the two arched structures have not considered any architectural view points. Or considered the appropriate catenary prior to the start of printing. The targeted dimensions has merely been set to 1m rise and span. A better way of doing could be 1) Find the appropriate funicular form using the hardened properties of the material. 2) Based on the results of the form finding a possible division of the geometry that defines the path of the printing can be defined. 3) Verify the form by making a model of the structure and see how it can be refined with combining the printing constraints.

Limitations of material models

Material non-linearity has been accounted for in time dependent equation definitions, however, further non-linearity of the material models has not been accounted for due to lack of experimental testing and data from literature. The resulting structures all have a fabrication time that is less than 1 hour. This means that only the first equation defined for strength and stiffness development is used. None of the structures take more than 2 hours to print meaning that the other equations defined have not been used. Optimisation of printing time can see the use of the other equations. Nevertheless, the material models defined over 20 and 28 days gives the target hardened properties which can be useful for construction planning.

Limitation of geometric considerations -characterisation of shell

When designed properly shell structures can take large loads through membrane action while their thickness can be much less than plates or slabs covering the same area. Depending on the a/t ratio where a is the radius and t is the thickness of the shell, shell structures can be divided into different categories varying from thick to thin shells [169].

- Very thick shells ($a/t \leq 5$): 3D effects and solid elements
- Thick shells ($5 \leq a/t \leq 15$): In-plane membrane forces, out of plane bending and higher order transverse shear included
- Moderate shells ($15 \leq a/t \leq 30$): In-plane membrane forces, out of plane bending and linear transverse shear included
- Thin shells ($30 \leq a/t \leq 4000$): In-plane membrane forces, out of plane bending and shear included, though transverse shear deformation neglected
- Membrane ($4000 \leq a/t$): In-plane membrane forces only

Where:

$$a = \frac{1}{2}s + \frac{1}{8}\frac{l^2}{s} \quad (7.9)$$

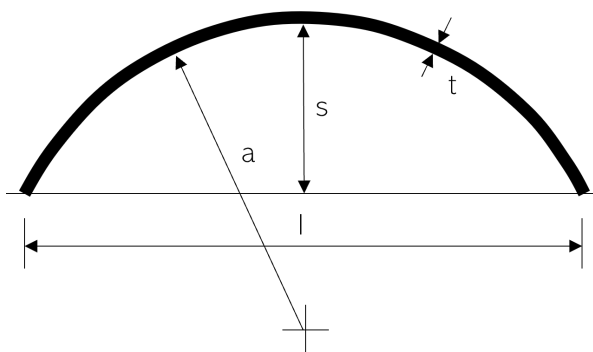


Figure 7.33: a / t ratio (adapted from Ref [169])

This results in the shell considered in this analysis to be "very thick shells" given that s and l are both 1, resulting in a/t ratio to be 4.1667. Most analysis programmes are developed for thin shells. Although the shell structures in this work are considered very thick shells, it has been analysed as a thin shell. More consideration of the geometry, either scaling up the dimensions or lowering the section thickness is recommended.

Limitations of Karamba and analysis method

Linear elastic vs. non-linear analysis

The analysis performed here utilises the Analyse THII component in Karamba which takes into account second order theory. Therefore, the type of analysis performed is considered geometrically non-linear but considering a linear elastic material. To verify that it is indeed what Karamba has done. The hand check using eqns. 7.5 -7.8 has been done to see how many layers can be printed if a first order analysis was considered. By checking against the allowable stresses for the cement stabilised upper bound model, the results showed that 37 layers would be possible in a first order analysis vs. 21 layers possible in a second order analysis. This is in line with the shell theory as seen in Fig. 7.34.

Karamba is limited to material linear elastic calculations. The limitation of idealising the material as linear elastic is that it will incorrectly predict tensile stresses that the material is not capable of supporting. Therefore, the critical failure load may not be predicted correctly. In masonry vaults, linear elastic methods are incapable of predicting the actual behaviour or failure state. Plastic design approach, or equilibrium approach, allows for the existence of many possible load paths within a structure. If one equilibrium state can be found for a structure given a set of loads, the structure can be demonstrated as safe. The equilibrium approach

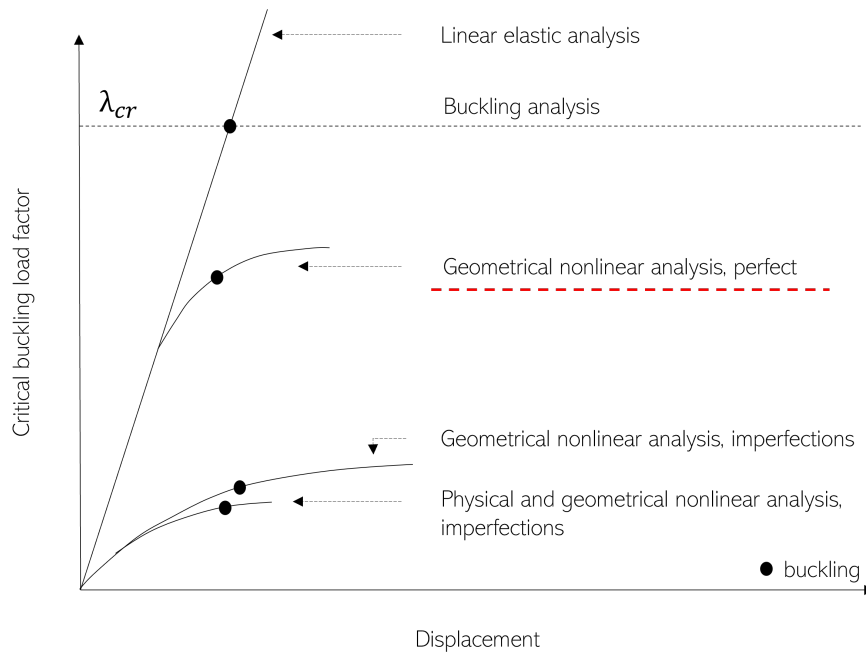


Figure 7.34: Finite element analysis of shells (adapted from Ref [170])

can be carried out using e.g. graphic statics.

Furthermore, for FE analysis, Karamba only uses triangular elements, which can be bad in terms of accuracy, as a lot elements are required to get a decent accuracy out of constant strain triangles. Therefore, enough mesh and proper convergence is required for the results. The speed of Karambas calculations is a result of the limitations of the software.

Consideration of displacements

The consideration of displacements is a serviceability limit state requirement and have not been considered in the analysis. It can be seen from the results that some structures result in very big displacements. If a displacement criterion were to be included, more design criteria with regards to e.g. the function of the structure can be taken more into account through optimising fabrication parameters or geometrical shape. However, displacement limits would have to be agreed upon amongst stakeholders involved. This has not been considered in this work.

Consideration of imperfections

Imperfections have not been considered in this model. Due to the big field of research into imperfections in non-linear analysis, it is hard to determine the appropriate knockdown factor. However, if imperfections were considered, applying a factor of 3 can be considered to reach the real life physical shape. However, it must be noted that this value is a conservative estimate and more in depth considerations are required for more precise prediction of the imperfection factor. Fig. 7.35 and 7.36 compares the barrel vault and half dome, using unstabilised upper bound material model at printing speed 1000 mm/min., with and without the imperfection factor considered. The difference for the barrel vault is 11 layers while for the half dome it is 23 layers.

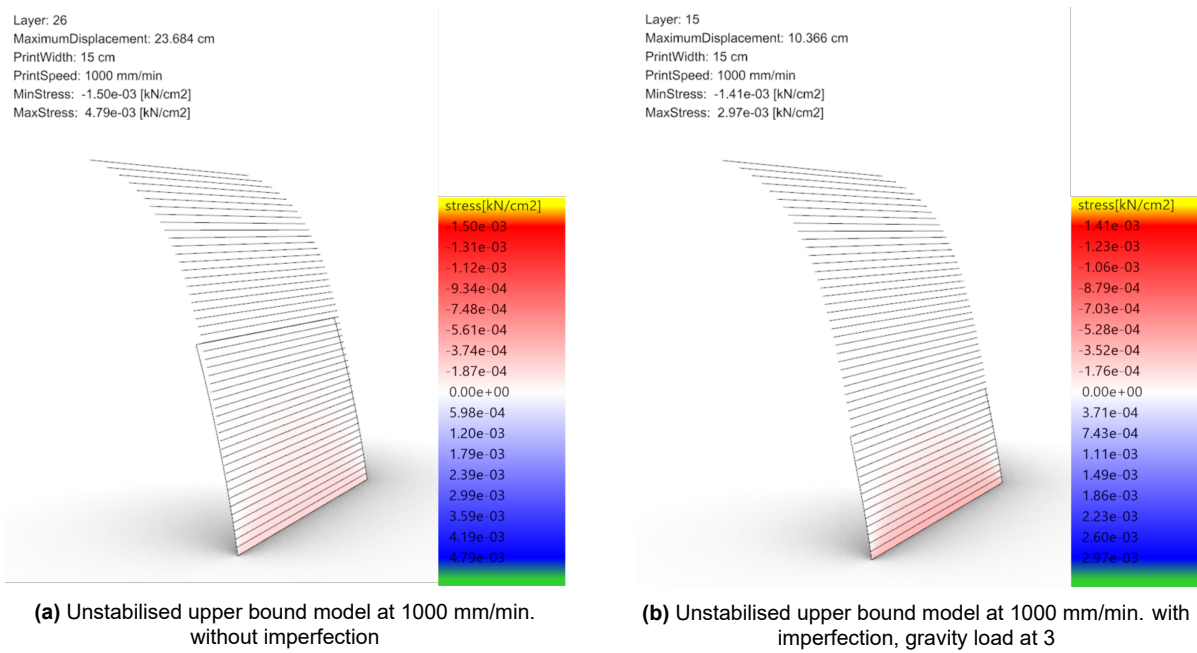


Figure 7.35: Comparison of barrel vault with (b) and without imperfections (a)

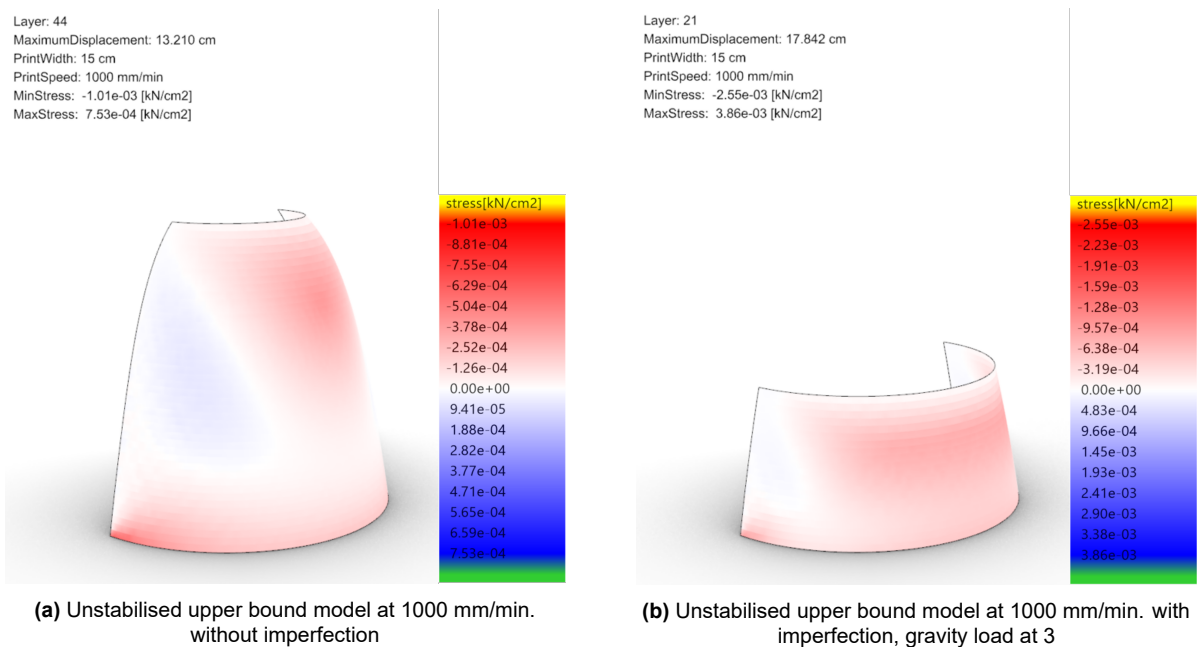
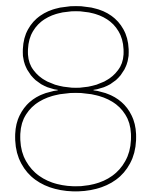


Figure 7.36: Comparison of half dome with (b) and without imperfections (a)



Conclusion

8.1. Main question: Fabrication feasibility of shotearth structures

What is the fabrication feasibility of robotically fabricated shotearth structures?

This thesis showcases the possibility of fabricating compression-only structures using shotearth material where a wall and two different arched structures were assessed for their possible dimensions and fabrication times. As shotearth is a novel printing technique using a material that is not widely understood, the assessment was performed through the development of different material models and the variation of printing speed. The structures were analysed according to limit state design using the geometrical non-linear finite element analysis method provided by Karamba3D. To achieve the results in this study, borrowed concepts from other areas, including soil mechanics/ geotechnical engineering, masonry design, concrete and shotcrete technology, 3D printing through the methods of extrusion and spraying, and shell structural analysis, were taken.

It is recognised that the fabrication feasibility of shotearth compression-only structures requires in-depth material understanding combined with optimal processing parameters. Fig. 8.1 show the main influences on a resulting printed shotearth geometry where the red boxes show the parameters taken into account in this study.

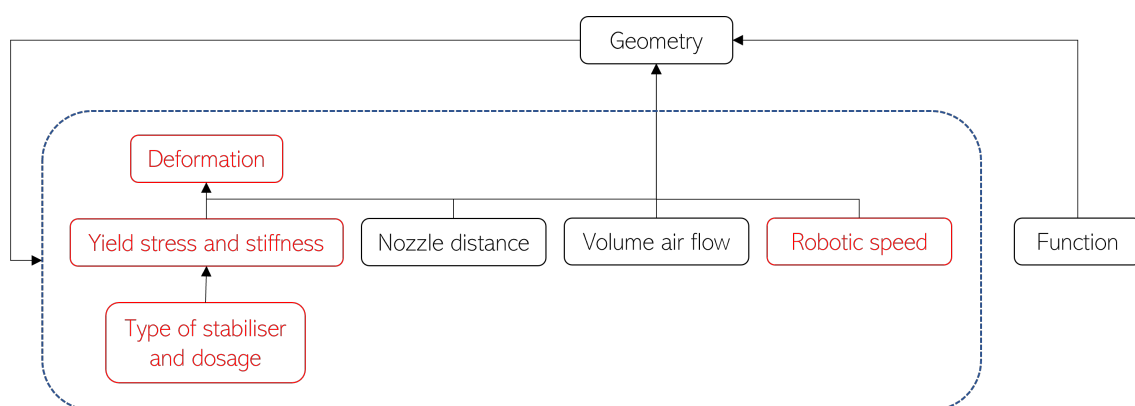


Figure 8.1: Design considerations taken into account in this work

Answer to sub question 1: Prediction of shotearth materials

What are the properties of earth building materials and 3D printed cementitious materials and how can this be used to predict shotearth material behaviour?

The prediction of shotearth material combined the theory from earth building material research and requirements for 3D printing of cementitious materials. The mechanical properties of earthen materials is impossible to predict or generalise without testing for its soil composition, mineralogy and water content. In literature, many different testing procedures have been adopted from other disciplines to measure their properties. This along with an infinite number of stabilisers, aggregates and other materials used in mix designs make it incredibly difficult to understand and compare. This means when looking for material properties from literature, one has to take the measured values with a pinch of salt. A suggested approach is to do statistical analysis of similar studies to get an average or a range of values, which can be used as an assumption.

The requirements for robotic shotearth material is similar to that of 3D concrete printing and shotcrete 3D printing in terms of consistency due to pumpability and extrudability /sprayability demands. This requires the material to be pasty. However, unlike concrete, extruded /sprayed earth materials require a longer drying process to achieve the mechanical properties desired. This again depends on the type of soil used and other materials in the mix design. Due to the ongoing debate of yes cement (stabilised) or no cement (unstabilised) in earth construction along with the few studies to date that have measured extruded and sprayed earth properties. Two assumptions were made for the robotic shotearth, one without and one with cement. Compressive strength and Young's modulus are the two most important properties when it comes to assessing the buildability of a structure.

The properties of unstabilised shotearth are assumed to lie within the range of rammed earth and extruded earth. As soil composition is impossible to compare, a study of the water content in these two types of earth construction techniques concluded that shotearth is closer to extruded earth in terms of consistency but has higher compaction due to the high air flow during fabrication. This results in a compressive strength value lying between those of rammed earth and extruded earth. Young's modulus of the material is inconclusive due to lack of data and varied testing procedures. The Young's modulus assumed in this study has been based on an existing measured value in extruded earth.

The properties of cement stabilised shotearth are, first, assumed to behave like concrete, second, assumed to reach a certain set of target values measured in one study, and third, assumed to lie within the range of 3D extruded and 3D sprayed concrete. The assumption is grossly based on one statement. The results are compressive strength and Young's modulus developments that closely follow the same curve. More certainty and predictability of the material behaviour is reached compared to the unstabilised models.

Answer to sub question 2: Structural design of earth structures

What are the design techniques of existing earthen wall and arch structures and how can these be applied to the design of a shotearth structures?

Earthen wall

3D printed structures have been related to masonry structures and can be considered as a new approach to masonry. In masonry, building components are built through the layer-by-layer stacking of elements joined by mortar. The 3D printing of aggregate based material

can be regarded as an infinite brick where components are also built through a layer-by-layer stacking. Existing earth building techniques that can also be related to masonry are rammed earth and earth blocks (e.g. compressed earth masonry (dry), adobe (wet)). To consider these techniques for the design of shotearth, the material consistencies of these techniques should be comparable to the 3D printing technique. For example, rammed earth (dry method) has different considerations during fabrication compared to 3D printing (wet method).

The structural design of existing planar earth wall structures cannot be applied to the structural design of shotearth wall structures, as there are no coherent guides or codes that specify requirements for the slenderness ratio and strength. This is due to each country or region having their own recommendations that are adapted to local conditions. Most of these also consider only the dry method building techniques. Due to the novelty of 3D printed structures, also no guides exist on how to design these and not all assessment procedures have been standardised in order to measure maximum dimensions (buildability) that can be achieved.

Earthen arches, vaults and domes

The structural design of ancient arches, vaults and domes structures using earth masonry elements can be used as a reference for the design of modern printed arch, vault and dome structures. However, methods to design efficient earthen arch structures as well as arched printed structures are currently unknown. Taking inspiration from masonry, for the design and fabrication of these shell structures, strength, stiffness and stability, especially during construction, are the most important aspects to take into account. The geometrical shape also plays a big role in terms of stability as it should be able to resist loads during fabrication as well as during its intended use and lifecycle. In ancient construction, catenaries were found as the most efficient type of shape as it is free of bending. To minimise reliance of formwork during construction, different layering techniques (roman, nubian, corbelling) can be applied and optimised for. Safety factors for earthen arch structures should account for variable soil compositions and imperfections which depend on the shape analysed. Strategies to protect projects from moisture to ensure durability should be taken into account throughout the whole design process.

Answer to sub question 3: Fabrication times and dimensions of shotearth structures

What are the possible fabrication times and dimensions of shotearth structures?

Monolithic wall

It can be concluded that for a 1 m wide wall, a wall height between 0.12 -0.62 m can be printed when using an unstabilised mix, while a cement stabilised mix can give wall heights between 0.32 -0.54 m. When assessing the dimensions from the upper bound materials at the lowest printing speed of 1000 mm/min. considered, unstabilised (0.62 m) and cement stabilised (0.54 m) walls are shown to reach similar heights. This gives to conclude that unstabilised shotearth has as much potential as stabilised shotearth to build walls. There is of course a lot of uncertainty involved. Nevertheless, this prediction shows and takes part in the discussion of when to stabilise earthen walls, if the raw earth wall may work just as well.

Overhang with roman layering technique

With the current available computational tools and the assumptions made, more so an overhang rather than a full arch has been achieved. The printing speed has been assessed at 1000 mm/min and 6000 mm/min. The result of both the barrel vault and half dome show that for the unstabilised material a possible overhanging angle around 9 -10 degrees. For the cement stabilised material, it is around the same. For the case of the half dome, considering both upper bound models, the results show that almost the full structure can be printed at the printing

speed 1000 mm/min. Although, this is not taking into account any shell imperfections, it shows that there is possibility. Due to the important time dependent nature of printed materials, one could imagine starting the print overnight at a much lower speed and have components ready the next day. This gives even more potential to achieve full geometries.

Overhang with nubian layering technique

The result of both the barrel vault and half dome using the nubian layering technique also show that for the unstabilised and stabilised materials a possible overhang of around 9 -10 degrees can be achieved. This is the case for the half dome structure. The barrel vault structure shows that inclined layering can be possible but more attention to the layer angle and print parameters are required for better assessment. The nubian layering technique have a possibility to result in larger overhangs as proven in ancient construction and has also been demonstrated in printed concrete but is unclear from this research due to no form finding on the geometry has been performed and little attention to the layering angle. Variation of layering angle could result in a bigger and better overhang.

The result of both the barrel vault and half dome structures along with projects demonstrated so far show that it is possible to use to earth material to print compression-only structures using either unstabilised and cement stabilised material until a certain point. To print a full vault or dome, using the tool developed by Witteveen +Bos, formwork is unavoidable at a certain point of the print, as the closer to the apex it gets during printing, the bigger the tension stresses will be at the bottom layers, and so to avoid this, the solution will have to include tensile reinforcement or formwork. To minimise or optimise the need for formwork or reinforcement more consideration is required for the fabrication and processing aspects. An idea is to either divide the structure into different sections with different dimensions and different printing parameters to then be assembled (like masonry), or use formwork during printing at the apex of the structure.

Effect of printing speed

This study has measured the effects of possible dimensions and fabrication time through the variation of robotic print speed. From the monolithic wall structure, it can be concluded that slower printing speeds give more layers. However, this also depends on the material. Raw earth materials take more time to develop strength compared to a stabilised material. For both the upper and lower bound unstabilised materials, it has been observed that the maximum allowable compressive strength did not change much with the change of printing speed. Especially, when looking at the unstabilised lower bound material model applied to a wall, it can be seen that regardless of printing speed applied, a maximum of 6 layers can be printed at the lowest speed and 5 layers at the highest speed before the structure fails by material crushing. The same conditions apply for the two arch structures. The cement stabilised material models resulted in dimensions closer to each other. This can be attributed to the hydration products in concrete that gives higher material strength in the early ages compared to the unstabilised.

Answer to sub question 4: Considerations required for real construction

What are the design considerations required for real construction?

To fully design, simulate and fabricate a shotearth vault or overhanging structure, four main considerations are required. Where each consideration need their own special attention in order to reach an optimal result. These are understanding of early-age material behaviour, influence of processing parameters on the material properties and shape, the structural safety

of the shape to be fabricated both during construction and intended service life, and the simulation tool used.

Not considered in this study:

- Geometry: a vault was created without considering its shape
- Material: rebound effects, shrinkage effects, bond strength between layers, environmental conditions
- Processing: optimised print path, inter-layer time, nozzle type and distance to target, material deposition direction.

To properly model shotearth, one should consider developing a simulation tool that can predict the flow of material, which gives opportunity for an in-depth process parameter study, as well as structural behaviour.

Other considerations

Environmental conditions play a big role in mechanical strength which has not been considered. This gives difficulty when applying the method on site. The high water content required to print earthen elements will undergo shrinkage in the hardening process, leading to possible cracking and other technical issues. This must be considered in the design. So far, no studies address this aspect [171].

8.2. Future outlook on earth and shotearth construction

The past few years has seen an increase in digital manufacturing research and demonstrations using earthen materials. They show a great potential of creating a new architectural style for earth building and construction, while providing many benefits to urban spaces in terms of circularity and sustainability, better indoor environments. Further development in this field could also start to integrate functionally graded materials for future construction, which have potential to optimise building performances even more. Craveiro et al. [120] explored this possibility through the demonstration of a design tool. Earth buildings as a wider term provides many opportunities for poverty alleviation and is a solution to world housing crisis. Here earth masonry elements and rammed earth play a big role, in terms of being more low tech but still very efficient and impactful solution. Interest in earth arches, vaults and domes offer the contemporary designer rich possibilities for achieving radical new designs. Improvements in design tools, an increase in environmentally sustainable building techniques will contribute to the continued relevance, innovation and growth. Thousands of years after these materials and methods first appeared, earthen vaults have untapped potential to create exceptional buildings.

8.2.1. Standardisation

One of the biggest issues regarding earth materials is the absence of standardisation in the material and products. Given the novelty of the robotic shotearth fabrication technique and the need for large scale rigorous testing to understand the material and influence of processes. In digital manufacturing the experiments and prototypes are in the early ages and is fragmented, as with earth construction in general. Many projects, showcase the design possibilities of AM in earth construction but do not provide scientific information on the fabrication feasibility e.g. workflow and processes, material standards, and performance aspects e.g. structural, thermal and environmental. The lack of information prevents the industry from implementing and

considering this material + construction method, and authorities from regulating it. Therefore, shotearth is unlikely to become standardised and used as a common construction method for the time being. More promise can be found in earth structural masonry or raw earth bricks. Earth masonry is a commercial product produced in the same way as commercial bricks but unfired. The manufacturing process can ensure high density and uniformity of bricks given that the material is the same. Compared to other forms of earth construction: cob, rammed earth. Earth masonry have higher strengths. Systematic structural testing of earth components will provide a roadmap for standardisation [171].

8.2.2. Sustainability

Digital construction methods have the potential of being sustainable in all aspects of the material and fabrication chain through resource utilisation, energy consumption and cleaner + efficient production. However, few studies have explored the the environmental impact of AM technology in construction, Agusti-Juan and Habert [172] found that digital fabrication provides environmental benefits when applied for complex structures rather than simple wall structures. Currently very little data is available on the energy consumption of AM processes and must be further assessed [173]. 3D concrete printing, which currently has the interest of most researchers and industry stakeholders, is not yet environmentally friendly as most mixtures have more than 40% higher binder content than conventional mould cast concrete. The binder system is the most energy-intensive part of the concrete [174]. Several studies have focused on alternative binders and recycled aggregates to improve sustainability; however, more research is still needed to understand mechanical properties. This also applies to the case of earth construction, where cement is the most utilised stabilising material. Much more focus on material development and research to improve and understand the sustainability of earth construction and AM technologies.

8.2.3. Cost benefits

Economic benefits of earth construction in general is not clear. The general conception and most attractive thing about earth is that it is in principle free and abundant. Though it is obvious that material sourced further away from site and any stabiliser added increases costs, modern earth constructions are in general more expensive than projects using conventional materials. This is mainly due to lack of training and experience among engineers and builders which require specialists to realise these projects. AM technologies can automate large parts of the manual work required, however, economic benefits of AM technologies in general are also not yet clear. The geometric freedom that comes with this technology enables designers to apply topology optimisation to reduce material usage. In the cases of no formwork even further material reduction can be achieved. Weng et al. [175] found that 3DCP, compared to precast structures due to no formwork, can reduce overall costs by 25%. However, machine and material cost could be higher.

8.3. Recommendations and further work

The work in this thesis presented numerical work based on assumptions from literature and related theory. In order to further the knowledge in earth building and construction, more research into material behaviour, 3D printing simulation and structural analysis is recommended to do.

Material

To obtain more accurate material models, it is recommended to first do material testing for its time-dependent strength and stiffness behaviour and then feed this data to a FE analysis model. In order to do proper material testing, the following is recommended to do [176].

- identify the PSD and Proctor compaction curves of the soil intended to study
- measure the suction to obtain the Soil Water Retention Curve (SWRC)

To measure strength and stiffness time dependent behaviour, procedures in 3D concrete printing can be followed. In 3D printing, stiffness is tested and monitored based on deformation, which depends on young's modulus and is quantified by either stress-strain relation using the unconfined compression test for cylindrical specimens (ASTM D4648), optical metrology, or PZT (piezoelectrical transducers) that assess stiffness gain and damage evolution, thereby ensuring stability of the stacking process. Time-dependent yield stress depends on cohesiveness of cement paste, which is suggested by authors to resemble the behaviour of a cohesive soil, as failure in compression results from relative movement of particles. Strength is attributed to a combination of inter-particle friction and cohesion, which can be translated by a Mohr-Coulomb yield criterion, similar to cohesive soils. An alternative way to perform yield stress analysis is through the dynamic stress sweep method using an oscillatory rheometer, which allows proper reproducibility of results and minimizes wall slippage problems in high-viscosity mortars.

Understanding stiffness

Stiffness in existing earth material research sees a large uncertainty in values. Proper guidelines for understanding earth stiffness and how to measure this property is recommended to look into first.

Material non-linearity

This work has assumed linear material curing rates. For the unstabilised material models, a linear material curing rate (strength development rate) is assumed for the upper bound one from 0 to 3 days, while the lower bound one based on Perrot's data shows that it is not. The upper bound model has not accounted for material non-linearity as this data is not available, given that natural soils exhibit very little plasticity. The model can be an accurate prediction in real world application but has to be verified through experiments. Shrinkage is not considered.

For the cement stabilised material models, a linear material curing rate has been taken for both the upper and lower bound models. While it may be true for the lower bound, the upper bound model shows a non-linear development. Furthermore in 3DCP studies from Suiker and Wolfs, compare linear and exponentially decaying curing rates in their FE models and find a difference.

Reinforcement integration

To increase tensile capacity, it is recommended to look into reinforcement integration. Steel reinforcement is not recommended for earth materials due to bonding behaviour and risk of efflorescence which can ruin the appearance of earth walls. Fibers and bamboo is recommended. Also to keep in line with the natural aspects of the material.

Computational modelling

Different computational tools have been developed and are under development to better predict 3D printed structures. Most advancements have been made for the development of 3D printed structures using the extrusion process.

Wolfs method and Voxelprint

Other modelling methods incl. Wolfs method for 3DCP. Testing to verify predictions.

Non-linear structural model with non-linear material model

Only linear elastic model. look into non-linear models. Describe other models that are better to model soil behaviour.

Discrete element modelling

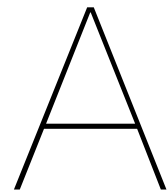
Discrete element analysis methods is an alternative computational approach to assess collapse of earthen arches. It is a numerical solution based on finite-difference principles used to describe the behaviour of discontinuous blocks and has been used to validate earth masonry design to validate basic lab tests [29]. It has been used in one published study on rammed earth walls [9], which showed the superior results predicting the failure mode of a set of rammed earth walls compared to equivalent FEM results. Time-dependent properties can be modelled here.

Optimising processing parameters and toolpath generation

Processing parameters have an influence on the mechanical properties of printed structures and resulting behaviour. More research in general understanding of how these affect structures is recommended. Varying flow of material, printing speed, inter-layer time etc. These can be done through testing.

Modelling methods for Arches

Stability of an arch is important during construction. To design a fully printed arch with no or minimal formwork, analysis of a full arch structure using the final hardened properties can be taken into consideration first to find a form that will work. This can be done using thrust line analysis or limit analysis. Further work towards finding a modelling method that can form-find printed arch structures with time-dependent properties is recommended.



Additives, biopolymers and fibres found in earth material research

Additive type	Additive source	Main effects studied
<u>Animal origin</u>		
Pig hair	W	M
Wool sheep fibers	W/BY	M
Chitosan	BY	M D
Casein and sodium caseinate biopolymers	-	M
Cow-dung	W	M D
Cow blood	BY	M

(W): waste materials, (BY): by-product, (W/BY): case of uncertain classification, (-): not specified, (M): mechanical properties, (H): hygroscopic, (T): thermal properties, (D): durability, (B): biological risk

Table A.1: Natural additives and fibers of animal origin for earthen material stabilisation classified by their additive source (adapted from Ref [177])

Additive type	Additive source	Main effects studied
<u>Plant origin</u>		
Pine needles	-	M
Kenaf fibers, hibiscus cannabinus fibers	-	M D T
Thypha spadixes wool fibers	-	M H T
Hemp fibers	-	M
Flax fibers	-	M
Chips of phragmites and thypha spadixes	-	H
Bamboo particles	-	M D
Oat fibers	W/BY	M H T B D
Sunflower bark, pith	W/BY	M H T D
Banana fibers	W	M
Pineapple leaves	W	M D
Coconut husk	W	M D
Sugarcane bagasse	W	M D
Cassava peels	W	M D
Fescue	BY	M
Rice husk	W	M D
Wheat straw	W/BY	M T D
Rape straw	W/BY	M H T D
Barley straw	W/BY	M H T D B
Straw fibers	W/BY	M D
Lavender straw	W/BY	M T D B
Corn plant	W/BY	M
Corn pith	W/BY	H T
Oil palm fruit, bunch	W/BY	M D
Date palm fibers	W/BY	M D
Olive fibers	W	H T
Olive stones	BY	M
Burned olive waste	W	M D
Wood shavings	W	M D
Seaweed fibers	W	M D
Posidonia seagrass	W	M
Carrageenan	-	M D
Cuar	-	M
Xanthan gum	-	M
Gellan and agar gum	-	M D
Alginate	-	M
Tannins	-	M
Residues of beetroot and tomatoes	W	M D
Lignin/lignin sulfonate	BY	M D
Cooking oil	W	M
Linseed oil	-	H D

(W): waste materials, (BY): by-product, (W/BY): case of uncertain classification, (-): not specified, (M): mechanical properties, (H): hygroscopic, (T): thermal properties, (D): durability, (B): biological risk

Table A.2: Natural additives and fibers of plant origin for earthen material stabilisation classified by their additive source (adapted from Ref [177])

B

Overview of earth building standards, codes and normative documents

No.	Country	Document Name	Earth building material	Soil gradation	Soil plasticity, PI [%]
1	Brazil	NBR 8491-2, 10832-6, 12023-5, 13554-5 (1984-96)	CSEB		≤18 LL ≤ 45
2	India	IS: 2110 (1998)	CS earth	Content of sand fraction ≤ 35 % d = 0.075 -4.75 mm	8.5 -10.5, LL ≤ 27
3	India	IS: 1725 (2010)	CSCEB	10 -15 % clay d < 0.002 mm >65 % sand d = 0.075 -4.75 mm	≤ 12
4	Kyrgyzstan	PCH-2-87 (1988)	CSRE	Content of soil particles d < 0.005 mm (10-30 %) d > 0.005 mm (70-90 %)	2 -9
5	Peru	NTE E.080 (2000)	EB, unstabilised	55 -70 % sand 15 -25 % silt 10 -20 % clay	
6	Spain	UNE 41410	CEB	≥10 % clay	
7	Sri Lanka	SLS 1382-1 (2009)	CSCEB	10 -15 % clay, d < 0.002 mm 5 -20 % silt, d =0.002 -0.06 mm > 65 % sand +gravel, max. particle size ≤ 12 mm	≤ 12
8	Zimbabwe	SAZS 724 (2001)	RE, unstabilised	50 -70 % fine gravel and sand 15 -30 % silt 5 -15 % clay	

Table B.1: Overview of numerical ranges of recommended soil gradation and plasticity for rammed earth and earth blocks from different countries (adapted from Ref [7])

No.	Country	Document Name	Soil	Building material	Construction system
1	Africa	ARS 671-683 (1996)		EB	EBM
2	Australia	CSIRO Bulletin 5, 4 th ed. (1995)	E	EB, CSEB, EMM	RE, EBM
3	Australia	EBAA (2004)	E	EB, EMM	EBM, RE
4	Brazil	NBR 8491-2, 10832-6, 12023-5, 13554-5 (1984-96)		CSEB	
5	Brazil	NBR 13553 (1996)			CSRE
6	Columbia	NTC 5324 (2004)		CSEB	
7	France	AFNOR XRP13-901 (2001)		EB	
8	Germany	Lehmbau Regeln (2009)	E	C, LC, EB, EM, CP	RE, C, EBM, EP, EI, WL
9	Germany	RL 0803 (2004)		EP	
10	Germany	TM 01 (2008)		EP	
11	Germany	TM 02 (2011)		EB	
12	Germany	TM 03 (2011)		EMM	
13	Germany	TM 04 (2011)		EP	
14	Germany	TM 05 (2011)	E		
15	India	IS: 2110 (1998)	E, ES		RE
16	India	IS: 13827 (1998)		EB	EBM, RE
17	India	IS: 1725 (2011)		CSEB	
18	Kenya	KS02-1070 (1999)		CSEB	
19	Kyrgyzstan	PCH-2-87 (1988)	E, ES		RE
20	New Zealand	NZS 4297-9 (1998)		E, EB	RE, EBM, EP
21	Nigeria	NIS 369 (1997)		CSEB	
22	Nigeria	NBC 10.23 (2006)			EBM, RE
23	Peru	NTE E.080 (2000)		EB	EBM
24	Spain	MOPT Tapial (1992)			RE
25	Spain	UNE 41410 (2008)		CEB	
26	Sri Lanka	Specification for CSEB, SLS 1382 part 1-3 (2009)		CSEB	EBM
27	Switzerland	Regeln zum Bauen mit Lehm (1994)	E	EB, LE, EM	EBM, RE, EI, WL
28	Tunisia	NT 21.33, 21.35 (1998)		CEB	
29	Turkey	TS 537, 2514, 2515 (1985-97)		CSEB	
30	USA	UBS, Sec. 2405 (1982)			EBM
31	USA	14.7.4 NMAC (2006)		EB, EMM	EBM, RE
32	USA	ASTM E2392/E2392M (2010)	E	EB, EM	C, EBM, RE, EM, WL
33	Zimbabwe	SAZS 724 (2001)	E		RE

(C): Cob, (CP): Clay panel, (E, ES): Earth, earth stabilised with cement, (EB): Earth block, (CEB): Compressed earth block, (CSEB): Compressed stabilised earth blocks, (PEB): Poured earth blocks, (EBM): Earth block masonry, (EM): Earth mortar, (EP): Earth plaster, (EMM): Earth masonry mortar, (ESM): Earth spray mortar, (EI): Earth infill, (WD): Wattle and Daub, (PEI): Poured earth infill, (LC): Light clay, (RE): Rammed earth, (CSRE): Cement stabilised rammed earth, (WL): Wall lining.

Table B.2: Overview of earth building guidelines from different countries (adapted from Ref [7])

No.	Country	Document		
		Name	Earth building material	
			Entire content of soluble salts [% by mass]	
1	Australia	EBAA (2004)	EB, EMM	To an extent which will not 'impair the strength of durability of a wall'
2	Germany	TM 02, 03 (2011)	EB, EM	< 0.12
3	India	IS: 2110 (1998)	CS earth	≤ 1; sodium salts ≤ 0.1
4	Kyrgyzstan	PCH-2-87 (1988)	CSRE	≤ 3
5	New Zealand	NZS 4298 (1998)	E, EB	To an extent which will not 'impair the strength of durability of a wall'
6	Peru	NTE E.080 (2000)	EB	Free of 'alien materials'
7	USA /New Mexico	14.7.4 NMAC (2006)	EB, RE	≤ 2
8	Zimbabwe	SAZS 724 (2001)	RE	Free

Table B.3: Permissible levels of salt content in earth building standards (adapted from Ref [7])

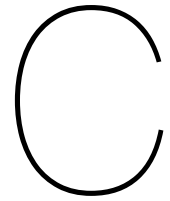
No.	Country	Document		
		Name	Design UCS [N/mm ²]	
			Specimen details/ characteristic UCS [N/mm ²]	
1	Australia	CSIRO Bull. 5, 4 th ed. (1995) EBAA (2004)	0.7 a 1.0 a	Height to thickness or diameter ratio (0.4 -5.0 or more) with aspect ratio factors /5.2)
2	Germany	Lehmbau Regeln (2009)	0.3 -0.5	Cube, 20 cm ³ /2 -4; 1 sample of 3 or more individuals, the lowest is standard
3	India	IS: 2110 (1998)	1.4 a, b	Cylinder, height /diameter (mm): Fine -grained soils: 100 /50 Medium -grained soils: 200 /100
4	Kyrgyzstan	PCH-2-87 (1988)	0.63 -3.6 b	Cube 15 cm ³ /0.95 -0.4.7; 1 sample of 3 or more individuals after 3, 7, 28 days
5	New Zealand	NZS 4297-9 (1998)	0.5	Height to thickness or diameter ratio (0.4 -5.0 or more) with aspect ratio factors /1 sample of 5 or more individuals, the lowest must be > 1.3 N/mm ² is aspect ration factor = 1
6	Spain	MOPT Tapial (1992)	0.2 c 0.1 c, wet environment	Cube 30 cm ² ; 1 sample of 10 individuals /compress. Crushing strengths at 5 cm ³ cubes cut from a wall: Low strength 0.6, Medium strength 1.2, High strength 1.8
7	Switzerland	Regeln zum Bauen mit Lehm (1994)	0.3 -0.5	Cube 20 cm ³ / 2-4
8	USA	14.7.4 NMAC (2006)		Cube 10.2 cm ³ / 2.07; 1 sample of 5 or more individuals, the lowest may be < 2.07 N/mm ² but ≥ 1.725 N/mm ²
9	Zimbabwe	SAZS 724 (2001)		1.5 for one-storey walls up to 400 mm thick 2.0 for two-storey walls

a) 'Design' and 'characteristic' values not distinguished

b) Cement -stabilised

c) E/I: Exterior/ Interior walls

Table B.4: Recommended design values of UCS and speciment details (adapted from Ref [7])



Unstabilised shotearth calculations

C.1. Data entries for predictions

Perrots data -without Alginate (unstabilised)					
		Compressive strength			
Time (min)	Time (hours)	fcm (kPa)	fcm (MPa)	fcm (kN/cm2)	
1.0002	0.01667	2.96	0.00296	0.000296	
4.9998	0.08333	3.2	0.0032	0.00032	
64.9998	1.08333	5.99	0.00599	0.000599	
124.9998	2.08333	8.99	0.00899	0.000899	
1246.9998	20.78333	15.58	0.01558	0.001558	
2662.0002	44.36667	58.13	0.05813	0.005813	
7131	118.85	958.86	0.95886	0.095886	
8437.0002	140.61667	1827.83	1.82783	0.182783	
9993	166.55	2157.44	2.15744	0.215744	
30000	500	2249	2.249	0.2249	
		Elastic modulus			
Time (min)	Time (hours)	E (kPa)	E (MPa)	E (kN/cm2)	
1.0002	0.01667	18	0.0018	0.0018	
4.9998	0.08333	18.6	0.00186	0.00186	
64.9998	1.08333	29.7	0.00297	0.00297	
124.9998	2.08333	37.8	0.00378	0.00378	
1246.9998	20.78333	68.4	0.00684	0.00684	
2662.0002	44.36667	424.2	0.04242	0.04242	
7131	118.85	6468	0.6468	0.6468	
8437.0002	140.61667	14850	1.485	1.485	
9993	166.55	15336	1.5336	1.5336	
15000	250	15050	1.505	1.505	

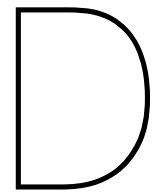
Table C.1: Measured data for stress and stiffness development, original data received from Perrot

Assumed -Unstabilised Rammed Earth development					
Slopes for assumed URE					
Time (hour)	Strength (MPa)	Slope	Notes		
0	0.5	0.026041667	At zero hours, strength is 0.5 MPa		
72	2.375		Assumed 95 % of strength reached at 72 hours		
Stiffness (MPa)		0.791416667 <th colspan="3">Notes</th>	Notes		
0	0.018		No data, same stiffness taken as Perrot		
72	57	Assumed 95 % of stiffness reached at 72 hours			
URE: fcm	y= 0.002604*x+0.05				
URE: E	y= 0.079141*x+0.0018				
Compressive strength					
Time (min)	Time (hours)	fcm (kPa)	fcm (MPa)	fcm (kN/cm2)	
1.0002	0.01667	500.4341146	0.500434115	0.050043411	
4.9998	0.08333	502.1700521	0.502170052	0.050217005	
10.0002	0.16667	504.3403646	0.504340365	0.050434036	
60	1	526.0416667	0.526041667	0.052604167	
120	2	552.0833333	0.552083333	0.055208333	
180	3	578.125	0.578125	0.0578125	
1360.9998	22.68333	1090.711719	1.090711719	0.109071172	
2701.9998	45.03333	1672.742969	1.672742969	0.167274297	
4320	72	2375	2.375	0.2375	
7171.9998	119.53333	2500	2.5	0.25	
8497.0002	141.61667	2500	2.5	0.25	
10035	167.25	2500	2.5	0.25	
15000	250	2500	2.5	0.25	
30000	500	2500	2.5	0.25	
Elastic modulus					
Time (min)	Time (hours)	E (kPa)	E (MPa)	E (kN/cm2)	
1.0002	0.01667	31.19291583	0.031192916	0.003119292	
4.9998	0.08333	83.94875083	0.083948751	0.008394875	
64.9998	1.08333	875.3654175	0.875365418	0.087536542	
124.9998	2.08333	1666.782084	1.666782084	0.166678208	
1246.9998	20.78333	16466.27375	16.46627375	1.646627375	
2662.0002	44.36667	35130.52208	35.13052208	3.513052208	
3000	50	39588.83333	39.58883333	3.958883333	
3600	60	47503	47.503	4.7503	
4320	72	57000	57	5.7	
4800	80	60000	60	6	
7131	118.85	60000	60	6	
8437.0002	140.61667	60000	60	6	
9993	166.55	60000	60	6	
15000	250	60000	60	6	

Table C.2: Data for stress and stiffness development assumed for URE

Proposed -shotearth development					
Slopes for proposed shotearth					
Time (hour)	Strength (MPa)	Slope	Notes		
0	0.00296	0.015180267	At zero hours, assumed same as Perrot		
150	2.28		Assumed 95 % of strength reached at 150 hours		
Stiffness (MPa)					
0	0.018	0.166546667	No data, same stiffness taken as Perrot		
150	25		Assumed 95 % of stiffness reached at 150 hours		
Shotearth: fcm		$y = 0.01518 * x + 0.00296$			
Shotearth: E		$y = 0.1665 * x + 0.0018$			
Compressive strength					
Time (min)	Time (hours)	fcm (kPa)	fcm (MPa)	fcm (kN/cm ²)	
1.0002	0.01667	3.213055045	0.003213055	0.000321306	
4.9998	0.08333	4.224971621	0.004224972	0.000422497	
10.0002	0.16667	19.40523829	0.019405238	0.001940524	
60	1	34.58550495	0.034585505	0.003458555	
120	2	318.4564916	0.318456492	0.031845649	
180	3	676.4578817	0.676457882	0.067645788	
1360.9998	22.68333	761.9733333	0.761973333	0.076197333	
2701.9998	45.03333	913.776	0.913776	0.0913776	
4320	72	1065.578667	1.065578667	0.106557867	
7171.9998	119.53333	1217.381333	1.217381333	0.121738133	
8497.0002	141.61667	1807.134693	1.807134693	0.180713469	
10035	167.25	2137.558548	2.137558548	0.213755855	
15000	250	2400	2.4	0.24	
30000	500	2400	2.4	0.24	
Elastic modulus					
Time (min)	Time (hours)	E (kPa)	E (MPa)	E (kN/cm ²)	
1.0002	0.01667	20.77633293	0.020776333	0.002077633	
4.9998	0.08333	31.87833373	0.031878334	0.003187833	
64.9998	1.08333	198.4250004	0.198425	0.0198425	
124.9998	2.08333	364.9716671	0.364971667	0.036497167	
1246.9998	20.78333	3479.394334	3.479394334	0.347939433	
2662.0002	44.36667	7407.121	7.407121	0.7407121	
3000	50	8345.333333	8.345333333	0.834533333	
3600	60	10010.8	10.0108	1.00108	
4320	72	11676.26667	11.67626667	1.167626667	
4800	80	13341.73333	13.34173333	1.334173333	
7131	118.85	19812.07133	19.81207133	1.981207133	
8437.0002	140.61667	23437.23767	23.43723767	2.343723767	
9993	166.55	25000	25	2.5	
15000	250	25000	25	2.5	

Table C.3: Data for stress and stiffness development proposed for unstabilised shotearth



Cement stabilised shotearth calculations

D.1. Concrete and shotcrete models

D.1.1. Eurocode 2 and ACI

Eurocode 2

In Eurocode 2 [178] concrete strength at time, t , for various types of cement can be found through equation (D.1). This relationship can be used to predict shotcrete where [179] suggests using $s = 0.20$. Eurocode 2 specifies that the relationship is valid for concrete from 3-28 days. Concrete younger than 3 days should be determined from experimental testing.

$$f_{cm}(t) = \beta_{cc}(t) f_{cm} \quad (D.1)$$

where $f_{cm}(t)$ is the mean compressive strength at an age of t days and f_{cm} is determined at 28 days.

$$\beta_{cc}(t) = \exp \left\{ s \left[1 - \left(\frac{28}{t} \right)^{1/2} \right] \right\} \quad (D.2)$$

s depends on type of cement where:

$s = 0.20$ for rapid hardening cement (Class R)

$s = 0.25$ for normal hardening cement (Class N)

$s = 0.38$ for slow hardening cement (Class S)

Also in Eurocode 2, Young's modulus at time, t , can be derived knowing the stress at t .

$$E_{cm}(t) = (f_{cm}(t)/f_{cm})^{0.3} E_{cm} \quad (D.3)$$

where E_{cm} and f_{cm} are values determined at 28 days.

ACI

The American Concrete Institute (ACI 209r-92) similarly has stress relationships at time t .

$$(f'_c)_t = \frac{t}{a + \beta t} (f'_c)_{28} \quad (D.4)$$

where $f_c(t)$ is the compressive strength at t days, a and b are constants and f_{c28} is mean compressive strength at 28 days.

To predict Young's modulus ACI 318-14 proposes the following for normal weight concrete:

$$E_c = 4700\sqrt{f'_c} \quad (D.5)$$

D.1.2. Shotcrete models

The following shotcrete models were found and plotted using the known target strength and stiffness found by Curto et al.

CEB-FIP (1990)

According to CEB-FIP code, strength and Young's modulus as a function of time can be found with the following relationships, where $s = 25$ was used.

Strength

$$f_{cp}(t) = f_{cp,28} \exp \left[s \left(1 - \sqrt{\frac{t_{28}}{t}} \right) \right] \quad (D.6)$$

Young's modulus

$$E(t) = E_{28} \exp \left[s \left(1 - \sqrt{\frac{t_{28}}{t}} \right) \right]^{0.5} \quad (D.7)$$

Weber (1979)

According to Weber, strength and Young's modulus as a function of time can be found with the following relationships.

Strength

$$f_{cp}(t) = a f_{cp,28} \exp \left(\frac{c}{t^{0.55}} \right) \quad (D.8)$$

where $a = 1.45$ and $c = -2.32$ was used

Cement class	Z 25	Z 35 F	Z 55
	Z 35 L	Z 45 F	
	Z 45 L		
a	1.45	1.27	1.20
c	-2.32	-1.49	-1.14

(D.9)

Young's modulus

$$E(t) = a E_{28} \exp \left(\frac{c}{t^{0.6}} \right) \quad (D.10)$$

where $a = 1.132$ and $c = -0.915$ was used

Cement class	Z 25	Z 35 F	Z 55
	Z 35 L	Z 45 F	
	Z45 L		
a	1.132	1.084	1.062
c	-0.915	-0.596	-0.445

(D.11)

Chang (1994)

According to Chang, strength and Young's modulus as a function of time can be found with the following relationships.

Strength

$$f_{cp} = 1.105 f_{cp,28} \exp\left(\frac{-0.743}{t^{0.7}}\right) \quad (\text{D.12})$$

Young's modulus

$$E(t) = 1.062 E_{28} \exp\left(\frac{-0.446}{t^{0.7}}\right) \quad (\text{D.13})$$

Aldrian (1991) with Schubert (1988)

According to Aldrian, strength as a function of time can be found with the following relationships.

Strength -Aldrian

$$f_c(t) = \begin{cases} f_{c,28} \cdot 0.03t, & 0 < t < 8h \\ f_{c,28} \cdot \sqrt{\frac{t-5}{45+0.925t}}, & t > 8h \end{cases} \quad (\text{D.14})$$

Aldrian did not define a relationship for Young's modulus, therefore Schubert's definition for Young's modulus as a function of time is used, as Schubert did not define a relationship for strength. At least it has not been found.

Young's modulus -Schubert

$$E(t) = E_{28} \sqrt{\frac{t}{4.2 + 0.85t}} \quad (\text{D.15})$$

Golser (1990) and Aydan (1992)

The following two models were also tested but values for strength and stiffness were vastly underestimated and thus not plotted with the other models.

Strength -Golser

$$f_{cp}(t) = f_{cp,28} \sqrt{\frac{t}{101 + 0.85t}} \quad (\text{D.16})$$

Young's modulus -Aydan

$$E(t) = 5000 (1 - \exp^{-0.42t}) \quad (\text{D.17})$$

Other

Shotcrete models for tunnelling is an active field of research. The development of robotic shotcrete or shotearth could follow conventions defined or take inspiration here. If more values for strength and stiffness after 1 day was measured. Further work could be to test the following two models.

Two of the most widely used shotcrete models are the model by Meschke (viscoplastic model) and the model by Schädlich and Schweiger. The Meschke model can represent the evolution of stiffness, strength, shrinkage, creep, hardening material behaviour in compressive loading and mixed loading and softening behaviour in tensile loading. The Schädlich and Schweiger model can represent the evolution of material stiffness and strength, creep, shrinkage and plastic material behaviour including hardening and softening [180].

D.2. Data on early age strength and stiffness development for 3DCP and SC3DP

D.2.1. Suiker's data

Suiker's data points is based on the following relationships:

Strength

$$\hat{\sigma}_{p*}(t) = 5.984 + 0.147t \quad \text{with } \sigma_{p*} \text{ in kPa and } t \text{ in min.} \quad (\text{D.18})$$

Young's modulus:

$$\hat{E}_*(t) = 0.0781 + 0.0012t \quad \text{with } E_* \text{ in MPa and } t \text{ in min.} \quad (\text{D.19})$$

D.2.2. Dressler's data

Original data points for strength from Dressler was received and is found in Table. D.1. Assumed stiffness calculation for Dressler is found in Table D.2.

Dresslers data -0 % accelerator	
Time [min]	fcm [kPa]
5	11.2
10	13.08
15	15.26
20	22.72
25	20.94
30	24.52
40	30.75
50	36.85
60	45.46
70	63.07
80	81.51
90	110.89

Table D.1: Original data from Dressler with 0 % accelerator

Suiker data					Dressler data	Assumed E
Time (min)	fcm [MPa]	Ecm [MPa]	Time (min)	fcm/Ecm	fcm [MPa]	E [Mpa]
0	0.005984	0.0781				
5	0.006719	0.0841	5	0.079892985	0.0112	0.140187528
10	0.007454	0.0901	10	0.0827303	0.01308	0.158104105
15	0.008189	0.0961	15	0.085213319	0.01526	0.179079985
20	0.008924	0.1021	20	0.087404505	0.02272	0.259940834
25	0.009659	0.1081	25	0.089352451	0.02094	0.234352832
30	0.010394	0.1141	30	0.09109553	0.02452	0.269167982
35	0.011129	0.1201				
40	0.011864	0.1261	40	0.09408406	0.03075	0.326835384
45	0.012599	0.1321				
50	0.013334	0.1381	50	0.096553222	0.03685	0.381654792
55	0.014069	0.1441				
60	0.014804	0.1501	60	0.098627582	0.04546	0.460925831
65	0.015539	0.1561				
70	0.016274	0.1621	70	0.100394818	0.06307	0.628219676
75	0.017009	0.1681				
80	0.017744	0.1741	80	0.101918438	0.08151	0.799757157
85	0.018479	0.1801				
90	0.019214	0.1861	90	0.103245567	0.11089	1.074041272
95	0.019949	0.1921				
100	0.020684	0.1981				
105	0.021419	0.2041				
110	0.022154	0.2101				
115	0.022889	0.2161				
120	0.023624	0.2221				

Table D.2: Assumed stiffness calculation for Dressler based on Suiker's data

D.2.3. Perrot's data

Perrots data -with Alginate (stabilised)					
		Compressive strength			
Time (min)	Time (hours)	fcm (kPa)	fcm (MPa)	fcm (kN/cm2)	
1.0002	0.01667	3.46	0.00346	0.000346	
4.9998	0.08333	35.96	0.03596	0.003596	
10.0002	0.16667	37.46	0.03746	0.003746	
60	1	39.85	0.03985	0.003985	
120	2	45.25	0.04525	0.004525	
180	3	48.54	0.04854	0.004854	
1360.9998	22.68333	166.3	0.1663	0.01663	
2701.9998	45.03333	294.25	0.29425	0.029425	
7171.9998	119.53333	1402.34	1.40234	0.140234	
8497.0002	141.61667	1797.87	1.79787	0.179787	
10035	167.25	2300	2.3	0.23	
15000	250	2500	2.5	0.25	
30000	500	2600	2.6	0.26	
		Elastic modulus			
Time (min)	Time (hours)	E (kPa)	E (MPa)	E (kN/cm2)	
1.0002	0.01667	24	0.024	0.0024	
4.9998	0.08333	132	0.132	0.0132	
10.0002	0.16667	151.5	0.1515	0.01515	
60	1	224.4	0.2244	0.02244	
120	2	240	0.24	0.024	
180	3	291	0.291	0.0291	
1360.9998	22.68333	975	0.975	0.0975	
2701.9998	45.03333	2097	2.097	0.2097	
7171.9998	119.53333	13200	13.2	1.32	
8497.0002	141.61667	14070	14.07	1.407	
10035	167.25	16500	16.5	1.65	
15000	250	16550	16.55	1.655	

Table D.3: Measured data for stress and stiffness development, original data received from Perrot

D.3. Curvefitting calculation

Stress development -Upper bound					
	Time (day)	Time (min)	fc _m [MPa]	fc _m [kN/cm ²]	
<u>SC3DP</u>	0.003472222	5	0.0112	0.00112	
	0.006944444	10	0.01308	0.001308	
	0.010416667	15	0.01526	0.001526	
	0.013888889	20	0.02272	0.002272	
	0.017361111	25	0.02094	0.002094	
	0.020833333	30	0.02452	0.002452	
	0.027777778	40	0.03075	0.003075	
	0.034722222	50	0.03685	0.003685	
	0.041666667	60	0.04546	0.004546	
	0.048611111	70	0.06307	0.006307	
	0.055555556	80	0.08151	0.008151	
	0.0625	90	0.11089	0.011089	
0.0625	90	0.018981013	0.001898101		
<u>Curve fitting</u>	0.069444444	100	0.054130907	0.005413091	
	0.076388889	110	0.054130907	0.005413091	
	0.083333333	120	0.081080587	0.008108059	
	0.125	180	0.241171647	0.024117165	
	0.166666667	240	0.398541679	0.039854168	
	0.208333333	300	0.553236931	0.055323693	
	0.25	360	0.705302866	0.070530287	
	0.291666667	420	0.854784173	0.085478417	
	0.333333333	480	1.001724784	0.100172478	
	0.375	540	1.146167881	0.114616788	
	0.416666667	600	1.288155914	0.128815591	
	1	1440	3.040334651	0.304033465	
2	2880	5.219161329	0.521916133		
<u>CEB-FIP</u>	3	4320	5.683283705	0.568328371	
	4	5760	6.29561885	0.629561885	
	5	7200	6.750953946	0.675095395	
	6	8640	7.108065134	0.710806513	
	7	10080	7.398607439	0.739860744	
	8	11520	7.641428982	0.764142898	
	9	12960	7.84858489	0.784858489	
	10	14400	8.028211576	0.802821158	
	12	17280	8.326227652	0.832622765	
	13	18720	8.451907079	0.845190708	
	14	20160	8.565464889	0.856546489	
	15	21600	8.668768794	0.866876879	
	16	23040	8.763302965	0.876330297	
	17	24480	8.850264315	0.885026431	
	18	25920	8.930630672	0.893063067	
	19	27360	9.005210095	0.900521009	
	20	28800	9.074677202	0.90746772	
	21	30240	9.139600395	0.913960039	
	22	31680	9.200462561	0.920046256	
	23	33120	9.257677029	0.925767703	
	24	34560	9.311600013	0.931160001	
	25	36000	9.362540434	0.936254043	
	26	37440	9.410767738	0.941076774	
	27	38880	9.456518197	0.94565182	
	28	40320	9.5	0.95	

Table D.4: Curvefitting fcm upper

Stress development -Lower bound					
	Time (day)	Time (min)	fc _m [MPa]	fc _m [kN/cm ²]	
Suiker		0	0	0.005984	0.0005984
	0.003472222		5	0.006719	0.0006719
	0.006944444		10	0.007454	0.0007454
	0.010416667		15	0.008189	0.0008189
	0.013888889		20	0.008924	0.0008924
	0.017361111		25	0.009659	0.0009659
	0.020833333		30	0.010394	0.0010394
	0.024305556		35	0.011129	0.0011129
	0.027777778		40	0.011864	0.0011864
	0.03125		45	0.012599	0.0012599
	0.034722222		50	0.013334	0.0013334
	0.038194444		55	0.014069	0.0014069
	0.041666667		60	0.014804	0.0014804
	0.045138889		65	0.015539	0.0015539
	0.048611111		70	0.016274	0.0016274
	0.052083333		75	0.017009	0.0017009
	0.055555556		80	0.017744	0.0017744
	0.059027778		85	0.018479	0.0018479
	0.0625		90	0.019214	0.0019214
	0.065972222		95	0.019949	0.0019949
	0.069444444		100	0.020684	0.0020684
	0.072916667		105	0.021419	0.0021419
	0.076388889		110	0.022154	0.0022154
	0.079861111		115	0.022889	0.0022889
	0.083333333		120	0.023624	0.0023624
	Curve fitting	0.125	180	0.094526579	0.009452658
		0.166666667	240	0.188112604	0.01881126
		0.208333333	300	0.280767431	0.028076743
0.25		360	0.372500328	0.037250033	
0.291666667		420	0.463320467	0.046332047	
0.333333333		480	0.553236931	0.055323693	
0.375		540	0.642258711	0.064225871	
0.416666667		600	0.730394709	0.073039471	
0.458333333		660	0.81765374	0.081765374	
0.5		720	0.904044529	0.090404453	
0.541666667		780	0.989575715	0.098957571	
0.583333333		840	1.074255851	0.107425585	
0.625		900	1.158093406	0.115809341	
0.666666667		960	1.241096764	0.124109676	
0.708333333		1020	1.323274224	0.132327422	
0.75		1080	1.404634005	0.1404634	
0.791666667		1140	1.485184242	0.148518424	
0.833333333		1200	1.564932992	0.156493299	
0.875		1260	1.643888228	0.164388823	
0.916666667		1320	1.722057846	0.172205785	
0.958333333	1380	1.799449663	0.179944966		
1	1440	1.876071419	0.187607142		
2	2880	3.502805368	0.350280537		
Weber	3	4320	3.876743013	0.387674301	
	4	5760	4.667096225	0.466709622	
	5	7200	5.288534607	0.528853461	
	6	8640	5.794339347	0.579433935	
	7	10080	6.216922303	0.62169223	
	8	11520	6.577207027	0.657720703	
	9	12960	6.889378052	0.688937805	
	10	14400	7.16344145	0.716344145	
	12	17280	7.62458396	0.762458396	
	13	18720	7.821308151	0.782130815	
	14	20160	8.000131216	0.800013122	
	15	21600	8.163650437	0.816365044	
	16	23040	8.313959989	0.831395999	
	17	24480	8.452770338	0.845277034	
	18	25920	8.581494618	0.858149462	
	19	27360	8.701312288	0.870131229	
	20	28800	8.813216837	0.881321684	
	21	30240	8.918052052	0.891805205	
	22	31680	9.016539973	0.901653997	
	23	33120	9.109302699	0.91093027	
	24	34560	9.196879585	0.919687959	
	25	36000	9.279740945	0.927974094	
	26	37440	9.358299065	0.935829906	
	27	38880	9.432917141	0.943291714	
	28	40320	9.503916581	0.950391658	

Table D.5: Curvefitting fcm lower

Stiffness development -Upper bound					
	day	min		Ecm [MPa]	Ecm [kN/cm ²]
<u>SC3DP</u>	0.003472222		5	0.140187528	0.014018753
	0.006944444		10	0.158104105	0.015810411
	0.010416667		15	0.179079985	0.017907999
	0.013888889		20	0.259940834	0.025994083
	0.017361111		25	0.234352832	0.023435283
	0.020833333		30	0.269167982	0.026916798
	0.027777778		40	0.326835384	0.032683538
	0.034722222		50	0.381654792	0.038165479
	0.041666667		60	0.460925831	0.046092583
	0.048611111		70	0.628219676	0.062821968
0.055555556		80	0.799757157	0.079975716	
0.0625		90	1.074041272	0.107404127	
<u>Curve fitting</u>	0.069444444		100	55.31039123	5.531039123
	0.076388889		110	82.8472901	8.28472901
	0.083333333		120	110.3056244	11.03056244
	0.125		180	273.4182821	27.34182821
	0.166666667		240	433.7585539	43.37585539
	0.208333333		300	591.3735616	59.13735616
	0.25		360	746.3096256	74.63096256
	0.291666667		420	898.6122795	89.86122795
	0.333333333		480	1048.326282	104.8326282
	0.375		540	1195.495633	119.5495633
0.416666667		600	1340.163583	134.0163583	
	1	1440	3125.413365	312.5413365	
	2	2880	5345.363745	534.5363745	
<u>CEB-FIP</u>		3	4320	7507.976336	750.7976336
		4	5760	7902.09853	790.209853
		5	7200	8182.872788	818.2872788
		6	8640	8396.512258	839.6512258
		7	10080	8566.397433	856.6397433
		8	11520	8705.83672	870.583672
		9	12960	8823.053384	882.3053384
		10	14400	8923.446654	892.3446654
		12	17280	9087.561595	908.7561595
		13	18720	9155.890369	915.5890369
		14	20160	9217.193323	921.7193323
		15	21600	9272.608782	927.2608782
		16	23040	9323.031255	932.3031255
		17	24480	9369.174928	936.9174928
		18	25920	9411.618001	941.1618001
		19	27360	9450.834364	945.0834364
		20	28800	9487.216683	948.7216683
		21	30240	9521.093517	952.1093517
	22	31680	9552.742213	955.2742213	
	23	33120	9582.398765	958.2398765	
	24	34560	9610.265437	961.0265437	
	25	36000	9636.516739	963.6516739	
	26	37440	9661.30415	966.130415	
	27	38880	9684.759898	968.4759898	
	28	40320	9707	970.7	

Table D.6: Curvefitting E upper

Stiffness development -Lower bound						
	day	min	Ecm [MPa]	Ecm [kN/cm ²]		
Suiker		0	0	0.0781	0.00781	
	0.003472222		5	0.0841	0.00841	
	0.006944444		10	0.0901	0.00901	
	0.010416667		15	0.0961	0.00961	
	0.013888889		20	0.1021	0.01021	
	0.017361111		25	0.1081	0.01081	
	0.020833333		30	0.1141	0.01141	
	0.024305556		35	0.1201	0.01201	
	0.027777778		40	0.1261	0.01261	
	0.03125		45	0.1321	0.01321	
	0.034722222		50	0.1381	0.01381	
	0.038194444		55	0.1441	0.01441	
	0.041666667		60	0.1501	0.01501	
	0.045138889		65	0.1561	0.01561	
	0.048611111		70	0.1621	0.01621	
	0.052083333		75	0.1681	0.01681	
	0.055555556		80	0.1741	0.01741	
	0.059027778		85	0.1801	0.01801	
	0.0625		90	0.1861	0.01861	
	0.065972222		95	0.1921	0.01921	
	0.069444444		100	0.1981	0.01981	
	0.072916667		105	0.2041	0.02041	
	0.076388889		110	0.2101	0.02101	
	0.079861111		115	0.2161	0.02161	
	0.083333333		120	0.2221	0.02221	
	Curve fitting	0.125		180	144.5184023	14.45184023
		0.166666667		240	286.8852058	28.68852058
		0.208333333		300	427.1324438	42.71324438
0.25			360	565.2916725	56.52916725	
0.291666667			420	701.3939782	70.13939782	
0.333333333			480	835.4699846	83.54699846	
0.375			540	967.5498593	96.75498593	
0.416666667			600	1097.663321	109.7663321	
0.458333333			660	1225.839645	122.5839645	
0.5			720	1352.107673	135.2107673	
0.541666667			780	1476.495814	147.6495814	
0.583333333			840	1599.032058	159.9032058	
0.625			900	1719.743974	171.9743974	
0.666666667			960	1838.658724	183.8658724	
0.708333333			1020	1955.803065	195.5803065	
0.75			1080	2071.203353	207.1203353	
0.791666667			1140	2184.885554	218.4885554	
0.833333333			1200	2296.875248	229.6875248	
0.875			1260	2407.197633	240.7197633	
0.916666667			1320	2515.877532	251.5877532	
0.958333333		1380	2622.939397	262.2939397		
1		1440	2728.40732	272.840732		
2		2880	4838.201098	483.8201098		
Weber	3		4320	6845.012976	684.5012976	
	4		5760	7378.396745	737.8396745	
	5		7200	7755.983296	775.5983296	
	6		8640	8041.078344	804.1078344	
	7		10080	8265.992195	826.5992195	
	8		11520	8449.172485	844.9172485	
	9		12960	8602.020162	860.2020162	
	10		14400	8732.010543	873.2010543	
	12		17280	8942.470101	894.2470101	
	13		18720	9029.277232	902.9277232	
	14		20160	9106.716342	910.6716342	
	15		21600	9176.340265	917.6340265	
	16		23040	9239.36511	923.936511	
	17		24480	9296.758541	929.6758541	
	18		25920	9349.301352	934.9301352	
	19		27360	9397.63136	939.763136	
	20		28800	9442.275343	944.2275343	
	21		30240	9483.67267	948.367267	
	22		31680	9522.193068	952.2193068	
	23		33120	9558.150173	955.8150173	
	24		34560	9591.811993	959.1811993	
	25		36000	9623.409079	962.3409079	
	26		37440	9653.14099	965.314099	
	27		38880	9681.181429	968.1181429	
	28		40320	9707.682394	970.7682394	

Table D.7: Curvefitting E lower



Assessment of shotearth structures

E.1. Recommendations for the design of earthen walls

No.	Country	Document Name	Design UCS [N/mm ²]	Wall type	Min. thickness t of wall [mm]	Max. height h [mm]	Max. slenderness h/t	Max. distance of laterally supported walls [mm]
1	Australia	EBAA (2004)	EBM	E/I	200/125	4000/2700 or	20/21.6	3500
			RE	E/I	200/200	3000/4000	15/20	3500
2	Germany	Lehmbau Regeln (2009)	RE	E/I	325/240	3250	10	4500
			EBM	E/I	365/240	3250	13.5	4500
			C	E/I	400/400	3250	8.1	4500
3	India	IS: 2110 (1998)	CSCEBM	L/NL	300/200	3200	10.7/16	
			CSRE	L/NL	300/200			
4	India	IS: 13827 (1998)	EBM RE			8 x T		10 x t or 64 x t ² /h
5	New Zealand	NZS 4297-9 (1998)	RE		250	3300	6 c	
			CEBM		130	3300	16 c	
6	Peru	NTE E.080 (2000)	EBM		400-500	2.4-3.0	< 6	d
7	Sri Lanka	SLS 1382 -1 (2009)	CSCEBM				BS5628: Pt.1, clause 25	
8	Switzerland	Regeln zum Bauen mit Lehm (1994)	RE	E/I	300/500 b	3500	11.6/7	5000
			EBM	E/I	200/300 b	3500	17.5/11.7	5000
9	USA	14.7.4 NMAC (2006)	RE	E/I	457/305	2438-3048		7315 max. length
			EBM		254/356 b			
10	USA	ASTM E2392/ E2392M					e	
11	Zimbabwe	SAZS 724 (2001)	RE		300		12 unstabilised 16 cem.stabilised	9000 max. length

Figure E.1: Recommended values for wall thickness and slenderness of earth walls (adapted from Ref [7])

E.2. Linear regression of data for material models

Upper bound strength development
Assumed URE

```

10
11 import rhinoscriptsyntax as rs
12 import math as m
13
14
15 def function(t,e_min):
16     if t <= e_min:
17         y = 4*10**-05*t + 0.05 + testValue
18     elif t > e_min:
19         y = 0.25 + testValue
20     return y
21
22 fct=function(float(t),4320)
23

```

Upper bound stiffness development
Assumed URE

```

10
11 import rhinoscriptsyntax as rs
12 import math as m
13
14
15 def function(t,e_min):
16     if t <= e_min:
17         y = 0.0013*t + 0.0018 + testValue
18     elif t > e_min:
19         y = 6 + testValue
20     return y
21
22 fct=function(float(t),4320)
23

```

Lower bound strength development
3DPE Perrot

```

10
11 import rhinoscriptsyntax as rs
12 import math as m
13
14
15 def function(t,e_min,six_daymin):
16     if t <= e_min:
17         y = 2*10**-06*t + 0.0003 + testValue
18     elif e_min < t and t < six_daymin:
19         y = 3*10**-05*t + 0.075 + testValue
20     elif t > six_daymin:
21         y = 5*10**-07*t + 0.2112 + testValue
22     return y
23
24 fct=function(float(t),2662,9993)
25

```

Lower bound stiffness development
3DPE Perrot

```

10
11 import rhinoscriptsyntax as rs
12 import math as m
13
14
15 def function(t,e_min,six_daymin):
16     if t <= e_min:
17         y = 1*10**-05*t + 0.0004 + testValue
18     elif e_min < t and t < six_daymin:
19         y = 0.0002*t + 0.6144 + testValue
20     elif t > six_daymin:
21         y = 1.5 + testValue
22     return y
23
24 fct=function(float(t),2662,8437)
25

```

Proposed shotearth strength development

```

10
11 import rhinoscriptsyntax as rs
12 import math as m
13
14
15 def function(t,e_min):
16     if t <= e_min:
17         y = 3*10**-05*t + 0.0003 + testValue
18     elif e_min < t:
19         y = 0.24 + testValue
20     return y
21
22 fct=function(float(t),8437)
23

```

Proposed shotearth stiffness development

```

10
11 import rhinoscriptsyntax as rs
12 import math as m
13
14
15 def function(t,e_min):
16     if t <= e_min:
17         y = 0.0003*t + 0.0018 + testValue
18     elif e_min < t:
19         y = 2.5 + testValue
20     return y
21
22 fct=function(float(t),8437)
23

```

Figure E.2: Python code: conditions for unstabilised material models

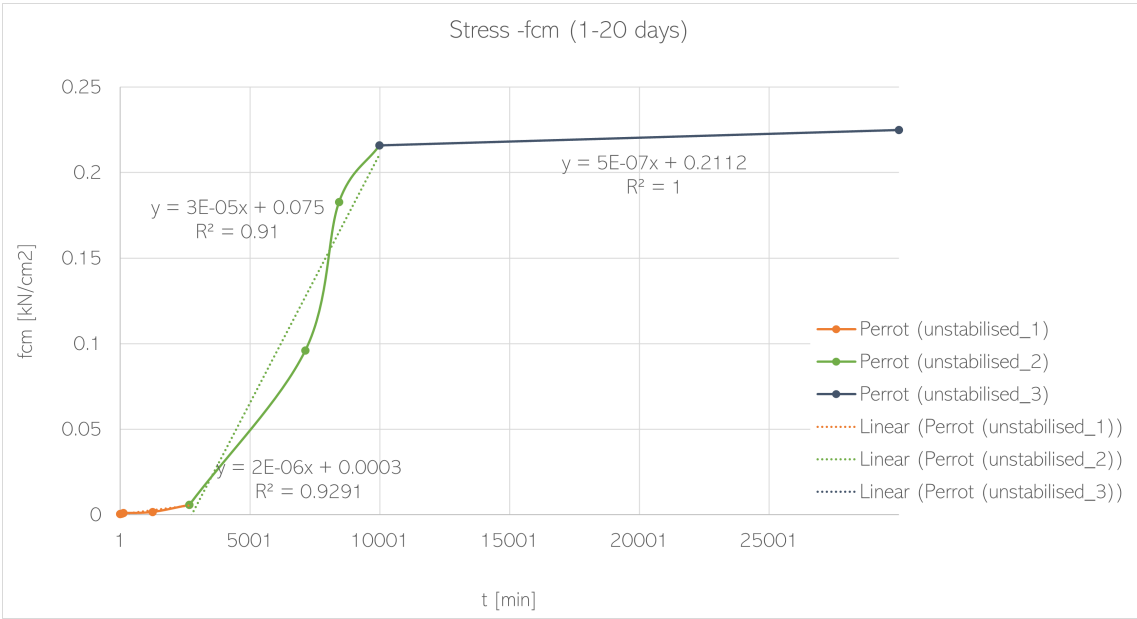


Figure E.3: Linear regression of Perrots stress development

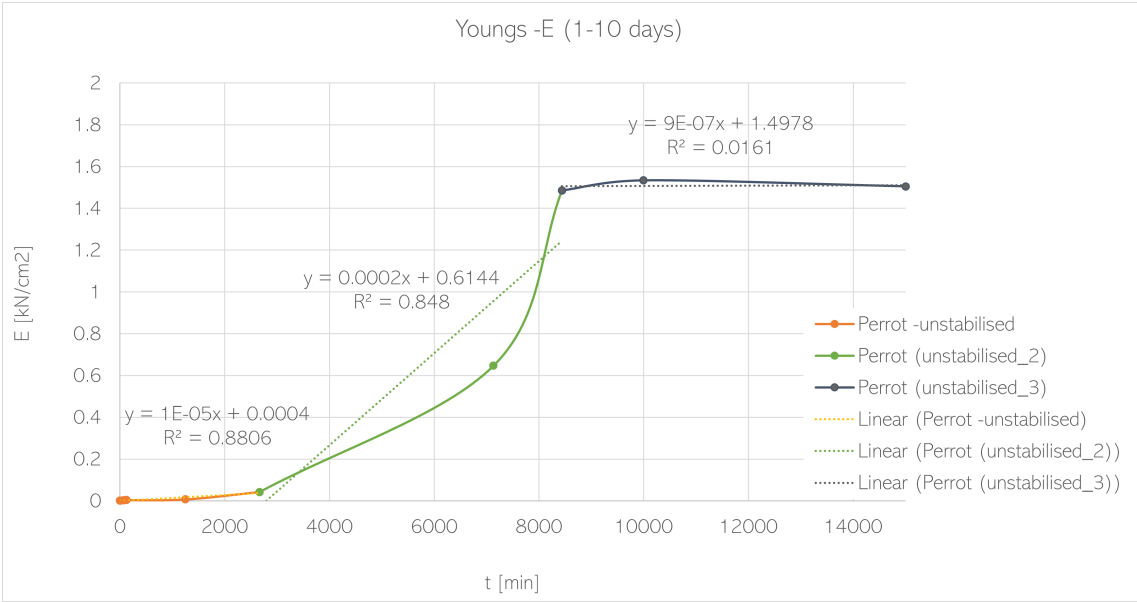


Figure E.4: Linear regression of Perrots stiffness development



Figure E.5: Linear regression of assumed URE stress development

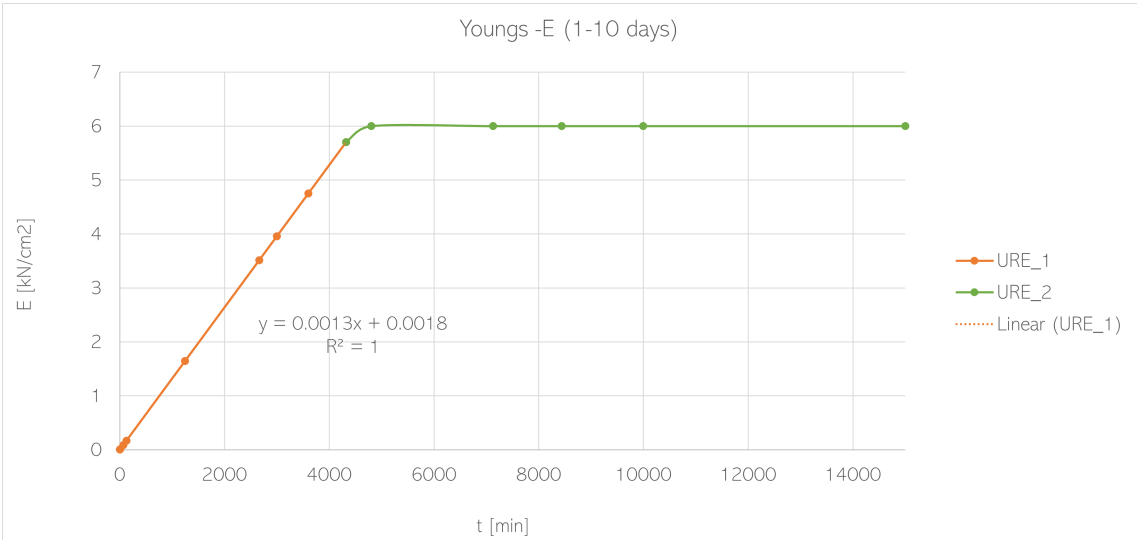


Figure E.6: Linear regression of assumed URE stiffness development

Upper bound strength development
SC3DP to CEP-FIP

Upper bound stiffness development
SC3DP to CEP-FIP

```

10
11 import rhinoscriptsyntax as rs
12 import math as m
13
14
15 def function(t,e_min,three_daymin):
16     if t <= e_min:
17         y = 0.0001*t +0.0003 + testValue
18     elif e_min < t and t < three_daymin:
19         y = (-3*10**-8*t**2) + (0.0003*t) - 0.0223 + testValue
20     elif three_daymin <= t:
21         y = (-3*10**-10*t**2) + (2*10**-05*t) + 0.5204 +testValue
22     return y
23
24 fct=function(float(t),120,4320)
25
10
11 import rhinoscriptsyntax as rs
12 import math as m
13
14
15 def function(t,e_min,three_daymin):
16     if t <= e_min:
17         y = 0.001*t + 0.0014 + testValue
18     elif e_min < t and t < three_daymin:
19         y = -3*10**-05*t**2 + 0.2728*t - 20.541 + testValue
20     elif three_daymin <= t:
21         y = -2*10**-07*t**2 + 0.0136*t + 726.7 +testValue
22     return y
23
24 fct=function(float(t),120,4320)
25
    
```

Lower bound strength development
Suiker to Weber

Lower bound stiffness development
Suiker to Weber

```

10
11 import rhinoscriptsyntax as rs
12 import math as m
13
14
15 def function(t,e_min,three_daymin):
16     if t <= e_min:
17         y = 0.0005984 + 0.000014*t + testValue
18     elif e_min < t and t < three_daymin:
19         y = (-1*10**-8*t**2) + (0.0002*t) - 0.0184 + testValue
20     elif three_daymin <= t:
21         y = (-4*10**-10*t**2) + (3*10**-05*t) + 0.3068 +testValue
22     return y
23
24 fct=function(float(t),120,4320)
25
10
11 import rhinoscriptsyntax as rs
12 import math as m
13
14
15 def function(t,e_min,three_daymin):
16     if t <= e_min:
17         y = 0.00781 + 0.00012*t + testValue
18     elif e_min < t and t < three_daymin:
19         y = -2*10**-05*t**2 + 0.2406*t - 27.158 + testValue
20     elif three_daymin <= t:
21         y = -3*10**-07*t**2 + 0.018*t + 654.34 +testValue
22     return y
23
24 fct=function(float(t),120,4320)
25
    
```

Figure E.7: Python code: conditions for stabilised material models

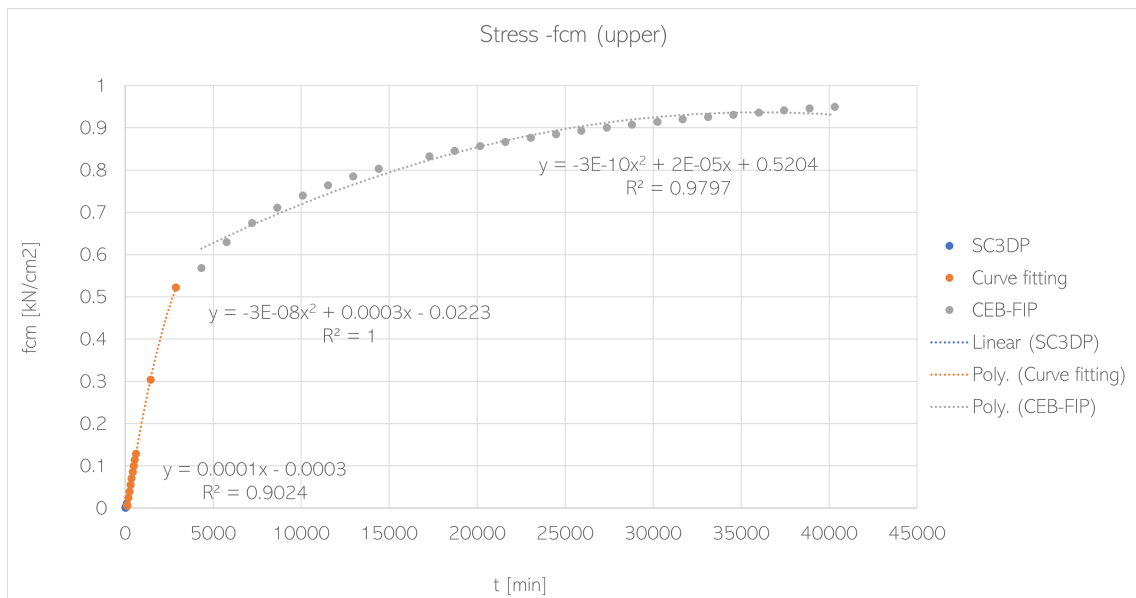


Figure E.8: Linear regression of stress data, upper

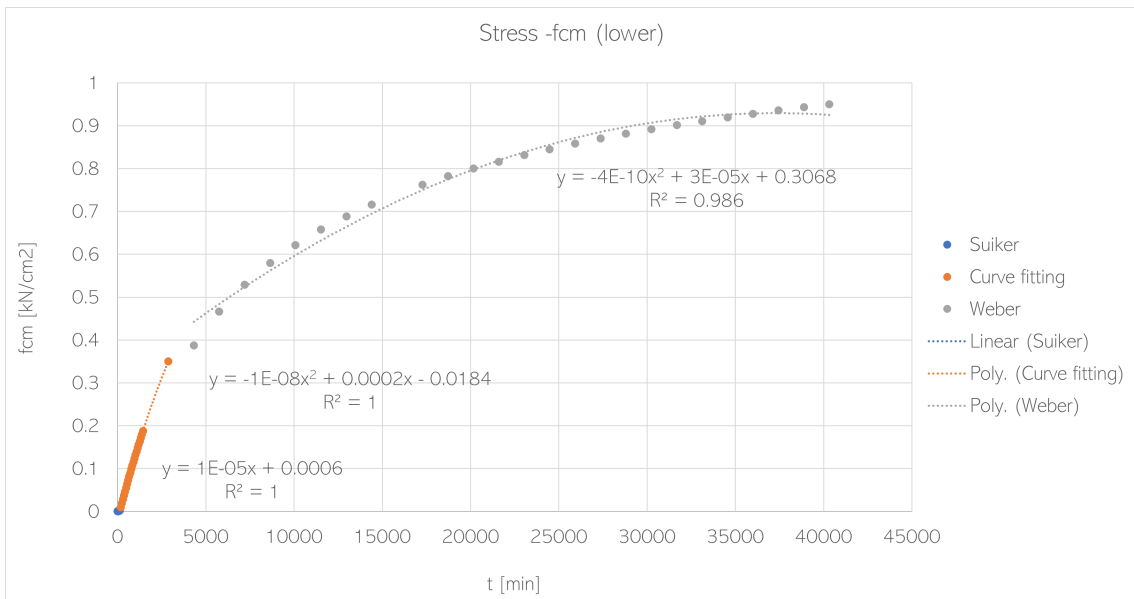


Figure E.9: Linear regression of stress data, lower

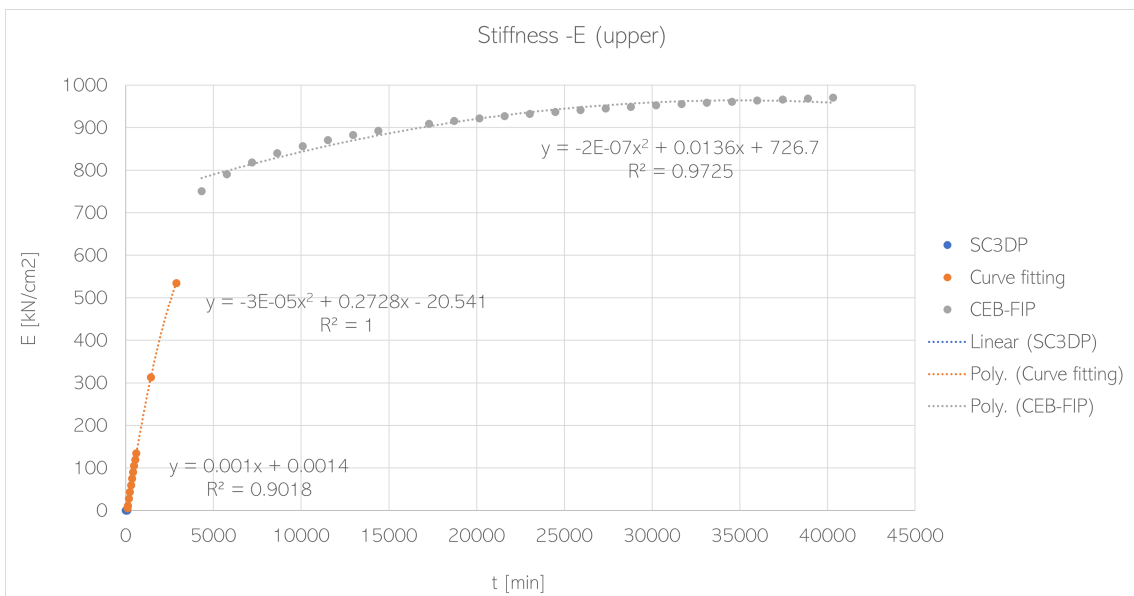


Figure E.10: Linear regression of stiffness data, upper

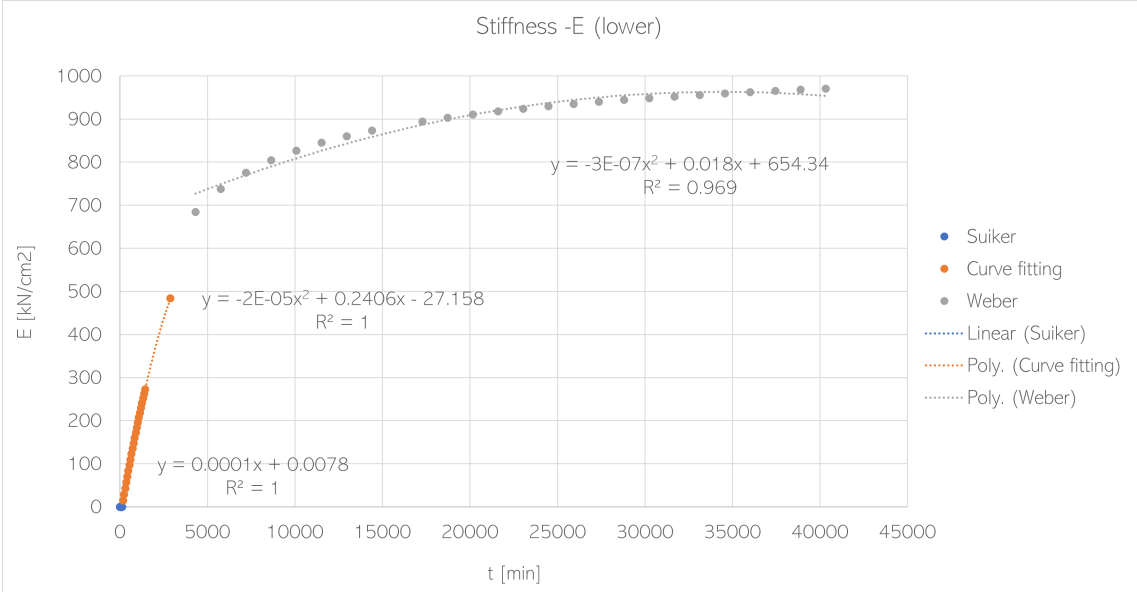


Figure E.11: Linear regression of stiffness data, lower

E.3. Monolithic wall

Wall model results -U: lower bound								
Gravity load	1							
Position	0 center of elements							
From shellview component					Allowable			
Principal 1			Principal 2					
Print speed [mm/min]	Max layer height	Max stress tension [MPa]	Min stress compression [MPa]	BLF (first)	Time to print [min]	Max compression [MPa]	Max tension [MPa]	
1000	6	0.00012	-0.00306	1.929	6	-0.00312	0.000312	
2000	5	0.000905	-0.00232	2.473	2.5	-0.00305	0.000305	
3000	5	0.000916	-0.00232	2.438	1.6667	-0.003033334	0.000303333	
4000	5	0.000922	-0.00233	2.42	1.25	-0.003025	0.0003025	
5000	5	0.000926	-0.00233	2.409	1	-0.00302	0.000302	
6000	5	0.000928	-0.00233	2.402	0.8333	-0.003016666	0.000301667	
Wall model results -U: upper bound								
Gravity load	1							
Position	0 center of elements							
From shellview component					Allowable			
Principal 1			Principal 2					
Print speed [mm/min]	Max layer height	Max stress tension [MPa]	Min stress compression [MPa]	BLF (first)	Time to print [min]	Max compression [MPa]	Max tension [MPa]	
1000	31	0.000159	-0.0195	1.071	31	-0.5124	0.05124	
2000	23	0.000178	-0.0141	1.027	11.5	-0.5046	0.05046	
3000	19	0.000181	-0.0114	1.121	4.75	-0.5019	0.05019	
4000	18	0.000197	-0.0107	1.025	4.5	-0.5018	0.05018	
5000	17	0.000204	-0.01	1.006	3.4	-0.50136	0.050136	
6000	16	0.000204	-0.00935	1.039	2.667	-0.5010668	0.05010668	
Wall model results -C: lower bound								
Gravity load	1							
Position	0 center of elements							
From shellview component					Allowable			
Principal 1			Principal 2					
Print speed [mm/min]	Max layer height	Max stress tension [MPa]	Min stress compression [MPa]	BLF (first)	Time to print [min]	Max compression [MPa]	Max tension [MPa]	
1000	16	0.00019	-0.00786	2.095	16	0.008224	0.0008224	
2000	14	0.000161	-0.00672	2.835	7	0.006964	0.0006964	
3000	13	0.000147	-0.00616	3.43	4.333	0.00659062	0.000659062	
4000	13	0.000147	-0.00615	3.38	3.25	0.006439	0.0006439	
5000	13	0.000148	-0.00615	3.36	2.6	0.006348	0.0006348	
6000	13	0.000148	-0.00615	3.343	2.16667	0.006287334	0.000628733	
Wall model results -C: upper bound								
Gravity load	1							
Position	0 center of elements							
From shellview component					Allowable			
Principal 1			Principal 2					
Print speed [mm/min]	Max layer height	Max stress tension [MPa]	Min stress compression [MPa]	BLF (first)	Time to print [min]	Max compression [MPa]	Max tension [MPa]	
1000	27	0.000946	-0.0148	1.024	27	0.284	0.0284	
2000	20	0.000106	-0.0107	1.047	10	0.114	0.0114	
3000	18	0.000111	-0.0089	1.089	5.6667	0.070667	0.0070667	
4000	16	0.00012	-0.00832	1.018	4	0.054	0.0054	
5000	15	0.000122	-0.00773	1.026	3	0.044	0.0044	
6000	14	0.000121	-0.00713	1.089	2.333	0.03733	0.003733	

Table E.1: Stress and buckling checks for wall model at different print speeds

E.4. Overhang roman layering

E.4.1. Barrel vault

Vault_roman results -U: lower bound									
Gravity load	1								
Position	0 center of elements								
From shellview component					Allowable				
Principal 1					Principal 2				
Print speed [mm/min]	Max layer height	Max stress tension [MPa]	Min stress compresio [MPa]	BLF (first)	Time to print [min]	Max compression [MPa]	Max tension [MPa]	Angle of overhang	
1000	5	0.000624	-0.00293		2.16	5	-0.0031	0.00031	8.922
2000	5	0.000648	-0.00296		2.51	2.5	-0.00305	0.000305	8.922
3000	5	0.000656	-0.00297		2.47	1.6667	-0.003033334	0.000303333	8.922
4000	5	0.000661	-0.00297		2.45	1.25	-0.003025	0.0003025	8.922
5000	5	0.000663	-0.00297		2.44	1	-0.00302	0.000302	8.922
6000	5	0.000665	-0.00298		2.44	0.8333	-0.003016666	0.000301667	8.922

Vault_roman results -U: upper bound									
Gravity load	1								
Position	0 center of elements								
From shellview component					Allowable				
Principal 1					Principal 2				
Print speed [mm/min]	Max layer height	Max stress tension [MPa]	Min stress compresio [MPa]	BLF (first)	Time to print [min]	Max compression [MPa]	Max tension [MPa]	Angle of overhang	
1000	26	0.0479	-0.0681		1.4	26	-0.5104	0.05104	10.18
1000 with imperfector	15	0.0297	-0.0647		1.5	15	-0.506	0.0506	9.73
3000									
4000									
5000									
6000	15	0.0091	-0.0415	1.16		2.5	-0.501	0.0501	9.669

Vault_roman results -C: lower bound									
Gravity load	1								
Position	0 center of elements								
From shellview component					Allowable				
Principal 1					Principal 2				
Print speed [mm/min]	Max layer height	Max stress tension [MPa]	Min stress compresio [MPa]	BLF (first)	Time to print [min]	Max compression [MPa]	Max tension [MPa]	Angle of overhang	
1000	10	0.000145	-0.00711		7.79	10	-0.007384	0.0007384	9.36
2000	9	0.0000999	-0.00602		10.03	4.5	-0.006614	0.0006614	9.28
3000	9	0.000101	-0.00602		9.85	3	-0.006404	0.0006404	9.28
4000									
5000									
6000	9	0.000102	0.00603		9.66	1.5	-0.006194	0.0006194	9.28
Compression stress is the governing									

Vault_roman results -C: upper bound									
Gravity load	1								
Position	0 center of elements								
From shellview component					Allowable				
Principal 1					Principal 2				
Print speed [mm/min]	Max layer height	Max stress tension [MPa]	Min stress compresio [MPa]	BLF (first)	Time to print [min]	Max compression [MPa]	Max tension [MPa]	Angle of overhang	
1000	21	0.0183	-0.0348		1.67	21	-0.224	0.0224	10.02
2000									
3000									
4000									
5000									
6000	11	0.0016	-0.0106		1.91	1.833	-0.03233	0.003233	9.44

Table E.2: Results from the barrel vault roman layering where the highlighted cell is the governing failure mode

E.4.2. Half dome

HalfDome_roman results -U: lower bound									
Gravity load	1								
Position	0 center of elements								
From shellview component					Allowable				
Principal 1					Principal 2				
Print speed [mm/min]	Max layer height	Max stress tension [MPa]	Min stress compressio	BLF (first)	Time to print [min]	Max compression [MPa]	Max tension [MPa]	Angle of overhang	
1000	5	0.000082	-0.00291		2.78	7.63	-0.0031526	0.00031526	8.92
2000									
3000									
4000									
5000									
6000	5	0.0000908	-0.00298		2.49	1.27	-0.0030254	0.00030254	8.92
HalfDome_roman results -U: upper bound									
Gravity load	1								
Position	0 center of elements								
From shellview component					Allowable				
Principal 1					Principal 2				
Print speed [mm/min]	Max layer height	Max stress tension [MPa]	Min stress compressio	BLF (first)	Time to print [min]	Max compression [MPa]	Max tension [MPa]	Angle of overhang	
1000	44	0.00753	-0.0549	1.19	55.32	-0.522128	0.0522128	9.95	
1000 with imperfection €	21	0.0386	-0.013	1.34	30.23	-0.512092	0.0512092	10.18	
3000									
4000									
5000									
6000	17	0.00852	-0.0313	1.38	4.15	-0.50166	0.050166	9.73	
HalfDome_roman results -C: lower bound									
Gravity load	1								
Position	0 center of elements								
From shellview component					Allowable				
Principal 1					Principal 2				
Print speed [mm/min]	Max layer height	Max stress tension [MPa]	Min stress compressio	BLF (first)	Time to print [min]	Max compression [MPa]	Max tension [MPa]	Angle of overhang	
1000	11	0.000115	-0.00814		7.98	16.46	-0.0082884	0.00082884	9.44
2000	10	0.0000962	-0.00696		9.29	8.23	-0.0071362	0.00071362	9.36
3000	9	0.0000856	-0.00587		11.8	4.52	-0.0066168	0.00066168	9.28
4000	9	0.0000871	-0.00587		11.65	3.39	-0.0064586	0.00064586	9.28
5000	9	0.0000871	-0.00587		11.55	2.71	-0.0063634	0.00063634	9.28
6000	9	0.0000877	-0.00587		11.5	2.26	-0.0063004	0.00063004	9.28
HalfDome_roman results -C: upper bound									
Gravity load	1								
Position	0 center of elements								
From shellview component					Allowable				
Principal 1					Principal 2				
Print speed [mm/min]	Max layer height	Max stress tension [MPa]	Min stress compressio	BLF (first)	Time to print [min]	Max compression [MPa]	Max tension [MPa]	Angle of overhang	
1000	39	0.0104	-0.062	1.17	51	-0.524	0.0524	10.099	
2000									
3000									
4000									
5000									
6000	14	0.00358	-0.0188		1.33	3.45	-0.0485	0.00485	9.67

Table E.3: Results from the half dome roman layering where the highlighted cell is the governing failure mode

E.5. Overhang nubian layering

E.5.1. Barrel vault

Vault_nubian results -U: lower bound									
Gravity load	1								
Position	0 center of elements								
From shellview component					Allowable				
		Principal 1	Principal 2						
Print speed [mm/min]	Max layer height	Max stress tension [MPa]	Min stress compressi [MPa]	BLF (first)	Time to print [min]	Max compression [MPa]	Max tension [MPa]	Angle of overhang	
1000	3	0.00088	-0.000191	1.69	0.27	-0.0030054	0.00030054	N/A	
Vault_nubian results -U: upper bound									
Gravity load	1								
Position	0 center of elements								
From shellview component					Allowable				
		Principal 1	Principal 2						
Print speed [mm/min]	Max layer height	Max stress tension [MPa]	Min stress compressi [MPa]	BLF (first)	Time to print [min]	Max compression [MPa]	Max tension [MPa]	Angle of overhang	
1000	9	0.00183	-0.00465	1.311	2.46	-0.500984	0.0500984	N/A	
Vault_nubian results -C: lower bound									
Gravity load	1								
Position	0 center of elements								
From shellview component					Allowable				
		Principal 1	Principal 2						
Print speed [mm/min]	Max layer height	Max stress tension [MPa]	Min stress compressi [MPa]	BLF (first)	Time to print [min]	Max compression [MPa]	Max tension [MPa]	Angle of overhang	
1000		0.00334	-0.00628	1.48	5.03	-0.0066882	0.00066882	N/A	
Vault_nubian results -C: upper bound									
Gravity load	1								
Position	0 center of elements								
From shellview component					Allowable				
		Principal 1	Principal 2						
Print speed [mm/min]	Max layer height	Max stress tension [MPa]	Min stress compressi [MPa]	BLF (first)	Time to print [min]	Max compression [MPa]	Max tension [MPa]	Angle of overhang	
1000	8	0.00168	0.00423	1.24	1.95	-0.0335	0.00335	N/A	

Table E.4: Results from the barrel vault nubian layering where the highlighted cell is the governing failure mode

E.5.2. Half dome

HalfDome_nubian results -U: lower bound								
Gravity load	1							
Position	0	center of elements						
			From shellview component			Allowable		
		Principal 1	Principal 2					
Print speed [mm/min]	Max layer height	Max stress tension [I]	Min stress compressi	BLF (first)	Time to print [min]	Max compression [M]	Max tension [MPa]	Angle of overhang
1000	2	0.000217	-0.000546	2.78	0.86	-0.0030172	0.00030172	8.63
		Not feasible						
HalfDome_nubian results -U: upper bound								
Gravity load	1							
Position	0	center of elements						
			From shellview component			Allowable		
		Principal 1	Principal 2					
Print speed [mm/min]	Max layer height	Max stress tension [I]	Min stress compressi	BLF (first)	Time to print [min]	Max compression [M]	Max tension [MPa]	Angle of overhang
1000	16	0.00447	-0.00532	1.43	17.69	-0.507076	0.0507076	10.02
			geometry					
HalfDome_nubian results -C: lower bound								
Gravity load	1							
Position	0	center of elements						
			From shellview component			Allowable		
		Principal 1	Principal 2					
Print speed [mm/min]	Max layer height	Max stress tension [I]	Min stress compressi	BLF (first)	Time to print [min]	Max compression [M]	Max tension [MPa]	Angle of overhang
1000	16	0.00432	-0.00516	2.46	17.69	-0.0084606	0.00084606	10.02
			geometry					
HalfDome_nubian results -C: upper bound								
Gravity load	1							
Position	0	center of elements						
			From shellview component			Allowable		
		Principal 1	Principal 2					
Print speed [mm/min]	Max layer height	Max stress tension [I]	Min stress compressi	BLF (first)	Time to print [min]	Max compression [M]	Max tension [MPa]	Angle of overhang
1000	15	0.00414	-0.00493	2.37	16.09	-0.1749	0.01749	9.96
			geometry					

Table E.5: Results from the half dome nubian layering where the highlighted cell is the governing failure mode

Bibliography

- [1] F. Pacheco-Torgal and S. Jalali, "Earth construction: Lessons from the past for future eco-efficient construction", *Construction and building materials*, vol. 29, pp. 512–519, 2012.
- [2] D. Gallipoli, A. W. Bruno, C. Perlot, and J. Mendes, "A geotechnical perspective of raw earth building", *Acta Geotechnica*, vol. 12, no. 3, pp. 463–478, 2017.
- [3] Y. Etzion and M. Saller, "Earth construction" a review of needs and methods", *Architectural Science Review*, vol. 30, no. 2, pp. 43–48, 1987.
- [4] U. Habitat, *Global housing strategy: Framework document*, 2016.
- [5] R. Rael, *Earth architecture*. Princeton architectural press, 2009.
- [6] M. Santamouris and D. Kolokotsa, "Passive cooling dissipation techniques for buildings and other structures: The state of the art", *Energy and Buildings*, vol. 57, pp. 74–94, 2013.
- [7] M. R. Hall, R. Lindsay, and M. Krayenhoff, *Modern earth buildings: Materials, engineering, constructions and applications*. Elsevier, 2012.
- [8] B. Medvey and G. Dobszay, "Durability of stabilized earthen constructions: A review", *Geotechnical and Geological Engineering*, vol. 38, no. 3, pp. 2403–2425, 2020.
- [9] L. ton erde. "Lkh feldkirch". (1993), [Online]. Available: <https://www.lehmtonerde.at/en/projects/project.php?pID=17> (visited on 02/19/2022).
- [10] Ricola. "Ricola eröffnet kräuterzentrum in laufen". (2014), [Online]. Available: <https://www.ricola.com/de/ricola/media/medienmitteilungen/international/ricola-eroffnung-krauterzentrum> (visited on 02/19/2022).
- [11] Z. news. "The arch of ctesiphon in iraq." (2021), [Online]. Available: <https://www.zenger.news/2021/02/21/wonder-lost-iraqs-arch-of-ctesiphon-could-go-extinct-after-authorities-neglect-it/> (visited on 02/19/2022).
- [12] Archdaily. "Stadium kigali rwanda". (2017), [Online]. Available: <https://www.archdaily.com/886036/rwanda-cricket-stadium-light-earth-designs/5a3e9fc3b22e3879e10003ef-rwanda-cricket-stadium-light-earth-designs-image> (visited on 02/19/2022).
- [13] FuturArc. "Sharanam center for rural development". (2016), [Online]. Available: <https://www.futurarc.com/project/sharanam-centre-for-rural-development/> (visited on 02/19/2022).
- [14] S. Jeske. "Outer shell of l'orangerie in context". (2020), [Online]. Available: https://www.dachverband-lehm.de/lehm2020_online/pdf/lehm2020_b_jeske-cva_en.pdf (visited on 02/19/2022).
- [15] B. R. Group. "Rammed earth vault". (2014), [Online]. Available: <https://block.arch.ethz.ch/brg/teaching/rammed-earth-vault> (visited on 02/19/2022).
- [16] archello. "Tecla -technology and clay". (2021), [Online]. Available: <https://archello.com/project/tecla-technology-and-clay> (visited on 02/19/2022).

- [17] M. Gomaa, J. Vaculik, V. Soebarto, M. Griffith, and W. Jabi, "Feasibility of 3dp cob walls under compression loads in low-rise construction", *Construction and Building Materials*, vol. 301, p. 124 079, 2021.
- [18] C. Beckett, P. Jaquin, and J.-C. Morel, "Weathering the storm: A framework to assess the resistance of earthen structures to water damage", *Construction and Building Materials*, vol. 242, p. 118 098, 2020.
- [19] H. Schroeder, *Sustainable building with earth*. Springer, 2016.
- [20] J. Dethier, *The Art of Earth Architecture: Past, Present, Future*. Thames and Hudson, 2020.
- [21] E. Hamard, B. Cazacliu, A. Razakamanantsoa, and J.-C. Morel, "Cob, a vernacular earth construction process in the context of modern sustainable building", *Building and Environment*, vol. 106, pp. 103–119, 2016.
- [22] S. Piesik, *Habitat: vernacular architecture for a changing planet*. Thames & Hudson, 2017.
- [23] D. Gandreau and L. Delboy, "Patrimoine mondial, inventaire et situation des biens construits en terre", *Paris, France: CRAterre-ENSAG*, 2010.
- [24] C. F. Horne, C. H. W. Johns, *et al.*, *The code of Hammurabi*. Forgotten Books, 1915.
- [25] A. Al Rashid, S. A. Khan, S. G. Al-Ghamdi, and M. Koç, "Additive manufacturing: Technology, applications, markets, and opportunities for the built environment", *Automation in Construction*, vol. 118, p. 103 268, 2020.
- [26] Gashtour. "The windcatchers of yazd". (2020), [Online]. Available: <https://irangash ttour.com/2020/03/03/windcatchers/> (visited on 02/19/2022).
- [27] Twitterpost. "Catal hüyük reconstruction 7000 bce". (2020), [Online]. Available: <https://twitter.com/sumerianhittite/status/1279276569727565830?lang=ar-x-fm> (visited on 02/19/2022).
- [28] Wikipedia. "White temple ziggurat in uruk 2020". (2020), [Online]. Available: <https://en.wikipedia.org/wiki/Uruk> (visited on 02/19/2022).
- [29] SuperStock. "Irak. assyrian dur sharrukin". (2020), [Online]. Available: https://www.google.com/url?sa=i&url=https%3A%2F%2Fwww.superstock.com%2Fstock-photos-images%2F1788-27929&psig=A0vVaw3TbdvjDvdXuHbHkFdrKZWc&ust=1645372022656000&source=images&cd=vfe&ved=0CAsQjRxqFwoTCIC_hM20jPYCFQAAAAAdAAAAABAE (visited on 02/19/2022).
- [30] N. Geographic. "The manhattan of the desert". (2017), [Online]. Available: <https://www.nationalgeographic.com/travel/article/shibam-mud-skyscraper-yemen> (visited on 02/19/2022).
- [31] C. Muse. "Alhambra palace". (2020), [Online]. Available: <https://cliomusetours.com/a-brief-history-of-the-alhambra-palace/> (visited on 02/19/2022).
- [32] Wikipedia. "Jiayu pass". (2022), [Online]. Available: https://www.google.com/url?sa=i&url=https%3A%2F%2Fnl.pinterest.com%2Fpin%2F435019645236897148%2F&psig=A0vVaw1MAb2clwlp1Q31KLIn6VG&ust=1645471957417000&source=images&cd=vfe&ved=0CAsQjRxqFwoTCKDqp0Cj_YCFQAAAAAdAAAAABAS (visited on 02/19/2022).
- [33] A. CG. "Fujian tulou". (2019), [Online]. Available: <https://www.aimircg.com/fujian-tulou/> (visited on 02/19/2022).

- [34] Forbes. "Santa fe, new mexico". (2021), [Online]. Available: <https://www.forbes.com/sites/forbes-global-properties/2021/08/07/santa-fe-new-mexico-where-the-luxury-home-buying-dollar-goes-far/> (visited on 02/19/2022).
- [35] arctic adventures. "Turf houses". (2022), [Online]. Available: <https://adventures.is/iceland/attractions/turf-houses-iceland/> (visited on 02/19/2022).
- [36] wikipedia. "Ennis house". (2022), [Online]. Available: https://en.wikipedia.org/wiki/Ennis_House (visited on 02/19/2022).
- [37] S. Atlas. "Hasan fathy". (2020), [Online]. Available: <https://www.sensesatlas.com/territory/hassan-fathy-building-in-the-desert-in-new-baris/> (visited on 02/19/2022).
- [38] G. Barnes, *Soil mechanics: principles and practice*. Macmillan International Higher Education, 2016.
- [39] F. Wu, G. Li, H.-N. Li, and J.-Q. Jia, "Strength and stress–strain characteristics of traditional adobe block and masonry", *Materials and structures*, vol. 46, no. 9, pp. 1449–1457, 2013.
- [40] H. Guillaud and H. Houben, "Earth construction: A comprehensive guide", *London, Intermediate Technology*, 1994.
- [41] F. Avila, E. Puertas, and R. Gallego, "Characterization of the mechanical and physical properties of unstabilized rammed earth: A review", *Construction and Building Materials*, p. 121 435, 2020.
- [42] J.-E. Aubert, A. Marcom, P. Oliva, and P. Segui, "Chequered earth construction in south-western france", *Journal of Cultural Heritage*, vol. 16, no. 3, pp. 293–298, 2015.
- [43] M. I. Gomes, T. D. Gonçalves, and P. Faria, "Unstabilized rammed earth: Characterization of material collected from old constructions in south portugal and comparison to normative requirements", *International Journal of Architectural Heritage*, vol. 8, no. 2, pp. 185–212, 2014.
- [44] F. Champiré, A. Fabbri, J.-C. Morel, H. Wong, and F. McGregor, "Impact of relative humidity on the mechanical behavior of compacted earth as a building material", *Construction and Building Materials*, vol. 110, pp. 70–78, 2016.
- [45] A. Fabbri, J.-C. Morel, and D. Gallipoli, "Assessing the performance of earth building materials: A review of recent developments", *RILEM Technical Letters*, vol. 3, pp. 46–58, 2018.
- [46] A. Bazara, "Erarbeitung einer konzeption zur konstruktiven und funktionellen rekonstruktion der stockwerk-lehmkonstruktionen in der vdr jemen", *Unpublished diploma thesis. Hochschule f. Architektur und Bauwesen, Sektion Bauingenieurwesen, Weimar*, 1986.
- [47] G. T. Pearson, *Conservation of clay and chalk buildings*. Routledge, 2015.
- [48] F. McDonald and P. Doyle, *Ireland's earthen houses*. A. & A. Farmar, 1997.
- [49] J. Q. Addo, T. G. Sanders, and M. Chenard, "Road dust suppression: Effect on maintenance stability, safety and the environment, phases 1-3", Tech. Rep., 2004.
- [50] P. Sherwood, *Soil stabilization with cement and lime*. 1993.
- [51] P. Walker, "Standards australia (2002) hb 195—the australian earth building handbook", *Standards Australia, Australia*,

- [52] T. S. Amhadi and G. J. Assaf, "Overview of soil stabilization methods in road construction", in *International Congress and Exhibition Sustainable Civil Infrastructures: Innovative Infrastructure Geotechnology*, Springer, 2018, pp. 21–33.
- [53] A. Mohajerani, S.-Q. Hui, M. Mirzababaei, *et al.*, "Amazing types, properties, and applications of fibres in construction materials", *Materials*, vol. 12, no. 16, p. 2513, 2019.
- [54] H. Van Damme and H. Houben, "Earth concrete. stabilization revisited", *Cement and Concrete Research*, vol. 114, pp. 90–102, 2018.
- [55] Y. Chen, "Soil–water retention curves derived as a function of soil dry density", *Geo-Hazards*, vol. 1, no. 1, pp. 3–19, 2020.
- [56] P. Jaquin, C. Augarde, D. Gallipoli, and D. Toll, "The strength of unstabilised rammed earth materials", *Géotechnique*, vol. 59, no. 5, pp. 487–490, 2009.
- [57] Q.-B. Bui, J.-C. Morel, S. Hans, and P. Walker, "Effect of moisture content on the mechanical characteristics of rammed earth", *Construction and Building materials*, vol. 54, pp. 163–169, 2014.
- [58] A. Aysen, *Soil mechanics: basic concepts and engineering applications*. CRC Press, 2002.
- [59] R. El Nabouch, "Mechanical behavior of rammed earth walls under pushover tests", Ph.D. dissertation, Université Grenoble Alpes, 2017.
- [60] J.-C. Morel, A. Pkla, and P. Walker, "Compressive strength testing of compressed earth blocks", *Construction and Building materials*, vol. 21, no. 2, pp. 303–309, 2007.
- [61] C. Kouakou and J.-C. Morel, "Strength and elasto-plastic properties of non-industrial building materials manufactured with clay as a natural binder", *Applied Clay Science*, vol. 44, no. 1-2, pp. 27–34, 2009.
- [62] A. Bruno, D. Gallipoli, C. Perlot, J. Mendes, and N. Salmon, "Mechanical properties of unstabilized earth compressed at high pressures", *Academic Journal of Civil Engineering*, vol. 33, no. 2, pp. 85–92, 2015.
- [63] G. F. Middleton and L. M. Schneider, "Earth-wall construction", 1987.
- [64] B. V. Reddy and P. P. Kumar, "Cement stabilised rammed earth. part b: Compressive strength and stress–strain characteristics", *Materials and structures*, vol. 44, no. 3, pp. 695–707, 2011.
- [65] B. Venkatarama Reddy and P. Prasanna Kumar, "Structural behavior of story-high cement-stabilized rammed-earth walls under compression", *Journal of materials in civil engineering*, vol. 23, no. 3, pp. 240–247, 2011.
- [66] C. Jayasinghe and N. Kamaladasa, "Compressive strength characteristics of cement stabilized rammed earth walls", *Construction and Building Materials*, vol. 21, no. 11, pp. 1971–1976, 2007.
- [67] M. Hall and Y. Djerbib, "Rammed earth sample production: Context, recommendations and consistency", *Construction and building materials*, vol. 18, no. 4, pp. 281–286, 2004.
- [68] V. Maniatidis and P. Walker, "Structural capacity of rammed earth in compression", *Journal of Materials in Civil Engineering*, vol. 20, no. 3, pp. 230–238, 2008.
- [69] J. Ruzicka, F. Havlik, J. Richter, and K. Stanek, "Advanced prefabricated rammed earth structures–mechanical, building physical and environmental properties", in *First International Conference on Rammed Earth Construction, Western Austrália*, 2015.

- [70] Q.-B. Bui, J.-C. Morel, S. Hans, and N. Meunier, "Compression behaviour of non-industrial materials in civil engineering by three scale experiments: The case of rammed earth", *Materials and structures*, vol. 42, no. 8, pp. 1101–1116, 2009.
- [71] B. King, *Buildings of earth and straw: structural design for rammed earth and straw-bale architecture*. 1996.
- [72] P. Walker, R. Keable, J. Martin, and V. Maniatidis, "Rammed earth: Design and construction guidelines", 2005.
- [73] B. Venkatarama Reddy, V. Suresh, and K. Nanjunda Rao, "Characteristic compressive strength of cement-stabilized rammed earth", *Journal of materials in civil engineering*, vol. 29, no. 2, p. 04 016 203, 2017.
- [74] P. Walker and S. Dobson, "Reinforced composite rammed earth in flexure", in *Proceedings 3rd International Conference on Non-Conventional Materials & Technologies*, 2002.
- [75] A. Standard, "Standard test methods for compressive strength of molded soil-cement cylinders", *ASTM International, West Conshohocken, PA*, 2017.
- [76] I. Hager, A. Golonka, and R. Putanowicz, "3d printing of buildings and building components as the future of sustainable construction?", *Procedia Engineering*, vol. 151, pp. 292–299, 2016.
- [77] R. L. Hartzler, "A program of investigation and laboratory research of acrylic-modified earthen mortar used at three prehistoric puebloan sites", 1996.
- [78] R. El-Nabouch, Q.-B. Bui, O. Ple, and P. Perrotin, "Assessing the in-plane seismic performance of rammed earth walls by using horizontal loading tests", *Engineering Structures*, vol. 145, pp. 153–161, 2017.
- [79] D. A. Shepherd, E. Kotan, and F. Dehn, "Plastic concrete for cut-off walls: A review", *Construction and Building Materials*, vol. 255, p. 119 248, 2020.
- [80] T.-T. Bui, Q.-B. Bui, A. Limam, and S. Maximilien, "Failure of rammed earth walls: From observations to quantifications", *Construction and Building Materials*, vol. 51, pp. 295–302, 2014.
- [81] L. Miccoli, U. Müller, and P. Fontana, "Mechanical behaviour of earthen materials: A comparison between earth block masonry, rammed earth and cob", *Construction and building materials*, vol. 61, pp. 327–339, 2014.
- [82] G. Minke, *Building with earth*. Birkhäuser, 2013.
- [83] V. Toufigh and E. Kianfar, "The effects of stabilizers on the thermal and the mechanical properties of rammed earth at various humidities and their environmental impacts", *Construction and Building Materials*, vol. 200, pp. 616–629, 2019.
- [84] N. Z. Standard, *Nzs 4298: Materials and workmanship for earth buildings*, 1998.
- [85] A. H. Narayanaswamy, "Mechanical testing procedure for local building materials: Rammed earth and laterite building stones", Ph.D. dissertation, Université de Lyon, 2016.
- [86] T.-T. Bui, Q.-B. Bui, A. Limam, and J.-C. Morel, "Modeling rammed earth wall using discrete element method", *Continuum Mechanics and Thermodynamics*, vol. 28, no. 1-2, pp. 523–538, 2016.
- [87] R. A. M. Silva, D. V. Oliveira, L. Schueremans, P. B. Lourenço, and T. F. Miranda, "Modelling of the structural behaviour of rammed earth components", 2014.

- [88] L. Miccoli, D. V. Oliveira, R. A. Silva, U. Müller, and L. Schueremans, "Static behaviour of rammed earth: Experimental testing and finite element modelling", *Materials and Structures*, vol. 48, no. 10, pp. 3443–3456, 2015.
- [89] Q.-B. Bui, T.-T. Bui, M.-P. Tran, T.-L. Bui, and H.-A. Le, "Assessing the seismic behavior of rammed earth walls with an I-form cross-section", *Sustainability*, vol. 11, no. 5, p. 1296, 2019.
- [90] M. Kosarimovahhed and V. Toufigh, "Sustainable usage of waste materials as stabilizer in rammed earth structures", *Journal of Cleaner Production*, vol. 277, p. 123 279, 2020.
- [91] M. CEB-FIP, "90, design of concrete structures. ceb-fip model code 1990", *British Standard Institution, London*, 1993.
- [92] F. McGregor, A. Heath, D. Maskell, A. Fabbri, and J.-C. Morel, "A review on the buffering capacity of earth building materials", *Proceedings of the Institution of Civil Engineers-Construction Materials*, vol. 169, no. 5, pp. 241–251, 2016.
- [93] U. Lustig-Rössler, *Untersuchungen zum Feuchteverhalten von Lehm als Baustoff*. na, 1992.
- [94] C. Rode, R. Peuhkuri, B. Time, K. Svennberg, and T. Ojanen, "Moisture buffer value of building materials", in *Heat-Air-Moisture Transport: Measurements on Building Materials*, ASTM International, 2007.
- [95] F. McGregor, A. Heath, E. Fodde, and A. Shea, "Conditions affecting the moisture buffering measurement performed on compressed earth blocks", *Building and Environment*, vol. 75, pp. 11–18, 2014.
- [96] D. Allinson and M. Hall, "Humidity buffering using stabilised rammed earth materials", *Proceedings of the Institution of Civil Engineers-Construction Materials*, vol. 165, no. 6, pp. 335–344, 2012.
- [97] K. Dierks and C. Ziegert, "Neue untersuchungen zum materialverhalten von stampflehm", *Steingass, P.: moderner lehmbau*, 2002.
- [98] A. N. Daza, E. Zambrano, and J. A. Ruiz, "Acoustic performance in raw earth construction techniques used in colombia",
- [99] J. D. Racusin and A. McArleton, *The natural building companion: a comprehensive guide to integrative design and construction*. Chelsea Green Publishing, 2012.
- [100] U. Röhlen and C. Ziegert, *Earth Building Practice: Planning-Design-Building*. Beuth Verlag, 2011.
- [101] A. W. Bruno, "Hygro-mechanical characterisation of hypercompacted earth for building construction", Ph.D. dissertation, Ph. D. thesis, 2016.
- [102] L. Birznieks, "Designing and building with compressed earth", 2013.
- [103] Q.-B. Bui, J.-C. Morel, B. V. Reddy, and W. Ghayad, "Durability of rammed earth walls exposed for 20 years to natural weathering", *Building and Environment*, vol. 44, no. 5, pp. 912–919, 2009.
- [104] A. Dahmen, "Who's afraid of raw earth? experimental wall in new england and the environmental cost of stabilization", in *Rammed Earth Construction*, CRC Press, 2015, pp. 95–98.
- [105] R. Kebao and D. Kagi, "Integral admixtures and surface treatments for modern earth buildings", in *Modern Earth Buildings*, Elsevier, 2012, pp. 256–281.

- [106] R. A. Buswell, R. C. Soar, A. G. Gibb, and A. Thorpe, "Freeform construction: Mega-scale rapid manufacturing for construction", *Automation in construction*, vol. 16, no. 2, pp. 224–231, 2007.
- [107] S. Martinez, C. Balaguer, A. Jardon, J. Navarro, A. Gimenez, and C. Barcena, "Robotized lean assembly in the building industry", in *Proceedings of the 25th International Symposium on Automation and Robotics in Construction, Vilnius, Lithuania*, Citeseer, 2008, pp. 26–29.
- [108] D. T. Pham and R. S. Gault, "A comparison of rapid prototyping technologies", *International Journal of machine tools and manufacture*, vol. 38, no. 10-11, pp. 1257–1287, 1998.
- [109] T. Wohlers, "Rapid prototyping & tooling state of the industry: 1998 worldwide progress report", *Materials Technology*, vol. 13, no. 4, pp. 174–176, 1998.
- [110] T. D. Ngo, A. Kashani, G. Imbalzano, K. T. Nguyen, and D. Hui, "Additive manufacturing (3d printing): A review of materials, methods, applications and challenges", *Composites Part B: Engineering*, vol. 143, pp. 172–196, 2018.
- [111] S. Lim, R. A. Buswell, T. T. Le, S. A. Austin, A. G. Gibb, and T. Thorpe, "Developments in construction-scale additive manufacturing processes", *Automation in construction*, vol. 21, pp. 262–268, 2012.
- [112] B. Khoshnevis, D. Hwang, K.-T. Yao, and Z. Yeh, "Mega-scale fabrication by contour crafting", *International Journal of Industrial and Systems Engineering*, vol. 1, no. 3, pp. 301–320, 2006.
- [113] N. Labonnote, A. Rønquist, B. Manum, and P. Rütther, "Additive construction: State-of-the-art, challenges and opportunities", *Automation in construction*, vol. 72, pp. 347–366, 2016.
- [114] I. Perkins and M. Skitmore, "Three-dimensional printing in the construction industry: A review", *International Journal of Construction Management*, vol. 15, no. 1, pp. 1–9, 2015.
- [115] F. Bos, R. Wolfs, Z. Ahmed, and T. Salet, "Additive manufacturing of concrete in construction: Potentials and challenges of 3d concrete printing", *Virtual and Physical Prototyping*, vol. 11, no. 3, pp. 209–225, 2016.
- [116] R. J. Wolfs, F. Bos, and T. Salet, "Early age mechanical behaviour of 3d printed concrete: Numerical modelling and experimental testing", *Cement and Concrete Research*, vol. 106, pp. 103–116, 2018.
- [117] A. Paolini, S. Kollmannsberger, and E. Rank, "Additive manufacturing in construction: A review on processes, applications, and digital planning methods", *Additive Manufacturing*, vol. 30, p. 100894, 2019.
- [118] R. A. Buswell, W. L. De Silva, S. Z. Jones, and J. Dirrenberger, "3d printing using concrete extrusion: A roadmap for research", *Cement and Concrete Research*, vol. 112, pp. 37–49, 2018.
- [119] B. Khoshnevis and R. Dutton, "Innovative rapid prototyping process makes large sized, smooth surfaced complex shapes in a wide variety of materials", *Materials Technology*, vol. 13, no. 2, pp. 53–56, 1998.
- [120] F. Craveiroa, J. P. Duarte, H. Bartolola, and P. J. Bartolod, "Additive manufacturing as an enabling technology for digital construction: A perspective on construction 4.0", *sustainable development*, vol. 4, p. 6, 2019.

- [121] ArchDaily. "Chinese company showcases ten 3d-printed houses". (2014), [Online]. Available: <https://www.archdaily.com/543518/chinese-company-showcases-ten20d-printed-houses> (visited on 09/07/2021).
- [122] Architect. "Gensler completes the world's first 3d-printed office building". (2016), [Online]. Available: https://www.architectmagazine.com/technology/gensler-designs-the-worlds-first-3d-printed-office-building-in-dubai_o (visited on 09/07/2021).
- [123] T. A. Salet, Z. Y. Ahmed, F. P. Bos, and H. L. Laagland, "Design of a 3d printed concrete bridge by testing", *Virtual and Physical Prototyping*, vol. 13, no. 3, pp. 222–236, 2018.
- [124] S. Engineering. "Bridge project". (2021), [Online]. Available: <https://www.summum.engineering/portfolio/3dcp-bridge/> (visited on 09/07/2021).
- [125] 3DPrintedHouse. "Project milestone". (2021), [Online]. Available: <https://3dprintedhouse.nl/en/project-info/project-milestone/> (visited on 09/07/2021).
- [126] COBOD. "Modular 3d construction printer". (2021), [Online]. Available: <https://cobod.com/bod2/> (visited on 09/07/2021).
- [127] A. C. University. "World's largest 3d printed building". (2021), [Online]. Available: <https://www.apis-cor.com/dubai-project> (visited on 09/07/2021).
- [128] CyBe. "Cybe construction". (2021), [Online]. Available: <https://cybe.eu/> (visited on 09/07/2021).
- [129] Arup. "Bringing 3d printing to construction". (2018), [Online]. Available: <https://www.arup.com/projects/3d-printed-concrete-house> (visited on 09/07/2021).
- [130] Xtree. "Xtree the large scale 3d". (2021), [Online]. Available: <https://xtreee.com/en/> (visited on 09/07/2021).
- [131] H. Lindemann, R. Gerbers, S. Ibrahim, *et al.*, "Development of a shotcrete 3d-printing (sc3dp) technology for additive manufacturing of reinforced freeform concrete structures", in *RILEM International Conference on Concrete and Digital Fabrication*, Springer, 2018, pp. 287–298.
- [132] H. Lindemann, H. Kloft, and N. Hack, "Gradual transition shotcrete 3d printing", *Advances in Architectural Geometry*, 2018.
- [133] S. Marcel, E. Elisabeth, G. Joschua, *et al.*, "Ten questions concerning the potential of digital production and new technologies for contemporary earthen constructions", *Building and Environment*, p. 108240, 2021.
- [134] A. Jipa and B. Dillenburger, "3d printed formwork for concrete: State-of-the-art, opportunities, challenges, and applications", *3D Printing and Additive Manufacturing*, 2021.
- [135] O. Kontovourkis and G. Tryfonos, "Robotic 3d clay printing of prefabricated non-conventional wall components based on a parametric-integrated design", *Automation in Construction*, vol. 110, p. 103005, 2020.
- [136] O. Kontovourkis and G. Tryfonos, "Integrating parametric design with robotic additive manufacturing for 3d clay printing: An experimental study", in *ISARC. Proceedings of the International Symposium on Automation and Robotics in Construction*, IAARC Publications, vol. 35, 2018, pp. 1–8.
- [137] A. Perrot, D. Rangeard, and E. Courteille, "3d printing of earth-based materials: Processing aspects", *Construction and Building Materials*, vol. 172, pp. 670–676, 2018.
- [138] S. Engineering. "Terramia". (2019), [Online]. Available: <https://www.summum.engineering/portfolio/terramia/> (visited on 09/07/2021).

- [139] A. Curto, L. Lanzoni, A. M. Tarantino, and M. Viviani, "Shot-earth for sustainable constructions", *Construction and Building Materials*, vol. 239, p. 117 775, 2020.
- [140] Y. W. D. Tay, G. H. A. Ting, Y. Qian, B. Panda, L. He, and M. J. Tan, "Time gap effect on bond strength of 3d-printed concrete", *Virtual and Physical Prototyping*, vol. 14, no. 1, pp. 104–113, 2019.
- [141] Y. Weng, M. Li, Z. Liu, *et al.*, "Printability and fire performance of a developed 3d printable fibre reinforced cementitious composites under elevated temperatures", *Virtual and physical prototyping*, vol. 14, no. 3, pp. 284–292, 2019.
- [142] J. Zhang, J. Wang, S. Dong, X. Yu, and B. Han, "A review of the current progress and application of 3d printed concrete", *Composites Part A: Applied Science and Manufacturing*, vol. 125, p. 105 533, 2019.
- [143] A. Bhardwaj, S. Z. Jones, N. Kalantar, *et al.*, "Additive manufacturing processes for infrastructure construction: A review", *Journal of Manufacturing Science and Engineering*, vol. 141, no. 9, p. 091 010, 2019.
- [144] B. Panda, N. A. Noor Mohamed, S. C. Paul, G. Bhagath Singh, M. J. Tan, and B. Šavija, "The effect of material fresh properties and process parameters on buildability and interlayer adhesion of 3d printed concrete", *Materials*, vol. 12, no. 13, p. 2149, 2019.
- [145] G. Duarte, N. Brown, A. Memari, and J. P. Duarte, "Learning from historical structures under compression for concrete 3d printing construction", *Journal of Building Engineering*, p. 103 009, 2021.
- [146] H. Kloft, M. Empelmann, N. Hack, E. Herrmann, and D. Lowke, "Reinforcement strategies for 3d-concrete-printing", *Civil Engineering Design*, vol. 2, no. 4, pp. 131–139, 2020.
- [147] V. Mechtcherine, R. Buswell, H. Kloft, *et al.*, "Integrating reinforcement in digital fabrication with concrete: A review and classification framework", *Cement and Concrete Composites*, p. 103 964, 2021.
- [148] B. Nematollahi, P. Vijay, J. Sanjayan, *et al.*, "Effect of polypropylene fibre addition on properties of geopolymers made by 3d printing for digital construction", *Materials*, vol. 11, no. 12, p. 2352, 2018.
- [149] M. Hambach, M. Rutzen, and D. Volkmer, "Properties of 3d-printed fiber-reinforced portland cement paste", in *3D Concrete Printing Technology*, Elsevier, 2019, pp. 73–113.
- [150] D. G. Soltan and V. C. Li, "A self-reinforced cementitious composite for building-scale 3d printing", *Cement and Concrete Composites*, vol. 90, pp. 1–13, 2018.
- [151] V. C. Li, F. P. Bos, K. Yu, *et al.*, "On the emergence of 3d printable engineered, strain hardening cementitious composites (ecc/shcc)", *Cement and Concrete Research*, vol. 132, p. 106 038, 2020.
- [152] R. Wolfs and A. Suiker, "Structural failure during extrusion-based 3d printing processes", *The International Journal of Advanced Manufacturing Technology*, vol. 104, no. 1, pp. 565–584, 2019.
- [153] Inhabitat. "Delta 3d printer". (2016), [Online]. Available: <https://inhabitat.com/worlds-largest-delta-style-3d-printer-can-print-nearly-zero-cost-housing-out-of-mud/> (visited on 02/19/2022).

- [154] Designboom. "Fabclay: Robotic additive manufacturing processes". (2012), [Online]. Available: <https://www.designboom.com/readers/fabclay-robotic-additive-manufacturing-processes/> (visited on 02/19/2022).
- [155] 3Dprint.com. "Ntu singapore researchers develop mobile 3d printing concrete collaborative robots". (2018), [Online]. Available: <https://3dprint.com/223728/mobile-robot-3d-print-construction/> (visited on 02/19/2022).
- [156] ing.dk. "Galleri: Sådan opføres dfab house med robotter og 3d-teknikker". (2017), [Online]. Available: <https://ing.dk/galleri/galleri-saadan-opfoeres-dfab-house-med-robotter-3d-teknikker-204648#1> (visited on 02/19/2022).
- [157] Y. Chen, K. Jansen, H. Zhang, *et al.*, "Effect of printing parameters on interlayer bond strength of 3d printed limestone-calcined clay-based cementitious materials: An experimental and numerical study", *Construction and Building Materials*, vol. 262, p. 120 094, 2020.
- [158] P. Carneau, R. Mesnil, N. Roussel, and O. Baverel, "Additive manufacturing of cantilever from masonry to concrete 3d printing", *Automation in Construction*, vol. 116, p. 103 184, 2020.
- [159] I. Dressler, N. Freund, and D. Lowke, "Control of strand properties produced with shotcrete 3d printing by accelerator dosage and process parameters", in *RILEM International Conference on Concrete and Digital Fabrication*, Springer, 2020, pp. 42–52.
- [160] V. Mechtcherine and V. N. Nerella, "3d printing with concrete: State-of-the art, trends, challenges", *Bautechnik*, vol. 95, no. 4, pp. 275–287, 2018.
- [161] A. Suiker, "Mechanical performance of wall structures in 3d printing processes: Theory, design tools and experiments", *International Journal of Mechanical Sciences*, vol. 137, pp. 145–170, 2018.
- [162] Z. Chang, E. Schlangen, and B. Šavija, "Extended lattice model to simulate the printing process of 3d printed cementitious materials", in *RILEM International Conference on Concrete and Digital Fabrication*, Springer, 2020, pp. 814–823.
- [163] I. Dressler, N. Freund, and D. Lowke, "The effect of accelerator dosage on fresh concrete properties and on interlayer strength in shotcrete 3d printing", *Materials*, vol. 13, no. 2, p. 374, 2020.
- [164] R. Schutz, "Numerical modelling of shotcrete for tunnelling", Ph.D. dissertation, Imperial College London, 2010.
- [165] C. Galán-Marín, C. Rivera-Gómez, and J. Petric, "Clay-based composite stabilized with natural polymer and fibre", *Construction and Building Materials*, vol. 24, no. 8, pp. 1462–1468, 2010.
- [166] M. Gohnert, I. Bulovic, and R. Bradley, "A low-cost housing solution: Earth block catenary vaults", in *Structures*, Elsevier, vol. 15, 2018, pp. 270–278.
- [167] J. Pegna, "Exploratory investigation of solid freeform construction", *Automation in construction*, vol. 5, no. 5, pp. 427–437, 1997.
- [168] C. B. Costanzi, Z. Ahmed, H. R. Schipper, F. Bos, U. Knaack, and R. Wolfs, "3d printing concrete on temporary surfaces: The design and fabrication of a concrete shell structure", *Automation in Construction*, vol. 94, pp. 395–404, 2018.
- [169] P. Hoogenboom, *Cie4143 shell analysis, theory and application*.
- [170] TUDelft. "Shell stability". (), [Online]. Available: http://homepage.tudelft.nl/p3r3s/b17_handout_8.pdf (visited on 02/24/2022).

- [171] M. Gomaa, W. Jabi, V. Soebarto, and Y. M. Xie, “Digital manufacturing for earth construction: A critical review”, *Journal of Cleaner Production*, p. 130 630, 2022.
- [172] I. Agustí-Juan, F. Müller, N. Hack, T. Wangler, and G. Habert, “Potential benefits of digital fabrication for complex structures: Environmental assessment of a robotically fabricated concrete wall”, *Journal of Cleaner Production*, vol. 154, pp. 330–340, 2017.
- [173] K. Kellens, R. Mertens, D. Paraskevas, W. Dewulf, and J. R. Duflou, “Environmental impact of additive manufacturing processes: Does am contribute to a more sustainable way of part manufacturing?”, *Procedia Cirp*, vol. 61, pp. 582–587, 2017.
- [174] M. K. Mohan, A. Rahul, K. Van Tittelboom, and G. De Schutter, “Rheological and pumping behaviour of 3d printable cementitious materials with varying aggregate content”, *Cement and Concrete Research*, vol. 139, p. 106 258, 2021.
- [175] Y. Weng, M. Li, S. Ruan, *et al.*, “Comparative economic, environmental and productivity assessment of a concrete bathroom unit fabricated through 3d printing and a precast approach”, *Journal of Cleaner Production*, vol. 261, p. 121 245, 2020.
- [176] H. Nowamooz and C. Chazallon, “Finite element modelling of a rammed earth wall”, *Construction and Building Materials*, vol. 25, no. 4, pp. 2112–2121, 2011.
- [177] A. Losini, A. Grillet, M. Bellotto, M. Woloszyn, and G. Dotelli, “Natural additives and biopolymers for raw earth construction stabilization—a review”, *Construction and Building Materials*, vol. 304, p. 124 507, 2021.
- [178] *EN 1992-1-1 Eurocode 2: Design of concrete structures - Part 1-1: General rules and rules for buildings*, EN, Brussels: CEN, 2005.
- [179] A.-L. Hammer, M. Thewes, and R. Galler, “Time-dependent material behaviour of shotcrete—new empirical model for the strength development and basic experimental investigations”, *Tunnelling and Underground Space Technology*, vol. 99, p. 103 238, 2020.
- [180] M. Neuner, T. Cordes, M. Drexel, and G. Hofstetter, “Time-dependent material properties of shotcrete: Experimental and numerical study”, *Materials*, vol. 10, no. 9, p. 1067, 2017.